MULTISCALE MODELING OF CROP EVAPOTRANSPIRATION AND CARBON DYNAMICS IN EAST-CENTRAL TEXAS USING SATELLITE REMOTE SENSING AND CROP GROWTH MODELS

A Dissertation

by

DOROTHY SCOTT MENEFEE

Submitted to the Office of Graduate and Professional Studies of
Texas A&M University
In partial fulfillment of the requirements for the degree of

DOCTOR OF PHILOSOPHY

Chair of Committee,	Nithya Rajan
Committee Members,	Ronnie Wayne Schnell Jason B. West Muthukumar V. Bagavathiannan
Head of Department,	David Baltensperger

December 2019

Major Subject: Agronomy

Copyright 2019 Dorothy Menefee

ABSTRACT

Over the past few decades, there have been increasing concerns over the impacts of agricultural practices on global carbon and water dynamics. Understanding these dynamics in agroecosystems will help efforts to reduce carbon emissions and improve water use efficiency in agriculture. Carbon and water vapor exchange from a continuous conventionally-tilled cotton (*Gossypium hirsutum*) field and a continuous conventionally-tilled corn (*Zea mays*) field in College Station, Texas were evaluated using two eddy covariance (EC) systems that were installed in early 2017.

Satellite imagery data from PlanetScope was incorporated to develop and validate gross primary productivity (GPP) models for both crops. Data from 2017 was used to develop the models and data from 2018 and 2019 was used to validate the models. The Decision Support System for Agrotechnology Transfer (DSSAT) software system was used to model crop growth and evapotranspiration (ET). In cotton, there were substantial differences in carbon fluxes between the years, which were driven by differences in meteorological conditions. A wet post-harvest season in 2018 spurred the growth of weeds, primarily volunteer cotton, morning glory (*Ipomoea cordatoriloba*), and Texas panicum (*Uruchloa texana*), resulting in substantial off-season carbon uptake in 2018 (374.2 g C m^{-2} in 2018 compared to 100.1 g C m^{-2} in 2017). The SAVI-based model was able to simulate GPP in corn production successfully; with a standard error for the model's validation of 1.74 g C m^{-2} in 2018 and 1.50 g C m^{-2} in 2019. The cotton GPP models performed adequately during the 2018 validation with an average standard error of 1.78 g C m^{-2}; however, there was significantly more error in the 2019 validation effort

(2.36 g C m^{-2}). The DSSAT system was able to estimate ET in dryland corn; however, the models had a tendency to underestimate ET, which was more pronounced in the Priestly-Taylor models. The average nRMSE was 0.36 mm for the Priestly-Taylor models and 0.35 mm for the FAO-56 models. There was mixed success in the ability of the DSSAT system to simulate ET in cotton. The model agreement with observed ET was low for 2019, with an average r^2 of 0.14.

DEDICATION

I dedicate my work to my family and friends who helped support me while I was pursuing my Ph.D. I would particularly like to thank my parents, Steve and Jenny Menefee, and my sister, Anna Menefee.

I would also like to dedicate this work to Dr. Dudley Smith and Ms. Angela Smith, whose family fellowship supported my work. Unfortunately, Dr. Dudley Smith passed away during the course of my studies.

ACKNOWLEDGMENTS

I would like to thank my committee chair, Dr. Nithya Rajan, and my committee members, Dr. Muthukumar Bagavathiannan, Dr. Ronnie Schnell, and Dr. Jason West, for their guidance and support throughout the course of this research.

I would also like to thank my colleagues in Dr. Rajan's lab group; Dr. Sumit Sharma, Dr. Ziana Zapata, Pramod Pokhrel, Jeff Sigfreid, and Rahul Raman.

I would like to thank Dr. Sanaz Shafian and Dr. Song Cui whose previous work helped direct my research projects.

I would like to thank our undergraduate student workers without whom this work would not be possible. Thank you to Bruno Fontana, Morgan Swaboda, Brad Knox, Ryan Kim, Ryan Leggett, and Michael Escobar.

I would like to thank the staff at the Texas A&M Research farm, particularly Mr. Alfred Nelson, for their assistance with planting and managing the crop fields.

Thanks also go to the Soil and Crop Sciences faculty and staff for making my time at Texas A&M University a great experience. I would like to the Soil and Crop Sciences Graduate Organization (SCGO) for creating an inviting community for graduate students at Texas A&M.

Finally, thanks to my mother and father for their encouragement and support.

CONTRIBUTORS AND FUNDING SOURCES

Contributors

This work was supervised by a thesis (or) dissertation committee consisting of Dr. Nithya Rajan, advisor, Dr. Muthukumar Bagavathiannan, and Dr. Ronnie Schnell of the Department of Soil and Crop Sciences and Dr. Jason West of the Department of Ecosystem Sciences and Management.

Satellite imagery data was received free of charge from Planet Labs Inc. through their "Research and Education Program". Training and assistance in using DSSAT were provided by the DSSAT Foundation. Missing meteorological data was provided by Dr. Don Conlee at the Department of Atmospheric Sciences at Texas A&M University.

All other work conducted for the dissertation was completed by the student independently.

Funding Sources

Graduate study was supported by the Dudley Smith Family Fellowship through the Department of Soil and Crop Sciences at Texas A&M University.

This work was made possible in part by NIFA-NLGCA under Grant Number 2016-70001-24636 and Project Accession Number 1008730 from the USDA National Institute of Food and Agriculture. Its contents are solely the responsibility of the authors and do not necessarily represent the official views of the USDA.

This work was also made possible in part by Cotton Incorporated under Grant Number 17-614. Its contents are solely the responsibility of the authors and do not necessarily represent the official views of Cotton Incorporated.

NOMENCLATURE

EC	Eddy Covariance
ET	Evapotranspiration
GPP	Gross Primary Productivity
NEE	Net Ecosystem Exchange
PAR	Photosynthetically Active Radiation
R_{eco}	Ecosystem Respiration
VPD	Vapor Pressure Deficit

TABLE OF CONTENTS

Page

LIST OF FIGURES

Page

LIST OF TABLES

Page

INTRODUCTION

1.1. About Carbon and Water Fluxes

The overarching goal of this dissertation is to improve our understanding of carbon and water fluxes in agroecosystems in East-Central Texas in order to improve the sustainability of cropping systems. Agroecosystems are unique from natural ecosystems due to the inputs and management that they receive (Foley et al., 2005; Tscharntke et al., 2005; Tian et al., 2010; Han et al., 2014). An agroecosystem is an agricultural system viewed from the perspective of ecosystem sciences. An agroecosystem includes the crop or livestock being produced plus the soil, water, microorganisms, weeds, insects, and the local environment (Tscharntke et al., 2005; Bennett et al., 2009).

The processes that occur in native ecosystems occur in agroecosystems and these processes are vital for the ability of the land to support agricultural production. Ecosystem services, like nutrient cycling, control of pests, and water infiltration and storage, are essential for agricultural production (Altieri, 1999; Foley et al., 2005; Tscharntke et al., 2005). Developing an understanding of agricultural lands as ecosystems can allow for better management practices that preserve ecosystem services and limit potential environmental harms associated with agricultural production. This can extend to a better ability to understand and manage carbon and water vapor fluxes, two extremely important components of ecosystem processes (Tscharntke et al., 2005; Bennett et al., 2009; Tian et al., 2010; Han et al., 2014).

Net ecosystem CO_2 exchange (NEE) and evapotranspiration (ET) are major components of ecosystem processes and global carbon and hydrologic cycles. Measuring and estimating NEE and ET can improve agricultural productivity and our ability to mitigate and adapt to climate change (Yuan et al., 2010; Mu et al., 2011). The development of the eddy covariance technique (EC) has allowed for large-scale measurements of NEE and ET, thus it has become widely used in ecosystem sciences. However, EC is less common agricultural sciences (Suyker et al., 2004a; Verma et al., 2005; Jans et al., 2010; Vitale et al., 2016). Eddy covariance calculates fluxes by taking the covariance of the wind velocity and the concentration of the gas of interest (i.e. CO_2) as follows:

$$CO_2\ Flux = \overline{\rho a * w' * s'}$$

Where ρa is the air density, w' is the deviation of the vertical wind speed, and s' is the deviation of the concentration of the gas of interest (Burba, 2013). The same applies to water vapor or any other gas of interest, such as methane. It is crucial to take these measurements from agroecosystems to further our understanding of the impact of climate change and management activities on agriculture. A greater understanding of NEE and ET from agriculture can also improve the ability of modeling efforts to predict changes and make management recommendations.

Evapotranspiration (ET) is the combined loss of water through soil evaporation and plant transpiration. This process is an important component of the hydrologic cycle and energy budget. Approximately 24% of incoming solar radiation is dissipated as latent heat flux (LE), which is the energy that is used to evaporate water. Over terrestrial

areas, LE is the energy equivalent of ET, where LE can be converted to ET given the known energetics of water evaporation (Lindsey, 2009; L'Ecuyer et al., 2015). Evapotranspiration is calculated from LE as follows:

$$ET = \frac{LE * 0.0018}{2.5}$$

Land management practices alter both the energy dynamics and the amount of water available for evaporation, thus altering ET compared to natural ecosystems (Li et al., 2008; Tian et al., 2010). Replacing deep-rooted forest vegetation with access to large amounts of groundwater with shallow-rooted crops that only access the surface soil reduces the amount of available water for ET. Applying irrigation water from aquifers in arid regions decreases the amount of water available for ET. Tillage and other soil management practices alter surface characteristics that in turn alters how energy is distributed (Oki and Shinjiro, 2006; Rost et al., 2008). For all these reasons, it is important to study agricultural ET to understand how our management practices affect this crucial natural process.

Directly measuring ET in agroecosystems can be applied to crop modeling efforts by allowing models to be validated with in-situ measurements. Modeling can allow for estimation of ET in areas where EC is not possible or practical (i.e. over areas too large or too small for EC, on slopes, and where EC equipment is too costly). Modeling can also predict how ET patterns will respond to hypothetical climate change scenarios or changes in crop management. However, having models backed up by actual ET measurements is essential for validating the accuracy of the models. Many agricultural ET models are backed with phenological (crop growth) data alone,

indicating a need for increased ET measurement efforts in agricultural settings (Collatz et al., 1991).

Similarly, to ET, agroecosystem carbon dynamics differ from their natural ecosystem counterparts (Lal, 2004; King et al., 2007; Kaplan et al., 2010). Net ecosystem exchange (NEE) is the sum of all positive and negative carbon fluxes from an ecosystem and represents the net balance of the carbon cycle. The most common sign convention is for positive numbers to indicate fluxes away from the ecosystem and for negative numbers to indicate fluxes toward the ecosystem. Negative NEE, thus represents net carbon sequestration and positive NEE represents net carbon emission. Gross primary productivity (GPP) is the total amount of carbon captured during photosynthesis in an ecosystem. Ecosystem respiration, R_{eco}, is the total amount of carbon released into the atmosphere by cellular respiration by all organisms in the ecosystem (plants, animals, and microbes). NEE thus is the sum of GPP and R_{eco}.

$$NEE = GPP + R_{eco}$$

As with ET, a variety of management practices can alter NEE in agroecosystems compared to their natural counterparts (Stoate et al., 2009). Possibly the largest impact on agricultural carbon dynamics is the introduction of tillage practices. Tillage incorporates plant residue, reduces the surface area of the residue, and aerates the soil, all of which increases the rate of R_{eco} (Murty et al., 2002; West and Post, 2002; Lal, 2004; Smith et al., 2014). In many cases, the increase in R_{eco} from tillage is not fully compensated by GPP and the ecosystem becomes a net carbon source as stored soil carbon is being used for microbial metabolism at a rate that exceeds carbon inputs. A

meta-analysis by Murty et al (2002) found that soil organic carbon (SOC) stocks had decreased by 22% (after correction for bulk density changes) over ten years following the conversion of native ecosystems to an agricultural system. This loss exacerbated in agricultural systems with residue harvest for fuel or animal feed, and/or intensive tillage practices. Similarly, Guo and Gifford (2002) found that conversion of forest or pasture to cropland resulted in a loss of 50% of topsoil (60 cm) SOC over 50 years. Most of this lost carbon was emitted to the atmosphere as CO_2, contributing to climate change. Despite this, better management practices can allow croplands to become net carbon sinks. Some improved management practices, like no-till, function by reducing R_{eco}, whereas others, such as cover cropping, function by increasing GPP (West and Post, 2002; Lal, 2004). Measuring carbon fluxes using EC can allow for the quantification of a net carbon balance from a cropping system. It can also be used to assist in predicting changes in soil carbon stocks due to management practices.

1.2. About The Region

In East-Central Texas, most of the agricultural land was converted from native ecosystems in the past century. Agricultural survey data shows that cropland in the South-Central USA (which includes this region of Texas) increased from 8.6% of total land area in 1860 to 30% in 2003 (Chen et al., 2006b). This change in land management has resulted in a loss of soil carbon and an increase in soil CO_2 emissions (Chen et al., 2006b; Woodbury et al., 2006). This decline in soil organic matter can reduce crop productivity and increase soil vulnerability to climate change (Brejda, 2000; Bronson et

al., 2004). The Southern US is an agriculturally important region and the study of ecosystem processes in agricultural systems in this region has been limited. Improving our knowledge of carbon dynamics in the Southern US is an important goal.

This study takes place in Burleson County, Texas, near College Station, Texas. The native ecosystem of this region is the Post-Oak Savannah. This is a sub-tropical mixed ecosystem consisting of post oak woodlands and tallgrass meadows (Texas Parks and Wildlife, 2019). The majority of land in this region is currently in pasture for grazing livestock. The most common row crops in Burleson County are corn (*Zea mays*), cotton (*Gossypium hirsutum*), soy (*Glycine max*), and sorghum (*Sorghum bicolor*) (USDA-NASS, 2017). This study will focus on corn and cotton, as they are two of the most common crops grown in this region.

Corn is a C4 monocot with a determinate vegetative growth pattern. After planting corn plants undergo rapid vegetative growth until around stage V6. At stage V6 reproductive growth typically begins as ear and tassel buds form. The tassel (male flower) matures before the ear (female flower). Once tasseling occurs, vegetative growth ceases and all of the plant's biomass accumulation is then allocated to reproductive growth. After the ear reaches maturity, the plant senesces (Bell, 2017). In Burleson County, corn is typically planted in early March and harvested in late July or early August. Corn is the 2nd largest crop in Burleson County by acreage, with 8,618 acres planted in 2017 (USDA-NASS, 2017).

Cotton is a C3 dicot with an indeterminate vegetative growth pattern. After planting, cotton grows very slowly, putting most of its energy into developing a root

system. Once the seedling is established with a sufficient root system, it begins vegetative growth. Pure vegetative growth continues until the plant accumulates 550 growing degree-days (GDD) or around the sixth vegetative node. At this point, the plant begins producing squares, which are the buds that will become flowers. Full bloom typically occurs after 950 GDD. After pollination, the bolls form and begin to develop. Throughout flowering and boll development, vegetative growth continues. Bolls mature 850 GDD after flowering (Ritchie et al., 2007; Main, 2012). Once the majority of the bolls are mature, the crop will typically be sprayed with a defoliant to halt vegetative growth and allow for an easier harvest. The defoliant is typically an herbicide that kills all photosynthetic structures. In Burleson County, cotton is typically planted in early to mid-April, defoliated in late August to mid-September and then harvested two to three weeks after defoliation. Cotton is the largest row crop in Burleson County by acreage and income, with 9,262 acres planted and worth $6,358,000 in sales (USDA-NASS, 2017).

1.3. Crop Modeling Systems

Crop growth and the environmental conditions associated with it can be modeled with crop modeling software systems. These systems can combine multiple individual mathematical models (i.e. growing degree-days, water infiltration, potential ET) into one system and compute them all simultaneously to simulate crop growth. Many of the modern crop modeling software platforms got their start in the 1980s when the USDA encouraged the development of such models for improved yield forecasting. Since then, crop modeling systems have expanded to a wide range of uses and crops (Jones et al.,

2017). This dissertation will utilize the Decision Support System for Agrotechnology Transfer (DSSAT) system to model corn and cotton. DSSAT was developed in the 1980s with the support of the USDA. DSSAT uses a modular approach that combines multiple modeling systems into one software platform. In this dissertation, we will use the CERES model within DSSAT for corn, and the CROPGRO model for cotton. CERES is a model that works with grass crops, such as corn, wheat, and rice. CROPGRO is a broadleaf model that was originally developed for soybean but has since been adapted for other broadleaf crops, including cotton (Hoogenboom et al., 2003; Jones et al., 2003, 2017).

1.4. Remote Sensing

The development of multispectral areal and satellite images has allowed plant scientists to take advantage of the unique spectral properties of plants. Chlorophyll in leaf tissue strongly absorbs visible light, particularly red, and reflects near-infrared (Asrar et al., 1984; Daughtry, 2000; Verlag et al., 2003). As such, it is possible to estimate plant productivity by comparing near-infrared reflectance to other wavelength bands of light. Vegetation indices (VI's) are indices that are typically a ratio of near-infrared to another band of light, often red. These VI's are commonly used in agricultural and ecosystem sciences for a wide range of purposes particularly yield forecasting (Gonzalez-Dugo et al., 2009; Peng et al., 2011; Shafian et al., 2018).

In 1977, Monteith developed a GPP model based on light use efficiency. In this model, GPP is the product of light use efficiency, photosynthetically active radiation, and the fraction of absorbed available radiation (Monteith, 1977). This model has been

commonly used with remote sensing data by replacing the LUE term with a VI. This method has been applied to native ecosystems and crops, particularly corn, wheat, and soy (Gonzalez-Dugo et al., 2009; Yan et al., 2009; Sakamoto et al., 2011; Gitelson, 2019). However, studies in cotton are limited compared to other crops. For that reason, it is important to include more studies involving cotton (Alganci et al., 2014; Ballester et al., 2019).

1.5. Overarching Goals

The overarching goal of this dissertation is to improve the understanding of carbon and water fluxes in corn and cotton production in East-Central Texas. This goal will be achieved through several sub-objectives.

1. To monitor carbon and water vapor fluxes in corn and cotton production fields using the eddy covariance method. Fluxes were monitored for three growing seasons and two full off-seasons. Fluxes in the cotton field are described and discussed in Chapter One: Carbon Exchange of a Dryland Cotton Field and its Relationship with PlanetScope Remote Sensing Data.
2. To model gross primary productivity in corn and cotton production using high-resolution satellite imagery. PlanetScope satellite data was used to develop and validate GPP models that were compared to observed fluxes from the eddy covariance system. The results of the modeling effort in corn are shown in Chapter Two: Modeling gross primary production of dryland corn using PlanetScope satellite imagery and eddy covariance data. The results of the same modeling effort in cotton are shown in Chapter Three: A comparison of modeled

primary production using PlanetScope satellite imagery to eddy covariance data in East-Central Texas cotton production.

3. To model evapotranspiration in corn and cotton production using the Decision Support System for Agrotechnology Transfer (DSSAT) crop modeling software platform. The DSSAT system was used to model evapotranspiration and the results were statistically compared to those from the eddy covariance flux-tower. The results of the modeling effort in corn are discussed in Chapter Four: Comparison of simulated ET using the DSSAT-CERES-MAIZE modeling system to measured ET using the eddy covariance method for a corn crop in East Texas. The results of the modeling efforts in cotton are discussed in Chapter Five: Comparison of simulated ET using DSSAT-CROPGRO-Cotton and measured ET using the eddy covariance method.

These goals will be addressed in the following chapters.

1.6. References

Adhikari, P., S. Ale, J.P. Bordovsky, K.R. Thorp, N.R. Modala, N. Rajan, and E.M. Barnes. 2016. Simulating future climate change impacts on seed cotton yield in the Texas High Plains using the CSM-CROPGRO-Cotton model. Agric. Water Manag. 164: 317–330. doi: 10.1016/j.agwat.2015.10.011.

Agam, N., W.P. Kustas, and M.C. Anderson. 2010. Application of the Priestley – Taylor Approach in a Two-Source Surface Energy Balance Model. Am. Meterorological Soc. 11: 185–198. doi: 10.1175/2009JHM1124.1.

Ahlrichs, J.S., and M.E. Bauer. 1983. Relation of Agronomic and Multispectral Reflectance Characteristics of Spring Wheat Canopies1. Agron. J. 75(6): 987–993. doi: 10.2134/agronj1983.00021962007500060029x.

Alganci, U., M. Ozdogan, E. Sertel, and C. Ormeci. 2014. Field Crops Research Estimating maize and cotton yield in southeastern Turkey with integrated use of satellite images , meteorological data and digital photographs. F. Crop. Res. 157: 8–19. doi: 10.1016/j.fcr.2013.12.006.

Altieri, M.A. 1999. The ecological role of biodiversity in agroecosystems. Agric. Ecosyst. Environ. 74(1–3): 19–31. doi: 10.1016/S0167-8809(99)00028-6.

Amouzou, K.A., J.B. Naab, J.P.A. Lamers, C. Borgemeister, M. Becker, and P.L.G. Vlek. 2018. CROPGRO-Cotton model for determining climate change impacts on yield, water- and N- use efficiencies of cotton in the Dry Savanna of West Africa. Agric. Syst. 165(November 2017): 85–96. doi: 10.1016/j.agsy.2018.06.005.

Anothai, J., C.M.T. Soler, A. Green, T.J. Trout, and G. Hoogenboom. 2013. Evaluation of two evapotranspiration approaches simulated with the CSM–CERES–Maize model under different irrigation strategies and the impact on maize growth, development and soil moisture content for semi-arid conditions. Agric. For. Meteorol. 176(July): 64–76.

Anthoni, P.M., B.E. Law, and M.H. Unsworth. 1999. Carbon and water vapor exchange of an open-canopied ponderosa pine ecosystem. Agric. For. Meteorol. 95(3): 151–168. doi: 10.1016/S0168-1923(99)00029-5.

Asrar, G., M. Fuchs, E.T. Kanemasu, and J.L. Hatfield. 1984. (1984) Estimating Absorbed Photosynthetic Radiation and Leaf Area Index from Spectral Reflectance in Wheat (AJ).

Aubinet, M., T. Vesala, and D. Papale. 2012. Eddy Covariance: A Practical Guide to Measurement and Data Analysis. Springer Atmospheric Sciences, Berlin, Germany.

Bagavathiannan, M., and J.K. Norsworthy. 2012. Late-Season Seed Production in Arable Weed Communities: Management Implications. Weed Sci. 60(3): 325–334.

Bai, J., J. Wang, X. Chen, G.P. Lou, H. Shi, L.H. Li, and J. Li. 2015. Seasonal and inter-variations in carbon fluxes and evapotranspiration over cotton field under drip irrigation and plastic mulch in an arid region of Northwest China. J. Arid Land 7(2): 272–282.

Baker, J.M., and T.J. Griffis. 2005. Examining strategies to improve the carbon balance of corn / soybean agriculture using eddy covariance and mass balance techniques. Agric. For. Meteorol. 128: 163–177. doi: 10.1016/j.agrformet.2004.11.005.

Baldocchi, D.D. 2003. Assessing the eddy covariance technique for evaluating carbon dioxide exchange rates of ecosystems: past, present and future. Glob. Chang. Biol. 9(4): 479–492. doi: 10.1046/j.1365-2486.2003.00629.x.

Ballester, C., J. Brinkhoff, W.C. Quayle, and J. Hornbuckle. 2019. Monitoring the Effects of Water Stress in Cotton Using the Green Red Vegetation Index and Red Edge Ratio. Remote Sens. 11(7).

Baret, F., and G. Guyot. 1991. Potentials and limits of vegetation indices for LAI and APAR assessment. Remote Sens. Environ. 35(2–3): 161–173. doi: 10.1016/0034-4257(91)90009-U.

Basso, B., L. Liu, and J.T. Ritchie. 2016. A Comprehensive Review of the CERES-Wheat, -Maize and -Rice Models' Performances. Elsevier Inc.

Bednarz, C.W., and R.L. Nichols. 2005. Phenological and Morphological Components of Cotton Crop Maturity. Crop Sci. 45(4): 1497–1503.

Bell, J. 2017. Corn Growth Stages and Development.

Bennett, E.M., G.D. Peterson, and L.J. Gordon. 2009. Understanding relationships among multiple ecosystem services. Ecol. Lett. 12(12): 1394–1404. doi: 10.1111/j.1461-0248.2009.01387.x.

Boman, R., and R. Lemon. 2005. Soil Temperatures for Cotton Planting. College Station, Texas.

Boote, K.J., and N.B. Pickering. 1994. Modeling Photosynthesis of Row Crop Canopies. HortScience 29(12): 1423–1434.

Bozorov, T.A., R.M. Usmanov, H.L. Yang, S.A. Hamdullaev, S. Musayev, J. Shakiev, S. Nabiev, D.Y. Zhang, and A.A. Abdullaev. 2018. Effect of water deficiency on relationships between metabolism, physiology, biomass, and yield of upland cotton (Gossypium hirsutum L.). J. Arid Land 10(3): 441–456.

Bruinsma, J. 2003. World Agriculture: Towards 2015/2030.

Burba, G. 2013. Eddy Covariance Method (R Nelson, Ed.). LI-COR Biosciences, Lincoln, NE.

Carberry, P.S. 1991. Test of leaf-area development in CERES-Maize: a correction. F. Crop. Res. 27: 159–167.

Carmelita, M., R. Alberto, R. Wassmann, R.J. Buresh, J.R. Quilty, T.Q. Correa, J.M. Sandro, C. Arloo, and R. Centeno. 2014. Field Crops Research Measuring methane flux from irrigated rice fields by eddy covariance method using open-path gas analyzer. F. Crop. Res. 160: 12–21. doi: 10.1016/j.fcr.2014.02.008.

Chen, J.M., A. Govind, O. Sonnentag, Y. Zhang, A. Barr, and B. Amiro. 2006a. Leaf area index measurements at Fluxnet-Canada forest sites. Agric. For. Meteorol. 140(1): 257–268.

Chen, H., H. Tian, M. Liu, J. Melillo, S. Pan, and C. Zhang. 2006b. Effect of Land-Cover Change on Terrestrial Carbon Dynamics in the Southern United States. J. Environ. Qual. 35(4): 1533. doi: 10.2134/jeq2005.0198.

Collatz, G.J., J.T. Ball, C. Grivet, and J.A. Berry. 1991. Physiological and environmental regulation of stomatal conductance, photosynthesis and transpiration: a model that includes a laminar boundary layer. Agric. For. Meteorol. 54(2–4): 107–136. doi: 10.1016/0168-1923(91)90002-8.

Collins, H.P., R.L. Blevins, L.G. Bundy, D.R. Christienson, W.A. Dick, D.R. Huggins, and E.A. Paul. 1999. Soil Carbon Dynamics in Corn-Based Agroecosystems:

Results from Carbon-13 Natural Abundance. Soil Sci. Soc. Am. J. 63(3): 584–591.

Contay, W.C., J.J. Burke, J.R. Mahan, J.E. Neilsen, and B.G. Sutton. 2012. Determining the Optimum Plant Temperature of Cotton Physiology and Yield to Improve Plant-Based Irrigation and Scheduling. Crop Sci. 52(July): 1828–1836.

Cook, B.D., K.J. Davis, W. Wang, A. Desai, B.W. Berger, R.M. Teclaw, J.G. Martin, P. V. Bolstad, P.S. Bakwin, C. Yi, and W. Heilman. 2004. Carbon exchange and venting anomalies in an upland deciduous forest in northern Wisconsin, USA. Agric. For. Meteorol. 126(3–4): 271–295. doi: 10.1016/j.agrformet.2004.06.008.

Daughtry, C. 2000. Estimating Corn Leaf Chlorophyll Concentration from Leaf and Canopy Reflectance. Remote Sens. Environ. 74(2): 229–239. doi: 10.1016/S0034-4257(00)00113-9.

Dejonge, K.C., and K.R. Thorp. 2017. Implementing Standardized Reference Evapotranspiration and Dual Crop Coefficient Approach in the DSSAT Cropping System Model. Am. Soc. Agric. Biol. Eng. 60(6): 1965–1981.

Dettori, M., C. Cesaraccio, A. Montroni, D. Spano, and P. Duce. 2011. Using CERES-Wheat to simulate durum wheat production and phenology in Southern Sardinia, Italy. F. Crop. Res. 120(1): 179–188.

Dokoohaki, H., M. Gheysari, S.F. Mousavi, S. Zand-Parsa, F.E. Miguez, S.V. Archontoulis, and G. Hoogenboom. 2016. Coupling and testing a new soil water module in DSSAT CERES-Maize model for maize production under semi-arid

condition. Agric. Water Manag. 163(1): 90–99.

Dolman, A.J., J. Noilhan, P. Durand, C. Sarrat, A. Brut, B. Piguet, A. Butet, N. Jarosz, Y. Brunet, D. Loustau, E. Lamund, L. Tolk, R. Ronda, F. Miglietta, B. Gioli, V. Magliulo, M. Esposito, C. Gerbig, S. Korner, P. Glademard, M. Ramonet, P. Ciais, B. Neininger, R.W.A. Hutjes, J.A. Elbers, R. Macatangay, O. Schrems, G. Perez-Landa, M.J. Sanz, Y. Scholz, G. Facon, E. Ceschia, and P. Beziat. 2006. The CarboEurope Regional Experiment Strategy. Am. Meteorol. Soc. (October): 1367–1379.

Doorenbos, J., and W.D. Pruitt. 1977. Guidelines for Predicting Crop Water Use. Rome, Italy.

Finnigan, J.J., R. Clement, Y. Malhi, R. Leuning, and H.A. Cleugh. 2003. A Re-Evaluation of Long-Term Flux Measurement Techniques Part 1: Averaging and Coordinate Rotation. Boundary-Layer Meteorol. (107): 1–48.

Foley, J.A., R. Defries, G.P. Asner, C. Barford, G. Bonan, S.R. Carpenter, F.S. Chapin, M.T. Coe, G.C. Daily, H.K. Gibbs, J.H. Helkowski, T. Holloway, E.A. Howard, C.J. Kucharik, C. Monfreda, J.A. Patz, I.C. Prentice, N. Ramankutty, and P.K. Snyder. 2005. Global Consequences of Land Use. Science (80-.). 309(July): 570–574. doi: 10.1126/science.1111772.

Food and Agriculture Organization. 2016. Land Use.

Frankenberg, C., J.B. Fisher, J. Worden, G. Badgley, S.S. Saatchi, J.E. Lee, G.C. Toon,

A. Butz, M. Jung, A. Kuze, and T. Yokota. 2011. New global observations of the terrestrial carbon cycle from GOSAT: Patterns of plant fluorescence with gross primary productivity. Geophys. Res. Lett. 38(17): 1–7. doi: 10.1029/2011GL048738.

Fritz, E., S. Richter, S. Schott, S. Hejja, and S. Trumbore. 2018. Partitioning Algorithm. Max Planck Inst. Biogeochem.

Garbulsky, M.F., J. Penuelas, D. Papale, J. Ardo, M.L. Goulden, K. Gerard, A.D. Richardson, E. Rotenberg, E.M. Veenendall, and I. Filella. 2010. Patterns and controls of the variability of radiation use efficiency and primary productivity across terrestrial ecosystems. Glob. Ecol. Biogeogr. 19: 253–267.

Gitelson, A.A. 2019. Remote estimation of fraction of radiation absorbed by photosynthetically active vegetation : generic algorithm for maize and soybean. Remote Sens. Lett. 10(3): 283–291. doi: 10.1080/2150704X.2018.1547445.

Gitelson, A.A., Y. Peng, J.G. Masek, D.C. Rundquist, S. Verma, A. Suyker, J.M. Baker, J.L. Hat, and T. Meyers. 2012. Remote estimation of crop gross primary production with Landsat data. Remote Sens. Environ. 121: 404–414. doi: 10.1016/j.rse.2012.02.017.

Glenn, E.P., A.R. Huete, P.L. Nagler, and S.G. Nelson. 2008. Relationship Between Remotely-sensed Vegetation Indices, Canopy Attributes and Plant Physiological Processes: What Vegetation Indices Can and Cannot Tell Us About the Landscape. : 2136–2160.

Godwin, D.C., and C.A. Jones. 1991. Nitrogen dynamics in soil-plant systems. p. 287–321. *In* Modeling plant and soil systems. ASA, CSSA, and SSSA, Madison, Wisconsin.

Godwin, D.C., and U. Singh. 1998. Nitrogen balance and crop response to nitrogen in upland and lowland cropping systems. p. 55–77. *In* Tsuji, G.Y., Hoogenboom, G., Thornton, P.K. (eds.), Understanding options for agricultural production. System approaches for sustainable agricultural development. Kluwer Academic Publishers, Dordrecht, Netherlands.

Gonias, E.D., D.M. Oosterhuis, and A.C. Bibi. 2011. Light interception and radiation use efficiency of okra and normal leaf cotton isolines. Environ. Exp. Bot. 72(2): 217–222.

Gonzalez-Dugo, M.P., C.M.U. Neale, L. Mateos, W.P. Kustas, J.H. Prueger, M.C. Anderson, and F. Li. 2009. A comparison of operational remote sensing-based models for estimating crop evapotranspiration. Agric. For. Meteorol. 149(11): 1843–1853. doi: 10.1016/j.agrformet.2009.06.012.

Guo, L.B., and R.M. Gifford. 2002. Soil carbon stocks and land use change: A meta analysis. Glob. Chang. Biol. 8(4): 345–360. doi: 10.1046/j.1354-1013.2002.00486.x.

Gutierrez, M., R. Norton, K.R. Thorp, and G. Wang. 2012. Association of Spectral Reflectance Indices with Plant Growth and Lint Yield in Upland Cotton. Crop Sci. 52(2): 849–857.

Gwathmey, C.O., D.D. Tyler, and X. Yin. 2010. Prospects for Monitoring Cotton Crop Maturity with Normalized Difference Vegetation Index. Agron. J. 102(5): 1352–1360.

Han, G., Q. Xing, J. Yu, Y. Luo, D. Li, L. Yang, G. Wang, P. Mao, B. Xie, and N. Mikle. 2014. Agricultural reclamation effects on ecosystem CO2exchange of a coastal wetland in the Yellow River Delta. Agric. Ecosyst. Environ. 196: 187–198. doi: 10.1016/j.agee.2013.09.012.

Harmel, R.D., D.R. Smith, R.L. Haney, and P.M. Allen. 2019. Comparison of nutrient loss pathways: Run-off and seepage flow in Vertisols. Hydrol. Process. 33(18): 2384–2393.

He, M., J.S. Kimball, M.P. Maneta, and B.D. Maxwell. 2018. Regional Crop Gross Primary Productivity and Yield Estimation Using Fused Landsat-MODIS Data. doi: 10.3390/rs10030372.

Hirschi, M., D. Michel, I. Lehner, and S.I. Seneviratne. 2017. A site-level comparison of lysimeter and eddy covariance flux measurements of evapotranspiration. Hydrol. Earth Syst. Sci. 21(3): 1809–1825. doi: 10.5194/hess-21-1809-2017.

Hoogenboom, G., J.W. Jones, C.H. Porter, P.W. Wilkens, K.J. Boote, W.D. Batchelor, L.A. Hunt, and G.Y. Tsuji. 2003. A Decision Support System for Agrotechnology Transfer Version 4.0. 4th ed. University of Hawaii, Honolulu, Hawaii.

Houghton, R.A. 2007. Balancing the Global Carbon Budget. Annu. Rev. Earth Planet.

Sci. 35(1): 313–347. doi: 10.1146/annurev.earth.35.031306.140057.

Houghton, R.A., A. Baccini, and W.S. Walker. 2018. Where is the residual terrestrial carbon sink? Glob. Chang. Biol. 24(8): 3277–3279.

Howell, T.A., S.R. Evett, J.A. Tolk, and A.D. Schneider. 2004. Evapotranspiration of full-, deficit-irrigated, and dryland cotton on the Northern Texas High Plains. J. Irrig. Drain. Eng. 130(4).

Huemmrich, K.F., P. Campbell, D. Landis, and E. Middleton. 2019. Developing a common globally acceptable method for optical remote sensing of ecosystem light use efficiency. Remote Sens. Environ. 230.

Huete, A.R., H.Q. Liu, K. Batchily, and L. van W. J. 1997. A comparsion of vegetation indices over a Global set of TM images for EO -MODIS. Remote Sens. Environ. 59(Table 1): 440–451. doi: 10.1016/S0034-4257(96)00112-5.

Ibell, P.T., Z. Xu, and T.J. Blumfield. 2010. Effects of weed control and fertilization on soil carbon and nutrient pools in an exotic pine plantation of subtropical Australia. J. Soils Sediments (10): 1027–1038. doi: 10.1007/s11368-010-0222-6.

Ibrahim, M.E., and D.R. Buxton. 1981. Early Vegetative Growth of Cotton as Influenced by Leaf Type. Crop Sci. 21(5): 639–643.

Jaafar, H.H., and F.A.. Ahmad. 2015. Relationships Between Primary Production and Crop Yields in Semi-Arid and Arid Irrigated Agroecosystems. Int. Symp. Remote Sens. Environ. 47(W3): 27–30.

Jalota, S.K., S. Sukhvinder, G.B.S. Chahal, S.S. Ray, S. Panigraphy, F. Bhupinder-Singh, and K.B.. Singh. 2010. Soil texture, climate and management effects on plant growth, grain yield and water use by rainfed maize–wheat cropping system: Field and simulation study. Agric. Water Manag. 97(1): 83–90.

Jans, W.W.P., C.M.J. Jacobs, B. Kruijt, J.A. Elbers, S. Barendse, and E.J. Moors. 2010. Carbon exchange of a maize (Zea mays L.) crop: Influence of phenology. Agric. Ecosyst. Environ. 139(3): 316–324. doi: 10.1016/j.agee.2010.06.008.

Johnson, D.M. 2016. A comprehensive assessment of the correlations between field crop yields and commonly used MODIS products. Int. J. Appl. EARTH Obs. Geoinf. 52: 65–81.

Jones, J.W. 1993. Decision Support System for agricultural development. p. 459–471. *In* de Vries, F.P., Teng, P., Metselaar, K. (eds.), Systems Approaches for Agricultural Development. Kluwer Academic Publishers, Boston.

Jones, J.W., J.M. Antle, B. Basso, K.J. Boote, R.T. Conant, I. Foster, H.C.J. Godfray, M. Herrero, R.E. Howitt, S. Janssen, B.A. Keating, R. Munoz-Carpena, C.H. Porter, C. Rosenzweig, and T.R. Wheeler. 2017. Brief history of agricultural systems modeling. Agric. Syst. 155(June): 240–254. doi: 10.1016/j.agsy.2016.05.014.

Jones, J.W., K.J. Boote, G. Hoogenboom, S.S. Jagtap, and G.G. Wilkerson. 1989. Soybean Crop Growth Simulation Model. Gainsville.

Jones, J.W., G. Hoogenboom, C.H. Porter, K.J. Boote, W.D. Batchelor, L.A. Hunt, P.W.

Wilkens, U. Singh, and A.J. Gijsman. 2003. The DSSAT Cropping System Model.

Jones, J.W., and J.T. Ritchie. 1991. Crop Growth Models. p. 63–89. *In* Hoffman, G.J., Howell, T.A., Soloman, K.H. (eds.), Management of Farm Irrigation System. 9th ed. American Society of Agricultural Engineers.

Kaplan, J.O., K.M. Krumhardt, E.C. Ellis, F. Ruddiman, C. Lemmen, and K.K. Goldewijk. 2010. Holocene carbon emissions as a result of anthropogenic land cover change. The Holocene 21(June). doi: 10.1177/0959683610386983.

Kerr, J.T., and M. Ostrovsky. 2003. From space to species: Ecological applications for remote sensing. Trends Ecol. Evol. 18(6): 299–305. doi: 10.1016/S0169-5347(03)00071-5.

Kessavalou, A., A.R. Mosier, J.W. Doran, R.A. Drijber, D.J. Lyon, and O. Heinemeyer. 1998. Fluxes of Carbon Dioxide, Nitrous Oxide, and Methane in Grass Sod and Winter Wheat-Fallow Tillage Management. J. Environ. Qual. (27): 1094–1104.

King, A.W., L. Dilling, G.P. Zimmerman, D.M. Fairman, R.A. Houghton, G.H. Marland, A.Z. Rose, and T.J. Wilbanks. 2007. The North American Carbon Budget and Implications for the Global Carbon Cycle.

L'Ecuyer, T.S., H.K. Beaudoing, M. Rodell, W. Olson, B. Lin, S. Kato, C.A. Clayson, E. Wood, J. Sheffield, R. Adler, G. Huffman, M. Bosilovich, G. Gu, F. Robertson, P.R. Houser, D. Chambers, J.S. Famiglietti, E. Fetzer, W.T. Liu, X. Gao, C.A. Schlosser, E. Clark, D.P. Lettenmaier, and K. Hilburn. 2015. The observed state of

the energy budget in the early twenty-first century. J. Clim. 28(21): 8319–8346. doi: 10.1175/JCLI-D-14-00556.1.

Laitala, K., and I.G. Klepp. 2015. Age and active life of clothing. Prod. Lifetimes Environ.: 182–186.

Lal, R. 2004. Soil Carbon Sequestration Impacts on Global Climate Change and Food Security. Am. Assoc. Adv. Sci. 304(5677): 1623–7. doi: 10.1126/science.1097396.

LI-COR. 2015. SmartFlux System Instruction Manual.

Li, S., S. Kang, F. Li, and L. Zhang. 2008. Evapotranspiration and crop coefficient of spring maize with plastic mulch using eddy covariance in northwest China. Agric. Water Manag. 95(11): 1214–1222. doi: 10.1016/j.agwat.2008.04.014.

Li, X., L. Liu, H. Yang, and Y. Li. 2018. Relationships between carbon fluxes and environmental factors in a drip-irrigated, film-mulched cotton field in arid region. PLoS One 13(2): 1–18. doi: 10.1371/journal.pone.0192467.

Lindsey, R. 2009. Climate and Earth's Energy Budget. NASA Earth Obs.: 1–12. doi: 10.1007/s10712-011-9165-8.

Liu, P. 2017. The future of food and agriculture: Trends and challenges.

Lopez-Cedron, F.X., K.J. Boote, J. Pineiro, and F. Sau. 2008. Improving the CERES-Maize model ability to simulate water deficit impact on maize production and yield components. Agron. J. 100: 296–307.

Main, C.L. 2012. Cotton Growth and Development.

Matocha, M., C. Allen, R. Boman, G. Morgan, and P. Baumann. 2009. Crop Profile for Cotton in Texas. College Station, Texas.

Meyers, T.P. 2001. A comparison of summertime water and CO2fluxes over rangeland for well watered and drought conditions. Agric. For. Meteorol. 106(3): 205–214. doi: 10.1016/S0168-1923(00)00213-6.

Modala, N.R., S. Ale, N. Rajan, C.L. Munster, P.B. DeLaune, K.R. Thorp, S.S. Nair, and E.M. Barnes. 2015. Evaluation of the CSM-CROPGRO-COTTON MODEL for the Texas Rolling Plains Region and Simulation of Deficit Irrigation Strategies for Increasing Water Use Efficiency. Trans. ASABE 58(3): 658–696.

Möller, M., J. Tanny, Y. Li, and S. Cohen. 2004. Measuring and predicting evapotranspiration in an insect-proof screenhouse. Agric. For. Meteorol. 127(1–2): 35–51. doi: 10.1016/j.agrformet.2004.08.002.

Monteith, J.L. 1977. Climate and Efficiency of Crop Production in Britain. Phil. Trans. R. Soc. Lond. 281(980).

Monteith, J.L. 1986. How do crops manipulate water supply and demand ? Phil. Trans. R. Soc. Lond. 316: 245–259.

Mu, Q., M. Zhao, and S.W. Running. 2011. Improvements to a MODIS global terrestrial evapotranspiration algorithm. Remote Sens. Environ. 115(8): 1781–1800. doi: 10.1016/j.rse.2011.02.019.

Mubeen, M., A. Ahmad, T. Khaliqu, and A. Bakhsh. 2013. Evaluating CSM-

CERESMaize model for irrigation scheduling in semi-arid conditions of Punjab, Pakistan. Int. J. Agric. Biol. 15(1): 1–10.

Murty, D., M.U.F. Kirschbaum, R.E. Mcmurtrie, and H. Mcgilvray. 2002. Does conversion of forest to agricultural land change soil carbon and nitrogen? A review of the literature. Glob. Chang. Biol. 8(2): 105–123. doi: 10.1046/j.1354-1013.2001.00459.x.

Myneni, R.B., R.R. Nemani, and S.W. Running. 1997. Estimation of global leaf area index and absorbed par using radiative transfer models. IEEE Trans. Geosci. Remote Sens. 35(6): 1380–1393.

National Oceanic and Atmospheric Administration. 2011. Climate Data Online. Natl. Centers Environ. Inf.

Oki, T., and K. Shinjiro. 2006. Global Hydrological Cycles and World Water Resources. Science (80-.). 313(August): 1068–1073.

Pace, P.F., H.T. Cralle, S.H.M. El-Halawany, J.T. Cothren, and S.A. Senseman. 1999. Drought-induced Changes in Shoot and Root Growth of Young Cotton Plants. J. Cotton Sci. 3(183–187).

Padilla, F.L.M., S.J. Maas, M.P. Gonzalez-Dugo, N. Rajan, F. Mansilla, P. Gavilan, and J. Dominguez. 2012. Wheat Yield Monitoring in Southern Spain Using the GRAMI Model and a Series of Satellite Images. F. Crop. Res. 139(29): 145–145.

Pathak, T.B., J.W. Jones, C.W. Fraisse, D. Wright, and G. Hoogenboom. 2012.

Uncertainty analysis and parameter estimation for the CSM-CROPGRO-cotton model. Agron. J. 104(5): 1363–1373. doi: 10.2134/agronj2011.0349.

Patil, N.G., and G.S. Rajput. 2009. Evaluation of Water Retention Functions and Computer Program “Rosetta” in Predicting Soil Water Characteristics of Seasonally Impounded Shrink-Swell Soils. J. Irrig. Drain. Eng. 135(3): 286–294.

Paw, K.T., D.D. Baldocchi, T.P. Meyers, and K.B. Wilson. 2000. Correction of Eddy-Covariance Measurements Incorporating Both Advective Effects and Density Fluxes. Boundary-Layer Meteorol. (47): 487–511.

Pegelow, E.J., D.R. Buxton, R.E. Briggs, H. Muramoto, and W.G. Gensler. 1977. Canopy Photosynthesis and Transpiration of Cotton as Affected by Leaf Type. Crop Sci. 17(1): 1–4.

Peng, Y., and A.A. Gitelson. 2011. Application of chlorophyll-related vegetation indices for remote estimation of maize productivity. Agric. For. Meteorol. 151(9): 1267–1276.

Peng, Y., and A.A. Gitelson. 2012. Remote estimation of gross primary productivity in soybean and maize based on total crop chlorophyll content. Remote Sens. Environ. 117: 440–448. doi: 10.1016/j.rse.2011.10.021.

Peng, Y., A.A. Gitelson, G. Keydan, D.C. Rundquist, and W. Moses. 2011. Remote estimation of gross primary production in maize and support for a new paradigm based on total crop chlorophyll content. Remote Sens. Environ. 115(4): 978–989.

Pettigrew, W.T. 2004. Physiological Consequences of Moisture Deficit Stress in Cotton. Crop Sci. 44(4): 1265–1272.

PhytoGen. 2019. PhytoGen Cotton Varieties. Corteva Agriscience. https://phytogencottonseed.com/varieties.

Planet Team. 2017. Planet Application Program Interface: In Space for Life on Earth. San Francisco, CA.

Planet Team. 2018. No Title. Planet Inc.

Priestly, C.H.B., and R.J. Taylor. 1972. On the Assessment of Surface Heat Flux and Evaporation Using Large-Scale Parameters. Mon. Weather Rev. 100(February): 81–92.

Qin, S., S. Li, S. Kang, T. Du, L. Tong, and R. Ding. 2016. Can the drip irrigation under film mulch reduce crop evapotranspiration and save water under the sufficient irrigation condition? Agric. Water Manag. 177: 128–137. doi: 10.1016/j.agwat.2016.06.022.

Rajan, N., S.J. Maas, and S. Cui. 2013a. Extreme Drought Effects on Carbon Dynamics of a Semi Arid Pasture. Crop Ecol. Physiol. 105(6): 1749–1760.

Rajan, N., S.J. Maas, and S. Cui. 2013b. Extreme Drought Effects on Carbon Dynamics of a Semi-arid Pasture. 2013 105(6): 1749–1760.

Ramankutty, N., A.T. Evan, C. Monfreda, and J.A. Foley. 2008. Farming the planet : 1 . Geographic distribution of global agricultural lands in the year 2000. 22(February

2007): 1–19. doi: 10.1029/2007GB002952.

Raper, T.B., J.J. Varco, and K.J. Hubbard. 2013. Canopy-Based Normalized Difference Vegetation Index Sensors for Monitoring Cotton Nitrogen Status. Agron. J. 105(5): 1345–1354.

Reichstein, M., E. Falge, D. Baldocchi, D. Papale, M. Aubinet, P. Berbigier, C. Bernhofer, N. Buchmann, T. Gilmanov, A. Granier, T. Grunwald, K. Havrankova, H. Ilvesniemi, D. Janous, A. Knohl, T. Laurila, A. Lohila, D. Loustau, G. Matteucci, T. Meyers, F. Miglietta, J.-M. Ourcival, J. Pumpanen, S. Rambal, E. Rotenberg, M. Sanz, J. Tenhunen, G. Seufert, F. Vaccari, T. Vesala, D. Yakir, and R. Valentini. 2005. On the separation of net ecosystem exchange into assimilation and ecosystem respiration : review and improved algorithm. Glob. Chang. Biol. (11): 1424–1439. doi: 10.1111/j.1365-2486.2005.001002.x.

Ringrose-Voase, A.J., and A.J. Nadelko. 2013. Deep drainage in a Grey Vertosol under furrow-irrigated cotton. Crop Pasture Sci. 64(12): 1155–1170.

Ritchie, J.T. 1972. Model for Predicting Evaporation from a Row Crop with Incomplete Cover. Water Resour. Res. 8(5): 1204–1213.

Ritchie, J.T. 1998. Soil water balance and plant stress. p. 41–54. *In* Tsuji, G.Y., Hoogenboom, G., Thornton, P.K. (eds.), Understanding options for agricultural production. System approaches for sustainable agricultural development. Kluwer Academic Publishers, Dordrecht, Netherlands.

Ritchie, G.L., C.W. Bednarz, P.H. Jost, and S.M. Brown. 2007. Cotton Growth and Development.

Ritchie, J.T., and S. Otter. 1985. Description and performance of CERES-Wheat: A User-oriented wheat yield model. ARS Wheat Yield Proj. 38: 159–175.

Ritchie, J.T., C.H. Porter, J. Judge, J.W. Jones, and A.A. Suleiman. 2009. Extension of an Existing Model for Soil Water Evaporation and Redistribution under High Water Content Conditions. Soil Sci. Soc. Am. J. 73(3): 792. doi: 10.2136/sssaj2007.0325.

Ritchie, G.L., D.G. Sullivan, W.K. Vencill, C.W. Bednarz, and J.E. Hook. 2010. Sensitivities of Normalized Difference Vegetation Index and a Green/Red Ratio Index to Cotton Ground Cover Fraction. Crop Sci. 50(3): 1000–1010.

Rodell, M., H.K. Beaudoing, T.S. L'Ecuyer, W.S. Olson, J.S. Famiglietti, P.R. Houser, R. Adler, M.G. Bosilovich, C.A. Clayson, D. Chambers, E. Clark, E.J. Fetzer, X. Gao, G. Gu, K. Hilburn, G.J. Huffman, D.P. Lettenmair, W.T. Liu, F.R. Robertson, C.A. Schlosser, J. Sheffield, and E.F. Wood. 2015. The Observed State of the Water Cycle in the Early Twenty-First Century. J. Clim. 28(November): 8289–8318. doi: 10.1175/JCLI-D-14-00555.1.

Rost, S., D. Gerten, A. Bondeau, W. Lucht, and J. Rohwer. 2008. Agricultural green and blue water consumption and its influence on the global water system. Water Resour. Res. 44: 1–17. doi: 10.1029/2007WR006331.

Saigusa, N., S. Yamamoto, S. Murayama, H. Kondo, and N. Nishimura. 2002. Gross

primary production and net ecosystem exchange of a cool-temperate deciduous forest estimated by the eddy covariance method. Agric. For. Meteorol. 112: 203–215.

Sakamoto, T., A.A. Gitelson, B.D. Wardlow, S.B. Verma, and A.E. Suyker. 2011. Estimating daily gross primary production of maize based only on MODIS WDRVI and shortwave radiation data. Remote Sens. Environ. 115(12): 3091–3101.

Saseendran, S.A., L. Ma, D.C. Nielsen, M.F. Vigil, and L.R. Ahuju. 2005. imulating planting date effects on corn production using RZWQM and CERES-Maize models. Agron. J. 97(1): 58–71.

Sau, F., K.J. Boote, M. Bostick, J.W. Jones, and M.I. Minguez. 2004. Testing and Improving Evapotranspiration and Soil Water Balance of the DSSAT Crop Models. Agron. J. 96(September): 1243–1257.

Schindler, D.W. 1999. The mysterious missing sink. Nature 398: 105–107.

Seligman, N.C., and H. Van Keulen. 1981. PAPRAN: a simulation model of annual pasture production limited by rainfall and nitrogen. p. 192–221. *In* Frissel, M.J., Van Veen, J.A. (eds.), Simulation of nitrogen behavior of soil-plant systems. Centrum voor Landbouwpublikaties en Landbouwdocumentatie, Wageningen, Netherlands.

Shafian, S., N. Rajan, R. Schnell, M. Bagavathiannan, J. Valasek, Y. Shi, and J. Olsenholler. 2018. Unmanned Aerial Systems-Based Remote Sensing for

Monitoring Sorghum Growth and Development. PLoS One 13(5).

Sharma, S., N. Rajan, S. Cui, K. Casey, S. Ale, R. Jessup, and S. Maas. 2017. Seasonal variability of evapotranspiration and carbon exchanges over a biomass sorghum field in the Southern U.S. Great Plains. Biomass and Bioenergy 105: 392–401.

Shelton, M.L. 1987. Irrigation induced change in vegetation and evapotranspiration in the Central Valley of California. Landsc. Ecol. 1(2): 95–105.

Sinclair, T.R., and R.C. Muchow. 2001. System Analysis of Plant Traits to Increase Grain Yield on Limited Water Supplies. 93(2): 263–270.

Skinner, H.R. 2007. High Biomass Removal Limits Carbon Sequestration Potential of Mature Temperate Pastures. J. Environ. Qual. 37(4): 1319–1326.

Smith, P., M. Bustamante, H. Ahammad, H. Clark, H. Dong, E.A. Elsiddi, H. Haberl, R. Harper, J. House, M. Jafari, O. Masera, C. Mbow, N.H. Ravindranath, C.W. Rice, C.R. Abad, A. Romanovskaya, F. Sperling, and F. Tubiello. 2014. Agriculture, forestry and other land use.

Snowden, M.C., G.L. Ritchie, F.R. Simao, and J.P. Bordovsky. 2014. Timing of Episodic Drought Can Be Critical in Cotton. Agron. J. 106(2): 452–458.

Soldevilla-Martinez, M., M. Quemada, R. Lopez-Urrea, R. Munoz-Carpena, and J.I. Lizaso. 2014. Soil water balance: Comparing two simulation models of different levels of complexity with lysimeter observations. Agric. Water Manag. 139(June): 53–63.

Soler, C.M.T., P.C. Sentelhas, and G. Hoogenboom. 2007. Application of the CSM-CERES-Maize model for planting date evaluation and yield forecasting for maize grown off-season in a subtropical environment. Eur. J. Agron. 27(2–4): 165–177. doi: 10.1016/j.eja.2007.03.002.

Sonnentag, O., M. Detto, R. Vargas, Y. Ryu, B.R.K. Runkle, M. Kelly, and D.D. Baldocchi. 2011. Agricultural and Forest Meteorology Tracking the structural and functional development of a perennial pepperweed (Lepidium latifolium L .) infestation using a multi-year archive of webcam imagery and eddy covariance measurements. Agric. For. Meteorol. 151(7): 916–926. doi: 10.1016/j.agrformet.2011.02.011.

Spera, S.A., G.L. Galford, and M.T. Coe. 2016. Land-use change affects water recycling in Brazil ' s last agricultural frontier. Glob. Chang. Biol. 22: 3405–3413. doi: 10.1111/gcb.13298.

Suleiman, A.A., and G. Hoogenboom. 2007. Comparison of Priestley–Taylor and FAO-56 Penman–Monteith for daily reference evapotranspiration estimation in Georgia, USA. J. Irrig. Drain. Eng. 133(2).

Suleiman, A.A., and J.T. Ritchie. 2003. Modeling Soil Water Redistribution during Second-Stage Evaporation. Soil Sci. Soc. Am. J. 67(2): 377–386. doi: 10.2136/sssaj2003.0377.

Suleiman, A.A., C.M.T. Soler, and G. Hoogenboom. 2007. Evaluation of FAO-56 crop coefficient procedures for deficit irrigation management of cotton in a humid

climate. Agric. Water Manag. 91(1): 33–42.

Suyker, A.E., S.B. Verma, G.G. Burba, T.J. Arkebauer, D.T. Walters, and K.G. Hubbard. 2004a. Growing season carbon dioxide exchange in irrigated and rainfed maize. Agric. For. Meteorol. 124(1–2): 1–13. doi: 10.1016/j.agrformet.2004.01.011.

Suyker, A.E., S.B. Verma, G.G. Burba, T.J. Arkebauer, D.T. Walters, and K.G. Hubbard. 2004b. Growing season carbon dioxide exchange in irrigated and rainfed maize. Agric. For. Meteorol. 124(1): 1–13.

Texas A&M Agrilife. 2019. Cotton Production Regions of Texas. Cott. Insect Manag. Guid.

Texas Parks and Wildlife. 2019. Post Oak Savannah and Blackland Prairie Wildlife Management. Habitats.

Thorp, K.R., E.M. Barnes, D.J. Hunsaker, and B.A. Kimball. 2014. Evaluation of CSM-CROPGRO-Cotton for Simulating Effects of Management and Climate Change on Cotton Growth and Evapotranspiration In An Arid Environment. Trans. ASABE 57(6): 1627–1642.

Thorp, K.R., D.J. Hunsaker, A.N. French, E. Bautista, and K.F. Bronson. 2015. Integrating geospatial data and cropping system simulation within a geographic information system to analyze spatial seed cotton yield, water use, and irrigation requirements. Precis. Agric. 16(5): 532–557.

Tian, H., G. Chen, M. Liu, C. Zhang, G. Sun, C. Lu, X. Xu, W. Ren, S. Pan, and A. Chappelka. 2010. Model estimates of net primary productivity, evapotranspiration, and water use efficiency in the terrestrial ecosystems of the southern United States during 1895-2007. For. Ecol. Manage. 259(7): 1311–1327. doi: 10.1016/j.foreco.2009.10.009.

Tscharntke, T., A.M. Klein, A. Kruess, I. Steffan-Dewenter, and C. Thies. 2005. Landscape perspectives on agricultural intensification and biodiversity - Ecosystem service management. Ecol. Lett. 8(8): 857–874. doi: 10.1111/j.1461-0248.2005.00782.x.

Tubiello, F.N., M. Salvatore, R.D. Cóndor Golec, A. Ferrara, S. Rossi, R. Biancalani, S. Federici, H. Jacobs, and A. Flammini. 2014. Agriculture, Forestry and Other Land Use Emissions by Sources and Removals by Sinks. ESS Work. Pap. No.2 2: 4–89. doi: 10.13140/2.1.4143.4245.

Twine, T.E., W.P. Kustas, J.M. Norman, D.R. Cook, P.R. Houser, and T.P. Meyers. 2000. Correcting eddy-covariance flux underestimates over a grassland. Agric. For. Meteorol. 103: 279–300.

Uddin, J., R.J. Smith, N.H. Hancock, and J.P. Foley. 2013. Evaporation and sapflow dynamics during sprinkler irrigation of cotton. Agric. Water Manag. 125: 35–45. doi: 10.1016/j.agwat.2013.04.001.

USDA-NASS. 2017. 2017 Census of Agriculture County Profile: Burleson County Texas.

Verlag, F., A.A. Gitelson, Y. Gritz, and M.N. Merzlyak. 2003. Relationships between leaf chlorophyll content and spectral reflectance and algorithms for non-destructive chlorophyll assessment in higher plant leaves. J. Plant Physiol. 160(3): 271–282.

Verma, S.B., A. Dobermann, K.G. Cassman, D.T. Walters, J.M. Knops, T.J. Arkebauer, A.E. Suyker, G.G. Burba, B. Amos, H. Yang, D. Ginting, K.G. Hubbard, A.A. Gitelson, and E.A. Walter-Shea. 2005. Annual carbon dioxide exchange in irrigated and rainfed maize-based agroecosystems. Agric. For. Meteorol. 131(1–2): 77–96. doi: 10.1016/j.agrformet.2005.05.003.

Vitale, L., P. Di Tommasi, G. D'Urso, and V. Magliulo. 2016. The response of ecosystem carbon fluxes to LAI and environmental drivers in a maize crop grown in two contrasting seasons. Int. J. Biometeorol. 60(3): 411–420. doi: 10.1007/s00484-015-1038-2.

Wang, Y., C.E. Woodcock, W. Buermann, P. Stenberg, P. Voipio, H. Smolander, T. Hame, Y. Tian, H. Jiannan, Y. Knyazikhin, and R.B. Myneni. 2004. Evaluation of the MODIS LAI algorithm at a coniferous forest site in Finland. Remote Sens. Environ. 91(1): 114–127.

Wang, C., Z. Zhang, S. Fan, R. Mwiya, and M. Xie. 2018. Effects of straw incorporation on desiccation cracking patterns and horizontal flow in cracked clay loam. Soil Tillage Res. 182: 130–143.

Webb, E.K., G.I. Pearman, and R. Leuning. 1980. Correction of flux measurements for density effects due to heat and water vapour transfer. Q. J. R. Meteorol. Soc.

106(447): 85–100.

West, T.O., and W.M. Post. 2002. Soil Organic Carbon Sequestration Rates by Tillage and Crop Rotation : A Global Data Analysis. Soil Sci. Soc. Am. J. 66(6): 1930–1946. doi: 10.2136/sssaj2002.1930.

Wharton, S., M. Falk, K. Bible, M. Schroeder, and K.T.U. Paw. 2012. Old-growth CO2 flux measurements reveal high sensitivity to climate anomalies across seasonal, annual and decadal time scales. Agric. For. Meteorol. 161: 1–14. doi: 10.1016/j.agrformet.2012.03.007.

Wilson, K., A. Goldstein, E. Falge, M. Aubinet, D. Baldocchi, P. Berbigier, C. Bernhofer, R. Ceulemans, H. Dolman, C. Field, A. Grelle, A. Ibrom, B.E. Law, A. Kowalski, T. Meyers, J. Moncrieff, R. Monson, W. Oechel, J. Tenhunen, R. Valentini, and S. Verma. 2002. Energy balance closure at FLUXNET sites. Agric. For. Meteorol. 113: 223–243.

Woodbury, P.B., L.S. Heath, and J.E. Smith. 2006. Land Use Change Effects on Forest Carbon Cycling Throughout the Southern United States. J. Environ. Qual. 35(4): 1348. doi: 10.2134/jeq2005.0148.

Wu, H., X. Wang, M. Xu, and J. Zhang. 2018. The Effect of Water Deficit and Waterlogging on the Yield Components of Cotton. Crop Sci. 58(4): 1751–1761.

Xevi, E., J. Gilley, and J. Feyen. 1996. Comparative study of two crop yield simulation models. Agric. Water Manag. 30(2): 155–173.

Xiao, J., G. Sun, J. Chen, H. Chen, S. Chen, G. Dong, S. Gao, H. Guo, J. Guo, S. Han, T. Kato, Y. Li, G. Lin, L. Weizhi, M. Ma, S. McNulty, C. Shao, X. Wang, and J. Zhou. 2013. Carbon fluxes, evapotranspiration, and water use efficiency of terrestrial ecosystems in China. Agric. For. Meteorol. 182(12): 76–90.

Xu, C.Y., and D. Chen. 2005. Comparison of seven models for estimation of evapotranspiration and groundwater recharge using lysimeter measurement data in Germany. Hydrol. Process. 19(18): 3717–3734. doi: 10.1002/hyp.5853.

Yan, H., Y. Fu, X. Xiao, H.Q. Huang, H. He, and L. Ediger. 2009. Modeling gross primary productivity for winter wheat-maize double cropping system using MODIS time series and CO2eddy flux tower data. Agric. Ecosyst. Environ. 129(4): 391–400. doi: 10.1016/j.agee.2008.10.017.

Yoder, B.J., and R.E. Pettigrew-Crosby. 1995. Predicting nitrogen and chlorophyll content and concentration for reflectance spectra (400 - 2500 nm) at leaf and canopy scales. Remote Sens. Environ. 53(September 1994): 199–211.

Yuan, W., S. Liu, G. Yu, J.M. Bonnefond, J. Chen, K. Davis, A.R. Desai, A.H. Goldstein, D. Gianelle, F. Rossi, A.E. Suyker, and S.B. Verma. 2010. Global estimates of evapotranspiration and gross primary production based on MODIS and global meteorology data. Remote Sens. Environ. 114(7): 1416–1431. doi: 10.1016/j.rse.2010.01.022.

Yu, G., X. Wen, X. Sun, B.D. Tanner, X. Lee, and J. Chen. 2006. Overview of ChinaFLUX and evaluation of its eddy covariance measurement. Agric. For.

Meteorol. 137: 125–137. doi: 10.1016/j.agrformet.2006.02.011.

Zapata, D., N. Rajan, and F. Hons. 2017. Does high soil moisture in no-till systems increase CO2 emissions and reduce carbon sequestration? Tampa, FL.

Zapata, D., N. Rajan, J. Mowrer, K. Casey, R. Schnell, and F. Hons. 2019. Impact of Long-Term Tillage on Soil CO2 Emissions and Soil Carbon Sequestration in Monoculture and Rotational Cropping Systems. Soil Tillage Res.

Zhao, M., F.A. Heinsch, R.R. Nemani, and S.W. Running. 2005. Improvements of the MODIS terrestrial gross and net primary production global data set. Remote Sens. Environ. 95(2): 164–176. doi: 10.1016/j.rse.2004.12.011.

Zheng, Y., L. Zhang, J. Xiao, W. Yuan, M. Yan, and T. Li. 2018. Sources of uncertainty in gross primary productivity simulated by light use efficiency models: Model structure, parameters, input data, and spatial resolution. Agric. For. Meteorol. 263(December 2017): 242–257. doi: 10.1016/j.agrformet.2018.08.003.

Zhou, Y., X. Xiao, P. Wagle, R. Bajgain, H. Mahan, J.B. Basara, J. Dong, Y. Qin, G. Zhang, Y. Luo, P.H. Gowda, J.P.S. Neel, P.J. Starks, and J.L. Steiner. 2017. Examining the short-term impacts of diverse management practices on plant phenology and carbon fluxes of Old World bluestems pasture. Agric. For. Meteorol. 237–238: 60–70. doi: 10.1016/j.agrformet.2017.01.018.

2. CARBON EXCHANGE OF A DRYLAND COTTON FIELD AND ITS RELATIONSHIP WITH PLANETSCOPE REMOTE SENSING DATA

2.1. Introduction

Understanding the dynamics of carbon sequestration and release in agricultural landscapes is pivotal as modern production practices have contributed substantially to rising greenhouse gas (GHG) emissions around the globe. The magnitude of carbon sequestration or release at a site depends upon a number of factors, including vegetation type, tillage practices, and meteorological conditions. The type of vegetation and its net primary production (NPP) can determine the amount of atmospheric carbon that can be converted into biomass carbon (Cao and Woodward, 1998; Prince et al., 2019). For perennial plant communities, such as forests, large amounts of carbon can be temporarily sequestered in standing plant biomass. This is not effective for agronomic cropping systems because the lifespan of the plants is short and significant amounts of aboveground biomass are removed during harvest. The remaining crop biomass is usually incorporated into the soil via tillage. Once in the soil, environmental factors such as temperature and soil moisture can have a large impact on the rates of decay and transformation of biomass carbon through regulation of microbial respiration (Davidson and Janssens, 2006; Valentini et al., 2019; Zapata et al., 2017). Tillage practices and soil disturbance increases the rate of soil respiration, which, when coupled with biomass removal via harvest leads to the decline in soil carbon stocks.

Measuring carbon fluxes from agricultural fields and estimating the seasonal and annual carbon budgets can provide important clues regarding how management practices are affecting crop development, carbon uptake, and release. After harvest, many producers in the southern U.S. states leave their fields fallow, leading to the growth of weeds, which can influence the off-season carbon dynamics. Collins et al (1999) studied carbon inputs from all sources, including weeds, at eight long-term continuous corn sites in the Great Lakes, central, and the south-central U.S. and found that weeds accounted for 20% of soil carbon inputs (Collins et al., 1999). Ibell et al (2010) found that complete weed removal (via high-frequency herbicide applications) in a pine plantation reduced soil carbon accumulation and negatively impacted nitrogen cycling. Further, eddy covariance (EC) measurement of a pepperweed (Lepidium latifolium) infestation in grass pasture found that weeds were a significant source of carbon flux (Sonnentag et al., 2011). Given that weeds can be an important part of carbon flux in crop fields, off-season measurements should be included for fully understanding the carbon dynamics of agricultural lands.

Eddy covariance is a commonly used micrometeorological method for measuring gas fluxes, particularly CO_2, water vapor, and methane. Eddy covariance has been widely used around the world for studying ecosystem carbon and water dynamics (Baldocchi, 2003; Dolman et al., 2006; Saigusa et al., 2002; Yu et al., 2006; Rajan et al., 2010). However, EC measurements from agricultural lands in the southern U.S. states are rare. Net ecosystem exchange (NEE) measured using this method is the balance between CO_2 uptake via photosynthesis (gross primary production or GPP) and CO_2

release via ecosystem respiration (R_{eco}). Both heterotrophic soil respiration (i.e. soil microorganisms) and autotrophic respiration (i.e. plant roots) are components of R_{eco}. Since daily NEE represents the balance between carbon uptake and release, it can effectively be used to study the source-sink dynamics of an ecosystem and its variation across both short-term and long-term time scales (Rajan et al., 2013; Wharton et al., 2012). Although this technique is one of the most accurate and direct methods for measuring turbulent fluxes, EC instruments are expensive, often limiting the number of locations that can be monitored. This method also assumes that the area within the instrument fetch is uniform and atmospheric conditions are stable, which requires large areas with uniform vegetation and minimal to no slope (Baldocchi, 2003; Burba, 2013).

The use of remote sensing technology can help alleviate some of the limitations of the eddy covariance method for estimating NEE and GPP. Combining EC with remote sensing can allow carbon dynamics to be upscaled from a single field to multiple fields in the landscape. Actively photosynthesizing plants strongly absorb red and blue lights and reflect near-infrared light, which can be measured using satellite, air, and ground-based remote sensing instruments (Asrar et al., 1984; Baret and Guyot, 1991; Yoder and Pettigrew-Crosby, 1995). This assessment of photosynthetic activity can help with estimating carbon fluxes in areas where EC measurements are impractical and over areas too large for EC measurements (Frankenberg et al., 2011; Yuan et al., 2010; Zhou et al., 2017). Advances in imaging and satellite technology have made high-resolution satellite data more readily available from both public and private sources. The recently launched PlanetScope satellite system is a network of 120 high-resolution Dove satellites

(spatial resolution of 3 meters) owned and managed by Planet Labs Inc. PlanetScope satellites take daily multi-spectral images from a 400 km sun-synchronous orbit (Planet Team, 2017). The use of high-resolution satellite data has the potential to expand the applications of remote sensing in agriculture. Currently, the majority of the large-scale agricultural remote sensing applications use low and medium-resolution satellite data, such as LANDSAT (30-meter) and MODIS (250-meter) (Chen et al., 2018; Cui et al., 2014; Padilla et al., 2012).

In this study, we investigated the effect of weeds and off-season fluxes on the annual carbon budget of conventionally managed cotton (Gossypium hirsutum), a major crop in South Central Texas. We examined the environmental and phenological driving factors of daily, seasonal and annual carbon fluxes. We also investigated the correlation between vegetation indices estimated from high-resolution PlanetScope satellite data and carbon fluxes measured using eddy covariance for broader scale applications.

2.2. Materials and Methods

2.2.1. Site Information

The study was conducted in a 12 ha conventionally managed dryland continuous cotton field located at the Texas A&M Agrilife Research Farm in Burleson County, Texas (30°32’46.2” N, 96°25’19.7” W), which is shown in Figure 2. An eddy covariance flux tower was established in this field on 28 February 2017 (DOY 59). Meteorological data prior to tower establishment was obtained from a weather station located at the Texas A&M Agrilife Research Farm (Conlee, 2019). Cotton (cultivar Phytogen 333WRF) was planted on 6 April (DOY 96) in 2017 and 18 April (DOY 108) in 2018

following conventional tillage in raised seedbeds. Nitrogen fertilizer was applied after planting at a rate of 95 kg ha^{-1} of N as urea ammonium nitrate (32-0-0). Glyphosate was applied for weed control after fertilization. The average plant population was 6.24 plants m^{-2} in 2017 and 6.22 plants m^{-2} in 2018. Cotton was harvested on 11 September in 2017 (DOY 254) and 17 September in 2018 (DOY 260) following defoliation. In cotton production, the plants are chemically defoliated to allow for easier harvest. The cotton crop was sprayed with Ginstar (Bayer CropScience, Monheim, Germany), a mixture of Thidiazuron and Diuron, which blocked photosynthesis. The cotton crop was defoliated on Aug 21 (DOY 233) in both years.

The dominant soil types in the field are the Weswood silt loam (Udifluventic Haplustepts, 38% clay in the surface horizon) and the Ships clay (Chromic Halpludert, 42% clay in the surface horizon), both of which are high in shrink-swell clay minerals. The climate of the location is humid subtropical (Köppen Cfa) with an average (30-year) annual temperature of 20.6°C and an average annual precipitation of 1018 mm (Zapata et al., 2019). Monthly 30-year averages for precipitation and temperature are shown in Figure 1. Summer months (June-September) regularly have temperatures above 35°C with a mild winter having only occasional freezing events. Precipitation follows a bimodal pattern with the highest precipitation in the months of May, June, and October (National Oceanic and Atmospheric Administration, 2011). Prominent weeds in this location include henbit (*Lamium amplexicaule*), morning glory (*Ipomoea cordatotriloba*), Palmer amaranth (*Amaranthus palmeri*), and grasses like Texas panicum (*Uruchloa texana*).

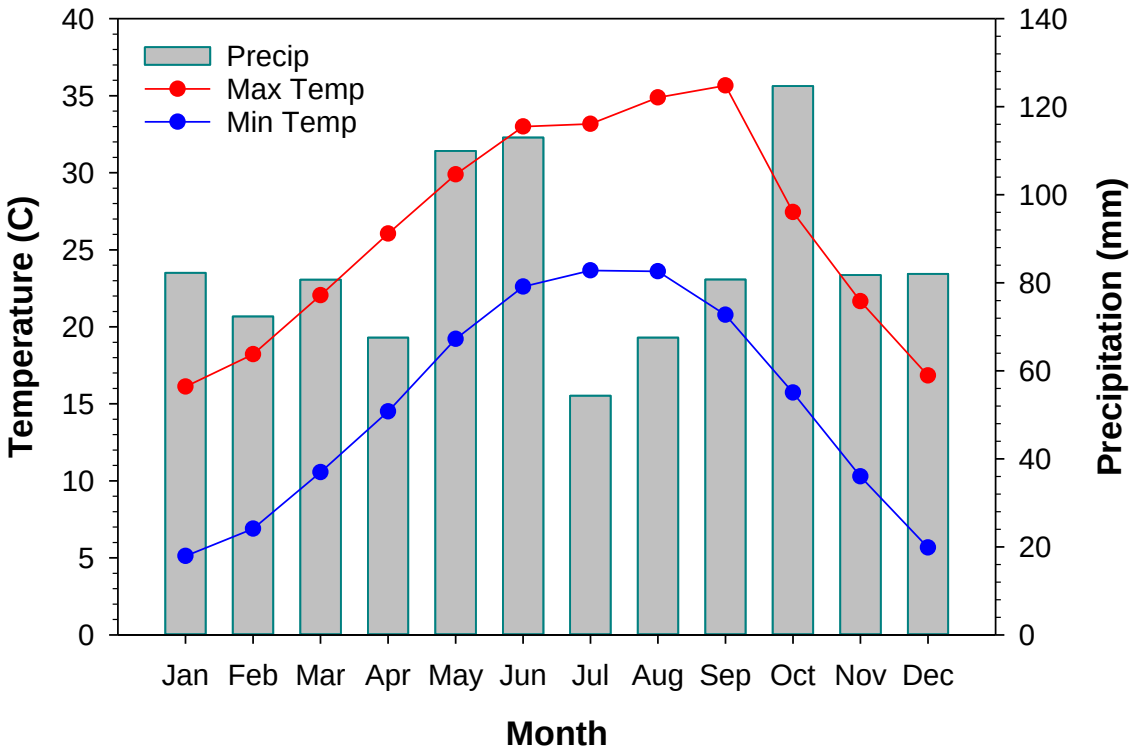

Figure 1: Monthly temperature and precipitation averages for Burleson County, Texas.

Data was obtained from the National Oceanic and Atmospheric Administration's current 30-year average (1981 – 210) from their weather station approximately 11-km from the study location. Precipitation has a bimodal average pattern with higher precipitation in fall and spring and lower precipitation in summer and winter. While average low temperatures do not drop below freezing, there are occasional freezing events, typically from November to February.

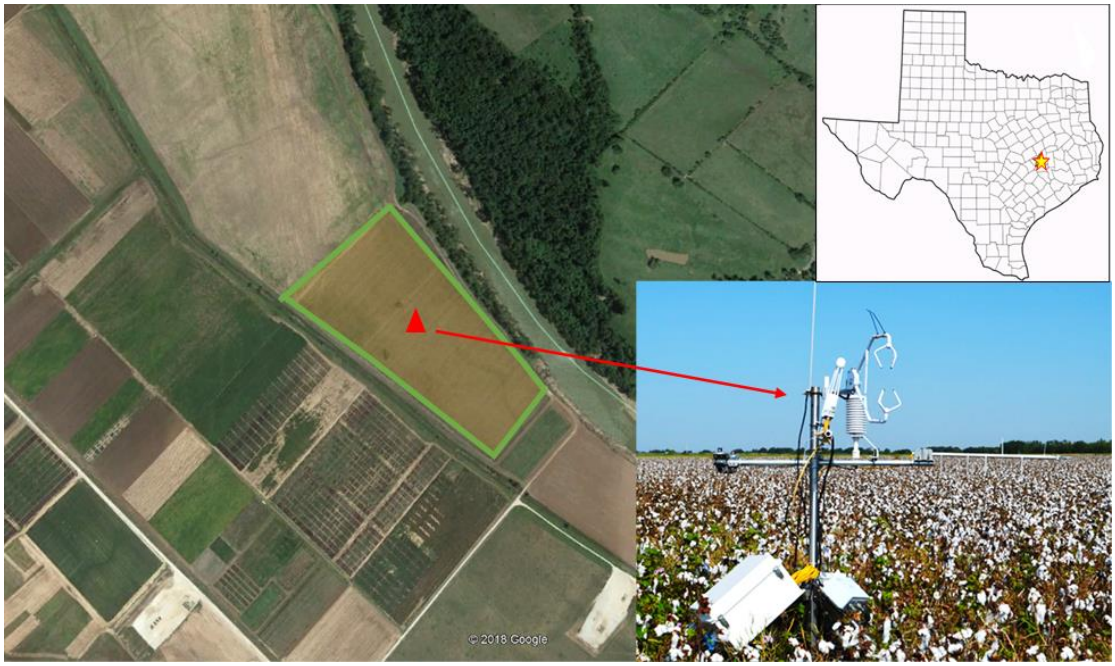

Figure 2: Image of the study site and location.
The image on the left is a Google Earth image of the study location with the green line highlighting the cotton field and the red triangle showing the location of the eddy covariance tower within the field. The blue line is the Brazos River. The upper right image is the location of the site within Texas, indicated by the red star. The image on the lower right is an image of the eddy covariance instrumentation (Google Earth, 2018).

2.2.2. Instrumentation

Carbon dioxide flux measurements were made continuously using an eddy covariance system at high frequency (10 Hz). The EC system consisted of a C-SAT3 Sonic Anemometer (Campbell Scientific, Logan, UT, USA) and an LI-7500 infrared gas analyzer (LI-COR, Lincoln, NE, USA). Both instruments were attached to a tripod and the height of the tripod mast was adjusted periodically to maintain the instruments at 2 m

above the plant canopy and thus maintain a constant fetch with a 200-meter radius. The instruments were installed facing south, in the direction of the prevailing winds. The gas analyzer was calibrated annually as recommended by the manufacturer and the internal chemicals were replaced annually.

Additional meteorological data was collected at the same location. Air temperature (T_{air}) and relative humidity (RH) were collected with a temperature and relative humidity probe (Model HMP155A; Vaisala, Vantaa, Finland). Precipitation was collected using a tipping bucket rain gauge (Model TE525; Texas Electronics, Dallas, TX, USA). Photosynthetically active radiation (PAR) was measured using a quantum sensor (Model LI-190R; LI-COR, Lincoln, NE, USA). Solar irradiance (Rs) was measured using a pyranometer (Model LI-200R; LI-COR, Lincoln, NE, USA) and net radiation (Rn) was measured using a net radiometer (Model NR-LITE2; Kipp and Zonen, Delft, The Netherlands). There was a gap in the Rn data during the late growing season of 2017 due to an instrument malfunction. Soil volumetric water content (VWC) and soil temperature (T_{soil}) was collected using seven soil moisture sensors (Model CS655; Campbell Scientific, Logan, UT, USA). Of the seven soil moisture sensors, three were placed horizontally at a depth of 4 cm; two were placed vertically between 10 and 20 cm, and the remaining two were placed vertically between 20 and 30 cm in the soil profile. All meteorological and soil instruments were connected to a Campbell Scientific CR3000 datalogger. Data was collected every 2 seconds and averaged at half-hourly intervals.

2.2.3. Eddy Covariance Data Processing

The sonic anemometer and gas analyzer were connected to LI-COR's SmartFlux system, which used EddyPro software (Version 6.2.2, LI-COR, Lincoln, NE, USA) to process 10 Hz data into 30-minute fluxes. EddyPro performs a number of corrections before computing NEE fluxes. This includes coordinate rotation, frequency response corrections, corrections for air density fluctuations and sensor separation delays (Burba, 2013; Carmelita et al., 2014; Finnigan et al., 2003; LI-COR, 2015; Paw et al., 2000; Qin et al., 2016; Webb et al., 1980). SmartFlux saved 30-minute flux calculations as .csv files onto a USB drive along with raw data (unprocessed) data files. The sign convention used was one where positive numbers indicated fluxes away from the canopy (net emission) and negative numbers indicated fluxes toward the canopy (net sequestration). The EddyPro software flagged NEE data for quality based on internal turbulence tests. High-quality data was marked with a '0', moderate quality with a '1' and low quality with a '2' (Burba, 2013; LI-COR, 2017). Gap filling was used to fill in low-quality data (flag '2') and data lost during rain events, calibration, power issues, and scheduled maintenance (i.e. instrument calibration) as well as manually removed low-quality data. Gap filling was done using the Max Plank Institute for Biogeochemistry's online R-based program using the default settings (Fritz et al., 2018). This program fills data gaps based on an algorithm that uses meteorological data to calculate missing data. If full meteorological data (temperature, humidity, and radiation) is available, then the missing value will be filled using a data point with similar conditions (temperature, humidity,

solar radiation) within a 14-day window of the missing point. If meteorological data is partial or missing, the program will use linear interpolation based on time of day to gap-fill, although this was uncommon (Fritz et al., 2018; Reichstein et al., 2005). The same gap-filling program also separates NEE fluxes into its component fluxes, assimilatory flux (GPP) and respiratory flux (R_{eco}). In the absence of photosynthesis assimilation of CO_2, nighttime NEE data represents ecosystem respiration (Reco). A reference temperature-based method based on nighttime Reco is used to estimate daytime Reco fluxes. The GPP flux is then calculated by subtracting Reco from NEE (GPP = NEE – R_{eco}). The estimates of GPP and R_{eco} are essential for understanding the processes that contribute to NEE (Aubinet et al., 2012; Reichstein et al., 2005).

2.2.4. Phenology

Phenology data was collected at biweekly intervals during the growing season. Plant height was measured at six locations in the field, with three from each soil type; locations were selected to form a circle around the EC tower. Fifteen plants were randomly selected at each location. Height was determined from the soil surface to the top of the apical bud. Leaf area and biomass were determined using destructive sampling (15 plants) at the same locations used for height measurements. Flowers, bolls, leaves, and stems were manually separated for subsequent measurements. Leaf area was measured using an LI-3100 Leaf Area Meter (LI-COR, Lincoln, NE, USA) immediately after destructive harvest. All plant samples were then placed in brown paper bags and dried in an oven at 40℃ until constant weight. Samples were then weighed and dry weight was recorded.

2.2.5. Vegetation Indices

Cloud-free multispectral PlanetScope satellite imagery was downloaded during the growing season. PlanetScope data has a spatial resolution of 3 m and a 16-bit radiometric resolution. Red and near-infrared (NIR) band values were extracted for the study site using ENVI image analysis software (Version 5.3; Harris Geospatial; Broomfield, Colorado, USA). An atmospheric correction was performed manually using the metadata file. Normalized Difference Vegetation Index (NDVI) was then calculated using the corrected band values, NDVI was selected, as it is very commonly used by most agricultural producers. NDV was calculated using the following equation.

$$NDVI = \frac{(NIR - RED)}{(NIR + RED)}$$

Daily NDVI was calculated by interpolating linearly between measurements.

2.2.6. Statistical Analysis

Regression analysis of GPP was performed using Sigmaplot (Version 14.0). GPP was statistically compared to PAR, precipitation, T_{air}, and NDVI using Sigmaplot's curve-fit capabilities.

2.3. Results and Discussion

2.3.1. Meteorological Conditions

Substantial differences in growing season (planting to defoliation; April – August) precipitation was recorded between 2017 and 2018 (Figure 3A). On average, approximately 40% of annual precipitation is generally received during the growing season. In 2017, after cotton defoliation, 590 mm of rainfall was received during a short

span of 4 days (DOY 239-243) from Hurricane Harvey. In 2017, about 30% of the annual average was received during the growing season (510 mm). However, in the 2018 growing season, only 15% of annual precipitation (184 mm) was received. While the growing season of 2018 was mostly dry, the post-harvest season was unusually wet. Nearly 68% of the annual precipitation for 2018 fell after cotton defoliation (848 mm). This heavy precipitation in September and October prevented the usual post-harvest tillage and spurred the growth of weeds in the field.

Precipitation variability between growing seasons influenced soil VWC, vapor pressure deficit (VPD), and T_{soil} (Figures 3A, 3B, and 3D). Average soil VWC at 4 cm during the 2018 growing season (0.19 ± 0.01) was lower than the average soil moisture in the 2017 growing season (0.35 ± 0.01), a similar trend was seen with the other depths. Drier conditions in the 2018 growing season resulted in high VPD compared to 2017. Although precipitation was well below average, 2018 was slightly cooler (19.66 ± 0.44℃) than 2017 (21.92 ± 0.37℃) due to lower temperatures in the winter months (January - February). However, the average growing season T_{air} in 2018 (26.73 ± 0.31℃) was higher than the growing season temperature in 2017 (25.77 ± 0.32℃). Average annual and seasonal T_{soil} at 4 cm followed similar trends. The average annual T_{soil} was 23.63 ± 0.35℃ in 2017 and 21.10 ± 0.44℃ in 2018. Similar to T_{air}, the average growing season T_{soil} in 2017 (27.12 ± 0.30℃) was slightly lower compared to 2018 (28.55 ± 0.30℃). During both growing seasons, there was no significant difference in incoming PAR. However, PAR during the post-harvest period was reduced in 2018 compared to 2017 due to the prevalence of cloudy conditions. There was no significant

difference in Rn during the growing season between 2017 and 2018. However, as with PAR, autumn (September - November), Rn was lower in 2018 compared to 2017.

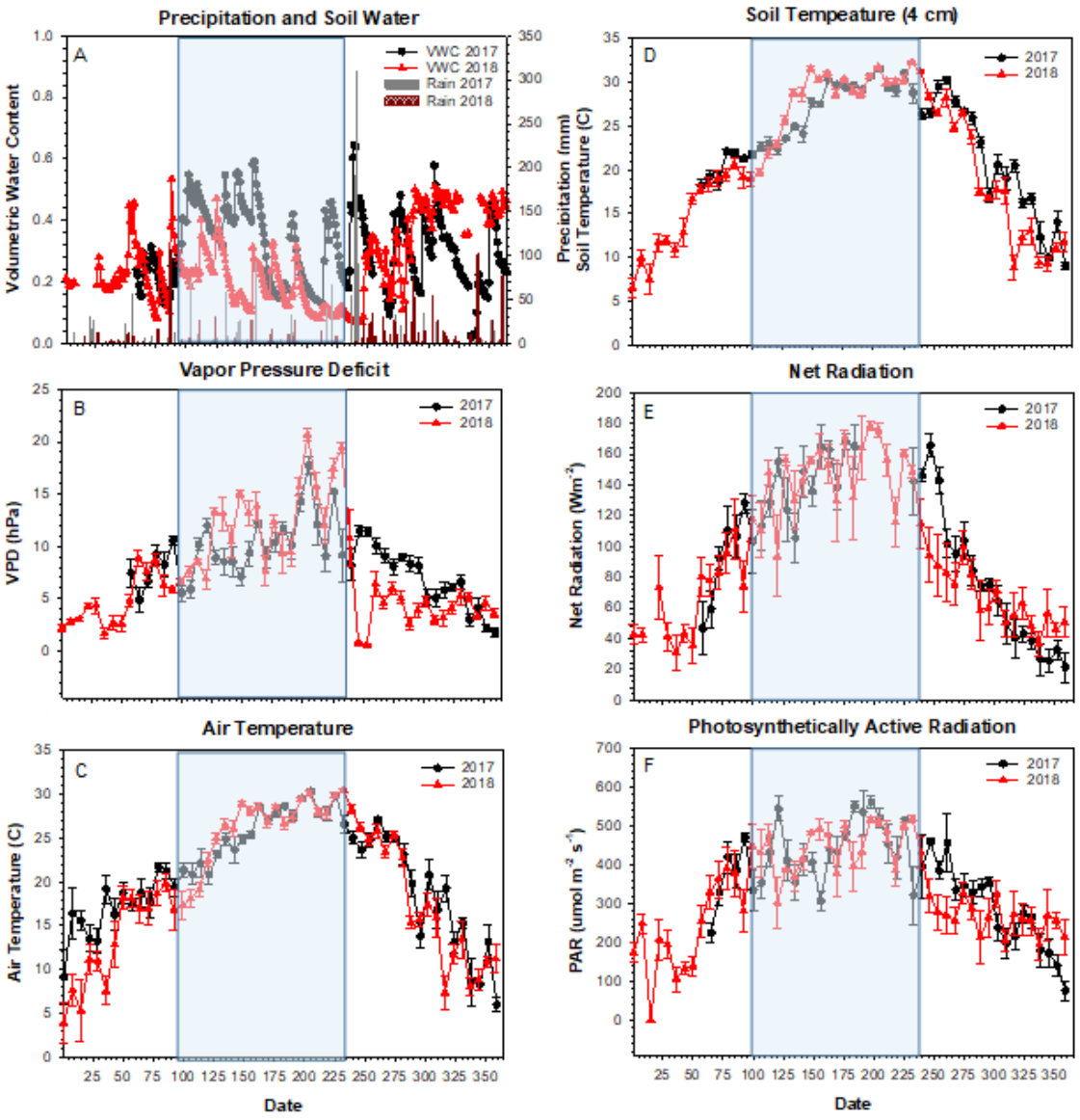

Figure 3: Auxiliary meteorological data for both 2017 and 2018 are presented in this figure.
Black lines refer to 2017 and red lines to 2018. Shaded areas highlight the growing season (planting to defoliation). Image "A" is daily precipitation and soil water content.

Image “B” is weekly average VPD. Images “C” and “D” are weekly averages for T_{air} and T_{soil}, respectively. Images “E” and “F” are weekly averages for Rn and PAR, respectively. Bars represent standard error of the mean.

2.3.2. Crop Phenological Development

In 2018, cotton plants developed faster in the early growing season likely due to dry and warm conditions. During the early growing season of 2018 (DOY 108 - 194), stored soil water and the limited rainfall was enough for plant establishment and growth. During July and August (boll filling stage), the dry conditions were most at their intense and caused reduced growth and wilting. The maximum growing season green LAI (Figure 4A) occurred earlier in 2018 than in 2017. The maximum LAI in 2017 was 2.55 (DOY 203) compared to in 2018 was 2.79 (DOY 194). While the 2018 crop reached maximum LAI earlier, LAI quickly declined due to dry conditions in the latter part of the growing season. Immediately prior to defoliation, LAI was 1.52 in 2017 and 0.66 in 2018. Drought conditions have been found to reduce leaf area by first a reduction of leaf expansion and second by the termination of established leaves (Pettigrew, 2004; Bozorov et al., 2018).

Plant height throughout the growing season was lower in 2018 compared to 2017 (Figure 4C). Mature plant height in 2017 was 90 cm (DOY 203) compared to 87 cm (DOY 194) in 2018. Dry conditions prior to squaring have been previously found to reduce mature plant height (Snowden et al., 2014). Total biomass was greater in 2017 compared to 2018 (Figure 4B). Lower growing season precipitation likely contributed to

the observed differences in biomass. The cotton lint yield was 2120.54 ± 129.7 kg ha^{-1} in 2017 and was 1081.97 ± 60.63 kg ha^{-1} in 2018. Reduced photosynthesis from dry conditions in the boll-filling stage of 2018 led to a significantly lower yield, which has been observed in other studies (Snowden et al., 2014; Wu et al., 2018). Studies of the effects of drought in cotton have found that earlier maturing verities (like Phytogen 333WRF) are more prone to yield loss from drought than later maturing varieties due to a lack of a growing window to recover from drought stress (Pace et al., 1999; Bednarz and Nichols, 2005).

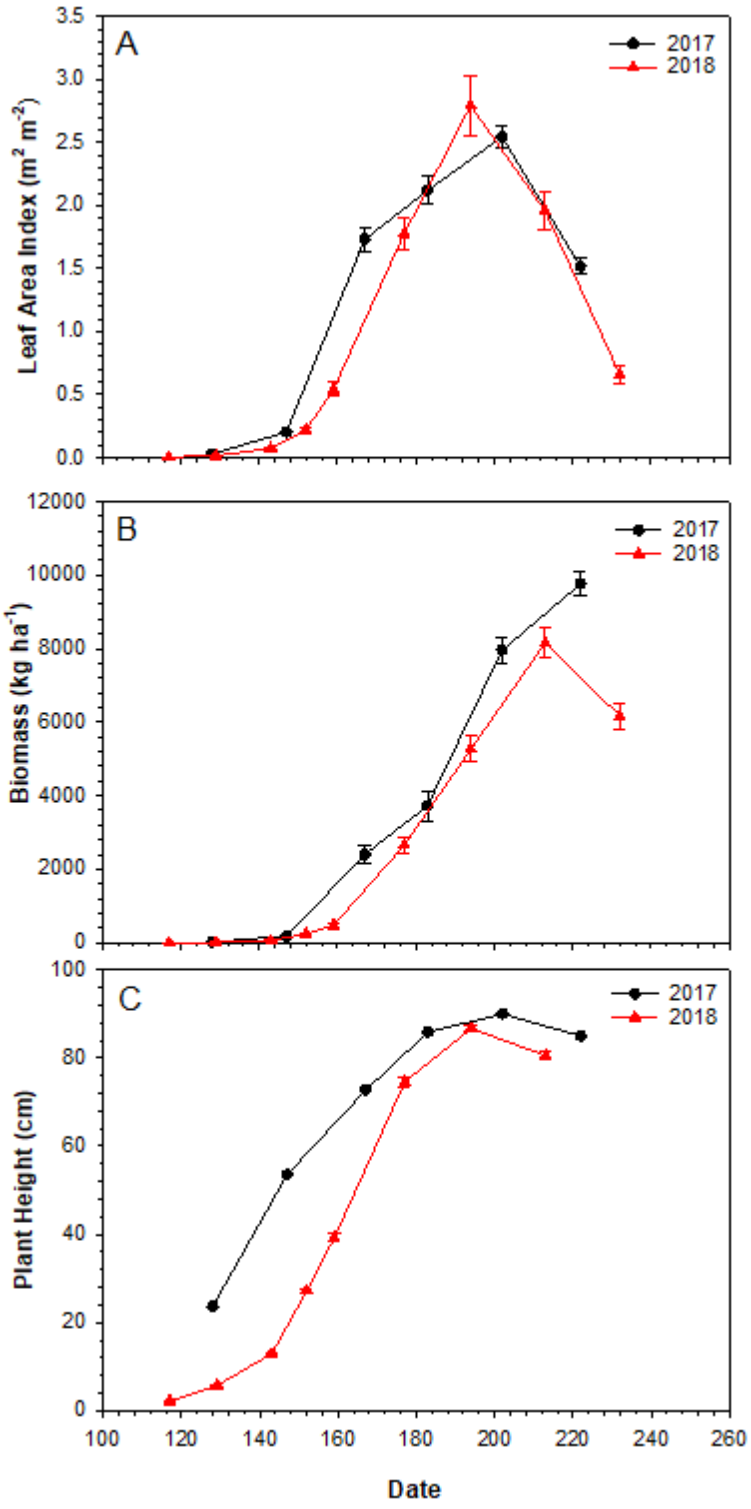

Figure 4: Cotton Phenological Development

Cotton plant phenological development during the 2017 (black lines) and 2018 (red lines) growing seasons is presented in this figure. Image “A” represents the leaf area index (LAI). Image “B” represents aboveground biomass. Image “C” represents plant height. Error bars associated with each point refer to the standard error of the mean. Sampling times were roughly biweekly with some variability due to weather conditions and ability to access the location.

2.3.3. Carbon Fluxes

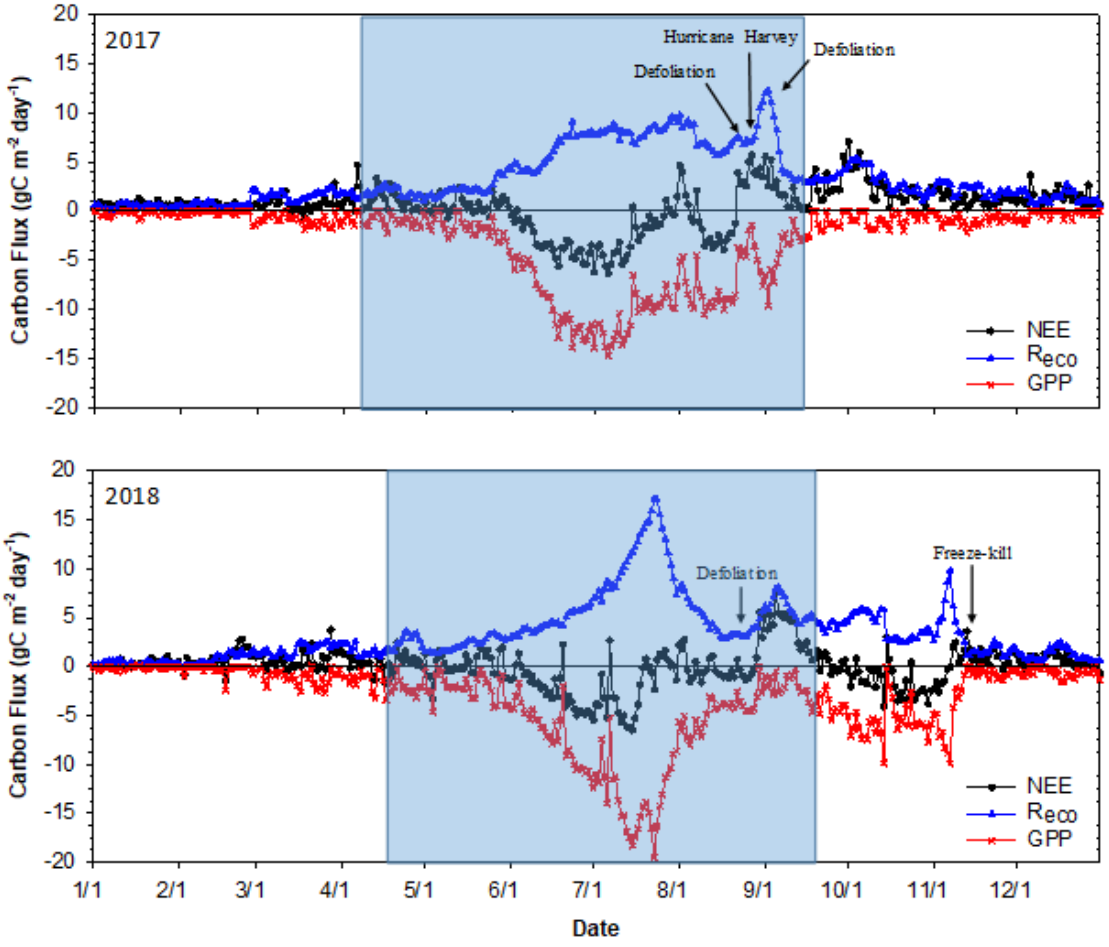

Figure 5: Daily Carbon Fluxes
Daily carbon flux for cotton for 2017 (above) and 2018 (below), the section highlighted in blue is the growing season (planting to harvest). A second defoliation was needed in 2017 due to regreening after Harvey. Freezing conditions occurred in December of 2017, but as carbon fluxes were already low, they did not result in a sudden change of fluxes.

Carbon fluxes (NEE, GPP, and R_{eco}) for 2017 and 2018 are shown in Figure 5. Precipitation variability between the years had a significant effect on determining carbon fluxes. In both years, maximum carbon uptake occurred in July, coinciding with the late flowering and boll filling stage. Net ecosystem CO_2 exchange was negative for most days during both growing seasons. During 2017, the highest daily net uptake was -6.38 g C m^{-2}, which occurred on July 6 (DOY 187). This was during the flowering and early boll-filling period of the growing season. There was little net uptake outside of the growing season in 2017. During 2018, the highest daily net uptake was -6.55 g C m^{-2}, which occurred on July 15 (DOY 196) during the boll-filling period, which is similar to what was observed in 2017. There was an additional period of net uptake from late-September to early-November due to weeds (primarily volunteer cotton, morning glories [*Ipomoea spp*], and Texas Panicum, [*Uruchloa texana*]) with daily net uptake as high as 4.1 g C m^{-2} (DOY 287). The weed-related carbon fluxes were greatly reduced in mid-November when the nighttime temperature fell below freezing. After the frost, carbon fluxes remained low for the remainder of 2018. Weed carbon uptake can be a significant contributor to carbon dynamics in agricultural settings, contributing as much as 25% of annual carbon uptake (Collins et al., 1999; Ibell et al., 2010).

There were a few days in the growing season where daily NEE was positive. Positive NEE values were common after rain events, especially when the soil was previously dry as the moisture enhances microbial activity (Zapata et al., 2017). The highest daily net emission in 2017 was 7.05 g C m^{-2}, which occurred on October 1 (DOY 283), which was shortly after harvest and residue shredding. There was another period of

high net emissions after Hurricane Harvey in 2017 with daily emissions around 5.0 g C m^{-2}. The highest daily net emission in 2018 was 7.52 g C m^{-2}, which occurred on September 5 (DOY 248). This was during the short window between defoliation and harvest and was the most prominent period of net emission during 2018. In dry soils, microbial activity is limited which in turn slows down carbon mineralization. When the soil becomes wet, it stimulates microbial activity and increases the rate of organic matter decomposition leading to emissions of CO_2 (Zapata et al., 2017, 2019). Since NEE is the balance of plant uptake and soil respiration (microbial and root), even when photosynthesis is high, enhanced soil respiration due to rainfall can still cause daily NEE to be positive (carbon source).

In 2017, R_{eco} was above 5 g C m^{-2} during most of the mid- and late- growing season. Following the extreme rain event associated with Hurricane Harvey (590 mm), R_{eco} increased to 12 g C m^{-2} for a brief period. There was a slight increase in R_{eco} following post-harvest tillage in 2017 (DOY 263), but it declined quickly afterward and remained low throughout the remainder of the 2017 post-harvest season, until planting in 2018. In 2018, R_{eco} was considerably higher during the growing season with many days above 10 g C m^{-2}. During the post-harvest season of 2018, R_{eco} remained between 4 and 5 g C m^{-2} for most days, although there were a few spikes due to weather events. On Nov 13 2018, (DOY 317) nighttime temperatures dropped below freezing and R_{eco} declined rapidly and remained around 1 g C m^{-2} for the rest of 2018.

Cumulative NEE, GPP, and R_{eco} by growing period are shown in Figure 6. Growing season cumulative NEE and GPP were both higher in 2017 than in 2018. In

Figure 6, growth periods 1 – 6 show different phases in the growth cycle of cotton. The first period shows the carbon fluxes from planting to seedling emergence with carbon uptake (if any) coming from weeds, R_{eco} exceeded GPP. The carbon balance in this period was a net emission of 19.6 g C m^{-2} in 2017 and 5.5 g C m^{-2} in 2018. The planting period of 2018 had weed growth (Predominantly henbit; *Lamium amplexicaule*) resulting in greater GPP, 1.4 g C m^{-2} in 2017 compared to 16.9 g C m^{-2} in 2018. The second period is the time between emergence and the development of the first square (cotton flower bud). During the beginning of this period, the cotton plant initially grows slowly, putting most of its energy into developing a root system, and then begins to grow quickly once established. During this period, GPP and R_{eco} are approximately equivalent to each other, resulting in a slight net emission of 1.6 g C m^{-2} in 2017 and 5.0 g C m^{-2} in 2018. The third period is the time between the first square and the first flower. During this time, rapid vegetative growth continues, but a small fraction of photosynthetic output is allocated to reproduction. There is a net uptake as the cotton plants accumulate more biomass and GPP exceeds R_{eco}. The fourth period is between flowering and the open boll phase (maturity). During this period, vegetative growth slows and the rate of photosynthesis remains high as the majority of the captured carbon is allocated to the growing reproductive structures. There is a net uptake as photosynthesis exceeds respiration; this period has the greatest cumulative GPP, with a fixation of 319.2 g C m^{-2} in 2017 and 469.3 in 2018. The fifth period is between open boll and defoliation. During this period, photosynthesis begins to decline as the plants begin to senesce. Once again, GPP and R_{eco} are similar to each other. During this phase, there was a net uptake of 25.4

g C m^{-2} in 2017 and a net uptake of 2.9 g C m^{-2} in 2018. The sixth period is between defoliation and harvest, at defoliation, all photosynthetic structures (leaves) are terminated with the application of the defoliant, an herbicide. As a result, GPP is greatly reduced while R_{eco} is largely unchanged, making the balance a net release of CO_2 to the atmosphere. Between defoliation and harvest, there was a net emission of 63.7 g C m^{-2} in 2017 and 75.5 g C m^{-2} in 2018.

Cumulative growing season, off-season and annual fluxes are presented as periods 7, 8 and 9 in Figure 6, respectively. The cumulative growing season GPP was 947.1 g C m^{-2} in 2017 and 882.7 g C m^{-2} in 2018. There was a net carbon uptake during both growing seasons; however, the net uptake was greater in 2017 as cumulative R_{eco} was similar between the two years and 2017 had a greater GPP. During the off-season (non-crop period), there was a net carbon emission in both years, however, the magnitude was different; the net emission during the off-season as 260.11 g C m^{-2} in 2017 and 48.79 g C m^{-2} in 2018. It is at this time where the differences between the two years were the greatest. In 2018, the post-harvest ecosystem respiration exceeded that of 2017 by 62.74 g C m^{-2}; however, the photosynthesis rate in the 2018 post-harvest season was considerably greater (GPP of 374.2 g C m^{-2} in 2018 compared to 100.1 g C m^{-2} in 2017) and more than compensated for the increased respiration. The annual carbon balance at the site shows a slight carbon sequestration of 5.1 g C m^{-2} in 2018 compared to a net emission of 175.4 g C m^{-2} in 2017, which is a striking difference in the span of two years. While there is little information on fluxes with cotton specifically, studies of other crop covers have found that differences in year-to-year weather patterns can

strongly affect the carbon balance and cause some years to be carbon sinks and other years to be carbon sources (Kessavalou et al., 1998; Meyers, 2001; Wharton et al., 2012). The prevalence of post-harvest weeds due to less tillage effectively acted as a cover crop, reducing the negative carbon impacts of fallow (Altieri, 1999; Kessavalou et al., 1998; Lal, 2004). Though, seed rain and seedbank replenishment from the post-harvest weed recruits is a valid concern (Bagavathiannan and Norsworthy, 2012).

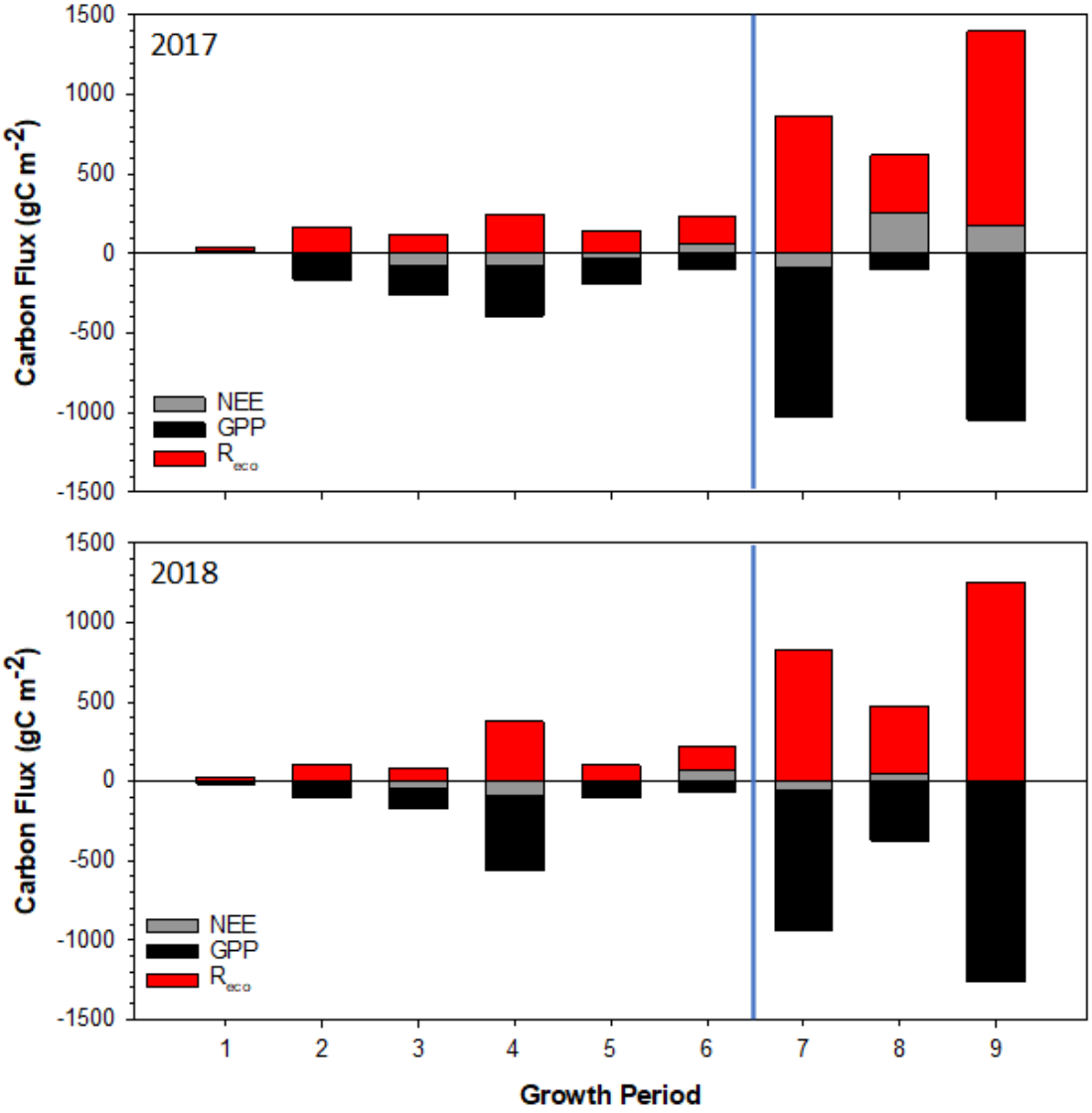

Figure 6: Cumulative Carbon Fluxes by Growth Period
NEE, GPP, and R_{eco} by the growth period are shown above. The blue line divides the growth stage fluxes from the annual fluxes. Growth period 1 is planting to seedling emergence, period 2 is emergence to the first square, period 3 is squaring to the first flower, period 4 is flowering to open boll, period 5 is open boll to defoliation, period 6 is defoliation to harvest, period 7 is total growing season, period 8 is off-season, and period

9 is full year. Negative numbers of NEE indicate net carbon uptake while positive numbers indicate net carbon release.

2.3.4. Effect of Cotton Lint Removal on Net Carbon Balance

Cotton lint is the largest natural fiber source in the textile industry. As cotton is a fiber crop, unlike bioenergy or food crops, it is not immediately consumed (by humans, animals, or as fuel) and could be thought of as a means of temporary sequestration. While the cotton seeds are typically used quickly via animal consumption or oil production, the fiber can remain for years. Well-cared-for and high-quality cotton fabrics can last for ten years or more. Most fabrics, however typically last between 2 and 5 years (Laitala and Klepp, 2015). Given the approximation that biomass is 50% carbon, the carbon removed as lint fiber was 1060.27 g C m^{-2} in 2017 and 540.99 g C m^{-2} in 2018. While this could be considered temporary carbon sequestration, overtime biomass removal can lead to depletion of soil carbon stocks, as carbon lost to microbial respiration is not replaced with new plant matter (Lal, 2004; Tubiello et al., 2014). A meta-analysis of 134 studies of change in soil carbon stocks in cropland found that soil carbon declines between 40% and 60% following the conversion of forest or pasture to cropland, mostly due to reduced inputs from biomass removal and increased respiration due to tillage practices (Guo and Gifford, 2002). An 8-year eddy covariance study of a hayfield in Pennsylvania found that once emissions from biomass removal via harvest was included, the field was a net carbon source (Skinner, 2007). The practice of tillage and other field operations increases soil respiration, which when coupled reduced

biomass inputs due to harvest, leads to a net emission of carbon from the site. This is particularly a problem for mono-cropping systems with heavy tillage (Chen et al., 2006b; Kaplan et al., 2010; Tubiello et al., 2014).

2.3.5. Meteorological Influences of GPP

Significant non-linear relationships were found between GPP and PAR, T_{air}, and precipitation. The relationship between weekly average GPP and T_{air} is shown in Figure 7a. The relationship between GPP and Tair was not different between the seasons and was non-linear. The best fit for the data with Sigmaplot was a 2-parameter power equation ($r^2 = 0.55$). As the temperature increased, GPP increased gradually until around 25°C. A substantial increase in GPP was observed between 25-30^{o}C. As the optimal temperature for cotton growth is between 26°C and 30°C, this increase pattern is expected as cotton grows very slowly at lower temperatures and then dramatically grows faster when temperature conditions are optimal (Suyker et al., 2004b; Boman and Lemon, 2005; Contay et al., 2012).

The relationship between weekly average daily GPP and daily PAR is shown in Figure 7b. The relationship between GPP and PAR was non-linear, the best fit for the data was found using Sigmaplot was a 2-parameter power model ($r^2 = 0.32$). There was no significant difference in the relationship between the two seasons. Most studies comparing GPP to PAR found a linear relationship (Suyker et al., 2004b; Sakamoto et al., 2011). However, in this study, we found a curvilinear relationship. This could be because of the unique growth pattern of cotton as these studies were in other crops, such as maize (*Zea mays*). During the early establishment period, aboveground biomass

development is slow as cotton is establishing its root system, even if PAR is high. Additionally, daily PAR is often still high at defoliation when the crop is chemically terminated and photosynthesis is halted.

The relationship between cumulative GPP and cumulative precipitation is shown in Figure 8. There was a significant difference in the relationship between the two seasons, with the correlation in 2017 being weaker than that of 2018. The low precipitation in 2018 likely contributed to the stronger correlation between GPP and precipitation. The overall curve for both years was non-linear, the best-fit using Sigmaplot was the polynomial quadratic model for both years (r^2 = 0.89 in 2017 and r^2 = 0.98 in 2018). The correlation between GPP and precipitation was stronger than any other meteorological variable. This relationship highlights the importance of precipitation in determining GPP in dryland systems. Garbulsky et al (2010) analyzed GPP and meteorological conditions from 35 sites in the Ameriflux and CarboEurope networks and found a similar trend with GPP and precipitation (Garbulsky et al., 2010; Xiao et al., 2013).

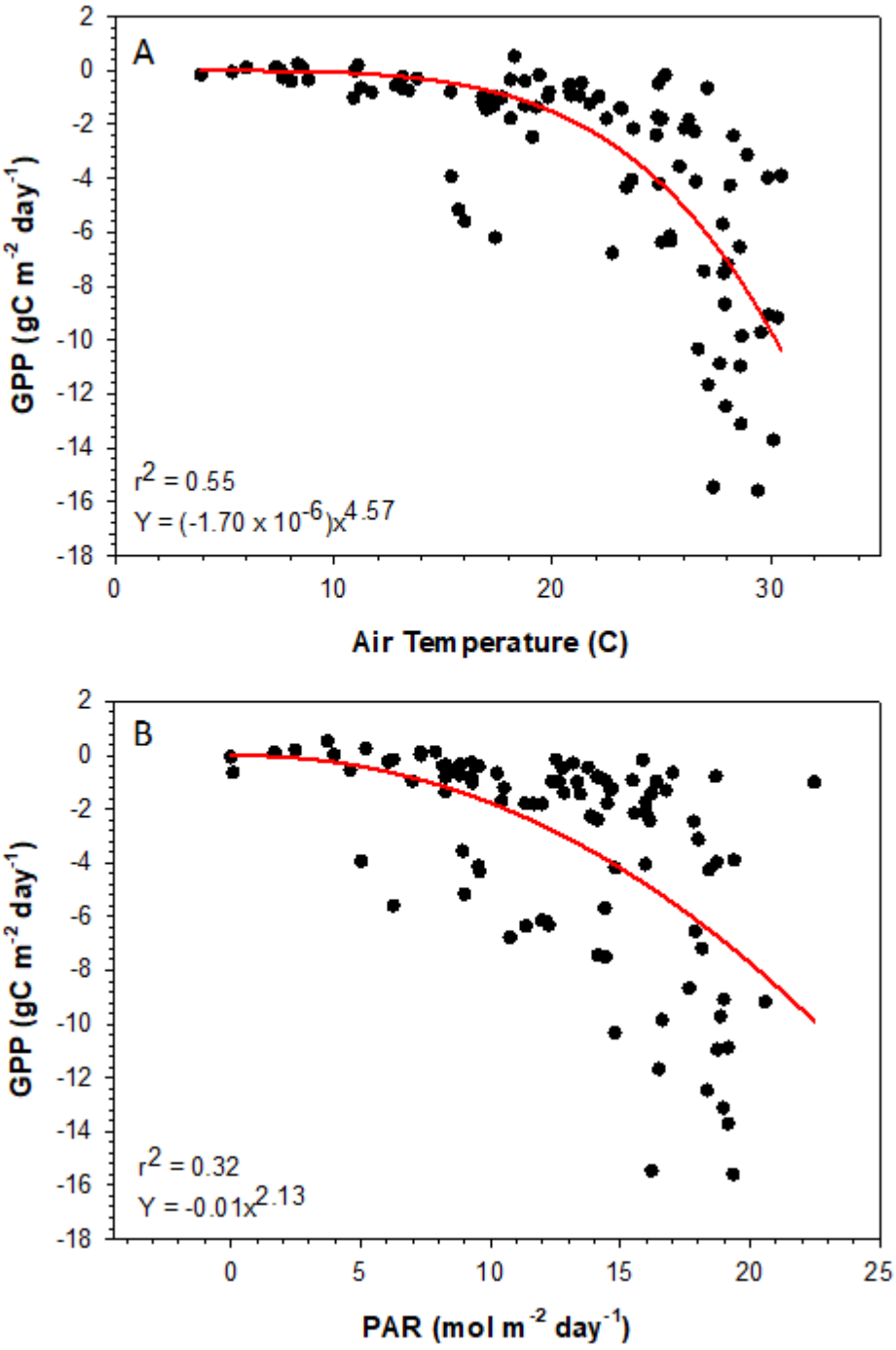

Figure 7: Correlation between GPP and Meteorological Conditions
The figure above shows the correlation between GPP and meteorological conditions.

Image "A" shows weekly average daily GPP plotted against weekly average air

temperature. Image “B” shows weekly average daily GPP plotted against daily PAR. The images contain data for both years combined, as there was no significant difference between the years.

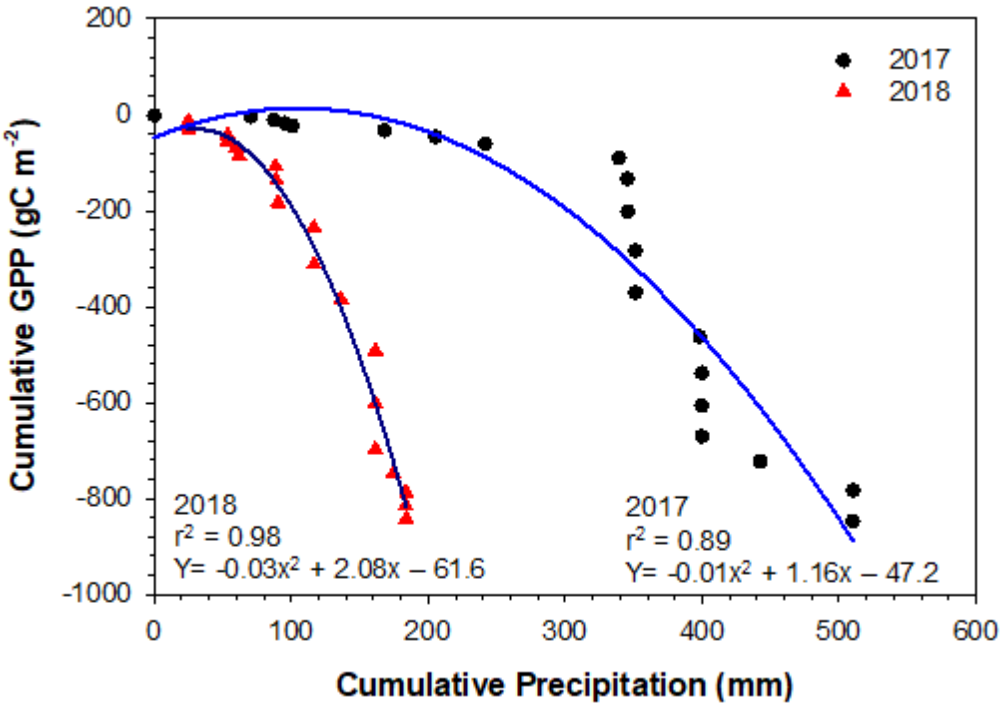

Figure 8: Correlation Between GPP and Precipitation
The correlation between cumulative GPP and cumulative precipitation is shown above. The curve fit was significantly different between the two growing seasons. The 2017 season is shown with black circles and a blue line. The 2018 season is shown with red triangles and a black line.

Relationship between PlanetScope NDVI and Carbon Fluxes

2.3.6. Relationship between PlanetScope NDVI and Carbon Fluxes

A time-series comparison of NDVI and GPP is shown in Figure 9. During 2017, NDVI increased between May and July, while carbon uptake was also increasing. Maximum NDVI in 2017 was 0.53 and occurred on DOY 189, following this date, NDVI remained around 0.50 until defoliation. NDVI decreased to 0.28 (DOY 255) following defoliation (DOY 231) and the senesce of leaves. Maximum NDVI in 2018 was 0.51 and occurred on DOY 199; following this date, NDVI quickly declined as dry conditions led to plant stress. Prior to defoliation in 2018 (DOY 230), NDVI was 0.39, and then following defoliation NDVI was 0.33 (DOY 243). During 2018, NDVI remained low during May, as did carbon uptake. In June and early July, carbon uptake increased rapidly as did NDVI. While NDVI reached the same peak in 2018 as it did in 2017, it did not remain high for as long. In late-July and August, as drought conditions prevailed, carbon uptake and NDVI greatly decreased. By defoliation in 2018, NDVI was already greatly reduced and a post-defoliation decline in NDVI was not as prominent.

Linear regression between NDVI and GPP is shown in Figure 10, which was performed using Sigmaplot's linear model. The correlation between GPP and NDVI was statistically significant in both years ($p < 0.001$). The r^2 value was higher in 2017 ($r^2 = 0.78$) compared to 2018 ($r^2 = 0.72$). The correlation between NDVI and GPP was weakest at high NDVI values, indicated by the greater spread in the data points. This effect was more notably prominent in 2018 compared to 2017. Satellite data has a lower

temporal resolution than EC data, and this might be partly responsible for the trend observed here. Thus, short-term fluxes associated with weather events are often not captured in satellite data. NDVI has additionally been found to correlate well with leaf area and the fraction of absorbed PAR, both of which are also important predictors of GPP (Asrar et al., 1984; Baret and Guyot, 1991).

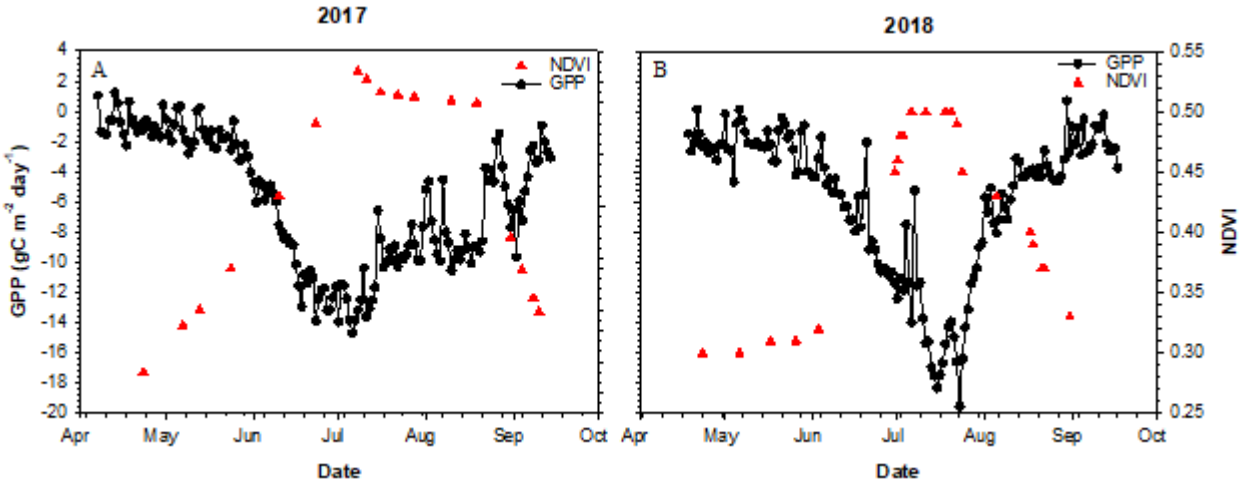

Figure 9: GPP and NDVI Time-series
The time-series of GPP and NDVI during the growing seasons is shown in the image above. Image "A" refers to 2017. Image "B" refers to 2018.

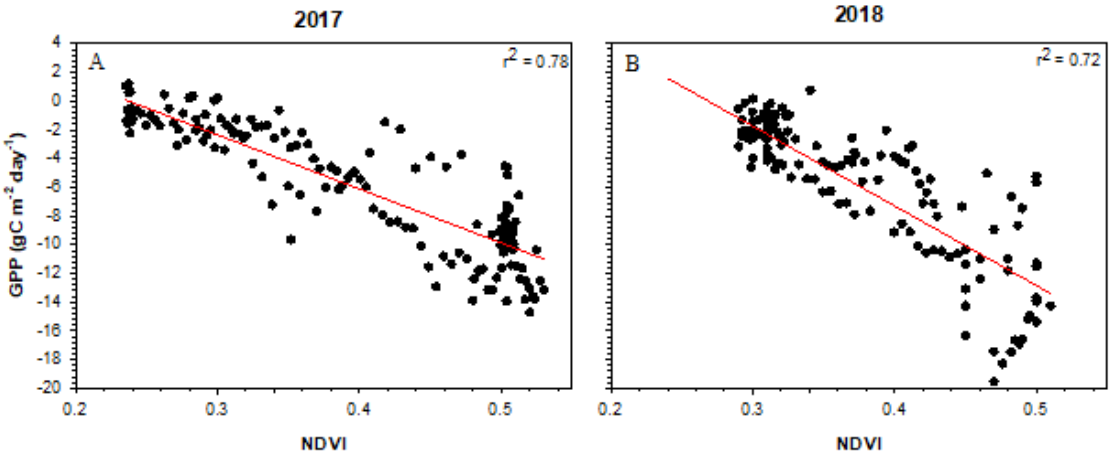

Figure 10: Linear Regression Between GPP and NDVI
Linear regression analysis of daily GPP and daily NDVI is shown in the image above. Image "A" refers to 2017. Image "B" refers to 2018.

2.4. Conclusions

In this study of carbon dynamics in cotton production, there were substantial differences in the carbon balance between the two years (2017 and 2018). Differences in precipitation between the two years were a major driving factor in the year-to-year variation in carbon balance. Precipitation during the growing season of 2017 was typical allowing for adequate crop growth. The carbon balance during the growing season was a net uptake of 947.1 g C m^{-2}. There was a brief period of high respiration following Hurricane Harvey, which occurred shortly after defoliation. Following harvest in 2017, respiration exceeded precipitation. The off-season net respiration exceeded the growing season's net photosynthesis, resulting in a net carbon emission of 175.4 g C m^{-2} for the entire year. Precipitation during the growing season of 2018 was unusually low,

resulting in reduced growing season carbon uptake compared to 2017 (882.7 g C m^{-2} vs 947.1 g C m^{-2}). While the growing season was dry, unusually wet conditions arrived in September of 2018 and carried through the rest of the year. The wet conditions following harvest prevented post-harvest tillage and fueled a growth of weeds, including re-greened cotton. This growth resulted in increased off-season carbon uptake. Despite the lower growing season carbon uptake, the increased off-season carbon uptake resulted in a slight net sequestration of 5.1 g C m^{-2} for the year as a whole. Carbon flux during the growing seasons followed the growth stages of the cotton crop, in both years; the greatest carbon uptake was during the boll-filling growth stage.

Of the meteorological variables, precipitation had the strongest correlation with GPP. The relationship between GPP and precipitation was strongest in 2018. There were also significant correlations between GPP and PAR and between GPP and air temperature. There was a significant correlation between GPP and NDVI from the satellite imagery data in both years. This correlation illustrated the potential value in including satellite imagery in studies of carbon dynamics. Given the high correlation between GPP and NDVI, satellite imagery data can be potentially used to estimate carbon uptake (Glenn et al., 2008; Yan et al., 2009; Yuan et al., 2010; Zheng et al., 2018). This study has allowed for a greater understanding of carbon dynamics in cotton production. The results of this study draw upon the importance of having carbon flux measurements for multiple years as different precipitation and temperature patterns can affect carbon balance.

2.5. Acknowledgment

This work is supported by NIFA-NLGCA [grant no. 2016-70001-24636/project accession no. 1008730] from the USDA National Institute of Food and Agriculture. This work was also supported partially through cotton incorporated grant # 17-614. This work was also supported by Planet's "Education and Research Program", which provided free access to PlanetScope imagery data. The authors would like to thank Dr. Don T. Conlee (Department of Atmospheric Sciences, Texas A&M University) for providing missing meteorological data. The authors would also like to thank Texas A&M Agrilife and the staff at the research farm, particularly Mr. Alfred Nelson (Farm Manager) for planting and managing the cotton field.

2.6. References

Adhikari, P., S. Ale, J.P. Bordovsky, K.R. Thorp, N.R. Modala, N. Rajan, and E.M. Barnes. 2016. Simulating future climate change impacts on seed cotton yield in the Texas High Plains using the CSM-CROPGRO-Cotton model. Agric. Water Manag. 164: 317–330. doi: 10.1016/j.agwat.2015.10.011.

Agam, N., W.P. Kustas, and M.C. Anderson. 2010. Application of the Priestley – Taylor Approach in a Two-Source Surface Energy Balance Model. Am. Meterorological Soc. 11: 185–198. doi: 10.1175/2009JHM1124.1.

Ahlrichs, J.S., and M.E. Bauer. 1983. Relation of Agronomic and Multispectral Reflectance Characteristics of Spring Wheat Canopies1. Agron. J. 75(6): 987–993. doi: 10.2134/agronj1983.00021962007500060029x.

Alganci, U., M. Ozdogan, E. Sertel, and C. Ormeci. 2014. Field Crops Research

Estimating maize and cotton yield in southeastern Turkey with integrated use of satellite images , meteorological data and digital photographs. F. Crop. Res. 157: 8–19. doi: 10.1016/j.fcr.2013.12.006.

Altieri, M.A. 1999. The ecological role of biodiversity in agroecosystems. Agric. Ecosyst. Environ. 74(1–3): 19–31. doi: 10.1016/S0167-8809(99)00028-6.

Amouzou, K.A., J.B. Naab, J.P.A. Lamers, C. Borgemeister, M. Becker, and P.L.G. Vlek. 2018. CROPGRO-Cotton model for determining climate change impacts on yield, water- and N- use efficiencies of cotton in the Dry Savanna of West Africa. Agric. Syst. 165(November 2017): 85–96. doi: 10.1016/j.agsy.2018.06.005.

Anothai, J., C.M.T. Soler, A. Green, T.J. Trout, and G. Hoogenboom. 2013. Evaluation of two evapotranspiration approaches simulated with the CSM–CERES–Maize model under different irrigation strategies and the impact on maize growth, development and soil moisture content for semi-arid conditions. Agric. For. Meteorol. 176(July): 64–76.

Anthoni, P.M., B.E. Law, and M.H. Unsworth. 1999. Carbon and water vapor exchange of an open-canopied ponderosa pine ecosystem. Agric. For. Meteorol. 95(3): 151–168. doi: 10.1016/S0168-1923(99)00029-5.

Asrar, G., M. Fuchs, E.T. Kanemasu, and J.L. Hatfield. 1984. (1984) Estimating Absorbed Photosynthetic Radiation and Leaf Area Index from Spectral Reflectance in Wheat (AJ).

Aubinet, M., T. Vesala, and D. Papale. 2012. Eddy Covariance: A Practical Guide to Measurement and Data Analysis. Springer Atmospheric Sciences, Berlin, Germany.

Bagavathiannan, M., and J.K. Norsworthy. 2012. Late-Season Seed Production in Arable Weed Communities: Management Implications. Weed Sci. 60(3): 325–334.

Bai, J., J. Wang, X. Chen, G.P. Lou, H. Shi, L.H. Li, and J. Li. 2015. Seasonal and inter-variations in carbon fluxes and evapotranspiration over cotton field under drip irrigation and plastic mulch in an arid region of Northwest China. J. Arid Land 7(2): 272–282.

Baker, J.M., and T.J. Griffis. 2005. Examining strategies to improve the carbon balance of corn / soybean agriculture using eddy covariance and mass balance techniques. Agric. For. Meteorol. 128: 163–177. doi: 10.1016/j.agrformet.2004.11.005.

Baldocchi, D.D. 2003. Assessing the eddy covariance technique for evaluating carbon dioxide exchange rates of ecosystems: past, present and future. Glob. Chang. Biol. 9(4): 479–492. doi: 10.1046/j.1365-2486.2003.00629.x.

Ballester, C., J. Brinkhoff, W.C. Quayle, and J. Hornbuckle. 2019. Monitoring the Effects of Water Stress in Cotton Using the Green Red Vegetation Index and Red Edge Ratio. Remote Sens. 11(7).

Baret, F., and G. Guyot. 1991. Potentials and limits of vegetation indices for LAI and APAR assessment. Remote Sens. Environ. 35(2–3): 161–173. doi: 10.1016/0034-4257(91)90009-U.

Basso, B., L. Liu, and J.T. Ritchie. 2016. A Comprehensive Review of the CERES-Wheat, -Maize and -Rice Models' Performances. Elsevier Inc.

Bednarz, C.W., and R.L. Nichols. 2005. Phenological and Morphological Components of Cotton Crop Maturity. Crop Sci. 45(4): 1497–1503.

Bell, J. 2017. Corn Growth Stages and Development.

Bennett, E.M., G.D. Peterson, and L.J. Gordon. 2009. Understanding relationships among multiple ecosystem services. Ecol. Lett. 12(12): 1394–1404. doi: 10.1111/j.1461-0248.2009.01387.x.

Boman, R., and R. Lemon. 2005. Soil Temperatures for Cotton Planting. College Station, Texas.

Boote, K.J., and N.B. Pickering. 1994. Modeling Photosynthesis of Row Crop Canopies. HortScience 29(12): 1423–1434.

Bozorov, T.A., R.M. Usmanov, H.L. Yang, S.A. Hamdullaev, S. Musayev, J. Shakiev, S. Nabiev, D.Y. Zhang, and A.A. Abdullaev. 2018. Effect of water deficiency on relationships between metabolism, physiology, biomass, and yield of upland cotton (Gossypium hirsutum L.). J. Arid Land 10(3): 441–456.

Bruinsma, J. 2003. World Agriculture: Towards 2015/2030.

Burba, G. 2013. Eddy Covariance Method (R Nelson, Ed.). LI-COR Biosciences, Lincoln, NE.

Carberry, P.S. 1991. Test of leaf-area development in CERES-Maize: a correction. F. Crop. Res. 27: 159–167.

Carmelita, M., R. Alberto, R. Wassmann, R.J. Buresh, J.R. Quilty, T.Q. Correa, J.M. Sandro, C. Arloo, and R. Centeno. 2014. Field Crops Research Measuring methane flux from irrigated rice fields by eddy covariance method using open-path gas analyzer. F. Crop. Res. 160: 12–21. doi: 10.1016/j.fcr.2014.02.008.

Chen, J.M., A. Govind, O. Sonnentag, Y. Zhang, A. Barr, and B. Amiro. 2006a. Leaf

area index measurements at Fluxnet-Canada forest sites. Agric. For. Meteorol. 140(1): 257–268.

Chen, H., H. Tian, M. Liu, J. Melillo, S. Pan, and C. Zhang. 2006b. Effect of Land-Cover Change on Terrestrial Carbon Dynamics in the Southern United States. J. Environ. Qual. 35(4): 1533. doi: 10.2134/jeq2005.0198.

Collatz, G.J., J.T. Ball, C. Grivet, and J.A. Berry. 1991. Physiological and environmental regulation of stomatal conductance, photosynthesis and transpiration: a model that includes a laminar boundary layer. Agric. For. Meteorol. 54(2–4): 107–136. doi: 10.1016/0168-1923(91)90002-8.

Collins, H.P., R.L. Blevins, L.G. Bundy, D.R. Christienson, W.A. Dick, D.R. Huggins, and E.A. Paul. 1999. Soil Carbon Dynamics in Corn-Based Agroecosystems: Results from Carbon-13 Natural Abundance. Soil Sci. Soc. Am. J. 63(3): 584–591.

Contay, W.C., J.J. Burke, J.R. Mahan, J.E. Neilsen, and B.G. Sutton. 2012. Determining the Optimum Plant Temperature of Cotton Physiology and Yield to Improve Plant-Based Irrigation and Scheduling. Crop Sci. 52(July): 1828–1836.

Cook, B.D., K.J. Davis, W. Wang, A. Desai, B.W. Berger, R.M. Teclaw, J.G. Martin, P. V. Bolstad, P.S. Bakwin, C. Yi, and W. Heilman. 2004. Carbon exchange and venting anomalies in an upland deciduous forest in northern Wisconsin, USA. Agric. For. Meteorol. 126(3–4): 271–295. doi: 10.1016/j.agrformet.2004.06.008.

Daughtry, C. 2000. Estimating Corn Leaf Chlorophyll Concentration from Leaf and Canopy Reflectance. Remote Sens. Environ. 74(2): 229–239. doi: 10.1016/S0034-4257(00)00113-9.

Dejonge, K.C., and K.R. Thorp. 2017. Implementing Standardized Reference Evapotranspiration and Dual Crop Coefficient Approach in the DSSAT Cropping System Model. Am. Soc. Agric. Biol. Eng. 60(6): 1965–1981.

Dettori, M., C. Cesaraccio, A. Montroni, D. Spano, and P. Duce. 2011. Using CERES-Wheat to simulate durum wheat production and phenology in Southern Sardinia, Italy. F. Crop. Res. 120(1): 179–188.

Dokoohaki, H., M. Gheysari, S.F. Mousavi, S. Zand-Parsa, F.E. Miguez, S.V. Archontoulis, and G. Hoogenboom. 2016. Coupling and testing a new soil water module in DSSAT CERES-Maize model for maize production under semi-arid condition. Agric. Water Manag. 163(1): 90–99.

Dolman, A.J., J. Noilhan, P. Durand, C. Sarrat, A. Brut, B. Piguet, A. Butet, N. Jarosz, Y. Brunet, D. Loustau, E. Lamund, L. Tolk, R. Ronda, F. Miglietta, B. Gioli, V. Magliulo, M. Esposito, C. Gerbig, S. Korner, P. Glademard, M. Ramonet, P. Ciais, B. Neininger, R.W.A. Hutjes, J.A. Elbers, R. Macatangay, O. Schrems, G. Perez-Landa, M.J. Sanz, Y. Scholz, G. Facon, E. Ceschia, and P. Beziat. 2006. The CarboEurope Regional Experiment Strategy. Am. Meteorol. Soc. (October): 1367–1379.

Doorenbos, J., and W.D. Pruitt. 1977. Guidelines for Predicting Crop Water Use. Rome, Italy.

Finnigan, J.J., R. Clement, Y. Malhi, R. Leuning, and H.A. Cleugh. 2003. A Re-Evaluation of Long-Term Flux Measurement Techniques Part 1: Averaging and Coordinate Rotation. Boundary-Layer Meteorol. (107): 1–48.

Foley, J.A., R. Defries, G.P. Asner, C. Barford, G. Bonan, S.R. Carpenter, F.S. Chapin, M.T. Coe, G.C. Daily, H.K. Gibbs, J.H. Helkowski, T. Holloway, E.A. Howard, C.J. Kucharik, C. Monfreda, J.A. Patz, I.C. Prentice, N. Ramankutty, and P.K. Snyder. 2005. Global Consequences of Land Use. Science (80-.). 309(July): 570–574. doi: 10.1126/science.1111772.

Food and Agriculture Organization. 2016. Land Use.

Frankenberg, C., J.B. Fisher, J. Worden, G. Badgley, S.S. Saatchi, J.E. Lee, G.C. Toon, A. Butz, M. Jung, A. Kuze, and T. Yokota. 2011. New global observations of the terrestrial carbon cycle from GOSAT: Patterns of plant fluorescence with gross primary productivity. Geophys. Res. Lett. 38(17): 1–7. doi: 10.1029/2011GL048738.

Fritz, E., S. Richter, S. Schott, S. Hejja, and S. Trumbore. 2018. Partitioning Algorithm. Max Planck Inst. Biogeochem.

Garbulsky, M.F., J. Penuelas, D. Papale, J. Ardo, M.L. Goulden, K. Gerard, A.D. Richardson, E. Rotenberg, E.M. Veenendall, and I. Filella. 2010. Patterns and controls of the variability of radiation use efficiency and primary productivity across terrestrial ecosystems. Glob. Ecol. Biogeogr. 19: 253–267.

Gitelson, A.A. 2019. Remote estimation of fraction of radiation absorbed by photosynthetically active vegetation : generic algorithm for maize and soybean. Remote Sens. Lett. 10(3): 283–291. doi: 10.1080/2150704X.2018.1547445.

Gitelson, A.A., Y. Peng, J.G. Masek, D.C. Rundquist, S. Verma, A. Suyker, J.M. Baker, J.L. Hat, and T. Meyers. 2012. Remote estimation of crop gross primary production

with Landsat data. Remote Sens. Environ. 121: 404–414. doi: 10.1016/j.rse.2012.02.017.

Glenn, E.P., A.R. Huete, P.L. Nagler, and S.G. Nelson. 2008. Relationship Between Remotely-sensed Vegetation Indices, Canopy Attributes and Plant Physiological Processes: What Vegetation Indices Can and Cannot Tell Us About the Landscape. : 2136–2160.

Godwin, D.C., and C.A. Jones. 1991. Nitrogen dynamics in soil-plant systems. p. 287–321. *In* Modeling plant and soil systems. ASA, CSSA, and SSSA, Madison, Wisconsin.

Godwin, D.C., and U. Singh. 1998. Nitrogen balance and crop response to nitrogen in upland and lowland cropping systems. p. 55–77. *In* Tsuji, G.Y., Hoogenboom, G., Thornton, P.K. (eds.), Understanding options for agricultural production. System approaches for sustainable agricultural development. Kluwer Academic Publishers, Dordrecht, Netherlands.

Gonias, E.D., D.M. Oosterhuis, and A.C. Bibi. 2011. Light interception and radiation use efficiency of okra and normal leaf cotton isolines. Environ. Exp. Bot. 72(2): 217–222.

Gonzalez-Dugo, M.P., C.M.U. Neale, L. Mateos, W.P. Kustas, J.H. Prueger, M.C. Anderson, and F. Li. 2009. A comparison of operational remote sensing-based models for estimating crop evapotranspiration. Agric. For. Meteorol. 149(11): 1843–1853. doi: 10.1016/j.agrformet.2009.06.012.

Google Earth, 2018. Map showing location of cotton field. earth.google.com/web/.

Guo, L.B., and R.M. Gifford. 2002. Soil carbon stocks and land use change: A meta analysis. Glob. Chang. Biol. 8(4): 345–360. doi: 10.1046/j.1354-1013.2002.00486.x.

Gutierrez, M., R. Norton, K.R. Thorp, and G. Wang. 2012. Association of Spectral Reflectance Indices with Plant Growth and Lint Yield in Upland Cotton. Crop Sci. 52(2): 849–857.

Gwathmey, C.O., D.D. Tyler, and X. Yin. 2010. Prospects for Monitoring Cotton Crop Maturity with Normalized Difference Vegetation Index. Agron. J. 102(5): 1352–1360.

Han, G., Q. Xing, J. Yu, Y. Luo, D. Li, L. Yang, G. Wang, P. Mao, B. Xie, and N. Mikle. 2014. Agricultural reclamation effects on ecosystem CO2exchange of a coastal wetland in the Yellow River Delta. Agric. Ecosyst. Environ. 196: 187–198. doi: 10.1016/j.agee.2013.09.012.

Harmel, R.D., D.R. Smith, R.L. Haney, and P.M. Allen. 2019. Comparison of nutrient loss pathways: Run-off and seepage flow in Vertisols. Hydrol. Process. 33(18): 2384–2393.

He, M., J.S. Kimball, M.P. Maneta, and B.D. Maxwell. 2018. Regional Crop Gross Primary Productivity and Yield Estimation Using Fused Landsat-MODIS Data. doi: 10.3390/rs10030372.

Hirschi, M., D. Michel, I. Lehner, and S.I. Seneviratne. 2017. A site-level comparison of lysimeter and eddy covariance flux measurements of evapotranspiration. Hydrol. Earth Syst. Sci. 21(3): 1809–1825. doi: 10.5194/hess-21-1809-2017.

Hoogenboom, G., J.W. Jones, C.H. Porter, P.W. Wilkens, K.J. Boote, W.D. Batchelor, L.A. Hunt, and G.Y. Tsuji. 2003. A Decision Support System for Agrotechnology Transfer Version 4.0. 4th ed. University of Hawaii, Honolulu, Hawaii.

Houghton, R.A. 2007. Balancing the Global Carbon Budget. Annu. Rev. Earth Planet. Sci. 35(1): 313–347. doi: 10.1146/annurev.earth.35.031306.140057.

Houghton, R.A., A. Baccini, and W.S. Walker. 2018. Where is the residual terrestrial carbon sink? Glob. Chang. Biol. 24(8): 3277–3279.

Howell, T.A., S.R. Evett, J.A. Tolk, and A.D. Schneider. 2004. Evapotranspiration of full-, deficit-irrigated, and dryland cotton on the Northern Texas High Plains. J. Irrig. Drain. Eng. 130(4).

Huemmrich, K.F., P. Campbell, D. Landis, and E. Middleton. 2019. Developing a common globally acceptable method for optical remote sensing of ecosystem light use efficiency. Remote Sens. Environ. 230.

Huete, A.R., H.Q. Liu, K. Batchily, and L. van W. J. 1997. A comparsion of vegetation indices over a Global set of TM images for EO -MODIS. Remote Sens. Environ. 59(Table 1): 440–451. doi: 10.1016/S0034-4257(96)00112-5.

Ibell, P.T., Z. Xu, and T.J. Blumfield. 2010. Effects of weed control and fertilization on soil carbon and nutrient pools in an exotic pine plantation of subtropical Australia. J. Soils Sediments (10): 1027–1038. doi: 10.1007/s11368-010-0222-6.

Ibrahim, M.E., and D.R. Buxton. 1981. Early Vegetative Growth of Cotton as Influenced by Leaf Type. Crop Sci. 21(5): 639–643.

Jaafar, H.H., and F.A.. Ahmad. 2015. Relationships Between Primary Production and

Crop Yields in Semi-Arid and Arid Irrigated Agroecosystems. Int. Symp. Remote Sens. Environ. 47(W3): 27–30.

Jalota, S.K., S. Sukhvinder, G.B.S. Chahal, S.S. Ray, S. Panigraphy, F. Bhupinder-Singh, and K.B.. Singh. 2010. Soil texture, climate and management effects on plant growth, grain yield and water use by rainfed maize–wheat cropping system: Field and simulation study. Agric. Water Manag. 97(1): 83–90.

Jans, W.W.P., C.M.J. Jacobs, B. Kruijt, J.A. Elbers, S. Barendse, and E.J. Moors. 2010. Carbon exchange of a maize (Zea mays L.) crop: Influence of phenology. Agric. Ecosyst. Environ. 139(3): 316–324. doi: 10.1016/j.agee.2010.06.008.

Johnson, D.M. 2016. A comprehensive assessment of the correlations between field crop yields and commonly used MODIS products. Int. J. Appl. EARTH Obs. Geoinf. 52: 65–81.

Jones, J.W. 1993. Decision Support System for agricultural development. p. 459–471. *In* de Vries, F.P., Teng, P., Metselaar, K. (eds.), Systems Approaches for Agricultural Development. Kluwer Academic Publishers, Boston.

Jones, J.W., J.M. Antle, B. Basso, K.J. Boote, R.T. Conant, I. Foster, H.C.J. Godfray, M. Herrero, R.E. Howitt, S. Janssen, B.A. Keating, R. Munoz-Carpena, C.H. Porter, C. Rosenzweig, and T.R. Wheeler. 2017. Brief history of agricultural systems modeling. Agric. Syst. 155(June): 240–254. doi: 10.1016/j.agsy.2016.05.014.

Jones, J.W., K.J. Boote, G. Hoogenboom, S.S. Jagtap, and G.G. Wilkerson. 1989. Soybean Crop Growth Simulation Model. Gainsville.

Jones, J.W., G. Hoogenboom, C.H. Porter, K.J. Boote, W.D. Batchelor, L.A. Hunt, P.W.

Wilkens, U. Singh, and A.J. Gijsman. 2003. The DSSAT Cropping System Model.

Jones, J.W., and J.T. Ritchie. 1991. Crop Growth Models. p. 63–89. *In* Hoffman, G.J., Howell, T.A., Soloman, K.H. (eds.), Management of Farm Irrigation System. 9th ed. American Society of Agricultural Engineers.

Kaplan, J.O., K.M. Krumhardt, E.C. Ellis, F. Ruddiman, C. Lemmen, and K.K. Goldewijk. 2010. Holocene carbon emissions as a result of anthropogenic land cover change. The Holocene 21(June). doi: 10.1177/0959683610386983.

Kerr, J.T., and M. Ostrovsky. 2003. From space to species: Ecological applications for remote sensing. Trends Ecol. Evol. 18(6): 299–305. doi: 10.1016/S0169-5347(03)00071-5.

Kessavalou, A., A.R. Mosier, J.W. Doran, R.A. Drijber, D.J. Lyon, and O. Heinemeyer. 1998. Fluxes of Carbon Dioxide, Nitrous Oxide, and Methane in Grass Sod and Winter Wheat-Fallow Tillage Management. J. Environ. Qual. (27): 1094–1104.

King, A.W., L. Dilling, G.P. Zimmerman, D.M. Fairman, R.A. Houghton, G.H. Marland, A.Z. Rose, and T.J. Wilbanks. 2007. The North American Carbon Budget and Implications for the Global Carbon Cycle.

L'Ecuyer, T.S., H.K. Beaudoing, M. Rodell, W. Olson, B. Lin, S. Kato, C.A. Clayson, E. Wood, J. Sheffield, R. Adler, G. Huffman, M. Bosilovich, G. Gu, F. Robertson, P.R. Houser, D. Chambers, J.S. Famiglietti, E. Fetzer, W.T. Liu, X. Gao, C.A. Schlosser, E. Clark, D.P. Lettenmaier, and K. Hilburn. 2015. The observed state of the energy budget in the early twenty-first century. J. Clim. 28(21): 8319–8346. doi: 10.1175/JCLI-D-14-00556.1.

Laitala, K., and I.G. Klepp. 2015. Age and active life of clothing. Prod. Lifetimes Environ.: 182–186.

Lal, R. 2004. Soil Carbon Sequestration Impacts on Global Climate Change and Food Security. Am. Assoc. Adv. Sci. 304(5677): 1623–7. doi: 10.1126/science.1097396.

LI-COR. 2015. SmartFlux System Instruction Manual.

Li, S., S. Kang, F. Li, and L. Zhang. 2008. Evapotranspiration and crop coefficient of spring maize with plastic mulch using eddy covariance in northwest China. Agric. Water Manag. 95(11): 1214–1222. doi: 10.1016/j.agwat.2008.04.014.

Li, X., L. Liu, H. Yang, and Y. Li. 2018. Relationships between carbon fluxes and environmental factors in a drip-irrigated, film-mulched cotton field in arid region. PLoS One 13(2): 1–18. doi: 10.1371/journal.pone.0192467.

Lindsey, R. 2009. Climate and Earth's Energy Budget. NASA Earth Obs.: 1–12. doi: 10.1007/s10712-011-9165-8.

Liu, P. 2017. The future of food and agriculture: Trends and challenges.

Lopez-Cedron, F.X., K.J. Boote, J. Pineiro, and F. Sau. 2008. Improving the CERES-Maize model ability to simulate water deficit impact on maize production and yield components. Agron. J. 100: 296–307.

Main, C.L. 2012. Cotton Growth and Development.

Matocha, M., C. Allen, R. Boman, G. Morgan, and P. Baumann. 2009. Crop Profile for Cotton in Texas. College Station, Texas.

Meyers, T.P. 2001. A comparison of summertime water and CO2fluxes over rangeland for well watered and drought conditions. Agric. For. Meteorol. 106(3): 205–214.

doi: 10.1016/S0168-1923(00)00213-6.

Modala, N.R., S. Ale, N. Rajan, C.L. Munster, P.B. DeLaune, K.R. Thorp, S.S. Nair, and E.M. Barnes. 2015. Evaluation of the CSM-CROPGRO-COTTON MODEL for the Texas Rolling Plains Region and Simulation of Deficit Irrigation Strategies for Increasing Water Use Efficiency. Trans. ASABE 58(3): 658–696.

Möller, M., J. Tanny, Y. Li, and S. Cohen. 2004. Measuring and predicting evapotranspiration in an insect-proof screenhouse. Agric. For. Meteorol. 127(1–2): 35–51. doi: 10.1016/j.agrformet.2004.08.002.

Monteith, J.L. 1977. Climate and Efficiency of Crop Production in Britain. Phil. Trans. R. Soc. Lond. 281(980).

Monteith, J.L. 1986. How do crops manipulate water supply and demand ? Phil. Trans. R. Soc. Lond. 316: 245–259.

Mu, Q., M. Zhao, and S.W. Running. 2011. Improvements to a MODIS global terrestrial evapotranspiration algorithm. Remote Sens. Environ. 115(8): 1781–1800. doi: 10.1016/j.rse.2011.02.019.

Mubeen, M., A. Ahmad, T. Khaliqu, and A. Bakhsh. 2013. Evaluating CSM-CERESMaize model for irrigation scheduling in semi-arid conditions of Punjab, Pakistan. Int. J. Agric. Biol. 15(1): 1–10.

Murty, D., M.U.F. Kirschbaum, R.E. Mcmurtrie, and H. Mcgilvray. 2002. Does conversion of forest to agricultural land change soil carbon and nitrogen? A review of the literature. Glob. Chang. Biol. 8(2): 105–123. doi: 10.1046/j.1354-1013.2001.00459.x.

Myneni, R.B., R.R. Nemani, and S.W. Running. 1997. Estimation of global leaf area index and absorbed par using radiative transfer models. IEEE Trans. Geosci. Remote Sens. 35(6): 1380–1393.

National Oceanic and Atmospheric Administration. 2011. Climate Data Online. Natl. Centers Environ. Inf.

Oki, T., and K. Shinjiro. 2006. Global Hydrological Cycles and World Water Resources. Science (80-.). 313(August): 1068–1073.

Pace, P.F., H.T. Cralle, S.H.M. El-Halawany, J.T. Cothren, and S.A. Senseman. 1999. Drought-induced Changes in Shoot and Root Growth of Young Cotton Plants. J. Cotton Sci. 3(183–187).

Padilla, F.L.M., S.J. Maas, M.P. Gonzalez-Dugo, N. Rajan, F. Mansilla, P. Gavilan, and J. Dominguez. 2012. Wheat Yield Monitoring in Southern Spain Using the GRAMI Model and a Series of Satellite Images. F. Crop. Res. 139(29): 145–145.

Pathak, T.B., J.W. Jones, C.W. Fraisse, D. Wright, and G. Hoogenboom. 2012. Uncertainty analysis and parameter estimation for the CSM-CROPGRO-cotton model. Agron. J. 104(5): 1363–1373. doi: 10.2134/agronj2011.0349.

Patil, N.G., and G.S. Rajput. 2009. Evaluation of Water Retention Functions and Computer Program “Rosetta” in Predicting Soil Water Characteristics of Seasonally Impounded Shrink-Swell Soils. J. Irrig. Drain. Eng. 135(3): 286–294.

Paw, K.T., D.D. Baldocchi, T.P. Meyers, and K.B. Wilson. 2000. Correction of Eddy-Covariance Measurements Incorporating Both Advective Effects and Density Fluxes. Boundary-Layer Meteorol. (47): 487–511.

Pegelow, E.J., D.R. Buxton, R.E. Briggs, H. Muramoto, and W.G. Gensler. 1977. Canopy Photosynthesis and Transpiration of Cotton as Affected by Leaf Type. Crop Sci. 17(1): 1–4.

Peng, Y., and A.A. Gitelson. 2011. Application of chlorophyll-related vegetation indices for remote estimation of maize productivity. Agric. For. Meteorol. 151(9): 1267–1276.

Peng, Y., and A.A. Gitelson. 2012. Remote estimation of gross primary productivity in soybean and maize based on total crop chlorophyll content. Remote Sens. Environ. 117: 440–448. doi: 10.1016/j.rse.2011.10.021.

Peng, Y., A.A. Gitelson, G. Keydan, D.C. Rundquist, and W. Moses. 2011. Remote estimation of gross primary production in maize and support for a new paradigm based on total crop chlorophyll content. Remote Sens. Environ. 115(4): 978–989.

Pettigrew, W.T. 2004. Physiological Consequences of Moisture Deficit Stress in Cotton. Crop Sci. 44(4): 1265–1272.

PhytoGen. 2019. PhytoGen Cotton Varieties. Corteva Agriscience. https://phytogencottonseed.com/varieties.

Planet Team. 2017. Planet Application Program Interface: In Space for Life on Earth. San Francisco, CA.

Planet Team. 2018. No Title. Planet Inc.

Priestly, C.H.B., and R.J. Taylor. 1972. On the Assessment of Surface Heat Flux and Evaporation Using Large-Scale Parameters. Mon. Weather Rev. 100(February): 81–92.

Qin, S., S. Li, S. Kang, T. Du, L. Tong, and R. Ding. 2016. Can the drip irrigation under film mulch reduce crop evapotranspiration and save water under the sufficient irrigation condition? Agric. Water Manag. 177: 128–137. doi: 10.1016/j.agwat.2016.06.022.

Rajan, N., S.J. Maas, and S. Cui. 2013a. Extreme Drought Effects on Carbon Dynamics of a Semi Arid Pasture. Crop Ecol. Physiol. 105(6): 1749–1760.

Rajan, N., S.J. Maas, and S. Cui. 2013b. Extreme Drought Effects on Carbon Dynamics of a Semi-arid Pasture. 2013 105(6): 1749–1760.

Ramankutty, N., A.T. Evan, C. Monfreda, and J.A. Foley. 2008. Farming the planet : 1 . Geographic distribution of global agricultural lands in the year 2000. 22(February 2007): 1–19. doi: 10.1029/2007GB002952.

Raper, T.B., J.J. Varco, and K.J. Hubbard. 2013. Canopy-Based Normalized Difference Vegetation Index Sensors for Monitoring Cotton Nitrogen Status. Agron. J. 105(5): 1345–1354.

Reichstein, M., E. Falge, D. Baldocchi, D. Papale, M. Aubinet, P. Berbigier, C. Bernhofer, N. Buchmann, T. Gilmanov, A. Granier, T. Grunwald, K. Havrankova, H. Ilvesniemi, D. Janous, A. Knohl, T. Laurila, A. Lohila, D. Loustau, G. Matteucci, T. Meyers, F. Miglietta, J.-M. Ourcival, J. Pumpanen, S. Rambal, E. Rotenberg, M. Sanz, J. Tenhunen, G. Seufert, F. Vaccari, T. Vesala, D. Yakir, and R. Valentini. 2005. On the separation of net ecosystem exchange into assimilation and ecosystem respiration : review and improved algorithm. Glob. Chang. Biol. (11): 1424–1439. doi: 10.1111/j.1365-2486.2005.001002.x.

Ringrose-Voase, A.J., and A.J. Nadelko. 2013. Deep drainage in a Grey Vertosol under furrow-irrigated cotton. Crop Pasture Sci. 64(12): 1155–1170.

Ritchie, J.T. 1972. Model for Predicting Evaporation from a Row Crop with Incomplete Cover. Water Resour. Res. 8(5): 1204–1213.

Ritchie, J.T. 1998. Soil water balance and plant stress. p. 41–54. *In* Tsuji, G.Y., Hoogenboom, G., Thornton, P.K. (eds.), Understanding options for agricultural production. System approaches for sustainable agricultural development. Kluwer Academic Publishers, Dordrecht, Netherlands.

Ritchie, G.L., C.W. Bednarz, P.H. Jost, and S.M. Brown. 2007. Cotton Growth and Development.

Ritchie, J.T., and S. Otter. 1985. Description and performance of CERES-Wheat: A User-oriented wheat yield model. ARS Wheat Yield Proj. 38: 159–175.

Ritchie, J.T., C.H. Porter, J. Judge, J.W. Jones, and A.A. Suleiman. 2009. Extension of an Existing Model for Soil Water Evaporation and Redistribution under High Water Content Conditions. Soil Sci. Soc. Am. J. 73(3): 792. doi: 10.2136/sssaj2007.0325.

Ritchie, G.L., D.G. Sullivan, W.K. Vencill, C.W. Bednarz, and J.E. Hook. 2010. Sensitivities of Normalized Difference Vegetation Index and a Green/Red Ratio Index to Cotton Ground Cover Fraction. Crop Sci. 50(3): 1000–1010.

Rodell, M., H.K. Beaudoing, T.S. L'Ecuyer, W.S. Olson, J.S. Famiglietti, P.R. Houser, R. Adler, M.G. Bosilovich, C.A. Clayson, D. Chambers, E. Clark, E.J. Fetzer, X. Gao, G. Gu, K. Hilburn, G.J. Huffman, D.P. Lettenmair, W.T. Liu, F.R. Robertson, C.A. Schlosser, J. Sheffield, and E.F. Wood. 2015. The Observed State of the

Water Cycle in the Early Twenty-First Century. J. Clim. 28(November): 8289–8318. doi: 10.1175/JCLI-D-14-00555.1.

Rost, S., D. Gerten, A. Bondeau, W. Lucht, and J. Rohwer. 2008. Agricultural green and blue water consumption and its influence on the global water system. Water Resour. Res. 44: 1–17. doi: 10.1029/2007WR006331.

Saigusa, N., S. Yamamoto, S. Murayama, H. Kondo, and N. Nishimura. 2002. Gross primary production and net ecosystem exchange of a cool-temperate deciduous forest estimated by the eddy covariance method. Agric. For. Meteorol. 112: 203–215.

Sakamoto, T., A.A. Gitelson, B.D. Wardlow, S.B. Verma, and A.E. Suyker. 2011. Estimating daily gross primary production of maize based only on MODIS WDRVI and shortwave radiation data. Remote Sens. Environ. 115(12): 3091–3101.

Saseendran, S.A., L. Ma, D.C. Nielsen, M.F. Vigil, and L.R. Ahuju. 2005. imulating planting date effects on corn production using RZWQM and CERES-Maize models. Agron. J. 97(1): 58–71.

Sau, F., K.J. Boote, M. Bostick, J.W. Jones, and M.I. Minguez. 2004. Testing and Improving Evapotranspiration and Soil Water Balance of the DSSAT Crop Models. Agron. J. 96(September): 1243–1257.

Schindler, D.W. 1999. The mysterious missing sink. Nature 398: 105–107.

Seligman, N.C., and H. Van Keulen. 1981. PAPRAN: a simulation model of annual pasture production limited by rainfall and nitrogen. p. 192–221. *In* Frissel, M.J., Van Veen, J.A. (eds.), Simulation of nitrogen behavior of soil-plant systems.

Centrum voor Landbouwpublikaties en Landbouwdocumentatie, Wageningen, Netherlands.

Shafian, S., N. Rajan, R. Schnell, M. Bagavathiannan, J. Valasek, Y. Shi, and J. Olsenholler. 2018. Unmanned Aerial Systems-Based Remote Sensing for Monitoring Sorghum Growth and Development. PLoS One 13(5).

Sharma, S., N. Rajan, S. Cui, K. Casey, S. Ale, R. Jessup, and S. Maas. 2017. Seasonal variability of evapotranspiration and carbon exchanges over a biomass sorghum field in the Southern U.S. Great Plains. Biomass and Bioenergy 105: 392–401.

Shelton, M.L. 1987. Irrigation induced change in vegetation and evapotranspiration in the Central Valley of California. Landsc. Ecol. 1(2): 95–105.

Sinclair, T.R., and R.C. Muchow. 2001. System Analysis of Plant Traits to Increase Grain Yield on Limited Water Supplies. 93(2): 263–270.

Skinner, H.R. 2007. High Biomass Removal Limits Carbon Sequestration Potential of Mature Temperate Pastures. J. Environ. Qual. 37(4): 1319–1326.

Smith, P., M. Bustamante, H. Ahammad, H. Clark, H. Dong, E.A. Elsiddi, H. Haberl, R. Harper, J. House, M. Jafari, O. Masera, C. Mbow, N.H. Ravindranath, C.W. Rice, C.R. Abad, A. Romanovskaya, F. Sperling, and F. Tubiello. 2014. Agriculture, forestry and other land use.

Snowden, M.C., G.L. Ritchie, F.R. Simao, and J.P. Bordovsky. 2014. Timing of Episodic Drought Can Be Critical in Cotton. Agron. J. 106(2): 452–458.

Soldevilla-Martinez, M., M. Quemada, R. Lopez-Urrea, R. Munoz-Carpena, and J.I. Lizaso. 2014. Soil water balance: Comparing two simulation models of different

levels of complexity with lysimeter observations. Agric. Water Manag. 139(June): 53–63.

Soler, C.M.T., P.C. Sentelhas, and G. Hoogenboom. 2007. Application of the CSM-CERES-Maize model for planting date evaluation and yield forecasting for maize grown off-season in a subtropical environment. Eur. J. Agron. 27(2–4): 165–177. doi: 10.1016/j.eja.2007.03.002.

Sonnentag, O., M. Detto, R. Vargas, Y. Ryu, B.R.K. Runkle, M. Kelly, and D.D. Baldocchi. 2011. Agricultural and Forest Meteorology Tracking the structural and functional development of a perennial pepperweed (Lepidium latifolium L .) infestation using a multi-year archive of webcam imagery and eddy covariance measurements. Agric. For. Meteorol. 151(7): 916–926. doi: 10.1016/j.agrformet.2011.02.011.

Spera, S.A., G.L. Galford, and M.T. Coe. 2016. Land-use change affects water recycling in Brazil ' s last agricultural frontier. Glob. Chang. Biol. 22: 3405–3413. doi: 10.1111/gcb.13298.

Suleiman, A.A., and G. Hoogenboom. 2007. Comparison of Priestley–Taylor and FAO-56 Penman–Monteith for daily reference evapotranspiration estimation in Georgia, USA. J. Irrig. Drain. Eng. 133(2).

Suleiman, A.A., and J.T. Ritchie. 2003. Modeling Soil Water Redistribution during Second-Stage Evaporation. Soil Sci. Soc. Am. J. 67(2): 377–386. doi: 10.2136/sssaj2003.0377.

Suleiman, A.A., C.M.T. Soler, and G. Hoogenboom. 2007. Evaluation of FAO-56 crop

coefficient procedures for deficit irrigation management of cotton in a humid climate. Agric. Water Manag. 91(1): 33–42.

Suyker, A.E., S.B. Verma, G.G. Burba, T.J. Arkebauer, D.T. Walters, and K.G. Hubbard. 2004a. Growing season carbon dioxide exchange in irrigated and rainfed maize. Agric. For. Meteorol. 124(1–2): 1–13. doi: 10.1016/j.agrformet.2004.01.011.

Suyker, A.E., S.B. Verma, G.G. Burba, T.J. Arkebauer, D.T. Walters, and K.G. Hubbard. 2004b. Growing season carbon dioxide exchange in irrigated and rainfed maize. Agric. For. Meteorol. 124(1): 1–13.

Texas A&M Agrilife. 2019. Cotton Production Regions of Texas. Cott. Insect Manag. Guid.

Texas Parks and Wildlife. 2019. Post Oak Savannah and Blackland Prairie Wildlife Management. Habitats.

Thorp, K.R., E.M. Barnes, D.J. Hunsaker, and B.A. Kimball. 2014. Evaluation of CSM-CROPGRO-Cotton for Simulating Effects of Management and Climate Change on Cotton Growth and Evapotranspiration In An Arid Environment. Trans. ASABE 57(6): 1627–1642.

Thorp, K.R., D.J. Hunsaker, A.N. French, E. Bautista, and K.F. Bronson. 2015. Integrating geospatial data and cropping system simulation within a geographic information system to analyze spatial seed cotton yield, water use, and irrigation requirements. Precis. Agric. 16(5): 532–557.

Tian, H., G. Chen, M. Liu, C. Zhang, G. Sun, C. Lu, X. Xu, W. Ren, S. Pan, and A.

Chappelka. 2010. Model estimates of net primary productivity, evapotranspiration, and water use efficiency in the terrestrial ecosystems of the southern United States during 1895-2007. For. Ecol. Manage. 259(7): 1311–1327. doi: 10.1016/j.foreco.2009.10.009.

Tscharntke, T., A.M. Klein, A. Kruess, I. Steffan-Dewenter, and C. Thies. 2005. Landscape perspectives on agricultural intensification and biodiversity - Ecosystem service management. Ecol. Lett. 8(8): 857–874. doi: 10.1111/j.1461-0248.2005.00782.x.

Tubiello, F.N., M. Salvatore, R.D. Cóndor Golec, A. Ferrara, S. Rossi, R. Biancalani, S. Federici, H. Jacobs, and A. Flammini. 2014. Agriculture, Forestry and Other Land Use Emissions by Sources and Removals by Sinks. ESS Work. Pap. No.2 2: 4–89. doi: 10.13140/2.1.4143.4245.

Twine, T.E., W.P. Kustas, J.M. Norman, D.R. Cook, P.R. Houser, and T.P. Meyers. 2000. Correcting eddy-covariance flux underestimates over a grassland. Agric. For. Meteorol. 103: 279–300.

Uddin, J., R.J. Smith, N.H. Hancock, and J.P. Foley. 2013. Evaporation and sapflow dynamics during sprinkler irrigation of cotton. Agric. Water Manag. 125: 35–45. doi: 10.1016/j.agwat.2013.04.001.

USDA-NASS. 2017. 2017 Census of Agriculture County Profile: Burleson County Texas.

Verlag, F., A.A. Gitelson, Y. Gritz, and M.N. Merzlyak. 2003. Relationships between leaf chlorophyll content and spectral reflectance and algorithms for non-destructive

chlorophyll assessment in higher plant leaves. J. Plant Physiol. 160(3): 271–282.

Verma, S.B., A. Dobermann, K.G. Cassman, D.T. Walters, J.M. Knops, T.J. Arkebauer, A.E. Suyker, G.G. Burba, B. Amos, H. Yang, D. Ginting, K.G. Hubbard, A.A. Gitelson, and E.A. Walter-Shea. 2005. Annual carbon dioxide exchange in irrigated and rainfed maize-based agroecosystems. Agric. For. Meteorol. 131(1–2): 77–96. doi: 10.1016/j.agrformet.2005.05.003.

Vitale, L., P. Di Tommasi, G. D'Urso, and V. Magliulo. 2016. The response of ecosystem carbon fluxes to LAI and environmental drivers in a maize crop grown in two contrasting seasons. Int. J. Biometeorol. 60(3): 411–420. doi: 10.1007/s00484-015-1038-2.

Wang, Y., C.E. Woodcock, W. Buermann, P. Stenberg, P. Voipio, H. Smolander, T. Hame, Y. Tian, H. Jiannan, Y. Knyazikhin, and R.B. Myneni. 2004. Evaluation of the MODIS LAI algorithm at a coniferous forest site in Finland. Remote Sens. Environ. 91(1): 114–127.

Wang, C., Z. Zhang, S. Fan, R. Mwiya, and M. Xie. 2018. Effects of straw incorporation on desiccation cracking patterns and horizontal flow in cracked clay loam. Soil Tillage Res. 182: 130–143.

Webb, E.K., G.I. Pearman, and R. Leuning. 1980. Correction of flux measurements for density effects due to heat and water vapour transfer. Q. J. R. Meteorol. Soc. 106(447): 85–100.

West, T.O., and W.M. Post. 2002. Soil Organic Carbon Sequestration Rates by Tillage and Crop Rotation : A Global Data Analysis. Soil Sci. Soc. Am. J. 66(6): 1930–

1946. doi: 10.2136/sssaj2002.1930.

Wharton, S., M. Falk, K. Bible, M. Schroeder, and K.T.U. Paw. 2012. Old-growth CO2 flux measurements reveal high sensitivity to climate anomalies across seasonal, annual and decadal time scales. Agric. For. Meteorol. 161: 1–14. doi: 10.1016/j.agrformet.2012.03.007.

Wilson, K., A. Goldstein, E. Falge, M. Aubinet, D. Baldocchi, P. Berbigier, C. Bernhofer, R. Ceulemans, H. Dolman, C. Field, A. Grelle, A. Ibrom, B.E. Law, A. Kowalski, T. Meyers, J. Moncrieff, R. Monson, W. Oechel, J. Tenhunen, R. Valentini, and S. Verma. 2002. Energy balance closure at FLUXNET sites. Agric. For. Meteorol. 113: 223–243.

Woodbury, P.B., L.S. Heath, and J.E. Smith. 2006. Land Use Change Effects on Forest Carbon Cycling Throughout the Southern United States. J. Environ. Qual. 35(4): 1348. doi: 10.2134/jeq2005.0148.

Wu, H., X. Wang, M. Xu, and J. Zhang. 2018. The Effect of Water Deficit and Waterlogging on the Yield Components of Cotton. Crop Sci. 58(4): 1751–1761.

Xevi, E., J. Gilley, and J. Feyen. 1996. Comparative study of two crop yield simulation models. Agric. Water Manag. 30(2): 155–173.

Xiao, J., G. Sun, J. Chen, H. Chen, S. Chen, G. Dong, S. Gao, H. Guo, J. Guo, S. Han, T. Kato, Y. Li, G. Lin, L. Weizhi, M. Ma, S. McNulty, C. Shao, X. Wang, and J. Zhou. 2013. Carbon fluxes, evapotranspiration, and water use efficiency of terrestrial ecosystems in China. Agric. For. Meteorol. 182(12): 76–90.

Xu, C.Y., and D. Chen. 2005. Comparison of seven models for estimation of

evapotranspiration and groundwater recharge using lysimeter measurement data in Germany. Hydrol. Process. 19(18): 3717–3734. doi: 10.1002/hyp.5853.

Yan, H., Y. Fu, X. Xiao, H.Q. Huang, H. He, and L. Ediger. 2009. Modeling gross primary productivity for winter wheat-maize double cropping system using MODIS time series and CO2eddy flux tower data. Agric. Ecosyst. Environ. 129(4): 391–400. doi: 10.1016/j.agee.2008.10.017.

Yoder, B.J., and R.E. Pettigrew-Crosby. 1995. Predicting nitrogen and chlorophyll content and concentration for reflectance spectra (400 - 2500 nm) at leaf and canopy scales. Remote Sens. Environ. 53(September 1994): 199–211.

Yuan, W., S. Liu, G. Yu, J.M. Bonnefond, J. Chen, K. Davis, A.R. Desai, A.H. Goldstein, D. Gianelle, F. Rossi, A.E. Suyker, and S.B. Verma. 2010. Global estimates of evapotranspiration and gross primary production based on MODIS and global meteorology data. Remote Sens. Environ. 114(7): 1416–1431. doi: 10.1016/j.rse.2010.01.022.

Yu, G., X. Wen, X. Sun, B.D. Tanner, X. Lee, and J. Chen. 2006. Overview of ChinaFLUX and evaluation of its eddy covariance measurement. Agric. For. Meteorol. 137: 125–137. doi: 10.1016/j.agrformet.2006.02.011.

Zapata, D., N. Rajan, and F. Hons. 2017. Does high soil moisture in no-till systems increase CO2 emissions and reduce carbon sequestration? Tampa, FL.

Zapata, D., N. Rajan, J. Mowrer, K. Casey, R. Schnell, and F. Hons. 2019. Impact of Long-Term Tillage on Soil CO2 Emissions and Soil Carbon Sequestration in Monoculture and Rotational Cropping Systems. Soil Tillage Res.

Zhao, M., F.A. Heinsch, R.R. Nemani, and S.W. Running. 2005. Improvements of the MODIS terrestrial gross and net primary production global data set. Remote Sens. Environ. 95(2): 164–176. doi: 10.1016/j.rse.2004.12.011.

Zheng, Y., L. Zhang, J. Xiao, W. Yuan, M. Yan, and T. Li. 2018. Sources of uncertainty in gross primary productivity simulated by light use efficiency models: Model structure, parameters, input data, and spatial resolution. Agric. For. Meteorol. 263(December 2017): 242–257. doi: 10.1016/j.agrformet.2018.08.003.

Zhou, Y., X. Xiao, P. Wagle, R. Bajgain, H. Mahan, J.B. Basara, J. Dong, Y. Qin, G. Zhang, Y. Luo, P.H. Gowda, J.P.S. Neel, P.J. Starks, and J.L. Steiner. 2017. Examining the short-term impacts of diverse management practices on plant phenology and carbon fluxes of Old World bluestems pasture. Agric. For. Meteorol. 237–238: 60–70. doi: 10.1016/j.agrformet.2017.01.018.

3. MODELING GROSS PRIMARY PRODUCTION OF DRYLAND CORN USING PLANETSCOPE SATELLITE IMAGERY

3.1. Introduction

Remote sensing technology has improved our ability to study the impact of human activities on ecosystem processes, including carbon cycling. Analysis of satellite and aerial images has greatly improved over the past few decades and has now become quite common in ecosystem and agricultural sciences. Remote sensing has improved our ability to understand global, regional, and local carbon fluxes by allowing for enhanced estimation over large areas of land. The main component of the carbon cycle that can be captured using remote sensing is gross primary productivity (GPP), which is the total amount of carbon uptake via photosynthesis. Gross primary production is the largest terrestrial carbon sink and is an important driver of ecosystem functions as it represents the carbon and energy available to the ecosystem. Understanding GPP is important for understanding carbon dynamics and ecosystem processes in both natural and managed ecosystems, such as croplands (Gitelson et al., 2012; Zheng et al., 2018). As human activities have increased the amount of carbon released into the atmosphere, satellite GPP estimations have assisted in determining the fate of this carbon. This better understanding of plant carbon uptake has allowed the "missing carbon sink" to be accounted for (Schindler, 1999; Houghton, 2007; King et al., 2007; Houghton et al., 2018). In agricultural settings, understanding carbon uptake can have additional benefits in improving crop productivity. Remote carbon uptake estimate can improve yield forecasts as carbon uptake via photosynthesis is tightly linked to the yield of the

agricultural product, such as grain or fiber (Alganci et al., 2014; He et al., 2018).

One of the more common methods of estimating GPP with imagery data is to use a light use efficiency (LUE) based model. This model was proposed by Monteith in 1977 and has since been widely used and modified to suit the needs of GPP modeling efforts. The most common modification is to replace LUE with a vegetation index (VI) from remote sensing. Vegetation Indices are ratios that utilize the spectral properties of growing vegetation to get a measure of plant productivity. They are typically a ratio of near-infrared (NIR) to another wavelength of light. Photosynthesizing plants reflect NIR more strongly than other wavelengths, which is how VI's are able to measure plant productivity. Multiple studies have shown that LUE and VI are well correlated and that VI can replace LUE in GPP models of agroecosystems (Glenn et al., 2008; Gitelson et al., 2012; Peng and Gitelson, 2012; Alganci et al., 2014; He et al., 2018; Zheng et al., 2018). Peng and Gitelson (2012) compared Ameriflux Eddy Covariance derived GPP to GPP modeled using vegetation indices at 16 sites. The corn models using the Green Chlorophyll Index was the most successful.

While satellite images can cover wider areas than possible with ground-based measurements, there is still a need for ground-based measurements of carbon dynamics. Ground-based measurements offer greater precision and when combined with satellite data they can act as a ground-truth to improve the accuracy of the satellite imagery-based model. One of the most common and effective methods to measure carbon dynamics in-situ is eddy covariance (EC). Eddy covariance measures trace gas flux, including CO_2, the gas of interest in photosynthesis, by taking the covariance of the gas

concentration and the vertical wind speed. Eddy covariance has been used worldwide for studying carbon dynamics, water use, and methane emissions, however, use in agricultural settings in the southern U.S. is still uncommon (Saigusa et al., 2002; Baldocchi, 2003; Dolman et al., 2006; Yu et al., 2006).

The primary objective of this study is to model GPP in conventional corn production using satellite remote sensing. This will be achieved by directly measuring carbon fluxes using an EC system and then using satellite data to model GPP with multiple vegetation indices as well as ground-based data. Modeled GPP will then be compared to observed GPP and the model with the best fit will be determined.

3.2. Materials and Methods

3.2.1. Site Information

The study was conducted in a 34 ha conventionally managed dryland production corn (*Zea mays*) field, located at the Texas A&M Agrilife Research Farm in Burleson County, Texas (30°32’46.2” N, 96°25’19.7” W), which is shown in Figure 11. The climate of the location is humid subtropical (Köppen Cfa) with an average annual temperature of 20.58°C and an average annual precipitation of 1018 mm. The rainfall pattern in this region is bimodal, with the highest rainfall in May, June, and October. The dominant soil types in the field are the Weswood silt loam (Udifluventic Haplustepts, 38% clay in surface horizon, floodplain) and Ships clay (Chromic Halpludert, 42% clay in the surface horizon), both of which contain predominantly shrink-swell clay minerals.

The corn crop was planted on March 10 in 2017, on March 6 in 2018, and on March 7 in 2019. Disc-tillage was performed prior to planting in 2017 and 2018. Due to

unusually wet soil conditions and a short planting window, pre-plant tillage was not performed in 2019. The variety planted was B-H 8845 VTB in 2017, Pioneer P1602 AM in 2018, and DeKalb 67-42 in 2019. Nitrogen fertilizer was broadcast at a rate of 135 kg N ha^{-1} as urea ammonium nitrate (32-0-0) after planting in all three years. Corn was harvested on July 25 in 2017, on July 19 in 2018, and on August 12 in 2019. Residues were shredded post-harvest and incorporated into the soil using disc tillage.

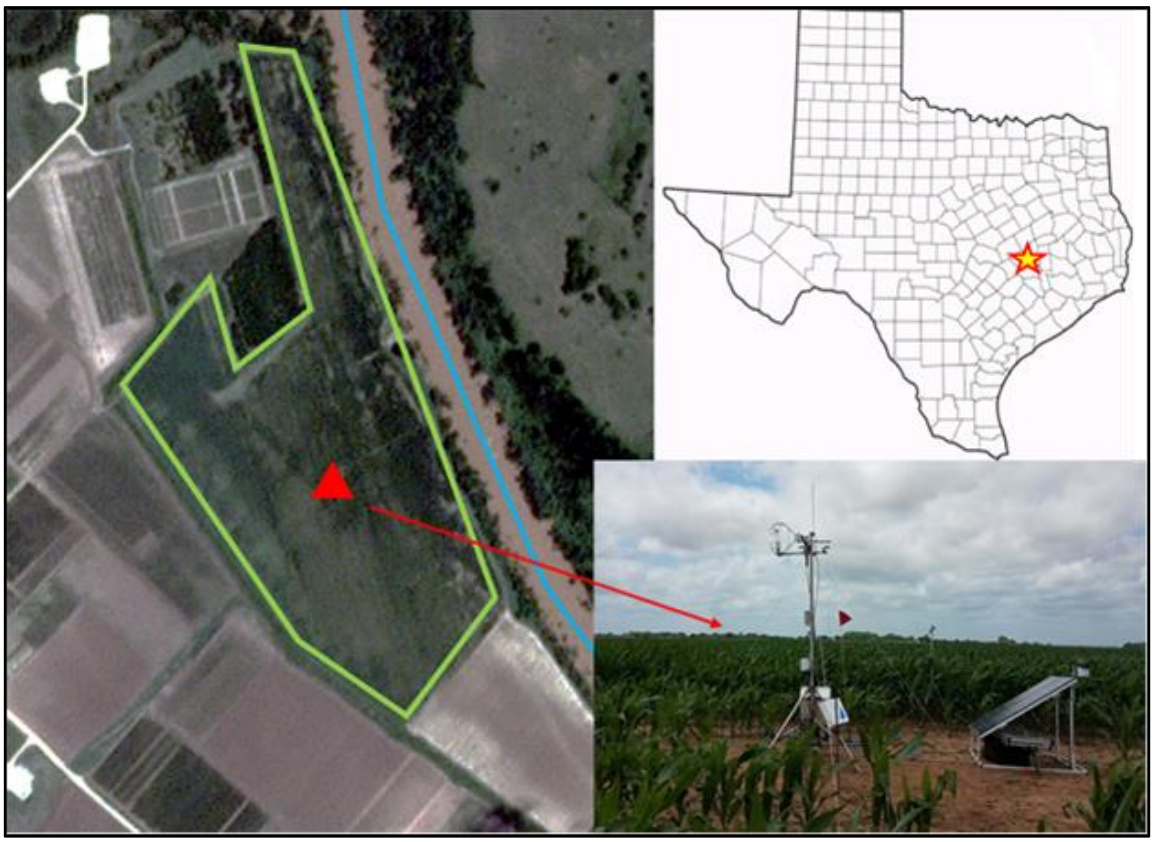

Figure 11: Image of Corn Field Location
Images of the site and location are shown above. The image on the left is a satellite image of the field. The field is outlined in green with the location of the EC tower indicated by a red triangle. The Brazos River is highlighted with a blue line. The image

on the upper right shows a map of Texas with the location of Burleson County marked with a star. The image on the lower right is a photograph of the EC tower.

3.2.2. Satellite Imagery Data

Satellite imagery from cloud-free days with full area coverage were downloaded from Planet Labs Inc. (San Francisco, CA, USA), 20 images were downloaded for 2017, 19 images for 2018, and 14 images for 2019. Selected images were captured using the PlanetScope Dove network of 120 multispectral imagery satellites. The satellites captured four wavelength bands: Red (590 – 670 nm), Green (500 – 590 nm), Blue (455 – 515 nm), and NIR (780 – 860 nm). They have an analytic radiometric resolution of 16 bit and a spatial resolution of 3 meters (Planet Team, 2017). Downloaded images were analyzed using ENVI (Version 5.3). The top of atmosphere correction was performed using the metadata included with the image. The band values were then extracted for calculated vegetation indices.

Vegetation indices (VI's) were manually calculated from the extracted band values. The following vegetation indices were calculated: Normalized Difference Vegetation Index (NDVI), Soil Adjusted Vegetation Index (SAVI), Weighted Difference Vegetation Index (WDVI), and Simplified Enhanced Vegetation Index (EVI). The equations for these indices are as follows:

$$NDVI = \frac{(NIR - RED)}{(NIR + RED)}$$

$$SAVI = \frac{(1 + 0.5)(NIR - RED)}{(NIR + RED + 0.5)}$$

$$WDVI = NIR - (1.06 * RED)$$

$$EVI = 2.5 * \frac{(NIR - RED)}{(1 + NIR + 2.4 * RED)}$$

Daily values for each VI were calculated by linearly interpolating between the known points using a manual calculation.

3.2.3. Eddy Covariance Data Processing

Continuous 10 Hz measurements of CO_2 flux were collected using an eddy covariance system (EC). The EC system consisted of a C-SAT3 Sonic Anemometer (Campbell Scientific, Logan, UT, USA) and an LI-7500 Infrared Gas Analyzer (IRGA; LI-COR, Lincoln, NE, USA). The Sonic Anemometer and IRGA were connected to LI-COR's SmartFlux system, which used EddyPro software (Version 6.2.2) to process the data collected at 10 Hz and compiled it into 30-minute summary files. The 30-minute summary files, along with the raw data, were saved to a USB drive for manual data collection. Eddy covariance instruments were installed facing south (the direction of the prevailing winds) on a tripod alongside additional meteorological instruments and maintained at 2 meters above the plant canopy. The IRGA was calibrated and had its internal chemicals (CO_2 and H_2O scrubbers) replaced annually, as recommended by the manufacturer.

Additional meteorological instrumentation consisted of a Temperature and Relative Humidity Probe (HMP155A, Vaisala, Vantaa, Finland), a Quantum Sensor (Plant Available Radiation (PAR); LI-190R, Li-COR, Lincoln, NE, USA), a

Pyranometer (LI-200R, LI-COR, Lincoln, NE, USA), a Net Radiometer (NR-LITE2, Kipp and Zonen, Delft, Netherlands), and a Rain Gauge (TE525, Texas Electronics, Dallas, TX, USA). Soil instruments consisted of seven soil moisture sensors (CS655, Campbell Scientific, Logan, UT, USA), four soil thermocouples (TCAV, Campbell Scientific, Logan, UT, USA), and four soil heat flux plates (HPF01SC Hukseflux, Delft, Netherlands). Three soil moisture sensors were placed horizontally at a depth of 4 cm; two were placed vertically between 10 and 20 cm, and the last two were placed vertically between 20 and 30 cm. Soil thermocouples were buried at 2 and 6 cm above the soil heat-flux plates. Soil heat-flux plates were placed in pairs, 1 meter apart, and buried at eight cm. Additional meteorological instruments and soil instruments were connected to a CR3000 datalogger (Campbell Scientific, Logan, UT, USA). Readings from the instruments were collected every 2 seconds and compiled into 30-minute summaries.

EddyPro (edition 6.2.2) computed the fluxes directly in the SmartFlux system, using a sign convention where positive numbers indicate fluxes away from the canopy (emission) and negative numbers indicate fluxes toward the canopy (sequestration). EddyPro performed a number of corrections before computing NEE fluxes. This includes coordinate rotation, frequency response corrections, corrections for air density fluctuations and sensor separation delays (Webb et al., 1980; Paw et al., 2000; Finnigan et al., 2003; Burba, 2013; Carmelita et al., 2014; LI-COR, 2015; Qin et al., 2016).

EddyPro also flagged data quality based on internal turbulence tests. High-quality data was marked with a “0”, moderate quality with a “1” and low quality with a

"2". Low-quality points were manually removed during data inspection for gap filling. Gap filling was used to fill in missing and removed data points. Gap filling and flux partitioning (partitioning CO_2 uptake {GPP} and respiration {R_{eco}}) were done simultaneously using the Max Plank Institute for Biogeochemistry's R program (R Gui 3.4.1) using their nighttime-based flux partitioning method (Reichstein et al., 2005; Fritz et al., 2018). This program fills data gaps based on an algorithm that uses meteorological conditions to calculate the missing data. If full meteorological data (temperature, humidity, and radiation) is available, then the missing value was filled using a data point with similar conditions within a 14-day window of the missing point. If meteorological data is partial or missing, then the program used linear interpolation based on time of day to gap-fill (Fritz et al., 2018; Reichstein et al., 2005). The same program also separates NEE fluxes into its component fluxes, assimilatory fluxes (GPP) and respiratory fluxes (R_{eco}). A reference temperature-based method based is used to estimate R_{eco}. The GPP flux is then calculated by subtracting R_{eco} from NEE (Aubinet et al., 2012; Reichstein et al., 2005).

3.2.4. Phenology Data Collection

Plant samples were collected every other week from six randomly selected areas within the field, three from each soil type. At each location, 15 plants were randomly selected and measured for height, growth stage, leaf area, and aboveground biomass. Plant height was measured from the top of the soil to the whorl and the plant stage was determined via manual inspection. Leaf area and biomass were measured via destructive sampling. Leaves, stems, and reproductive structures were separated manually. Leaf area

was measured by passing sampled leaves through an LI-3100 leaf area meter (LI-COR, Lincoln, NE, USA). The plant matter was then placed in brown paper bags and was oven-dried at 40°C and until sample weight was stable.

3.2.5. Model Development and Validation

Previous modeling work has established that GPP is proportional to light use efficiency (LUE) multiplied by the fraction of absorbed PAR (fPAR) and PAR (Monteith, 1977). In order to make this model more user-friendly, a few changes have been proposed by multiple authors. Primary productivity has been shown to be proportional to VI * PAR in a similar manner to LUE * PAR for a wide variety of crops, including corn (Gitelson et al., 2012; Peng and Gitelson, 2012; Alganci et al., 2014; He et al., 2018; Zheng et al., 2018). Additionally, Leaf Area Index (LAI) has been shown to correlate well with fPAR in grasslands and croplands where LAI < 4, which is typical of row crops including corn (Asrar et al., 1984; Glenn et al., 2008; Gitelson, 2019). As such, the model we are proposing is as follows:

$$GPP \propto VI * LAI * PAR$$

Where VI is obtained from the PlanetScope imagery data, LAI is obtained from destructive plant sampling, and PAR is obtained from the Quantum Sensor. The model was developed using the 2017 data and validated using the 2018 and 2019 data. For the 2017 data, VI * LAI * PAR was regressed against EC GPP using the linear model in Sigmaplot (Version 14.0). The equation of the regression curve was then applied to 2018 and 2019 data for model validation as follows:

$$GPP = slope * (VI * LAI * PAR) + intercept$$

Where the slope and intercept are from the linear regression using the 2017 data. Modeled GPP was then compared to measured GPP statically using Sigmaplot (Version 14.0) and R Gui (Version 3.4.1).

3.2.6. Statistical Analysis

The regression analysis was performed using Sigmaplot (Version 14.0). Root mean square error and standard error of the estimate were calculated manually. The index of agreement (d-index) was calculated manually using the following equation:

$$d = 1 - [\frac{\sum(x - \bar{x})^2}{\sum(|x - \bar{x}| + |y - \bar{y}|)^2}$$

Where x is the modeled value and y is the observed value. The d-index shows the degree of agreement between the modeled data and the measured data. A perfect 1:1 fit between the modeled and measured data will give a d-index of 1 and no correlation will give a d-index of 0 (Adhikari et al., 2016; Basso et al., 2016; Sharma et al., 2017). The slope of the linear regression between the modeled GPP and the measured GPP was compared to 1.0 using a t-test in R Gui (Version 3.4.1).

3.3. Results and Discussion

3.3.1. Vegetation Indices

There were some differences in the pattern of vegetation indices between the three seasons, which are shown in Figure 12. In 2017, NDVI increased more slowly over the course of the season and then declined more slowly during the senescence period when compared to 2018 and 2019. In 2018 and 2019, NDVI increased rapidly during the early vegetative growth season. However, the post-maturity senesce period in 2019 was

slower and followed a similar pattern to that of 2017. The maximum NDVI was 0.58 in 2017, 0.64 in 2018, and 0.57 in 2019. During the early growing season, SAVI was very similar between all three years. After approximately DOY 120, SAVI for 2018 continued to increase and remained above 2017 SAVI for the rest of the season. SAVI for 2019 did not continue to increase after DOY 120; however, the senescence period was more gradual compared to the previous two years. WDVI and EVI followed similar seasonal patterns. In both, the VI was higher in 2017 for the majority of the growing seasons compared to 2018 and 2019. The 2018 maximum WDVI and EVI was higher than that of 2019, however, both VI's dropped off quickly after maturity in 2018 but declined slowly during the senescence phase of 2019.

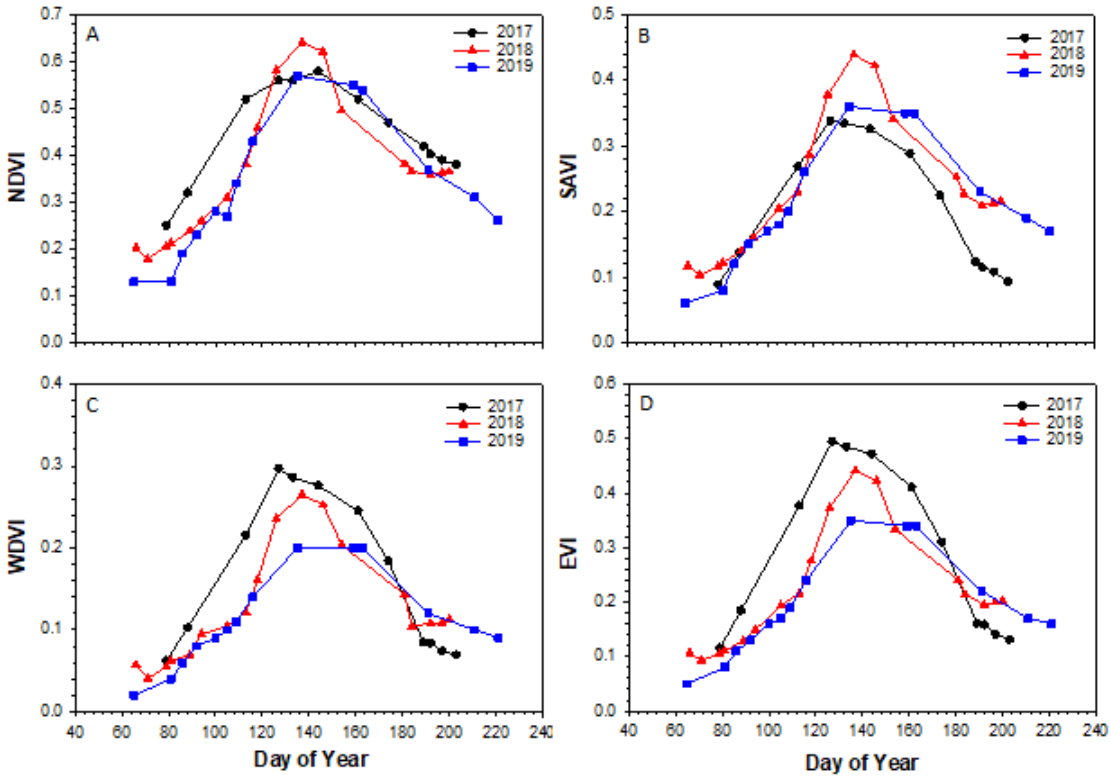

Figure 12: Vegetation Indices Over Corn Growing Season
Vegetation indices over the growing seasons are shown above. Image "A" refers to NDVI. Image "B" refers to SAVI. Image "C" refers to WDVI. Image "D" refers to EVI. Black lines with circles refer to 2017, red lines with triangles refer to 2018, and blue lines with squares refer to 2019.

3.3.2. Observed Gross Primary Productivity

There were some differences in measured GPP between the three seasons. Daily growing season GPP is shown in Figure 13. There was greater daily carbon uptake in the early part of the 2017 season compared to the 2018 and 2019 seasons. There was more carbon uptake in the senescence phase of the 2019 growing season compared to that of 2017 and

2018. The 2018 growing season had a larger daily maximum GPP (26.8 g C m^{-2}) than that of 2017 (20.9 g C m^{-2}) and 2019 (20.0 g C m^{-2}). These differences are likely explained by differences in soil temperature and moisture content between the years. March 2017 was warmer than 2018 and 2019 (Monthly average temperature of 19.1°C compared to 18.0°C in 2018 and 14.7°C in 2019), likely leading to more rapid seedling growth after planting. May and June of 2018 (25.6°C and 28.2°C, respectively) were warmer than that of 2017 (23.3°C 26.8°C) and 2019 (24.2°C 26.7°C). Higher temperatures increase the rate of metabolism, causing greater respiration and photosynthesis, which accounts for some of the differences in daily GPP between the three years (Wharton et al., 2012; Rajan et al., 2013a; Vitale et al., 2016; Zapata et al., 2017). Total growing season precipitation was 451.6 mm in 2017, 330.0 mm in 2018, and 618.5 mm in 2019. Greater precipitation in 2019 led to a slower decline in GPP following crop maturity. There was a small increase in GPP prior to harvest in 2019 due to the growth of warm-season weeds, particularly Bermuda grass *(Cynodon dactylon)* and Palmer amaranth (*Amaranthus palmeri*), greater soil moisture likely fueled this growth of weeds. Previous studies have found that weed growth can contribute significantly to GPP (Collins et al., 1999; Ibell et al., 2010; Sonnentag et al., 2011).

Despite some differences in the seasonal pattern of GPP, total carbon uptake between the three years was similar. Cumulative growing season GPP was 1360.8 g C m^{-2} in 2017, 1407.9 g C m^{-2} in 2018, and 1373.8 g C m^{-2} in 2019. The higher temperatures during the late vegetative and early reproductive stages in 2018 likely contributed to the greater cumulative GPP in 2018. Despite the higher cumulative and

daily maximum GPP in 2018, the aboveground crop biomass was less than that of 2017 and 2019. The maximum crop biomass was 12,800 kg ha^{-1} in 2017, 10,333 kg ha^{-1} in 2018, and 11,350 kg ha^{-1} in 2019. Warm and dry conditions can lead to a greater portion of GPP being allocated to respiration rather than biomass accumulation (Rajan et al., 2013b; Zapata et al., 2017).

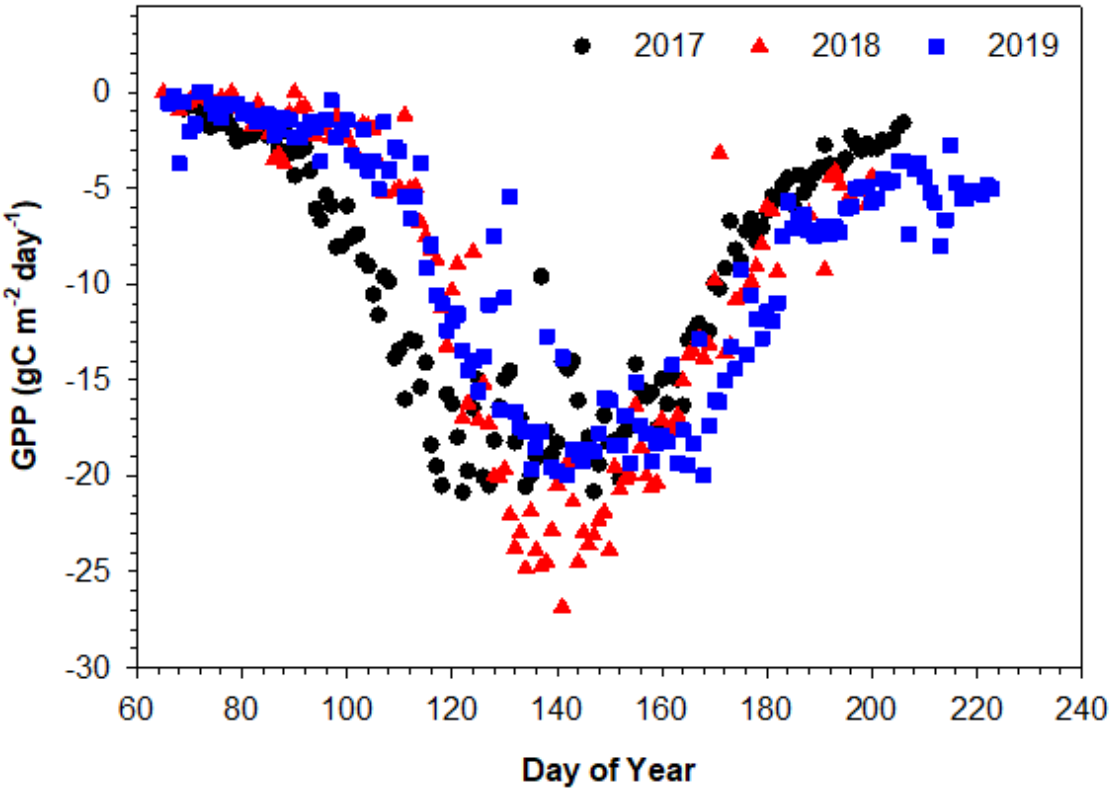

Figure 13: Daily Gross Primary Productivity for Corn
Daily gross primary productivity (GPP) for the three growing seasons is shown above. The period shown is from planting until harvest. Black circles represent 2017, red triangles represent 2018, and blue squares represent 2019.

3.3.3. Model Development

The models were developed by using the 2017 data to create a linear regression model of weekly averages of VI*PAR*LAI versus observed GPP. The sign of GPP was reversed for the purpose of model development and validation so that GPP is shown as a positive number. The linear models are shown in Figure 14 and their ANOVA tables are shown in Table 1. A separate linear model was created for each of the four selected vegetation indices using Sigmaplot's polynomial linear model. The models were all significant to $p < 0.0001$. The NDVI-based model had a slightly worse correlation with GPP ($r^2 = 0.92$) compared to those with the other VI's ($r = 0.95$). The RMSE for the fit between GPP and VI*PAR*LAI was 1.94 g C m^{-2} for NDVI, 1.49 g C m^{-2} for SAVI, 1.56 g C m^{-2} for WDVI, and 1.48 g C m^{-2} for EVI. The linear models were then used to estimate GPP for the 2018 and 2019 data. The linear model for NDVI is as follows:

NDVI: $GPP = 1.25 * (NDVI * LAI * PAR) + 1.90$

SAVI: $GPP = 2.22 * (SAVI * LAI * PAR) + 2.66$

WDVI: $GPP = 2.58 * (WDVI * LAI * PAR) + 2.87$

EVI: $GPP = 1.54 * (EVI * LAI * PAR) + 2.77$

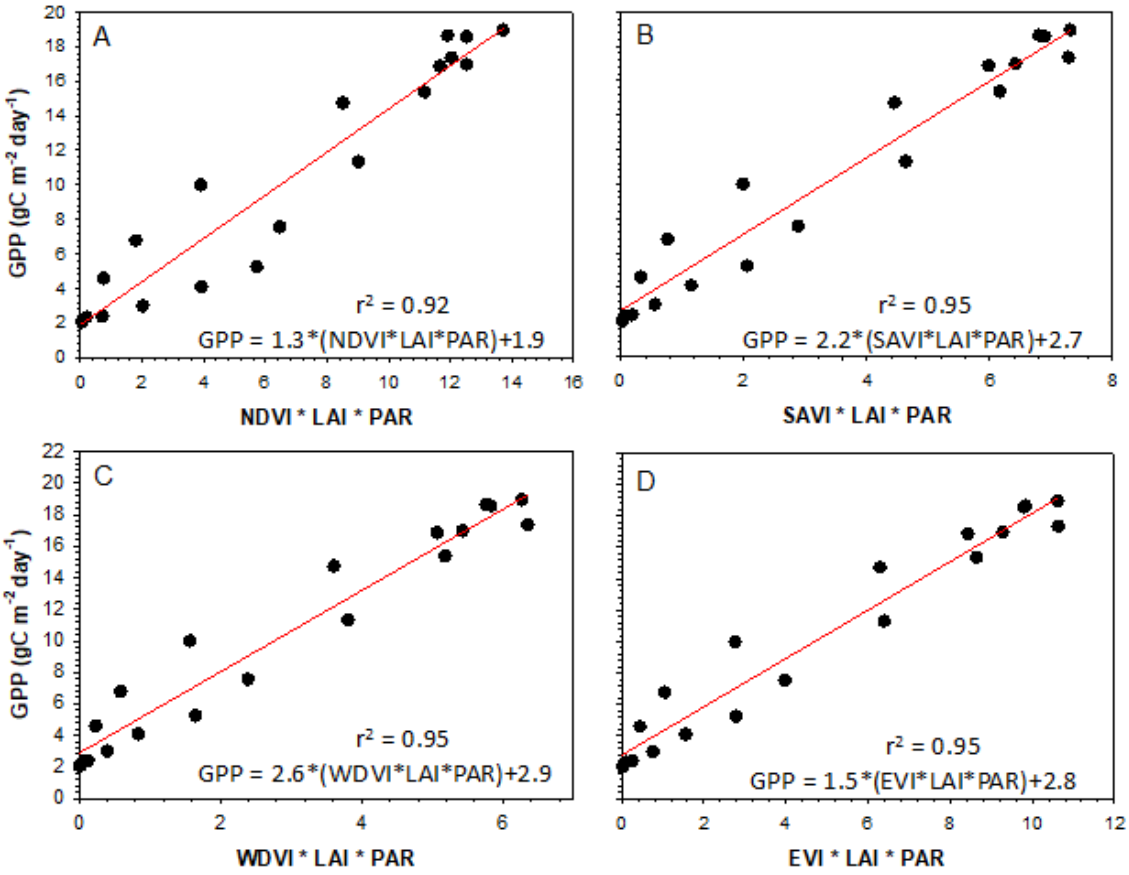

Figure 14: Corn VI based Models
The linear models for 2017 are shown above. The red line in each image refers to the best-fit model. Image "A" refers to NDVI. Image "B" refers to SAVI. Image "C" refers to WDVI. Image "D" refers to EVI. R-square and the best-fit equation are shown on the graphs.

Table 1: ANOVA for GPP versus VI*LAI*PAR

ANOVA for GPP versus VI * LAI * PAR					
NDVI					
	SS	MS	t	p	r^2
Regression	2738.2	1369.1	13.6	<0.0001	0.92
Residual	64.0	3.8			
Total	2802.2	147.5			
SAVI					
Regression	2764.4	1382.2	18.0	<0.0001	0.95
Residual	37.9	2.2			
Total	2802.2	147.5			
WDVI					
Regression	2761.6	1380.8	17.4	<0.0001	0.95
Residual	40.6	2.4			
Total	2802.2	147.5			
EVI					
Regression	2764.9	1382.4	18.2	<0.0001	0.95
Residual	37.4	2.2			
Total	2802.2	147.5			

3.3.4. Model Validation

The models developed were validated using data from 2018 and 2019. The validation using 2018 data is shown in Figure 15 and the validation using 2019 data is shown in Figure 16; with statistical analysis for both shown in Table 2. For the 2018 data, the NDVI, WDVI, and EVI-based models all underestimated the actual GPP, while the SAVI-based model came close to observed GPP. The SAVI-based model had a lower standard error (1.74 g C m^{-2}) than the other models (2.89 g C m^{-2} for NDVI, 3.62 g C m^{-2} for WDVI, and 3.72 g C m^{-2} for EVI). The t-test of the slope of the regression between modeled and observed data found that the NDVI, WDVI, and EVI models all had regression slopes that were significantly different from one. Conversely, the

regression slope for the SAVI-based model was not significantly different from 1.0, indicating an ideal fit between the modeled and measured GPP. All 2018 model validations had d-index values above 0.90, with the SAVI-based model having a d-index the closest to one (d-index 0.99).

For the 2019 data, the NDVI-based model significantly overestimated the actual GPP, while the WDVI and EVI-based models both underestimated the actual GPP. As with 2018, modeled GPP using the SAVI-based model was most similar to the observed GPP. The NDVI-based model produced a much higher error in 2019 than it did in 2018, 8.50 g C m^{-2} compared to 2.89 g C m^{-2}. The remaining three models from 2019 had a standard error similar to that of 2018, with the SAVI-based model having the lowest error (1.50 g C m^{-2} for SAVI, 3.21 g C m^{-2} for WDVI, and 3.10 g C m^{-2} for EVI). The t-test of the slope of the regression between modeled and observed GPP found that the slopes of the NDVI, WDVI, and EVI-based models all significantly differed from 1.0, while the SAVI-based model did not. The NDVI-based model had a low d-index, 0.79, compared to the other models, indicating less agreement between the modeled and observed GPP. The SAVI-based model had the d-index that was closest to 1.0 at 0.98. In both years, the SAVI-based model performed better than the other models.

While SAVI, WDVI, and EVI all preformed similarly for 2018 and 2019, there was a dramatic difference in the results of the NDVI-based model between the years. Differences in growing season weather conditions possibly affected model performance, possibly accounting for the dramatic difference in results with the NDVI-based model between 2018 and 2019. Weather conditions in the 2017 growing season (March – July)

were typical for the region with an average temperature of 23.84°C compared to the 30-year average of 23.67°C. Likewise, precipitation in 2017 was fairly typical with 451.6 mm of rain during the growing season compared to the 30-year average of 425.7 mm (National Oceanic and Atmospheric Administration, 2011). Compared to 2017 and the 30-year average, 2018 was unusually dry with only 330.0 mm of rain, and 2019 was unusually wet with 527.6 mm of rain. Average growing season temperatures were similar across 2018 and 2019 (23.65°C and 23.18°C, respectively). It is possible that the differences in weather conditions, particularly precipitation, were partly responsible for the differences in model success between the years, as similar trends have been observed in other studies. A large scale study of GPP modeling using the LUE method with satellite data at FLUXNET sites in Northeast China found that adding scalars for temperature and water stress improved the model success with the water stress scalar being particularly effective in croplands (Zheng et al., 2018). Plant water content has been found to affect reflectance across all wavelengths, which would alter vegetation indices (Ahlrichs and Bauer, 1983; Asrar et al., 1984). Additionally, changes in soil moisture and plant water stress can cause short-term changes in GPP that are not picked up by satellite-based methods because they have lower temporal resolution than EC measurements (Zhao et al., 2005; Yuan et al., 2010; Gitelson et al., 2012).

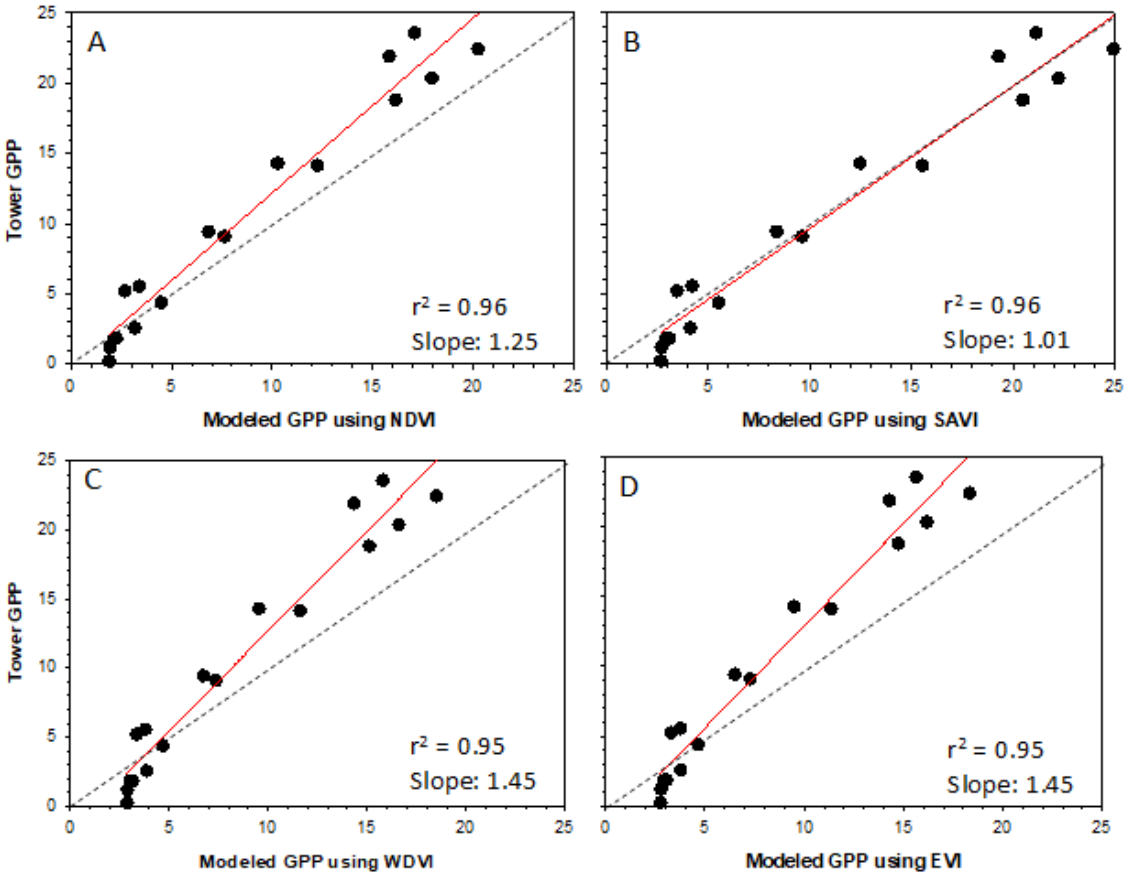

Figure 15: 2018 Corn GPP Model Validation
Model Validation with 2018 data is shown in the figure above. Image "A" refers to the model using NDVI. Image "B" refers to the model using SAVI. Image "C" refers to the model using WDVI. Image "D" refers to the model using EVI. The solid red line refers to the best-fit linear equation. The black dashed line refers to an ideal 1:1 line with a slope of one.

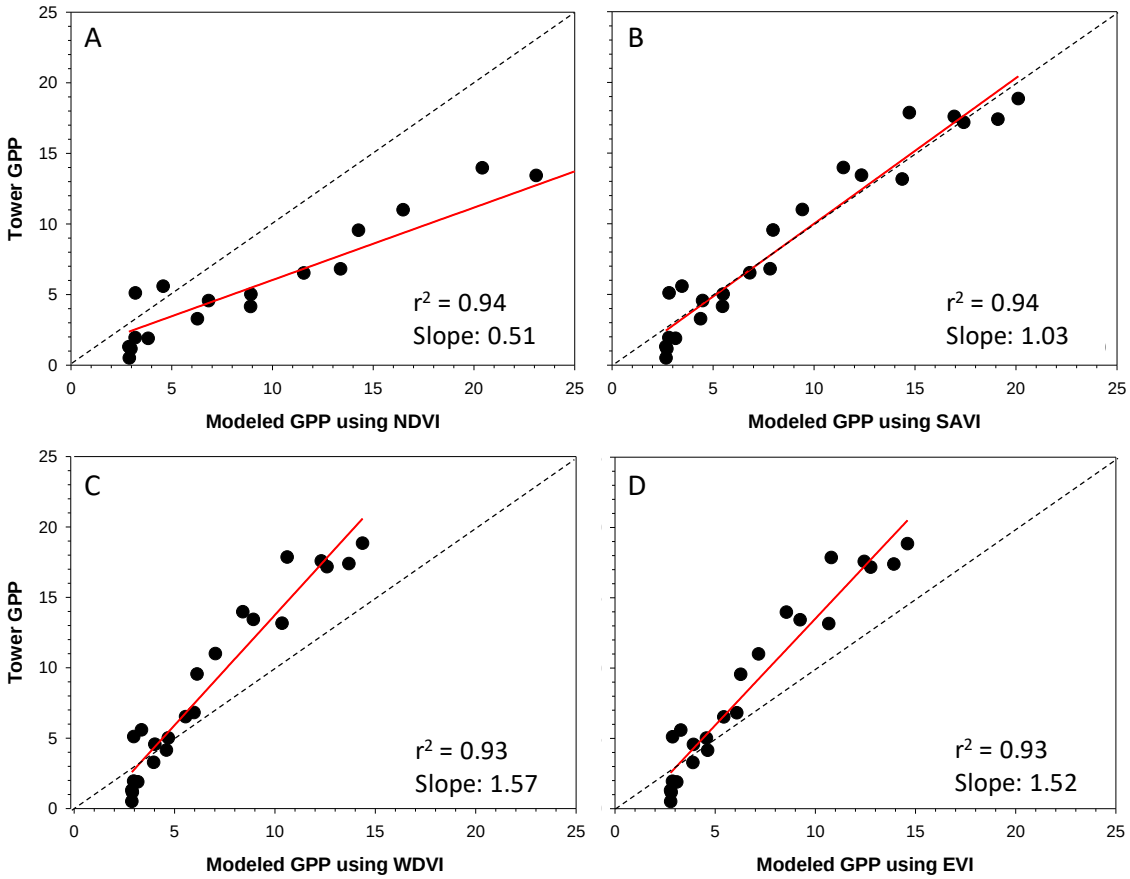

Figure 16: 2019 Corn GPP Model Validation
Model Validation with 2019 data is shown in the figure above. Image "A" refers to the model using NDVI. Image "B" refers to the model using SAVI. Image "C" refers to the model using WDVI. Image "D" refers to the model using EVI. The solid red line refers to the best-fit linear equation. The black dashed line refers to an ideal 1:1 line with a slope of one.

Table 2: Statistical Results for Model Validation

Statistical Results for Model Validation				
2018				
	RMSE	**D-index**	**Standard Error of Estimate**	**Does the slope of the model equal 1?**
NDVI	7.47	0.96	2.89	NO (>0.01)
SAVI	1.44	0.99	1.74	YES
WDVI	8.17	0.93	3.62	NO (>0.0001)
EVI	8.76	0.93	3.72	NO (>0.0001)
2019				
NDVI	30.73	0.79	8.50	NO (>0.0001)
SAVI	0.17	0.98	1.50	YES
WDVI	9.07	0.90	3.21	NO (>0.0001)
EVI	8.84	0.91	3.10	NO (>0.0001)

3.3.5. Implications for Producers

The model was able to simulate GPP, particularly the SAVI-based model. Other studies have found similarly successful results on efforts to model GPP using satellite-based methods (Zhao et al., 2005; Yan et al., 2009; Gitelson et al., 2012; Peng and Gitelson, 2012; Zhou et al., 2017). Tracking carbon dynamics from agricultural settings is important for determining the impacts of agricultural practices on the global carbon balance. Using models that have been validated with ground-truth observations such as this one, can improve estimates of carbon uptake. Given current proposals for regulating carbon in various industries, understanding carbon could become more important for producers. Keeping track of GPP in agricultural settings is beneficial beyond carbon monitoring. GPP correlates well with plant productivity and crop yield, and such models can be useful in precision agricultural by identifying highly productive zones (Gutierrez et al., 2012; Padilla et al., 2012; Johnson, 2016; He et al., 2018). Our research shows that

selection of vegetation index can make a difference in the success of the model. While NDVI may be the most commonly used vegetation index in agricultural settings, it may not always be the most appropriate. Producers may benefit from determining the best fit index for their cropping system (Ahlrichs and Bauer, 1983; Huete et al., 1997; Glenn et al., 2008).

3.4. Conclusions

There was a significant relationship between VI*LAI*PAR such that regression model of GPP was feasible. Given the good correlation values (r^2 above 0.9) for the 2017 regression of VI*LAI*PAR, that year's data was used as training data for model development. The models for each VI were validated using data from 2018 and 2019. The model using NDVI as the input vegetation index underestimated GPP in 2018 and overestimated GPP in 2019. The slope of the best fit between NDVI-modeled GPP and observed GPP was different from one in both years. The models using WDVI and EVI as inputs underestimated GPP in both validation years. The slope of the best fit between modeled and observed GPP was different from one for both EVI and WDVI for both years. The model using SAVI as the input slightly underestimated GPP in 2018 and slightly overestimated GPP in 2019; however, these differences were not statistically significant. The slope of the best fit between GPP modeled using SAVI and observed GPP was not different from one in both years, indicating and ideal fit between modeled and observed GPP. Differences in soil and weather conditions between the years likely affected the performance of the models, most significantly influencing the NDVI-based

model. The SAVI based model provided as more ideal fit likely because it better accounts for the effects of soil surface characteristics on reflectance values.

Overall, the variability of model results based on input vegetation index highlight the importance of selecting the ideal VI for a given situation. The model using SAVI as an input is likely to effective in other corn production systems in east-central Texas. The use of this modeling technique and new higher-resolution satellite data has the potential to improve estimates of carbon uptake from agricultural systems. While this study used ground-based inputs in the model (destructive LAI and PAR from the eddy covariance tower), all inputs can be obtained remotely. Future work on this would be to replace ground-based LAI and PAR terms with remote terms.

3.5. Acknowledgment

This work is supported by NIFA-NLGCA [grant no. 2016-70001-24636/project accession no. 1008730] from the USDA National Institute of Food and Agriculture. This work was also supported by Planet's "Education and Research Program", which provided free access to PlanetScope imagery data. The authors would like to thank Dr. Don T. Conlee (Department of Atmospheric Sciences, Texas A&M University) for providing missing meteorological data. The authors would also like to thank Texas A&M Agrilife and the staff at the research farm, particularly Mr. Alfred Nelson (Farm Manager) for managing the cornfield (planting, harvesting, fertilizing, tillage, and weed control).

3.6. References

Adhikari, P., S. Ale, J.P. Bordovsky, K.R. Thorp, N.R. Modala, N. Rajan, and E.M.

Barnes. 2016. Simulating future climate change impacts on seed cotton yield in the Texas High Plains using the CSM-CROPGRO-Cotton model. Agric. Water Manag. 164: 317–330. doi: 10.1016/j.agwat.2015.10.011.

Agam, N., W.P. Kustas, and M.C. Anderson. 2010. Application of the Priestley – Taylor Approach in a Two-Source Surface Energy Balance Model. Am. Meterorological Soc. 11: 185–198. doi: 10.1175/2009JHM1124.1.

Ahlrichs, J.S., and M.E. Bauer. 1983. Relation of Agronomic and Multispectral Reflectance Characteristics of Spring Wheat Canopies1. Agron. J. 75(6): 987–993. doi: 10.2134/agronj1983.00021962007500060029x.

Alganci, U., M. Ozdogan, E. Sertel, and C. Ormeci. 2014. Field Crops Research Estimating maize and cotton yield in southeastern Turkey with integrated use of satellite images , meteorological data and digital photographs. F. Crop. Res. 157: 8–19. doi: 10.1016/j.fcr.2013.12.006.

Altieri, M.A. 1999. The ecological role of biodiversity in agroecosystems. Agric. Ecosyst. Environ. 74(1–3): 19–31. doi: 10.1016/S0167-8809(99)00028-6.

Amouzou, K.A., J.B. Naab, J.P.A. Lamers, C. Borgemeister, M. Becker, and P.L.G. Vlek. 2018. CROPGRO-Cotton model for determining climate change impacts on yield, water- and N- use efficiencies of cotton in the Dry Savanna of West Africa. Agric. Syst. 165(November 2017): 85–96. doi: 10.1016/j.agsy.2018.06.005.

Anothai, J., C.M.T. Soler, A. Green, T.J. Trout, and G. Hoogenboom. 2013. Evaluation of two evapotranspiration approaches simulated with the CSM–CERES–Maize model under different irrigation strategies and the impact on maize growth,

development and soil moisture content for semi-arid conditions. Agric. For. Meteorol. 176(July): 64–76.

Anthoni, P.M., B.E. Law, and M.H. Unsworth. 1999. Carbon and water vapor exchange of an open-canopied ponderosa pine ecosystem. Agric. For. Meteorol. 95(3): 151–168. doi: 10.1016/S0168-1923(99)00029-5.

Asrar, G., M. Fuchs, E.T. Kanemasu, and J.L. Hatfield. 1984. (1984) Estimating Absorbed Photosynthetic Radiation and Leaf Area Index from Spectral Reflectance in Wheat (AJ).

Aubinet, M., T. Vesala, and D. Papale. 2012. Eddy Covariance: A Practical Guide to Measurement and Data Analysis. Springer Atmospheric Sciences, Berlin, Germany.

Bagavathiannan, M., and J.K. Norsworthy. 2012. Late-Season Seed Production in Arable Weed Communities: Management Implications. Weed Sci. 60(3): 325–334.

Bai, J., J. Wang, X. Chen, G.P. Lou, H. Shi, L.H. Li, and J. Li. 2015. Seasonal and inter-variations in carbon fluxes and evapotranspiration over cotton field under drip irrigation and plastic mulch in an arid region of Northwest China. J. Arid Land 7(2): 272–282.

Baker, J.M., and T.J. Griffis. 2005. Examining strategies to improve the carbon balance of corn / soybean agriculture using eddy covariance and mass balance techniques. Agric. For. Meteorol. 128: 163–177. doi: 10.1016/j.agrformet.2004.11.005.

Baldocchi, D.D. 2003. Assessing the eddy covariance technique for evaluating carbon dioxide exchange rates of ecosystems: past, present and future. Glob. Chang. Biol. 9(4): 479–492. doi: 10.1046/j.1365-2486.2003.00629.x.

Ballester, C., J. Brinkhoff, W.C. Quayle, and J. Hornbuckle. 2019. Monitoring the Effects of Water Stress in Cotton Using the Green Red Vegetation Index and Red Edge Ratio. Remote Sens. 11(7).

Baret, F., and G. Guyot. 1991. Potentials and limits of vegetation indices for LAI and APAR assessment. Remote Sens. Environ. 35(2–3): 161–173. doi: 10.1016/0034-4257(91)90009-U.

Basso, B., L. Liu, and J.T. Ritchie. 2016. A Comprehensive Review of the CERES-Wheat, -Maize and -Rice Models' Performances. Elsevier Inc.

Bednarz, C.W., and R.L. Nichols. 2005. Phenological and Morphological Components of Cotton Crop Maturity. Crop Sci. 45(4): 1497–1503.

Bell, J. 2017. Corn Growth Stages and Development.

Bennett, E.M., G.D. Peterson, and L.J. Gordon. 2009. Understanding relationships among multiple ecosystem services. Ecol. Lett. 12(12): 1394–1404. doi: 10.1111/j.1461-0248.2009.01387.x.

Boman, R., and R. Lemon. 2005. Soil Temperatures for Cotton Planting. College Station, Texas.

Boote, K.J., and N.B. Pickering. 1994. Modeling Photosynthesis of Row Crop Canopies. HortScience 29(12): 1423–1434.

Bozorov, T.A., R.M. Usmanov, H.L. Yang, S.A. Hamdullaev, S. Musayev, J. Shakiev, S. Nabiev, D.Y. Zhang, and A.A. Abdullaev. 2018. Effect of water deficiency on relationships between metabolism, physiology, biomass, and yield of upland cotton (Gossypium hirsutum L.). J. Arid Land 10(3): 441–456.

Bruinsma, J. 2003. World Agriculture: Towards 2015/2030.

Burba, G. 2013. Eddy Covariance Method (R Nelson, Ed.). LI-COR Biosciences, Lincoln, NE.

Carberry, P.S. 1991. Test of leaf-area development in CERES-Maize: a correction. F. Crop. Res. 27: 159–167.

Carmelita, M., R. Alberto, R. Wassmann, R.J. Buresh, J.R. Quilty, T.Q. Correa, J.M. Sandro, C. Arloo, and R. Centeno. 2014. Field Crops Research Measuring methane flux from irrigated rice fields by eddy covariance method using open-path gas analyzer. F. Crop. Res. 160: 12–21. doi: 10.1016/j.fcr.2014.02.008.

Chen, J.M., A. Govind, O. Sonnentag, Y. Zhang, A. Barr, and B. Amiro. 2006a. Leaf area index measurements at Fluxnet-Canada forest sites. Agric. For. Meteorol. 140(1): 257–268.

Chen, H., H. Tian, M. Liu, J. Melillo, S. Pan, and C. Zhang. 2006b. Effect of Land-Cover Change on Terrestrial Carbon Dynamics in the Southern United States. J. Environ. Qual. 35(4): 1533. doi: 10.2134/jeq2005.0198.

Collatz, G.J., J.T. Ball, C. Grivet, and J.A. Berry. 1991. Physiological and environmental regulation of stomatal conductance, photosynthesis and transpiration: a model that includes a laminar boundary layer. Agric. For. Meteorol. 54(2–4): 107–136. doi: 10.1016/0168-1923(91)90002-8.

Collins, H.P., R.L. Blevins, L.G. Bundy, D.R. Christienson, W.A. Dick, D.R. Huggins, and E.A. Paul. 1999. Soil Carbon Dynamics in Corn-Based Agroecosystems: Results from Carbon-13 Natural Abundance. Soil Sci. Soc. Am. J. 63(3): 584–591.

Contay, W.C., J.J. Burke, J.R. Mahan, J.E. Neilsen, and B.G. Sutton. 2012. Determining the Optimum Plant Temperature of Cotton Physiology and Yield to Improve Plant-Based Irrigation and Scheduling. Crop Sci. 52(July): 1828–1836.

Cook, B.D., K.J. Davis, W. Wang, A. Desai, B.W. Berger, R.M. Teclaw, J.G. Martin, P. V. Bolstad, P.S. Bakwin, C. Yi, and W. Heilman. 2004. Carbon exchange and venting anomalies in an upland deciduous forest in northern Wisconsin, USA. Agric. For. Meteorol. 126(3–4): 271–295. doi: 10.1016/j.agrformet.2004.06.008.

Daughtry, C. 2000. Estimating Corn Leaf Chlorophyll Concentration from Leaf and Canopy Reflectance. Remote Sens. Environ. 74(2): 229–239. doi: 10.1016/S0034-4257(00)00113-9.

Dejonge, K.C., and K.R. Thorp. 2017. Implementing Standardized Reference Evapotranspiration and Dual Crop Coefficient Approach in the DSSAT Cropping System Model. Am. Soc. Agric. Biol. Eng. 60(6): 1965–1981.

Dettori, M., C. Cesaraccio, A. Montroni, D. Spano, and P. Duce. 2011. Using CERES-Wheat to simulate durum wheat production and phenology in Southern Sardinia, Italy. F. Crop. Res. 120(1): 179–188.

Dokoohaki, H., M. Gheysari, S.F. Mousavi, S. Zand-Parsa, F.E. Miguez, S.V. Archontoulis, and G. Hoogenboom. 2016. Coupling and testing a new soil water module in DSSAT CERES-Maize model for maize production under semi-arid condition. Agric. Water Manag. 163(1): 90–99.

Dolman, A.J., J. Noilhan, P. Durand, C. Sarrat, A. Brut, B. Piguet, A. Butet, N. Jarosz, Y. Brunet, D. Loustau, E. Lamund, L. Tolk, R. Ronda, F. Miglietta, B. Gioli, V.

Magliulo, M. Esposito, C. Gerbig, S. Korner, P. Glademard, M. Ramonet, P. Ciais, B. Neininger, R.W.A. Hutjes, J.A. Elbers, R. Macatangay, O. Schrems, G. Perez-Landa, M.J. Sanz, Y. Scholz, G. Facon, E. Ceschia, and P. Beziat. 2006. The CarboEurope Regional Experiment Strategy. Am. Meteorol. Soc. (October): 1367–1379.

Doorenbos, J., and W.D. Pruitt. 1977. Guidelines for Predicting Crop Water Use. Rome, Italy.

Finnigan, J.J., R. Clement, Y. Malhi, R. Leuning, and H.A. Cleugh. 2003. A Re-Evaluation of Long-Term Flux Measurement Techniques Part 1: Averaging and Coordinate Rotation. Boundary-Layer Meteorol. (107): 1–48.

Foley, J.A., R. Defries, G.P. Asner, C. Barford, G. Bonan, S.R. Carpenter, F.S. Chapin, M.T. Coe, G.C. Daily, H.K. Gibbs, J.H. Helkowski, T. Holloway, E.A. Howard, C.J. Kucharik, C. Monfreda, J.A. Patz, I.C. Prentice, N. Ramankutty, and P.K. Snyder. 2005. Global Consequences of Land Use. Science (80-.). 309(July): 570–574. doi: 10.1126/science.1111772.

Food and Agriculture Organization. 2016. Land Use.

Frankenberg, C., J.B. Fisher, J. Worden, G. Badgley, S.S. Saatchi, J.E. Lee, G.C. Toon, A. Butz, M. Jung, A. Kuze, and T. Yokota. 2011. New global observations of the terrestrial carbon cycle from GOSAT: Patterns of plant fluorescence with gross primary productivity. Geophys. Res. Lett. 38(17): 1–7. doi: 10.1029/2011GL048738.

Fritz, E., S. Richter, S. Schott, S. Hejja, and S. Trumbore. 2018. Partitioning Algorithm.

Max Planck Inst. Biogeochem.

Garbulsky, M.F., J. Penuelas, D. Papale, J. Ardo, M.L. Goulden, K. Gerard, A.D. Richardson, E. Rotenberg, E.M. Veenendall, and I. Filella. 2010. Patterns and controls of the variability of radiation use efficiency and primary productivity across terrestrial ecosystems. Glob. Ecol. Biogeogr. 19: 253–267.

Gitelson, A.A. 2019. Remote estimation of fraction of radiation absorbed by photosynthetically active vegetation : generic algorithm for maize and soybean. Remote Sens. Lett. 10(3): 283–291. doi: 10.1080/2150704X.2018.1547445.

Gitelson, A.A., Y. Peng, J.G. Masek, D.C. Rundquist, S. Verma, A. Suyker, J.M. Baker, J.L. Hat, and T. Meyers. 2012. Remote estimation of crop gross primary production with Landsat data. Remote Sens. Environ. 121: 404–414. doi: 10.1016/j.rse.2012.02.017.

Glenn, E.P., A.R. Huete, P.L. Nagler, and S.G. Nelson. 2008. Relationship Between Remotely-sensed Vegetation Indices, Canopy Attributes and Plant Physiological Processes: What Vegetation Indices Can and Cannot Tell Us About the Landscape. : 2136–2160.

Godwin, D.C., and C.A. Jones. 1991. Nitrogen dynamics in soil-plant systems. p. 287–321. *In* Modeling plant and soil systems. ASA, CSSA, and SSSA, Madison, Wisconsin.

Godwin, D.C., and U. Singh. 1998. Nitrogen balance and crop response to nitrogen in upland and lowland cropping systems. p. 55–77. *In* Tsuji, G.Y., Hoogenboom, G., Thornton, P.K. (eds.), Understanding options for agricultural production. System

approaches for sustainable agricultural development. Kluwer Academic Publishers, Dordrecht, Netherlands.

Gonias, E.D., D.M. Oosterhuis, and A.C. Bibi. 2011. Light interception and radiation use efficiency of okra and normal leaf cotton isolines. Environ. Exp. Bot. 72(2): 217–222.

Gonzalez-Dugo, M.P., C.M.U. Neale, L. Mateos, W.P. Kustas, J.H. Prueger, M.C. Anderson, and F. Li. 2009. A comparison of operational remote sensing-based models for estimating crop evapotranspiration. Agric. For. Meteorol. 149(11): 1843–1853. doi: 10.1016/j.agrformet.2009.06.012.

Guo, L.B., and R.M. Gifford. 2002. Soil carbon stocks and land use change: A meta analysis. Glob. Chang. Biol. 8(4): 345–360. doi: 10.1046/j.1354-1013.2002.00486.x.

Gutierrez, M., R. Norton, K.R. Thorp, and G. Wang. 2012. Association of Spectral Reflectance Indices with Plant Growth and Lint Yield in Upland Cotton. Crop Sci. 52(2): 849–857.

Gwathmey, C.O., D.D. Tyler, and X. Yin. 2010. Prospects for Monitoring Cotton Crop Maturity with Normalized Difference Vegetation Index. Agron. J. 102(5): 1352–1360.

Han, G., Q. Xing, J. Yu, Y. Luo, D. Li, L. Yang, G. Wang, P. Mao, B. Xie, and N. Mikle. 2014. Agricultural reclamation effects on ecosystem CO2exchange of a coastal wetland in the Yellow River Delta. Agric. Ecosyst. Environ. 196: 187–198. doi: 10.1016/j.agee.2013.09.012.

Harmel, R.D., D.R. Smith, R.L. Haney, and P.M. Allen. 2019. Comparison of nutrient loss pathways: Run-off and seepage flow in Vertisols. Hydrol. Process. 33(18): 2384–2393.

He, M., J.S. Kimball, M.P. Maneta, and B.D. Maxwell. 2018. Regional Crop Gross Primary Productivity and Yield Estimation Using Fused Landsat-MODIS Data. doi: 10.3390/rs10030372.

Hirschi, M., D. Michel, I. Lehner, and S.I. Seneviratne. 2017. A site-level comparison of lysimeter and eddy covariance flux measurements of evapotranspiration. Hydrol. Earth Syst. Sci. 21(3): 1809–1825. doi: 10.5194/hess-21-1809-2017.

Hoogenboom, G., J.W. Jones, C.H. Porter, P.W. Wilkens, K.J. Boote, W.D. Batchelor, L.A. Hunt, and G.Y. Tsuji. 2003. A Decision Support System for Agrotechnology Transfer Version 4.0. 4th ed. University of Hawaii, Honolulu, Hawaii.

Houghton, R.A. 2007. Balancing the Global Carbon Budget. Annu. Rev. Earth Planet. Sci. 35(1): 313–347. doi: 10.1146/annurev.earth.35.031306.140057.

Houghton, R.A., A. Baccini, and W.S. Walker. 2018. Where is the residual terrestrial carbon sink? Glob. Chang. Biol. 24(8): 3277–3279.

Howell, T.A., S.R. Evett, J.A. Tolk, and A.D. Schneider. 2004. Evapotranspiration of full-, deficit-irrigated, and dryland cotton on the Northern Texas High Plains. J. Irrig. Drain. Eng. 130(4).

Huemmrich, K.F., P. Campbell, D. Landis, and E. Middleton. 2019. Developing a common globally acceptable method for optical remote sensing of ecosystem light use efficiency. Remote Sens. Environ. 230.

Huete, A.R., H.Q. Liu, K. Batchily, and L. van W. J. 1997. A comparsion of vegetation indices over a Global set of TM images for EO -MODIS. Remote Sens. Environ. 59(Table 1): 440–451. doi: 10.1016/S0034-4257(96)00112-5.

Ibell, P.T., Z. Xu, and T.J. Blumfield. 2010. Effects of weed control and fertilization on soil carbon and nutrient pools in an exotic pine plantation of subtropical Australia. J. Soils Sediments (10): 1027–1038. doi: 10.1007/s11368-010-0222-6.

Ibrahim, M.E., and D.R. Buxton. 1981. Early Vegetative Growth of Cotton as Influenced by Leaf Type. Crop Sci. 21(5): 639–643.

Jaafar, H.H., and F.A.. Ahmad. 2015. Relationships Between Primary Production and Crop Yields in Semi-Arid and Arid Irrigated Agroecosystems. Int. Symp. Remote Sens. Environ. 47(W3): 27–30.

Jalota, S.K., S. Sukhvinder, G.B.S. Chahal, S.S. Ray, S. Panigraphy, F. Bhupinder-Singh, and K.B.. Singh. 2010. Soil texture, climate and management effects on plant growth, grain yield and water use by rainfed maize–wheat cropping system: Field and simulation study. Agric. Water Manag. 97(1): 83–90.

Jans, W.W.P., C.M.J. Jacobs, B. Kruijt, J.A. Elbers, S. Barendse, and E.J. Moors. 2010. Carbon exchange of a maize (Zea mays L.) crop: Influence of phenology. Agric. Ecosyst. Environ. 139(3): 316–324. doi: 10.1016/j.agee.2010.06.008.

Johnson, D.M. 2016. A comprehensive assessment of the correlations between field crop yields and commonly used MODIS products. Int. J. Appl. EARTH Obs. Geoinf. 52: 65–81.

Jones, J.W. 1993. Decision Support System for agricultural development. p. 459–471. *In*

de Vries, F.P., Teng, P., Metselaar, K. (eds.), Systems Approaches for Agricultural Development. Kluwer Academic Publishers, Boston.

Jones, J.W., J.M. Antle, B. Basso, K.J. Boote, R.T. Conant, I. Foster, H.C.J. Godfray, M. Herrero, R.E. Howitt, S. Janssen, B.A. Keating, R. Munoz-Carpena, C.H. Porter, C. Rosenzweig, and T.R. Wheeler. 2017. Brief history of agricultural systems modeling. Agric. Syst. 155(June): 240–254. doi: 10.1016/j.agsy.2016.05.014.

Jones, J.W., K.J. Boote, G. Hoogenboom, S.S. Jagtap, and G.G. Wilkerson. 1989. Soybean Crop Growth Simulation Model. Gainsville.

Jones, J.W., G. Hoogenboom, C.H. Porter, K.J. Boote, W.D. Batchelor, L.A. Hunt, P.W. Wilkens, U. Singh, and A.J. Gijsman. 2003. The DSSAT Cropping System Model.

Jones, J.W., and J.T. Ritchie. 1991. Crop Growth Models. p. 63–89. *In* Hoffman, G.J., Howell, T.A., Soloman, K.H. (eds.), Management of Farm Irrigation System. 9th ed. American Society of Agricultural Engineers.

Kaplan, J.O., K.M. Krumhardt, E.C. Ellis, F. Ruddiman, C. Lemmen, and K.K. Goldewijk. 2010. Holocene carbon emissions as a result of anthropogenic land cover change. The Holocene 21(June). doi: 10.1177/0959683610386983.

Kerr, J.T., and M. Ostrovsky. 2003. From space to species: Ecological applications for remote sensing. Trends Ecol. Evol. 18(6): 299–305. doi: 10.1016/S0169-5347(03)00071-5.

Kessavalou, A., A.R. Mosier, J.W. Doran, R.A. Drijber, D.J. Lyon, and O. Heinemeyer. 1998. Fluxes of Carbon Dioxide, Nitrous Oxide, and Methane in Grass Sod and Winter Wheat-Fallow Tillage Management. J. Environ. Qual. (27): 1094–1104.

King, A.W., L. Dilling, G.P. Zimmerman, D.M. Fairman, R.A. Houghton, G.H. Marland, A.Z. Rose, and T.J. Wilbanks. 2007. The North American Carbon Budget and Implications for the Global Carbon Cycle.

L'Ecuyer, T.S., H.K. Beaudoing, M. Rodell, W. Olson, B. Lin, S. Kato, C.A. Clayson, E. Wood, J. Sheffield, R. Adler, G. Huffman, M. Bosilovich, G. Gu, F. Robertson, P.R. Houser, D. Chambers, J.S. Famiglietti, E. Fetzer, W.T. Liu, X. Gao, C.A. Schlosser, E. Clark, D.P. Lettenmaier, and K. Hilburn. 2015. The observed state of the energy budget in the early twenty-first century. J. Clim. 28(21): 8319–8346. doi: 10.1175/JCLI-D-14-00556.1.

Laitala, K., and I.G. Klepp. 2015. Age and active life of clothing. Prod. Lifetimes Environ.: 182–186.

Lal, R. 2004. Soil Carbon Sequestration Impacts on Global Climate Change and Food Security. Am. Assoc. Adv. Sci. 304(5677): 1623–7. doi: 10.1126/science.1097396.

LI-COR. 2015. SmartFlux System Instruction Manual.

Li, S., S. Kang, F. Li, and L. Zhang. 2008. Evapotranspiration and crop coefficient of spring maize with plastic mulch using eddy covariance in northwest China. Agric. Water Manag. 95(11): 1214–1222. doi: 10.1016/j.agwat.2008.04.014.

Li, X., L. Liu, H. Yang, and Y. Li. 2018. Relationships between carbon fluxes and environmental factors in a drip-irrigated, film-mulched cotton field in arid region. PLoS One 13(2): 1–18. doi: 10.1371/journal.pone.0192467.

Lindsey, R. 2009. Climate and Earth's Energy Budget. NASA Earth Obs.: 1–12. doi: 10.1007/s10712-011-9165-8.

Liu, P. 2017. The future of food and agriculture: Trends and challenges.

Lopez-Cedron, F.X., K.J. Boote, J. Pineiro, and F. Sau. 2008. Improving the CERES-Maize model ability to simulate water deficit impact on maize production and yield components. Agron. J. 100: 296–307.

Main, C.L. 2012. Cotton Growth and Development.

Matocha, M., C. Allen, R. Boman, G. Morgan, and P. Baumann. 2009. Crop Profile for Cotton in Texas. College Station, Texas.

Meyers, T.P. 2001. A comparison of summertime water and CO2fluxes over rangeland for well watered and drought conditions. Agric. For. Meteorol. 106(3): 205–214. doi: 10.1016/S0168-1923(00)00213-6.

Modala, N.R., S. Ale, N. Rajan, C.L. Munster, P.B. DeLaune, K.R. Thorp, S.S. Nair, and E.M. Barnes. 2015. Evaluation of the CSM-CROPGRO-COTTON MODEL for the Texas Rolling Plains Region and Simulation of Deficit Irrigation Strategies for Increasing Water Use Efficiency. Trans. ASABE 58(3): 658–696.

Möller, M., J. Tanny, Y. Li, and S. Cohen. 2004. Measuring and predicting evapotranspiration in an insect-proof screenhouse. Agric. For. Meteorol. 127(1–2): 35–51. doi: 10.1016/j.agrformet.2004.08.002.

Monteith, J.L. 1977. Climate and Efficiency of Crop Production in Britain. Phil. Trans. R. Soc. Lond. 281(980).

Monteith, J.L. 1986. How do crops manipulate water supply and demand ? Phil. Trans. R. Soc. Lond. 316: 245–259.

Mu, Q., M. Zhao, and S.W. Running. 2011. Improvements to a MODIS global terrestrial

evapotranspiration algorithm. Remote Sens. Environ. 115(8): 1781–1800. doi: 10.1016/j.rse.2011.02.019.

Mubeen, M., A. Ahmad, T. Khaliqu, and A. Bakhsh. 2013. Evaluating CSM-CERESMaize model for irrigation scheduling in semi-arid conditions of Punjab, Pakistan. Int. J. Agric. Biol. 15(1): 1–10.

Murty, D., M.U.F. Kirschbaum, R.E. Mcmurtrie, and H. Mcgilvray. 2002. Does conversion of forest to agricultural land change soil carbon and nitrogen? A review of the literature. Glob. Chang. Biol. 8(2): 105–123. doi: 10.1046/j.1354-1013.2001.00459.x.

Myneni, R.B., R.R. Nemani, and S.W. Running. 1997. Estimation of global leaf area index and absorbed par using radiative transfer models. IEEE Trans. Geosci. Remote Sens. 35(6): 1380–1393.

National Oceanic and Atmospheric Administration. 2011. Climate Data Online. Natl. Centers Environ. Inf.

Oki, T., and K. Shinjiro. 2006. Global Hydrological Cycles and World Water Resources. Science (80-.). 313(August): 1068–1073.

Pace, P.F., H.T. Cralle, S.H.M. El-Halawany, J.T. Cothren, and S.A. Senseman. 1999. Drought-induced Changes in Shoot and Root Growth of Young Cotton Plants. J. Cotton Sci. 3(183–187).

Padilla, F.L.M., S.J. Maas, M.P. Gonzalez-Dugo, N. Rajan, F. Mansilla, P. Gavilan, and J. Dominguez. 2012. Wheat Yield Monitoring in Southern Spain Using the GRAMI Model and a Series of Satellite Images. F. Crop. Res. 139(29): 145–145.

Pathak, T.B., J.W. Jones, C.W. Fraisse, D. Wright, and G. Hoogenboom. 2012. Uncertainty analysis and parameter estimation for the CSM-CROPGRO-cotton model. Agron. J. 104(5): 1363–1373. doi: 10.2134/agronj2011.0349.

Patil, N.G., and G.S. Rajput. 2009. Evaluation of Water Retention Functions and Computer Program "Rosetta" in Predicting Soil Water Characteristics of Seasonally Impounded Shrink-Swell Soils. J. Irrig. Drain. Eng. 135(3): 286–294.

Paw, K.T., D.D. Baldocchi, T.P. Meyers, and K.B. Wilson. 2000. Correction of Eddy-Covariance Measurements Incorporating Both Advective Effects and Density Fluxes. Boundary-Layer Meteorol. (47): 487–511.

Pegelow, E.J., D.R. Buxton, R.E. Briggs, H. Muramoto, and W.G. Gensler. 1977. Canopy Photosynthesis and Transpiration of Cotton as Affected by Leaf Type. Crop Sci. 17(1): 1–4.

Peng, Y., and A.A. Gitelson. 2011. Application of chlorophyll-related vegetation indices for remote estimation of maize productivity. Agric. For. Meteorol. 151(9): 1267–1276.

Peng, Y., and A.A. Gitelson. 2012. Remote estimation of gross primary productivity in soybean and maize based on total crop chlorophyll content. Remote Sens. Environ. 117: 440–448. doi: 10.1016/j.rse.2011.10.021.

Peng, Y., A.A. Gitelson, G. Keydan, D.C. Rundquist, and W. Moses. 2011. Remote estimation of gross primary production in maize and support for a new paradigm based on total crop chlorophyll content. Remote Sens. Environ. 115(4): 978–989.

Pettigrew, W.T. 2004. Physiological Consequences of Moisture Deficit Stress in Cotton.

Crop Sci. 44(4): 1265–1272.

PhytoGen. 2019. PhytoGen Cotton Varieties. Corteva Agriscience. https://phytogencottonseed.com/varieties.

Planet Team. 2017. Planet Application Program Interface: In Space for Life on Earth. San Francisco, CA.

Planet Team. 2018. No Title. Planet Inc.

Priestly, C.H.B., and R.J. Taylor. 1972. On the Assessment of Surface Heat Flux and Evaporation Using Large-Scale Parameters. Mon. Weather Rev. 100(February): 81–92.

Qin, S., S. Li, S. Kang, T. Du, L. Tong, and R. Ding. 2016. Can the drip irrigation under film mulch reduce crop evapotranspiration and save water under the sufficient irrigation condition? Agric. Water Manag. 177: 128–137. doi: 10.1016/j.agwat.2016.06.022.

Rajan, N., S.J. Maas, and S. Cui. 2013a. Extreme Drought Effects on Carbon Dynamics of a Semi Arid Pasture. Crop Ecol. Physiol. 105(6): 1749–1760.

Rajan, N., S.J. Maas, and S. Cui. 2013b. Extreme Drought Effects on Carbon Dynamics of a Semi-arid Pasture. 2013 105(6): 1749–1760.

Ramankutty, N., A.T. Evan, C. Monfreda, and J.A. Foley. 2008. Farming the planet : 1 . Geographic distribution of global agricultural lands in the year 2000. 22(February 2007): 1–19. doi: 10.1029/2007GB002952.

Raper, T.B., J.J. Varco, and K.J. Hubbard. 2013. Canopy-Based Normalized Difference Vegetation Index Sensors for Monitoring Cotton Nitrogen Status. Agron. J. 105(5):

1345–1354.

Reichstein, M., E. Falge, D. Baldocchi, D. Papale, M. Aubinet, P. Berbigier, C. Bernhofer, N. Buchmann, T. Gilmanov, A. Granier, T. Grunwald, K. Havrankova, H. Ilvesniemi, D. Janous, A. Knohl, T. Laurila, A. Lohila, D. Loustau, G. Matteucci, T. Meyers, F. Miglietta, J.-M. Ourcival, J. Pumpanen, S. Rambal, E. Rotenberg, M. Sanz, J. Tenhunen, G. Seufert, F. Vaccari, T. Vesala, D. Yakir, and R. Valentini. 2005. On the separation of net ecosystem exchange into assimilation and ecosystem respiration : review and improved algorithm. Glob. Chang. Biol. (11): 1424–1439. doi: 10.1111/j.1365-2486.2005.001002.x.

Ringrose-Voase, A.J., and A.J. Nadelko. 2013. Deep drainage in a Grey Vertosol under furrow-irrigated cotton. Crop Pasture Sci. 64(12): 1155–1170.

Ritchie, J.T. 1972. Model for Predicting Evaporation from a Row Crop with Incomplete Cover. Water Resour. Res. 8(5): 1204–1213.

Ritchie, J.T. 1998. Soil water balance and plant stress. p. 41–54. *In* Tsuji, G.Y., Hoogenboom, G., Thornton, P.K. (eds.), Understanding options for agricultural production. System approaches for sustainable agricultural development. Kluwer Academic Publishers, Dordrecht, Netherlands.

Ritchie, G.L., C.W. Bednarz, P.H. Jost, and S.M. Brown. 2007. Cotton Growth and Development.

Ritchie, J.T., and S. Otter. 1985. Description and performance of CERES-Wheat: A User-oriented wheat yield model. ARS Wheat Yield Proj. 38: 159–175.

Ritchie, J.T., C.H. Porter, J. Judge, J.W. Jones, and A.A. Suleiman. 2009. Extension of

an Existing Model for Soil Water Evaporation and Redistribution under High Water Content Conditions. Soil Sci. Soc. Am. J. 73(3): 792. doi: 10.2136/sssaj2007.0325.

Ritchie, G.L., D.G. Sullivan, W.K. Vencill, C.W. Bednarz, and J.E. Hook. 2010. Sensitivities of Normalized Difference Vegetation Index and a Green/Red Ratio Index to Cotton Ground Cover Fraction. Crop Sci. 50(3): 1000–1010.

Rodell, M., H.K. Beaudoing, T.S. L'Ecuyer, W.S. Olson, J.S. Famiglietti, P.R. Houser, R. Adler, M.G. Bosilovich, C.A. Clayson, D. Chambers, E. Clark, E.J. Fetzer, X. Gao, G. Gu, K. Hilburn, G.J. Huffman, D.P. Lettenmair, W.T. Liu, F.R. Robertson, C.A. Schlosser, J. Sheffield, and E.F. Wood. 2015. The Observed State of the Water Cycle in the Early Twenty-First Century. J. Clim. 28(November): 8289–8318. doi: 10.1175/JCLI-D-14-00555.1.

Rost, S., D. Gerten, A. Bondeau, W. Lucht, and J. Rohwer. 2008. Agricultural green and blue water consumption and its influence on the global water system. Water Resour. Res. 44: 1–17. doi: 10.1029/2007WR006331.

Saigusa, N., S. Yamamoto, S. Murayama, H. Kondo, and N. Nishimura. 2002. Gross primary production and net ecosystem exchange of a cool-temperate deciduous forest estimated by the eddy covariance method. Agric. For. Meteorol. 112: 203–215.

Sakamoto, T., A.A. Gitelson, B.D. Wardlow, S.B. Verma, and A.E. Suyker. 2011. Estimating daily gross primary production of maize based only on MODIS WDRVI and shortwave radiation data. Remote Sens. Environ. 115(12): 3091–3101.

Saseendran, S.A., L. Ma, D.C. Nielsen, M.F. Vigil, and L.R. Ahuju. 2005. imulating

planting date effects on corn production using RZWQM and CERES-Maize models. Agron. J. 97(1): 58–71.

Sau, F., K.J. Boote, M. Bostick, J.W. Jones, and M.I. Minguez. 2004. Testing and Improving Evapotranspiration and Soil Water Balance of the DSSAT Crop Models. Agron. J. 96(September): 1243–1257.

Schindler, D.W. 1999. The mysterious missing sink. Nature 398: 105–107.

Seligman, N.C., and H. Van Keulen. 1981. PAPRAN: a simulation model of annual pasture production limited by rainfall and nitrogen. p. 192–221. *In* Frissel, M.J., Van Veen, J.A. (eds.), Simulation of nitrogen behavior of soil-plant systems. Centrum voor Landbouwpublikaties en Landbouwdocumentatie, Wageningen, Netherlands.

Shafian, S., N. Rajan, R. Schnell, M. Bagavathiannan, J. Valasek, Y. Shi, and J. Olsenholler. 2018. Unmanned Aerial Systems-Based Remote Sensing for Monitoring Sorghum Growth and Development. PLoS One 13(5).

Sharma, S., N. Rajan, S. Cui, K. Casey, S. Ale, R. Jessup, and S. Maas. 2017. Seasonal variability of evapotranspiration and carbon exchanges over a biomass sorghum field in the Southern U.S. Great Plains. Biomass and Bioenergy 105: 392–401.

Shelton, M.L. 1987. Irrigation induced change in vegetation and evapotranspiration in the Central Valley of California. Landsc. Ecol. 1(2): 95–105.

Sinclair, T.R., and R.C. Muchow. 2001. System Analysis of Plant Traits to Increase Grain Yield on Limited Water Supplies. 93(2): 263–270.

Skinner, H.R. 2007. High Biomass Removal Limits Carbon Sequestration Potential of

Mature Temperate Pastures. J. Environ. Qual. 37(4): 1319–1326.

Smith, P., M. Bustamante, H. Ahammad, H. Clark, H. Dong, E.A. Elsiddi, H. Haberl, R. Harper, J. House, M. Jafari, O. Masera, C. Mbow, N.H. Ravindranath, C.W. Rice, C.R. Abad, A. Romanovskaya, F. Sperling, and F. Tubiello. 2014. Agriculture, forestry and other land use.

Snowden, M.C., G.L. Ritchie, F.R. Simao, and J.P. Bordovsky. 2014. Timing of Episodic Drought Can Be Critical in Cotton. Agron. J. 106(2): 452–458.

Soldevilla-Martinez, M., M. Quemada, R. Lopez-Urrea, R. Munoz-Carpena, and J.I. Lizaso. 2014. Soil water balance: Comparing two simulation models of different levels of complexity with lysimeter observations. Agric. Water Manag. 139(June): 53–63.

Soler, C.M.T., P.C. Sentelhas, and G. Hoogenboom. 2007. Application of the CSM-CERES-Maize model for planting date evaluation and yield forecasting for maize grown off-season in a subtropical environment. Eur. J. Agron. 27(2–4): 165–177. doi: 10.1016/j.eja.2007.03.002.

Sonnentag, O., M. Detto, R. Vargas, Y. Ryu, B.R.K. Runkle, M. Kelly, and D.D. Baldocchi. 2011. Agricultural and Forest Meteorology Tracking the structural and functional development of a perennial pepperweed (Lepidium latifolium L .) infestation using a multi-year archive of webcam imagery and eddy covariance measurements. Agric. For. Meteorol. 151(7): 916–926. doi: 10.1016/j.agrformet.2011.02.011.

Spera, S.A., G.L. Galford, and M.T. Coe. 2016. Land-use change affects water recycling

in Brazil ' s last agricultural frontier. Glob. Chang. Biol. 22: 3405–3413. doi: 10.1111/gcb.13298.

Suleiman, A.A., and G. Hoogenboom. 2007. Comparison of Priestley–Taylor and FAO-56 Penman–Monteith for daily reference evapotranspiration estimation in Georgia, USA. J. Irrig. Drain. Eng. 133(2).

Suleiman, A.A., and J.T. Ritchie. 2003. Modeling Soil Water Redistribution during Second-Stage Evaporation. Soil Sci. Soc. Am. J. 67(2): 377–386. doi: 10.2136/sssaj2003.0377.

Suleiman, A.A., C.M.T. Soler, and G. Hoogenboom. 2007. Evaluation of FAO-56 crop coefficient procedures for deficit irrigation management of cotton in a humid climate. Agric. Water Manag. 91(1): 33–42.

Suyker, A.E., S.B. Verma, G.G. Burba, T.J. Arkebauer, D.T. Walters, and K.G. Hubbard. 2004a. Growing season carbon dioxide exchange in irrigated and rainfed maize. Agric. For. Meteorol. 124(1–2): 1–13. doi: 10.1016/j.agrformet.2004.01.011.

Suyker, A.E., S.B. Verma, G.G. Burba, T.J. Arkebauer, D.T. Walters, and K.G. Hubbard. 2004b. Growing season carbon dioxide exchange in irrigated and rainfed maize. Agric. For. Meteorol. 124(1): 1–13.

Texas A&M Agrilife. 2019. Cotton Production Regions of Texas. Cott. Insect Manag. Guid.

Texas Parks and Wildlife. 2019. Post Oak Savannah and Blackland Prairie Wildlife Management. Habitats.

Thorp, K.R., E.M. Barnes, D.J. Hunsaker, and B.A. Kimball. 2014. Evaluation of CSM-CROPGRO-Cotton for Simulating Effects of Management and Climate Change on Cotton Growth and Evapotranspiration In An Arid Environment. Trans. ASABE 57(6): 1627–1642.

Thorp, K.R., D.J. Hunsaker, A.N. French, E. Bautista, and K.F. Bronson. 2015. Integrating geospatial data and cropping system simulation within a geographic information system to analyze spatial seed cotton yield, water use, and irrigation requirements. Precis. Agric. 16(5): 532–557.

Tian, H., G. Chen, M. Liu, C. Zhang, G. Sun, C. Lu, X. Xu, W. Ren, S. Pan, and A. Chappelka. 2010. Model estimates of net primary productivity, evapotranspiration, and water use efficiency in the terrestrial ecosystems of the southern United States during 1895-2007. For. Ecol. Manage. 259(7): 1311–1327. doi: 10.1016/j.foreco.2009.10.009.

Tscharntke, T., A.M. Klein, A. Kruess, I. Steffan-Dewenter, and C. Thies. 2005. Landscape perspectives on agricultural intensification and biodiversity - Ecosystem service management. Ecol. Lett. 8(8): 857–874. doi: 10.1111/j.1461-0248.2005.00782.x.

Tubiello, F.N., M. Salvatore, R.D. Cóndor Golec, A. Ferrara, S. Rossi, R. Biancalani, S. Federici, H. Jacobs, and A. Flammini. 2014. Agriculture, Forestry and Other Land Use Emissions by Sources and Removals by Sinks. ESS Work. Pap. No.2 2: 4–89. doi: 10.13140/2.1.4143.4245.

Twine, T.E., W.P. Kustas, J.M. Norman, D.R. Cook, P.R. Houser, and T.P. Meyers.

2000. Correcting eddy-covariance flux underestimates over a grassland. Agric. For. Meteorol. 103: 279–300.

Uddin, J., R.J. Smith, N.H. Hancock, and J.P. Foley. 2013. Evaporation and sapflow dynamics during sprinkler irrigation of cotton. Agric. Water Manag. 125: 35–45. doi: 10.1016/j.agwat.2013.04.001.

USDA-NASS. 2017. 2017 Census of Agriculture County Profile: Burleson County Texas.

Verlag, F., A.A. Gitelson, Y. Gritz, and M.N. Merzlyak. 2003. Relationships between leaf chlorophyll content and spectral reflectance and algorithms for non-destructive chlorophyll assessment in higher plant leaves. J. Plant Physiol. 160(3): 271–282.

Verma, S.B., A. Dobermann, K.G. Cassman, D.T. Walters, J.M. Knops, T.J. Arkebauer, A.E. Suyker, G.G. Burba, B. Amos, H. Yang, D. Ginting, K.G. Hubbard, A.A. Gitelson, and E.A. Walter-Shea. 2005. Annual carbon dioxide exchange in irrigated and rainfed maize-based agroecosystems. Agric. For. Meteorol. 131(1–2): 77–96. doi: 10.1016/j.agrformet.2005.05.003.

Vitale, L., P. Di Tommasi, G. D'Urso, and V. Magliulo. 2016. The response of ecosystem carbon fluxes to LAI and environmental drivers in a maize crop grown in two contrasting seasons. Int. J. Biometeorol. 60(3): 411–420. doi: 10.1007/s00484-015-1038-2.

Wang, Y., C.E. Woodcock, W. Buermann, P. Stenberg, P. Voipio, H. Smolander, T. Hame, Y. Tian, H. Jiannan, Y. Knyazikhin, and R.B. Myneni. 2004. Evaluation of the MODIS LAI algorithm at a coniferous forest site in Finland. Remote Sens.

Environ. 91(1): 114–127.

Wang, C., Z. Zhang, S. Fan, R. Mwiya, and M. Xie. 2018. Effects of straw incorporation on desiccation cracking patterns and horizontal flow in cracked clay loam. Soil Tillage Res. 182: 130–143.

Webb, E.K., G.I. Pearman, and R. Leuning. 1980. Correction of flux measurements for density effects due to heat and water vapour transfer. Q. J. R. Meteorol. Soc. 106(447): 85–100.

West, T.O., and W.M. Post. 2002. Soil Organic Carbon Sequestration Rates by Tillage and Crop Rotation : A Global Data Analysis. Soil Sci. Soc. Am. J. 66(6): 1930–1946. doi: 10.2136/sssaj2002.1930.

Wharton, S., M. Falk, K. Bible, M. Schroeder, and K.T.U. Paw. 2012. Old-growth CO2 flux measurements reveal high sensitivity to climate anomalies across seasonal, annual and decadal time scales. Agric. For. Meteorol. 161: 1–14. doi: 10.1016/j.agrformet.2012.03.007.

Wilson, K., A. Goldstein, E. Falge, M. Aubinet, D. Baldocchi, P. Berbigier, C. Bernhofer, R. Ceulemans, H. Dolman, C. Field, A. Grelle, A. Ibrom, B.E. Law, A. Kowalski, T. Meyers, J. Moncrieff, R. Monson, W. Oechel, J. Tenhunen, R. Valentini, and S. Verma. 2002. Energy balance closure at FLUXNET sites. Agric. For. Meteorol. 113: 223–243.

Woodbury, P.B., L.S. Heath, and J.E. Smith. 2006. Land Use Change Effects on Forest Carbon Cycling Throughout the Southern United States. J. Environ. Qual. 35(4): 1348. doi: 10.2134/jeq2005.0148.

Wu, H., X. Wang, M. Xu, and J. Zhang. 2018. The Effect of Water Deficit and Waterlogging on the Yield Components of Cotton. Crop Sci. 58(4): 1751–1761.

Xevi, E., J. Gilley, and J. Feyen. 1996. Comparative study of two crop yield simulation models. Agric. Water Manag. 30(2): 155–173.

Xiao, J., G. Sun, J. Chen, H. Chen, S. Chen, G. Dong, S. Gao, H. Guo, J. Guo, S. Han, T. Kato, Y. Li, G. Lin, L. Weizhi, M. Ma, S. McNulty, C. Shao, X. Wang, and J. Zhou. 2013. Carbon fluxes, evapotranspiration, and water use efficiency of terrestrial ecosystems in China. Agric. For. Meteorol. 182(12): 76–90.

Xu, C.Y., and D. Chen. 2005. Comparison of seven models for estimation of evapotranspiration and groundwater recharge using lysimeter measurement data in Germany. Hydrol. Process. 19(18): 3717–3734. doi: 10.1002/hyp.5853.

Yan, H., Y. Fu, X. Xiao, H.Q. Huang, H. He, and L. Ediger. 2009. Modeling gross primary productivity for winter wheat-maize double cropping system using MODIS time series and CO2eddy flux tower data. Agric. Ecosyst. Environ. 129(4): 391–400. doi: 10.1016/j.agee.2008.10.017.

Yoder, B.J., and R.E. Pettigrew-Crosby. 1995. Predicting nitrogen and chlorophyll content and concentration for reflectance spectra (400 - 2500 nm) at leaf and canopy scales. Remote Sens. Environ. 53(September 1994): 199–211.

Yuan, W., S. Liu, G. Yu, J.M. Bonnefond, J. Chen, K. Davis, A.R. Desai, A.H. Goldstein, D. Gianelle, F. Rossi, A.E. Suyker, and S.B. Verma. 2010. Global estimates of evapotranspiration and gross primary production based on MODIS and global meteorology data. Remote Sens. Environ. 114(7): 1416–1431. doi:

10.1016/j.rse.2010.01.022.

Yu, G., X. Wen, X. Sun, B.D. Tanner, X. Lee, and J. Chen. 2006. Overview of ChinaFLUX and evaluation of its eddy covariance measurement. Agric. For. Meteorol. 137: 125–137. doi: 10.1016/j.agrformet.2006.02.011.

Zapata, D., N. Rajan, and F. Hons. 2017. Does high soil moisture in no-till systems increase CO2 emissions and reduce carbon sequestration? Tampa, FL.

Zapata, D., N. Rajan, J. Mowrer, K. Casey, R. Schnell, and F. Hons. 2019. Impact of Long-Term Tillage on Soil CO2 Emissions and Soil Carbon Sequestration in Monoculture and Rotational Cropping Systems. Soil Tillage Res.

Zhao, M., F.A. Heinsch, R.R. Nemani, and S.W. Running. 2005. Improvements of the MODIS terrestrial gross and net primary production global data set. Remote Sens. Environ. 95(2): 164–176. doi: 10.1016/j.rse.2004.12.011.

Zheng, Y., L. Zhang, J. Xiao, W. Yuan, M. Yan, and T. Li. 2018. Sources of uncertainty in gross primary productivity simulated by light use efficiency models: Model structure, parameters, input data, and spatial resolution. Agric. For. Meteorol. 263(December 2017): 242–257. doi: 10.1016/j.agrformet.2018.08.003.

Zhou, Y., X. Xiao, P. Wagle, R. Bajgain, H. Mahan, J.B. Basara, J. Dong, Y. Qin, G. Zhang, Y. Luo, P.H. Gowda, J.P.S. Neel, P.J. Starks, and J.L. Steiner. 2017. Examining the short-term impacts of diverse management practices on plant phenology and carbon fluxes of Old World bluestems pasture. Agric. For. Meteorol. 237–238: 60–70. doi: 10.1016/j.agrformet.2017.01.018.

4. A COMPARISON OF MODELED PRIMARY PRODUCTION USING PLANETSCOPE SATELLITE IMAGERY TO EDDY COVARIANCE DATA IN EAST-CENTRAL TEXAS COTTON PRODUCTION

4.1. Introduction

With concerns over climate change and the need for increased food and fiber production, understanding the impact of agricultural lands on the global carbon cycle is more important than ever. Annual row cropland (i.e. corn, soy, cotton) currently makes up approximately 11% of the Earth's land area and is a significant contributor to the global carbon cycle (Bruinsma, 2003; Food and Agriculture Organization, 2016; Liu, 2017). Understanding carbon dynamics from cropping systems can help improve efforts to quantify the impacts of agricultural practices on the global carbon budget. Additionally, crop carbon uptake is strongly associated with crop yield, making understating these dynamics important for producers (Peng et al., 2011; Gitelson et al., 2012; He et al., 2018). In recent years, there have been efforts to improve our understanding of carbon fluxes from agricultural lands with the use of remote-sensing based estimates of gross primary productivity (GPP), the total carbon uptake via photosynthesis. Satellite remote sensing can allow for the carbon estimation in areas where ground-based measurements (i.e. eddy covariance) are not practical or possible (Kerr and Ostrovsky, 2003; Frankenberg et al., 2011).

Remote sensing-based GPP estimates generally function by utilizing vegetation indices (VI's). Vegetation indices are ratios of light reflectance wavelength bands that correlate well with plant growth and productivity, many compare the reflectance of near-

infrared (NIR) light to other types of light, often red. The mesophyll of plants reflects NIR, influenced by chlorophyll content, water, and nutrient status, making NIR ratios a good indicator of plant productivity (Yoder and Pettigrew-Crosby, 1995; Daughtry, 2000). Vegetation indices have been shown to correlate well with leaf area index (LAI), absorbed radiation and crop yield (Ahlrichs and Bauer, 1983; Asrar et al., 1984; Baret and Guyot, 1991; Alganci et al., 2014). Previous work in modeling GPP with remote sensing data has been successful with a variety of different VI's. The normalized difference vegetation index (NDVI) is probably one of the most widely used VI's, especially agricultural work, however others such as green chlorophyll index (CI_{Green}), and enhanced vegetation index (EVI) are also fairly common (Yan et al., 2009; Gitelson et al., 2012; Zheng et al., 2018).

Much of the work in modeling carbon dynamics with satellite remote sensing been with lower spatial resolution satellites, such as LANDSAT (30-meter) and MODIS (250-meter). Lower spatial resolution increases the risk of uncertainty due to mixed pixels, where an image pixel contains multiple land cover types (i.e. crop and bare soil or crop and pasture). With low spatial resolution, each image pixel corresponds to a larger ground area (i.e. 250 square meters for MODIS). Ideally, utilizing a finer spatial resolution could improve model success by reducing problems caused by mixed pixels (Zhou et al., 2017; Zheng et al., 2018). Recent developments in satellite technology have greatly increased the spatial resolution of satellite image data, allowing analysis that is more precise. The improvements in image resolution have the potential to improve the precision of satellite-based GPP models. Many of the high-resolution satellites are

privately owned, one such company is Planet Inc., a private satellite company that operates a network of 130+ imaging satellites, including 120 PlanetScope satellites. PlanetScope satellites have a spatial resolution of 3 meters compared to MODIS Terra's 250 meters and LANDSAT's 30 meters (Planet Team, 2017, 2018).

Most of the remote GPP models are based on a light use efficiency model that was first described by John L. Monteith in 1977. This method correlates GPP to the light use efficiency (LUE) of the plant multiplied by the photosynthetically available radiation (PAR), and the fraction of absorbed PAR (fPAR) (Monteith, 1977). This model is commonly modified for use with remote sensing data by replacing LUE and/or fPAR with vegetation indices or other more easily obtained data. In this study, the LUE term is replaced with a remote sensing VI, and fPAR is replaced with leaf area index (LAI). Multiple studies have previously found that LUE correlates well with a variety of vegetation indices – especially those that are related to or also correlate well with chlorophyll content (Peng and Gitelson, 2011; Peng et al., 2011; Huemmrich et al., 2019). Additionally, LAI has been successfully used to estimate fPAR (Myneni et al., 1997; Wang et al., 2004; Chen et al., 2006a; Shafian et al., 2018). The LAI calculation used by the MODIS Terra satellite is based on fPAR (Wang et al., 2004; Sakamoto et al., 2011). This study aims to do the reverse, estimate fPAR from LAI.

While the LUE-based methods have been used widely and successfully in corn, soy, and wheat, studies focusing on modeling GPP using remote sensing in cotton are limited (Gitelson et al., 2012; Alganci et al., 2014; Zheng et al., 2018). Cotton has a unique growth pattern that is different from other crops, which could affect the ability of

these models to work well with cotton. Cotton has a complex canopy structure and indeterminate vegetative growth, which could complicate modeling efforts (Bednarz and Nichols, 2005; Bozorov et al., 2018). Gross primary productivity modeled using the LUE method has been shown to correlate well with cotton yield in multiple studies, which is similar to findings in other crops. However, these studies do not include a ground truth for GPP from eddy covariance or another carbon monitoring method. (Alganci et al., 2014; Jaafar and Ahmad, 2015; Johnson, 2016). Including a ground truth allows for better validation, which greatly improves the modeling effort (Yuan et al., 2010; Frankenberg et al., 2011). This study aims to improve current efforts to model GPP in cotton production by validating a high-resolution satellite-based model using eddy covariance data. Three growing seasons of eddy covariance carbon flux and PlanetScope imagery data from a conventional, dryland cotton field in East-Central Texas is used to develop and validate a satellite remote sensing-based GPP model.

4.2. Materials and Methods

4.2.1. Site Information

The study was conducted in a 12.14 ha conventionally managed, dryland continuous cotton (*Gossypium hirsutum*) field, shown in Figure 17. The field was located at the Texas A&M Agrilife Research Farm in Burleson County, Texas (30°32’46.2” N, 96°25’19.7”W). An eddy covariance flux-tower was established in the center of the field in February 2017, and fluxes were monitored for three growing seasons. The cotton crop was planted on April 6 (DOY 96) in 2017, April 18 (DOY 108) in 2018, and April 30 (DOY 120) in 2019 following conventional tillage and the

formation of raised seedbeds. The delayed planting in 2019 was due to unusually wet conditions during planting. The cultivar, Phytogen 333WRF was used in 2017 and 2018, while the cultivar, Phytogen 350 was used in 2019. Nitrogen fertilizer was applied at a rate of 95 kg ha^{-1} as urea ammonium nitrogen (32-0-0) shortly after planting. Glyphosate was used for weed control as needed. The average plant population was 6.24 plants m^{-2} in 2017, 6.22 plants m^{-2} in 2018, and 6.11 plants m^{-2} in 2019. The cotton crop was chemically defoliated to allow for easier harvest with GinStar (Bayer CropScience, Monheim, Germany), a mixture of Thidiazuron and Diuron, which blocked photosynthesis. Defoliation occurred on Aug 21 (DOY 233) in 2017, Aug 21 (DOY 233) in 2018, and Sept 3 (DOY 246) in 2019. The cotton crop was harvested following defoliation on September 11 (DOY 254) in 2017, September 17 (DOY 260) in 2018, and September 16 (DOY 259) in 2019.

The climate of the location is humid subtropical (Köppen Cfa) with an average (30-year) annual temperature of 20.58°C and an average annual precipitation of 1018 mm. For the typical cotton growing season (April – September), the average (30-year) temperature was 26.38°C and precipitation was 413 mm (National Oceanic and Atmospheric Administration, 2011). The dominant soil types in the field are the Weswood silt loam (Udifluventic Haplustepts, 38% clay in surface horizon, floodplain) and Ships clay (Chromic Halpludert, 42% clay in the surface horizon). Both soils have a high content of shrink-swell minerals that cause the soil to form large cracks in dry weather.

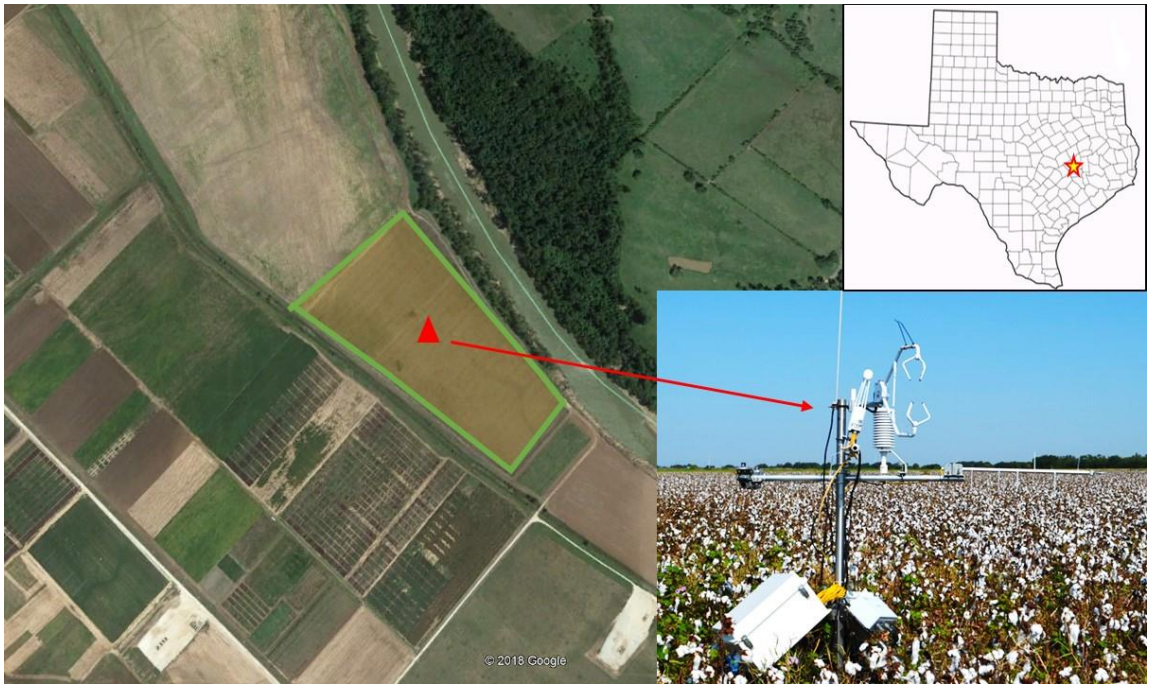

Figure 17: Image of Cotton Field Site
Image of the field site is shown above. Image on the left is a satellite photo of the field location with the field highlighted in green. The red triangle refers to the location of the eddy covariance tower, which is shown in the lower right image. The upper right image shows the location of the site in Texas (Google Earth, 2018).

4.2.2. Satellite Imagery Data

Satellite imagery was obtained from Planet, a private satellite imaging company. Selected images were captured using the PlanetScope (Dove) Satellite Network. The PlanetScope satellites are a network of 120 satellites. They collected four bands of data; Red (590 – 670 nm), Green (500 – 590 nm), Blue (455 – 515 nm), and NIR (780 – 860 nm). They have an analytic radiometric resolution of 16 bit and a spatial resolution of 3 meters (Planet Team, 2017, 2018). Downloaded images were analyzed using ENVI 5.3.

Vegetation indices (VI's) were calculated from the band values. The following vegetation indices were calculated: Normalized Difference Vegetation Index (NDVI), Soil Adjusted Vegetation Index (SAVI), Green Chlorophyll Index (CIGreen), and Simplified Enhanced Vegetation Index (EVI2).

$$NDVI = \frac{(NIR - RED)}{(NIR + RED)}$$

$$SAVI = \frac{(1 + 0.5)(NIR - RED)}{(NIR + RED + 0.5)}$$

$$CIGreen = \frac{NIR}{GREEN} - 1$$

$$EVI2 = 2.5 * \frac{(NIR - RED)}{(1 + NIR + 2.4 * RED)}$$

4.2.3. Eddy Covariance Data and Processing

Continuous (10 Hz) measurements of CO_2 and water vapor flux were made using an eddy covariance system (EC). The eddy covariance system consisted of a Campbell Scientific C-SAT3 Sonic Anemometer (Campbell Scientific, Logan, UT, USA) and an LI-7500 Infrared Gas Analyzer (IRGA; LI-COR, Lincoln, NE, USA). The Sonic Anemometer and IRGA were connected to a SmartFlux system (LI-COR, Lincoln, NE, USA), which used EddyPro software (version 6.2.2) to process data collected at 10 Hz and compiled it into 30 min summary files. Eddy covariance instruments were installed on a tripod with an adjustable mast to maintain instruments at a height of 2 meters above the plant canopy. Instruments were installed facing south, the direction of the prevailing

winds. The instruments were calibrated and had the internal chemicals changed annually, as recommended by the manufacturer.

Additional meteorological instruments were installed to supplement the EC data. The additional instruments consisted of the following: a temperature and relative humidity probe (HMP155A, Vaisala, Vantaa, Finland), a quantum (PAR) sensor (LI-190R, LI-COR, Lincoln, NE, 2019), a pyranometer (LI-200R, LI-COR, Lincoln, NE 2019), a net radiometer (NR-LITE2 Kipp and Zonen, Delft, The Netherlands), and a tipping bucket style rain gauge (TE525, Texas Electronics, Dallas, TX, USA). Soil instruments consisted of seven soil moisture sensors (CS655, Campbell Scientific, Logan, UT, USA), four soil thermocouples (TCAV, Campbell Scientific, Logan, UT, USA), and four soil heat-flux plates (HPF01SC, Hukseflux, Delft, The Netherlands). Three soil moisture sensors were placed horizontally at a depth of 4 cm; two were placed vertically between 10 and 20 cm; the last two were placed vertically between 20 and 30 cm. Soil heat-flux plates were placed in pairs, 1 meter apart, and buried at 8 cm. Soil thermocouples were buried at 2 and 6 cm above the soil heat-flux plates. Additional meteorological instruments and soil instruments were all connected to a datalogger (CR3000, Campbell Scientific, Logan, UT, USA). Readings were collected every 2 seconds and compiled into 30-minute summaries.

Eddy covariance fluxes were processed using a SmartFlux system, which was directly connected to the instruments. The SmartFlux system used embedded EddyPro (version 6.2.2) software to compute the fluxes and perform corrections. EddyPro performs a number of corrections before computing NEE fluxes. This includes

coordinate rotation, frequency response corrections, corrections for air density fluctuations and sensor separation delays (Webb et al., 1980; Paw et al., 2000; Finnigan et al., 2003; Burba, 2013; Carmelita et al., 2014; LI-COR, 2015; Qin et al., 2016). SmartFlux saved 30-minute flux calculations as .csv files onto a USB drive along with raw data (unprocessed) data files. The fluxes were calculated using a sign convention where positive numbers indicate fluxes away from the canopy and negative numbers indicate fluxes toward the canopy.

The EddyPro software flagged data for quality based on internal turbulence tests. High-quality data was marked with a "0", moderate quality with a "1" and low quality with a "2". Low-quality points were manually removed during data inspection for gap filling. Gap filling was used to fill in missing and removed data points. Gap filling and flux partitioning (partitioning CO_2 uptake {GPP} and respiration {R_{eco}}) were done using the Max Plank Institute for Biogeochemistry's online R-based (R Gui 3.4.1) program using the default settings. The program used a 14-day window and linear interpolation to points with similar meteorological conditions to gap-fill missing and removed points. Fluxes were separated using a reference temperature and nighttime fluxes to estimate daytime R_{eco} (Reichstein et al., 2005; Aubinet et al., 2012; Fritz et al., 2018). Gross Primary Productivity (GPP) was calculated from Net Ecosystem Exchange (NEE) and R_{eco} during the gap-filling process as follows:

$$GPP = NEE + R_{eco}$$

4.2.4. Phenology Data Collection

Destructive plant samples were collected every other week from six locations within the field, three from each soil type, forming a ring around the tower. At each location, 15 plants were randomly selected and measured for height, growth stage, leaf area, and above-ground biomass. After sampling, the leaves and flowers/bolls were removed from the stems. Leaves were put through a leaf area meter (LI-3100, LI-COR, Lincoln, NE, USA) to measure LAI. Leaves, stems, and flowers/bolls were dried in separate paper bags at 40°C and weighed to get above-ground biomass, leaf biomass, stem biomass, and reproductive biomass.

4.2.5. GPP Modelling

The model we are proposing is as follows:

$$GPP \propto VI * LAI * PAR$$

Where VI is obtained from the PlanetScope imagery data, LAI is obtained from destructive plant sampling, and PAR is obtained from the Quantum Sensor at the EC tower. For the 2017 data, VI * LAI * PAR was regressed against the actual GPP obtained from the EC tower. Regression was performed using SigmaPlot (Version 14.0) and the best-fit equation was found. The equation of the regression curve was then applied to the data for 2018 and 2019 for model validation as follows:

$$GPP = slope * (VI * LAI * PAR) + intercept$$

4.2.6. Statistical Analysis

Statistical analysis was performed using R Gui (version 3.4.1) and SigmaPlot (version 14.0). The slope of the regression for modeled GPP versus measured GPP was compared

to one with a t-test using R Gui. An ideal model will have a 1:1 relationship with the measured data. A slope less than one will indicate underestimation and a slope greater than one will indicate overestimation. The following model performance indices were calculated manually: root mean square error (RMSE), standard error of the estimate (SE), and the index of agreement (d-index). The d-index was calculated using the following equation:

$$d = 1 - [\frac{\sum(x - \bar{x})^2}{\sum(|x - \bar{x}| + |y - \bar{y}|)^2}$$

Where x is the modeled value and y is the observed value. The d-index shows the degree of agreement between the modeled data and the measured data. A perfect 1:1 fit between the modeled and measured data will give a d-index of 1 and no correlation will give a d-index of 0 (Adhikari et al., 2016; Basso et al., 2016; Sharma et al., 2017).

4.3. Results and Discussion

4.3.1. Vegetation Indices

The vegetation indices are shown in Figure 18. During the early growing season, NDVI (Figure 18A) was greater in 2017 compared to 2018 and 2019. Maximum NDVI was 0.68 in 2017 (DOY 189), 0.58 in 2018 (DOY 192), and 0.67 in 2019 (DOY 191). These maximum values are lower than reported in other studies, however most studies of vegetation indices in cotton focus on irrigated cotton, which is generally more productive. Lower VI values more similar to the ones seen here are found in dryland and limited irrigation cotton (Gwathmey et al., 2010; Gutierrez et al., 2012; Raper et al.,

2013). In 2018, NDVI quickly declined after its maximum due to drought conditions. There was a brief increase in NDVI late in the 2019 season due to a rain event (31.24 mm, DOY 237) causing leaf expansion. Immediately prior to defoliation NDVI was 0.58 in 2017 (DOY 231), 0.42 in 2018 (DOY 229), and 0.53 in 2019 (DOY 244). Total growing season precipitation was 510 mm in 2017, 184 mm in 2018, and 461 mm in 2019. The significantly lower precipitation in 2018 caused early senescence prior to defoliation, which was reflected in NDVI.

During the early growing season of 2019, SAVI (Figure 18B) was lower than that of 2017 and 2018. This is likely due to delayed planting in 2019, causing the cotton plants to be smaller than they were on the same date in previous years. Maximum SAVI was 0.47 in 2017 (DOY 189), 0.43 in 2018 (DOY 192), and 0.49 in 2019 (DOY 191). There was an increase in SAVI seen in the late 2019 growing season following the same rain event that affected NDVI. Prior to defoliation SAVI was 0.40 in 2017 (DOY 231), 0.28 in 2018 (DOY 229), and 0.36 in 2019 (DOY 244). During the early growing season, CI_{Green} followed a similar pattern to that of the other indices with higher values in 2017 compared to 2018 and 2019. Maximum CI_{Green} was 3.14 in 2017 (DOY 189), 2.24 in 2018 (DOY 192), and 3.00 in 2019 (DOY 191). Following the maximum, CI_{Green} declined rapidly in all years with brief increases following rain events. Prior to defoliation CI_{Green} was 2.20 in 2017 (DOY 231), 1.37 in 2018 (DOY 229), and 1.64 in 2019 (DOY 244). EVI followed a very similar trend to SAVI. Maximum EVI was 0.48 in 2017 (DOY 189), 0.43 in 2018 (DOY 192), and 0.50 in 2019 (DOY 191). Immediately prior to defoliation EVI was 0.40 in 2017 (DOY 231), 0.27 in 2018 (DOY

229), and 0.35 in 2019 (DOY 244). The reduction of multiple VI's seen in 2018 is typical for a season with limited water availability. Irrigation treatment studies in cotton have found that all VI's are reduced in deficit treatments, a similar trend between dry and wet years is expected (Ritchie et al., 2010; Ballester et al., 2019).

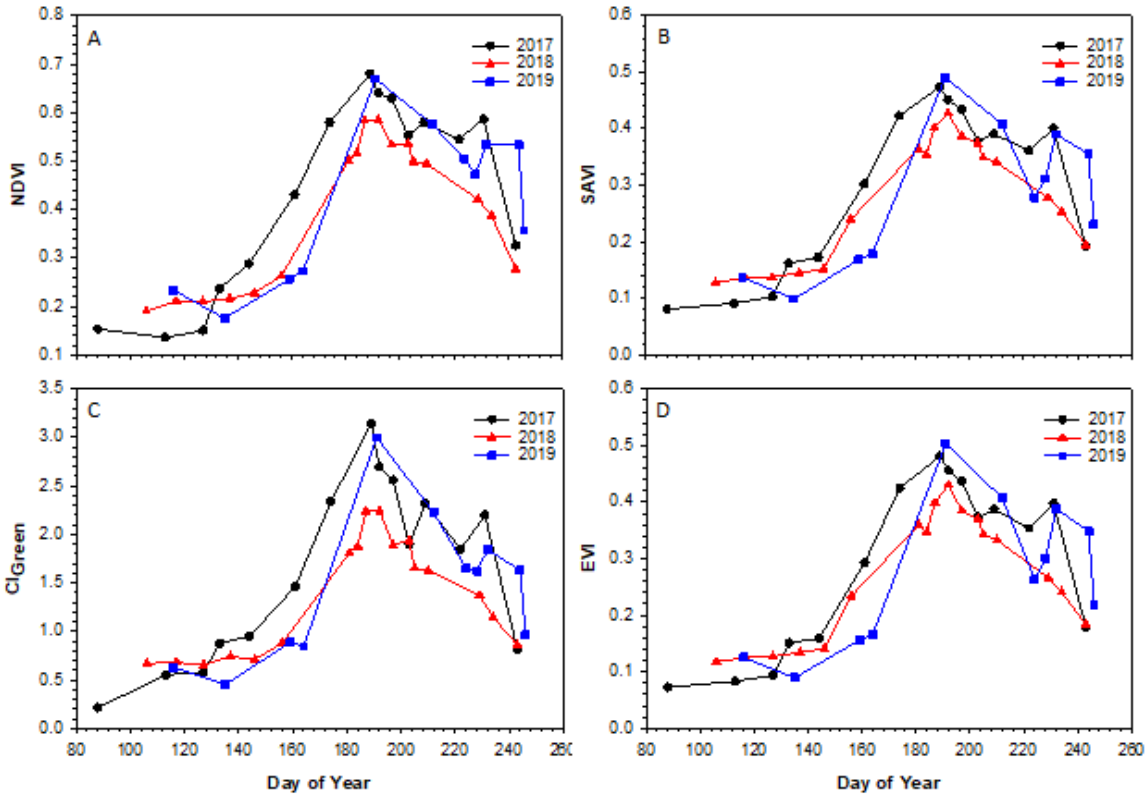

Figure 18: Cotton Vegetation Indices
Vegetation Indices over time are shown above. Image "A" refers to NDVI. Image "B" refers to SAVI. Image "C" refers to CI_{Green}. Image "D" refers to EVI. Black circles refer to 2017, red triangles to 2018, and blue squares to 2019.

4.3.2. Gross Primary Productivity

Growing season (planting to defoliation) gross primary productivity (GPP) is shown in Figure 19. The early growing season (DOY 90 – DOY 160) was characterized by similar fluxes between all three years. Following that, daily GPP for 2017 exceeds that of 2018 and 2019 until DOY 180. After that, daily GPP from 2018 exceeds daily GPP from 2017 and 2018 until approximately DOY 210. During the latter part of the growing seasons (DOY 220 – defoliation) daily GPP for 2017 and 2019 exceeded that of 2018. Maximum daily GPP was 14.70 gC m^{-2} day^{-1} for 2017 (DOY 187), 18.28 gC m^{-2} day^{-1} for 2018 (DOY 196), and 15.54 gC m^{-2} day^{-1} for 2019 (DOY 190). Cumulative growing season GPP was 947.1 gC m^{-2} for 2017, 882.7 gC m^{-2} for 2018, and 861.33 gC m^{-2} for 2019. The lowest cumulative GPP was in 2019, while daily fluxes were similar to that of 2017, delayed planting resulted in delayed early-season carbon uptake. The 2017 growing season was longer (138 days) than that of the subsequent years (126 and 127 days for 2018 and 2019 respectively). The cumulative GPP at this site is within the range reported by other studies. One study of irrigated cotton found an average (4 years) growing season GPP of 816.2 gC m^{-2}, which is similar to what was observed at this location (Bai et al., 2015; Li et al., 2018).

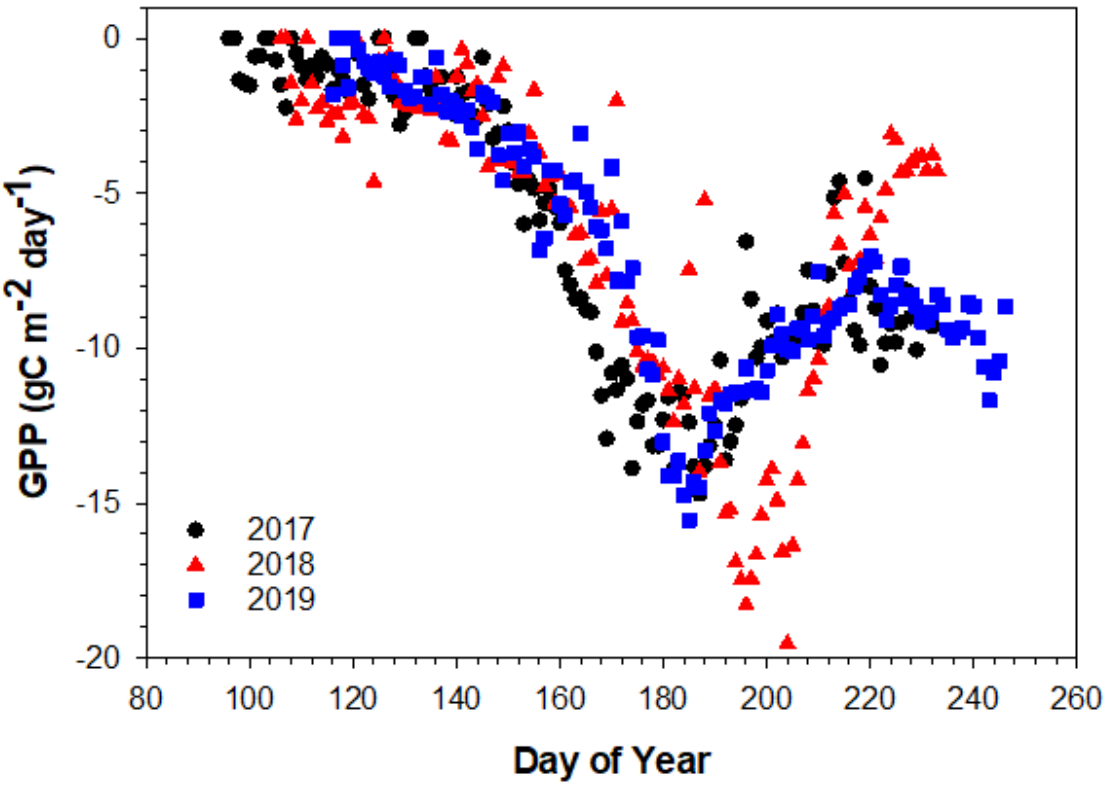

Figure 19: Cotton GPP Over Three Years
Growing season daily GPP is shown above with GPP on the Y-axis and Day of Year on the X-axis. Black circles show fluxes from 2017, red triangles show fluxes from 2018, and blue squares show fluxes from 2019.

4.3.3. Model Development

The model development phase using 2017 data is shown in Figure 20. The best-fit equation for NDVI*LAI*PAR versus inverse GPP was found to be linear using Sigmaplot. Inverse GPP is GPP shown with the inverse (positive) sign. The best-fit equations for the remaining three models were found to be quadratic using Sigmaplot. A

quadratic fit between GPP and VI*PAR*LAI has been found in previous studies (Gitelson et al., 2012; Peng and Gitelson, 2012). All relationships between GPP and VI*LAI*PAR were significant to $p < 0.001$. The relationship between NDVI*LAI*PAR and GPP had a slightly worse correlation ($r^2 = 0.87$) than the other VI's ($r^2 = 0.92$, 0.92, and 0.93 for SAVI, CI_{Green}, and EVI, respectively). Similar correlations have been found in a variety of crops such as corn, soy, wheat, and alfalfa, however little work in comparing GPP to vegetation indices has been performed in cotton specifically (Yan et al., 2009; Gitelson et al., 2012; He et al., 2018).

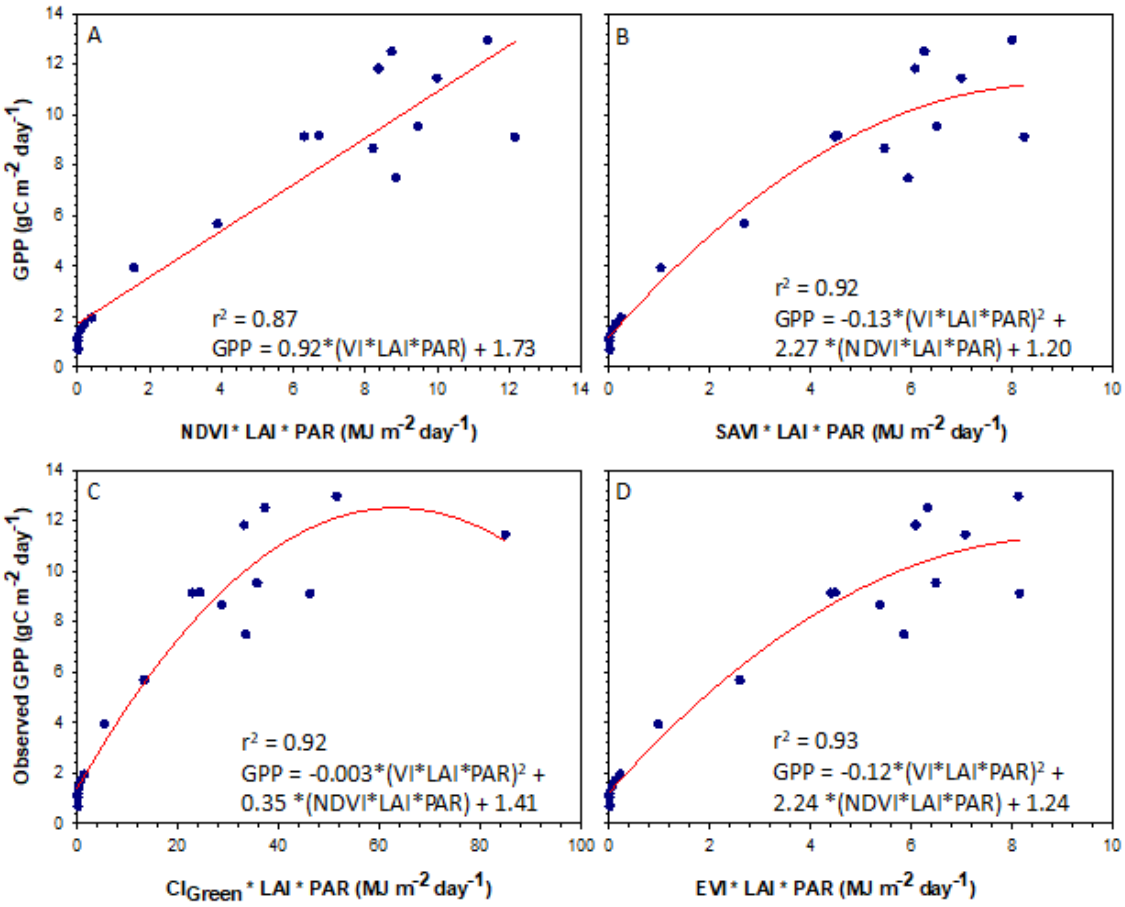

Figure 20: Regression Analysis Between GPP and VI*LAI*PAR
Regression analysis between VI*LAI*PAR and GPP is shown above. The Y-axis is observed GPP and the X-axis is VI*LAI*PAR. Image "A" refers to the graph where the VI is NDVI. Image "B" refers to the graph where the VI is SAVI. Image "C" refers to the graph where the VI is CI_{Green}. Image "D" refers to the graph where the VI is EVI.

4.3.4. Model Validation

The model validation using the 2018 data is shown in Figure 21 and the model validation using the 2019 data is shown in Figure 22, with statistical analysis for both

models shown in Table 3. Overall, the model validation using the 2018 data had a greater correlation with observed GPP (average $r^2 = 0.89$) than the model validation using the 2019 data (average $r^2 = 0.73$). The slope of the fit between NDVI-modeled GPP and observed GPP for 2018 was 1.05 and it was not statistically different ($p < 0.05$) from 1.0. The slope of the same model regression for 2019 was 0.68 and it was statistically different ($p < 0.05$) from 1.0. Despite being the best-fit model in 2018, the NDVI-based model was the worst fit in 2019. The lack of fit between the modeled GPP and observed GPP in 2019 suggests inadequacies in the model. Similar results were seen for the other vegetation indices.

The slope of the fit between SAVI-modeled GPP and observed GPP was 1.08 for 2018 and 0.81 for 2019. The slope was not statistically different ($p < 0.05$) from 1.0 in either year. While both years were not different from one, the correlation in 2019 ($r^2 = 0.76$) was weaker than that of 2018 ($r^2 = 0.85$). While still performing more poorly than any of the 2018 models, the 2019 SAVI-based model was the best fit for the 2019 models. The slope between CI_{Green}-modeled GPP and observed GPP was 1.14 for 2018 and 0.78 for 2019 and was not statistically different ($p < 0.05$) from 1.0 in either year. The correlation in 2019 ($r^2 = 0.75$) was substantially weaker than that of 2018 ($r^2 = 0.91$). The slope between CI_{Green}-modeled GPP and observed GPP was 1.08 for 2018 and 0.80 for 2019 and was not statistically different ($p < 0.05$) from 1.0 in either year. The correlation in 2019 ($r^2 = 0.76$) was substantially weaker than that of 2018 ($r^2 = 0.86$). While the model performance for 2019 was weaker than for 2018, similar results have

been seen in other studies of GPP modeling (Yan et al., 2009; He et al., 2018; Zheng et al., 2018).

In 2018, the SAVI-, CI_{Green}-, and EVI- based models all had a tendency to underestimate GPP in the latter part of the growing season. Since all four models used the same LAI and PAR data, yet this problem was not observed in the NDVI-based model, it is likely an issue with the vegetation index itself. Cotton has a more complex canopy structure than most of the crops are used in similar GPP modeling studies. Satellite images do not capture shaded leaves, which contribute (albeit less) to GPP. Differences in crop vegetative growth structure have been shown to alter the effectiveness of Satellite-based GPP models (Glenn et al., 2008; Yan et al., 2009; Zheng et al., 2018). A study on GPP modeling in a wheat/corn rotation found that the model had the greatest variability in the wheat crop compared to the corn crop. While both wheat and corn are grasses, wheat is C3 and has indeterminate vegetative growth (like cotton), whereas corn is C4 and has determinate vegetative growth (Yan et al., 2009). Even within a species, there can be differences in vegetative structure. The Phytogen 350 cultivar (2019) had smooth leaves compared to the Phytogen 333WRF cultivar (2017 and 2018), which was a hairy leaved variety (PhytoGen, 2019). Leaf-type in cotton plants has been shown to influence the CO_2 exchange rate, early vegetative growth rate, and radiation use efficiency (Pegelow et al., 1977; Ibrahim and Buxton, 1981; Gonias et al., 2011).

In 2019, all models had a tendency to underestimate GPP early in the season. Slow seedling growth in 2019 due to cold, wet soils may have resulted in issues with

mixed pixels (soil and plant) in the satellite data. During this period, the plants are only a few centimeters, yet the resolution of the satellite images is 3-meters meaning that the plants may not be properly captured by the imagery data. Mixed pixels have been shown to be a major source of uncertainty in other efforts of modeling GPP using satellite data (Zhao et al., 2005; He et al., 2018; Zheng et al., 2018). This is more likely for uncertainty in the early growing season when plants are considerably smaller than the image resolution causing mixed soil/plant pixels. Part of the differences in success between the years may also be influenced by the use of a different cultivar in 2019. The Phytogen 350 cultivar (2019) is slightly slower maturing than the Phytogen 333WRF cultivar (2017 and 2018), possibly causing uncertainty (PhytoGen, 2019).

Uncertainty in the observed GPP is another possible factor in the model uncertainty. Even with well-maintained towers, uncertainty in EC carbon flux data can be as high as 20% (Anthoni et al., 1999; Baldocchi, 2003; Baker and Griffis, 2005; Glenn et al., 2008; Burba, 2013). Errors in the carbon flux measurements come from a variety of sources, including calibration errors and sensor-time delays (Anthoni et al., 1999; Baldocchi, 2003; Burba, 2013). In addition to uncertainty from the direct measurements, there is uncertainty from the flux calculation, flux partitioning, and gap-filling processes. The method used and the assumptions it makes (i.e. the curve of the fit between R_{eco} and air temperature) can make a difference in outcomes. It is possible that uncertainty in the observed GPP measurements is affecting model success.

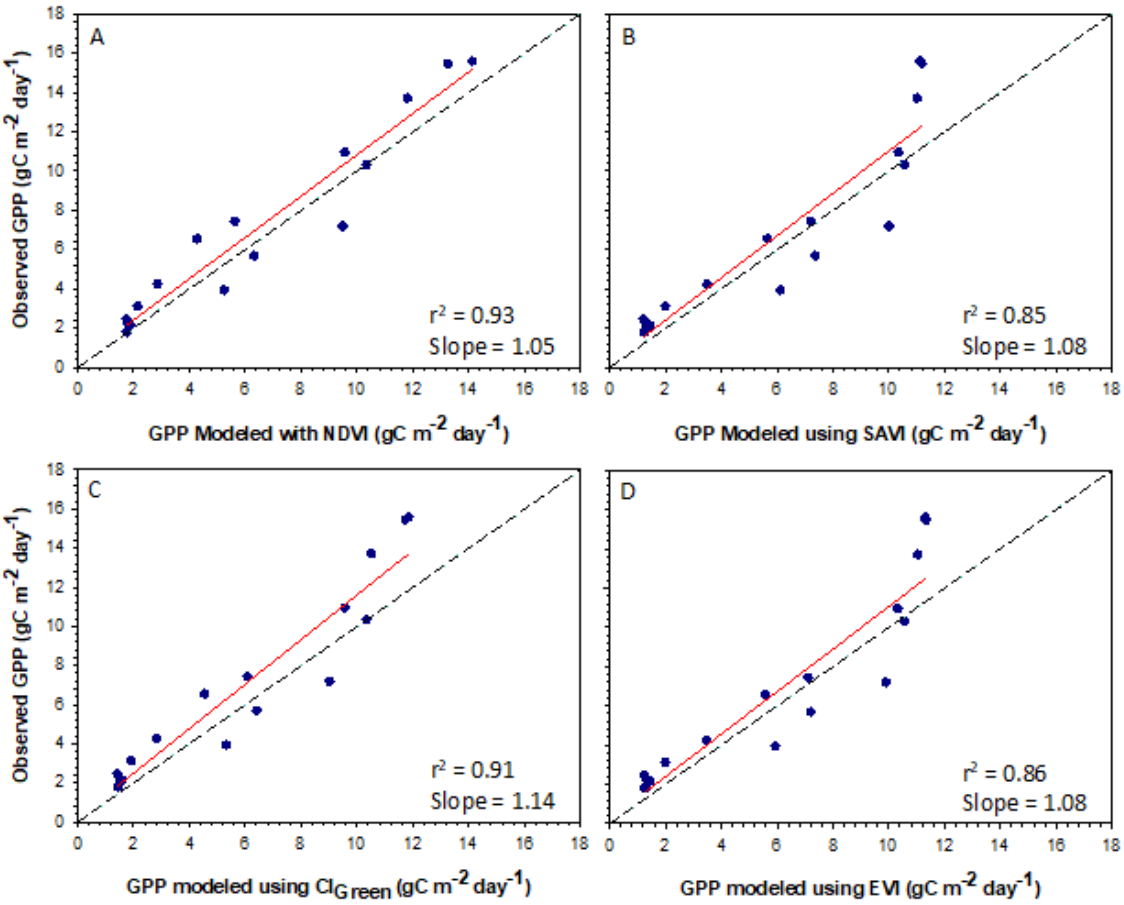

Figure 21: 2018 Cotton GPP Model Validation
Validation of 2018 GPP models is shown above. Image "A" refers to the validation of the NDVI-based GPP model. Image "B" refers to the validation of the SAVI-based GPP model. Image "C" refers to the validation of the CI_{Green}-based GPP model. Image "D" refers to the validation of the EVI-based GPP model. Y-axis on all graphs refers to observed (tower) GPP and x-axis refer to modeled GPP. The solid red line refers to the best fit between the measured and modeled GPP. The dashed black line shows the ideal 1:1 fit between measured and modeled GPP.

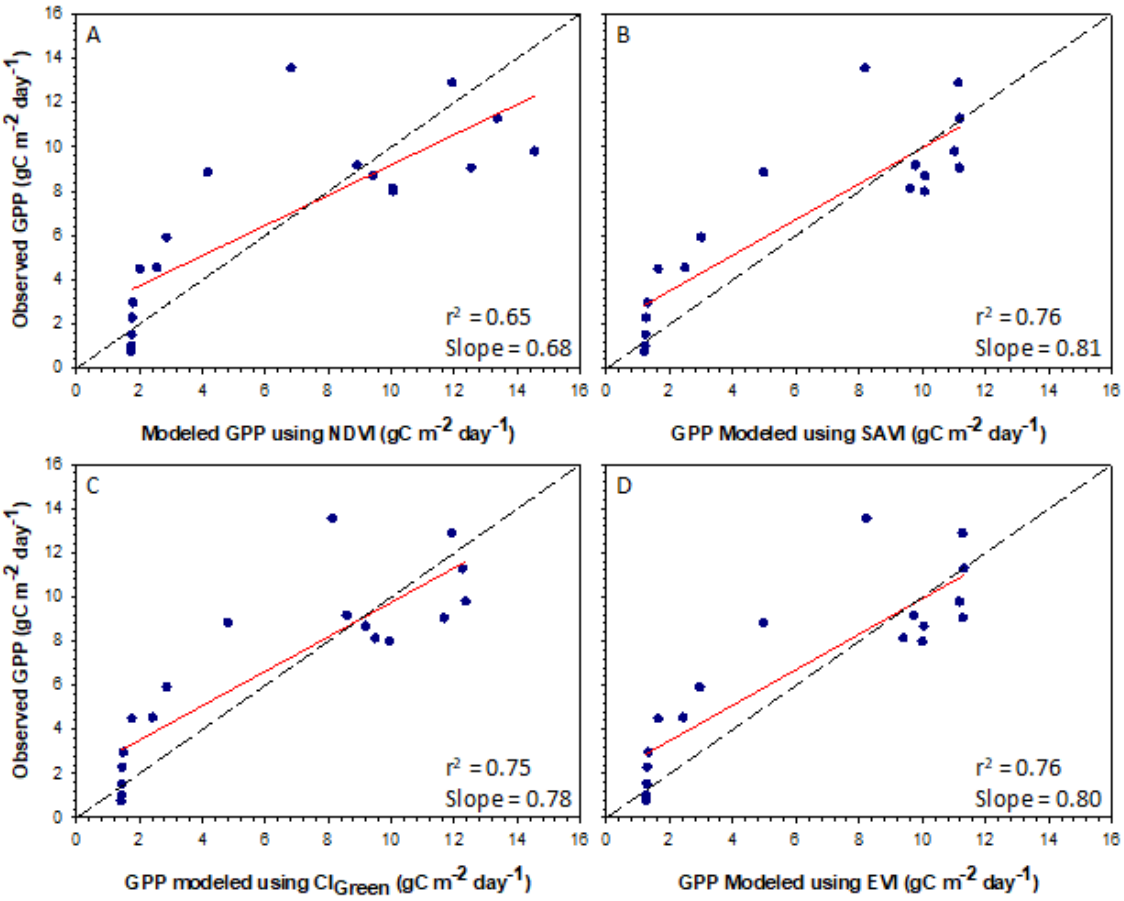

Figure 22: 2019 Cotton GPP Model Validation
Model validation for the 2019 GPP models. Image "A" refers to the validation of the NDVI-based GPP model. Image "B" refers to the validation of the SAVI-based GPP model. Image "C" refers to the validation of the CI_{Green}-based GPP model. Image "D" refers to the validation of the EVI-based GPP model. Y-axis on all graphs refers to observed (tower) GPP and x-axis refer to modeled GPP. The solid red line refers to the best fit between the measured and modeled GPP. The dashed black line shows the ideal 1:1 fit between measured and modeled GPP.

Table 3: Statistical Analysis of Cotton GPP Model Validation Statistical Analysis

2018	D-Index	r^2	Standard Error of the Mean	nRMSE	Different from 1?
NDVI	0.98	0.93	1.38	0.39	NO
SAVI	0.95	0.85	1.99	0.44	NO
CIGreen	0.95	0.91	1.84	0.62	NO
EVI	0.95	0.86	1.92	0.45	NO
2019	**D-Index**	**r^2**	**Standard Error of the Mean**	**nRMSE**	**Different from 1?**
NDVI	0.92	0.65	2.77	0.18	YES
SAVI	0.95	0.76	2.20	0.44	NO
CIGreen	0.95	0.75	2.26	0.37	NO
EVI	0.95	0.76	2.19	0.43	NO

4.4. Conclusions

There was some difficulty in modeling GPP in cotton using the modification of the LUE based method. While there has been success modeling GPP using this type of method in other crops, such as corn, little work has been done in cotton. Cotton has a more complex growth pattern, which proved tricky to model. There were several times during the growing seasons where PAR would be high yet GPP would be low, likely throwing off the accuracy of the model. During the early growing season, when temperatures are cool, the cotton plants grow slowly and uptake little carbon even if

there is sufficient incoming PAR. During the late growing season when the plants are senescing, they may once again uptake little carbon despite sufficient PAR.

The model validation using 2018 data was considerably more successful than the model validation effort in 2019. The average standard error was 1.78 gC m^{-2} for 2018 and 2.36 gC m^{-2} for 2019. In 2018, the best performing model was the NDVI-based model with an r^2 of 0.93 and nRMSE of 0.39 gC m^{-2} day^{-1}. In 2019, the best performing model was the EVI-based model with an r^2 of 0.76 and nRMSE of 0.43 gC m^{-2} day^{-1}. The delayed planting in 2019 likely increased severity of high incoming PAR values and low GPP found in the early growing season. The results from this study indicate that considerable uncertainty still exists in satellite-based GPP modeling for cotton and further work is likely needed to address this uncertainty. Cotton growth is more complex than other row crops and modeling cotton GPP successfully will need more work.

4.5. Acknowledgment

This work is supported by NIFA-NLGCA [grant no. 2016-70001-24636/project accession no. 1008730] from the USDA National Institute of Food and Agriculture. This work was also supported partially through cotton incorporated grant # 17-614. This work was also supported by Planet's "Education and Research Program", which provided free access to PlanetScope imagery data. The authors would like to thank Dr. Don T. Conlee (Department of Atmospheric Sciences, Texas A&M University) for providing missing meteorological data. The authors would also like to thank Texas A&M Agrilife and the staff at the research farm, particularly Mr. Alfred Nelson (Farm Manager) for planting and managing the cotton field.

4.6. References

Adhikari, P., Ale, S., Bordovsky, J.P., Thorp, K.R., Modala, N.R., Rajan, N., Barnes, E.M., 2016. Simulating future climate change impacts on seed cotton yield in the Texas High Plains using the CSM-CROPGRO-Cotton model. Agric. Water Manag. 164, 317–330. https://doi.org/10.1016/j.agwat.2015.10.011

Ahlrichs, J.S., Bauer, M.E., 1983. Relation of Agronomic and Multispectral Reflectance Characteristics of Spring Wheat Canopies1. Agron. J. 75, 987–993. https://doi.org/10.2134/agronj1983.00021962007500060029x

Alganci, U., Ozdogan, M., Sertel, E., Ormeci, C., 2014. Field Crops Research Estimating maize and cotton yield in southeastern Turkey with integrated use of satellite images , meteorological data and digital photographs. F. Crop. Res. 157, 8–19. https://doi.org/10.1016/j.fcr.2013.12.006

Anthoni, P.M., Law, B.E., Unsworth, M.H., 1999. Carbon and water vapor exchange of an open-canopied ponderosa pine ecosystem. Agric. For. Meteorol. 95, 151–168. https://doi.org/10.1016/S0168-1923(99)00029-5

Asrar, G., Fuchs, M., Kanemasu, E.T., Hatfield, J.L., 1984. (1984) Estimating Absorbed Photosynthetic Radiation and Leaf Area Index from Spectral Reflectance in Wheat (AJ).

Aubinet, M., Vesala, T., Papale, D., 2012. Eddy Covariance: A Practical Guide to Measurement and Data Analysis. Springer Atmospheric Sciences, Berlin, Germany.

Bai, J., Wang, J., Chen, X., Lou, G.P., Shi, H., Li, L.H., Li, J., 2015. Seasonal and inter-variations in carbon fluxes and evapotranspiration over cotton field under drip

irrigation and plastic mulch in an arid region of Northwest China. J. Arid Land 7, 272–282.

Baker, J.M., Griffis, T.J., 2005. Examining strategies to improve the carbon balance of corn / soybean agriculture using eddy covariance and mass balance techniques. Agric. For. Meteorol. 128, 163–177. https://doi.org/10.1016/j.agrformet.2004.11.005

Baldocchi, D.D., 2003. Assessing the eddy covariance technique for evaluating carbon dioxide exchange rates of ecosystems: past, present and future. Glob. Chang. Biol. 9, 479–492. https://doi.org/10.1046/j.1365-2486.2003.00629.x

Ballester, C., Brinkhoff, J., Quayle, W.C., Hornbuckle, J., 2019. Monitoring the Effects of Water Stress in Cotton Using the Green Red Vegetation Index and Red Edge Ratio. Remote Sens. 11.

Baret, F., Guyot, G., 1991. Potentials and limits of vegetation indices for LAI and APAR assessment. Remote Sens. Environ. 35, 161–173. https://doi.org/10.1016/0034-4257(91)90009-U

Basso, B., Liu, L., Ritchie, J.T., 2016. A Comprehensive Review of the CERES-Wheat, -Maize and -Rice Models' Performances, Advances in Agronomy. Elsevier Inc. https://doi.org/10.1016/bs.agron.2015.11.004

Bednarz, C.W., Nichols, R.L., 2005. Phenological and Morphological Components of Cotton Crop Maturity. Crop Sci. 45, 1497–1503.

Bozorov, T.A., Usmanov, R.M., Yang, H.L., Hamdullaev, S.A., Musayev, S., Shakiev, J., Nabiev, S., Zhang, D.Y., Abdullaev, A.A., 2018. Effect of water deficiency on

relationships between metabolism, physiology, biomass, and yield of upland cotton (Gossypium hirsutum L.). J. Arid Land 10, 441–456.

Bruinsma, J., 2003. World Agriculture: Towards 2015/2030.

Burba, G., 2013. Eddy Covariance Method. LI-COR Biosciences, Lincoln, NE.

Carmelita, M., Alberto, R., Wassmann, R., Buresh, R.J., Quilty, J.R., Correa, T.Q., Sandro, J.M., Arloo, C., Centeno, R., 2014. Field Crops Research Measuring methane flux from irrigated rice fields by eddy covariance method using the open-path gas analyzer. F. Crop. Res. 160, 12–21. https://doi.org/10.1016/j.fcr.2014.02.008

Chen, J.M., Govind, A., Sonnentag, O., Zhang, Y., Barr, A., Amiro, B., 2006. Leaf area index measurements at Fluxnet-Canada forest sites. Agric. For. Meteorol. 140, 257–268.

Daughtry, C., 2000. Estimating Corn Leaf Chlorophyll Concentration from Leaf and Canopy Reflectance. Remote Sens. Environ. 74, 229–239. https://doi.org/10.1016/S0034-4257(00)00113-9

Finnigan, J.J., Clement, R., Malhi, Y., Leuning, R., Cleugh, H.A., 2003. A Re-Evaluation of Long-Term Flux Measurement Techniques Part 1: Averaging and Coordinate Rotation. Boundary-Layer Meteorol. 1–48.

Food and Agriculture Organization, 2016. Land Use.

Frankenberg, C., Fisher, J.B., Worden, J., Badgley, G., Saatchi, S.S., Lee, J.E., Toon, G.C., Butz, A., Jung, M., Kuze, A., Yokota, T., 2011. New global observations of the terrestrial carbon cycle from GOSAT: Patterns of plant fluorescence with gross

primary productivity. Geophys. Res. Lett. 38, 1–7. https://doi.org/10.1029/2011GL048738

Fritz, E., Richter, S., Schott, S., Hejja, S., Trumbore, S., 2018. Partitioning Algorithm [WWW Document]. Max Planck Inst. Biogeochem.

Gitelson, A.A., Peng, Y., Masek, J.G., Rundquist, D.C., Verma, S., Suyker, A., Baker, J.M., Hat, J.L., Meyers, T., 2012. Remote estimation of crop gross primary production with Landsat data. Remote Sens. Environ. 121, 404–414. https://doi.org/10.1016/j.rse.2012.02.017

Glenn, E.P., Huete, A.R., Nagler, P.L., Nelson, S.G., 2008. Relationship between remotely-sensed vegetation indices, canopy attributes, and plant physiological processes: what vegetatio 2136–2160.

Gonias, E.D., Oosterhuis, D.M., Bibi, A.C., 2011. Light interception and radiation use efficiency of okra and normal leaf cotton isolines. Environ. Exp. Bot. 72, 217–222.

Google Earth, 2018. Map showing location of cotton field. earth.google.com/web/.

Gutierrez, M., Norton, R., Thorp, K.R., Wang, G., 2012. Association of Spectral Reflectance Indices with Plant Growth and Lint Yield in Upland Cotton. Crop Sci. 52, 849–857.

Gwathmey, C.O., Tyler, D.D., Yin, X., 2010. Prospects for Monitoring Cotton Crop Maturity with Normalized Difference Vegetation Index. Agron. J. 102, 1352–1360.

He, M., Kimball, J.S., Maneta, M.P., Maxwell, B.D., 2018. Regional Crop Gross Primary Productivity and Yield Estimation Using Fused Landsat-MODIS Data. https://doi.org/10.3390/rs10030372

Huemmrich, K.F., Campbell, P., Landis, D., Middleton, E., 2019. Developing a common globally acceptable method for optical remote sensing of ecosystem light use efficiency. Remote Sens. Environ. 230.

Ibrahim, M.E., Buxton, D.R., 1981. Early Vegetative Growth of Cotton as Influenced by Leaf Type. Crop Sci. 21, 639–643.

Jaafar, H.H., Ahmad, F.A.., 2015. Relationships Between Primary Production and Crop Yields in Semi-Arid and Arid Irrigated Agroecosystems. Int. Symp. Remote Sens. Environ. 47, 27–30.

Johnson, D.M., 2016. A comprehensive assessment of the correlations between field crop yields and commonly used MODIS products. Int. J. Appl. EARTH Obs. Geoinf. 52, 65–81.

Kerr, J.T., Ostrovsky, M., 2003. From space to species: Ecological applications for remote sensing. Trends Ecol. Evol. 18, 299–305. https://doi.org/10.1016/S0169-5347(03)00071-5

LI-COR, 2015. SmartFlux System Instruction Manual.

Li, X., Liu, L., Yang, H., Li, Y., 2018. Relationships between carbon fluxes and environmental factors in a drip-irrigated, film-mulched cotton field in arid region. PLoS One 13, 1–18. https://doi.org/10.1371/journal.pone.0192467

Liu, P., 2017. The future of food and agriculture: Trends and challenges., Fao. https://doi.org/ISBN 978-92-5-109551-5

Monteith, J.L., 1977. Climate and Efficiency of Crop Production in Britain. Phil. Trans. R. Soc. Lond. 281.

Myneni, R.B., Nemani, R.R., Running, S.W., 1997. Estimation of global leaf area index and absorbed par using radiative transfer models. IEEE Trans. Geosci. Remote Sens. 35, 1380–1393.

National Oceanic and Atmospheric Administration, 2011. Climate Data Online [WWW Document]. Natl. Centers Environ. Inf.

Paw, K.T., Baldocchi, D.D., Meyers, T.P., Wilson, K.B., 2000. Correction of Eddy-Covariance Measurements Incorporating Both Advective Effects and Density Fluxes. Boundary-Layer Meteorol. 487–511.

Pegelow, E.J., Buxton, D.R., Briggs, R.E., Muramoto, H., Gensler, W.G., 1977. Canopy Photosynthesis and Transpiration of Cotton as Affected by Leaf Type. Crop Sci. 17, 1–4.

Peng, Y., Gitelson, A.A., 2012. Remote estimation of gross primary productivity in soybean and maize based on total crop chlorophyll content. Remote Sens. Environ. 117, 440–448. https://doi.org/10.1016/j.rse.2011.10.021

Peng, Y., Gitelson, A.A., 2011. Application of chlorophyll-related vegetation indices for remote estimation of maize productivity. Agric. For. Meteorol. 151, 1267–1276.

Peng, Y., Gitelson, A.A., Keydan, G., Rundquist, D.C., Moses, W., 2011. Remote estimation of gross primary production in maize and support for a new paradigm based on total crop chlorophyll content. Remote Sens. Environ. 115, 978–989.

PhytoGen, 2019. PhytoGen Cotton Varieties [WWW Document]. Corteva Agriscience. URL https://phytogencottonseed.com/varieties

Planet Team, 2018. No Title [WWW Document]. Planet Inc.

Planet Team, 2017. Planet Application Program Interface: In Space for Life on Earth. San Francisco, CA.

Qin, S., Li, S., Kang, S., Du, T., Tong, L., Ding, R., 2016. Can the drip irrigation under film mulch reduce crop evapotranspiration and save water under the sufficient irrigation condition? Agric. Water Manag. 177, 128–137. https://doi.org/10.1016/j.agwat.2016.06.022

Raper, T.B., Varco, J.J., Hubbard, K.J., 2013. Canopy-Based Normalized Difference Vegetation Index Sensors for Monitoring Cotton Nitrogen Status. Agron. J. 105, 1345–1354.

Reichstein, M., Falge, E., Baldocchi, D., Papale, D., Aubinet, M., Berbigier, P., Bernhofer, C., Buchmann, N., Gilmanov, T., Granier, A., Grunwald, T., Havrankova, K., Ilvesniemi, H., Janous, D., Knohl, A., Laurila, T., Lohila, A., Loustau, D., Matteucci, G., Meyers, T., Miglietta, F., Ourcival, J.-M., Pumpanen, J., Rambal, S., Rotenberg, E., Sanz, M., Tenhunen, J., Seufert, G., Vaccari, F., Vesala, T., Yakir, D., Valentini, R., 2005. On the separation of net ecosystem exchange into assimilation and ecosystem respiration : review and improved algorithm. Glob. Chang. Biol. 1424–1439. https://doi.org/10.1111/j.1365-2486.2005.001002.x

Ritchie, G.L., Sullivan, D.G., Vencill, W.K., Bednarz, C.W., Hook, J.E., 2010. Sensitivities of Normalized Difference Vegetation Index and a Green/Red Ratio Index to Cotton Ground Cover Fraction. Crop Sci. 50, 1000–1010.

Sakamoto, T., Gitelson, A.A., Wardlow, B.D., Verma, S.B., Suyker, A.E., 2011.

Estimating daily gross primary production of maize based only on MODIS WDRVI and shortwave radiation data. Remote Sens. Environ. 115, 3091–3101.

Shafian, S., Rajan, N., Schnell, R., Bagavathiannan, M., Valasek, J., Shi, Y., Olsenholler, J., 2018. Unmanned Aerial Systems-Based Remote Sensing for Monitoring Sorghum Growth and Development. PLoS One 13.

Sharma, S., Rajan, N., Cui, S., Casey, K., Ale, S., Jessup, R., Maas, S., 2017. Seasonal variability of evapotranspiration and carbon exchanges over a biomass sorghum field in the Southern U.S. Great Plains. Biomass and Bioenergy 105, 392–401.

Wang, Y., Woodcock, C.E., Buermann, W., Stenberg, P., Voipio, P., Smolander, H., Hame, T., Tian, Y., Jiannan, H., Knyazikhin, Y., Myneni, R.B., 2004. Evaluation of the MODIS LAI algorithm at a coniferous forest site in Finland. Remote Sens. Environ. 91, 114–127.

Webb, E.K., Pearman, G.I., Leuning, R., 1980. Correction of flux measurements for density effects due to heat and water vapour transfer. Q. J. R. Meteorol. Soc. 106, 85–100.

Yan, H., Fu, Y., Xiao, X., Huang, H.Q., He, H., Ediger, L., 2009. Modeling gross primary productivity for winter wheat-maize double cropping system using MODIS time series and CO2eddy flux tower data. Agric. Ecosyst. Environ. 129, 391–400. https://doi.org/10.1016/j.agee.2008.10.017

Yoder, B.J., Pettigrew-Crosby, R.E., 1995. Predicting nitrogen and chlorophyll content and concentration for reflectance spectra (400 - 2500 nm) at leaf and canopy scales. Remote Sens. Environ. 53, 199–211.

Yuan, W., Liu, S., Yu, G., Bonnefond, J.M., Chen, J., Davis, K., Desai, A.R., Goldstein, A.H., Gianelle, D., Rossi, F., Suyker, A.E., Verma, S.B., 2010. Global estimates of evapotranspiration and gross primary production based on MODIS and global meteorology data. Remote Sens. Environ. 114, 1416–1431. https://doi.org/10.1016/j.rse.2010.01.022

Zhao, M., Heinsch, F.A., Nemani, R.R., Running, S.W., 2005. Improvements of the MODIS terrestrial gross and net primary production global data set. Remote Sens. Environ. 95, 164–176. https://doi.org/10.1016/j.rse.2004.12.011

Zheng, Y., Zhang, L., Xiao, J., Yuan, W., Yan, M., Li, T., 2018. Sources of uncertainty in gross primary productivity simulated by light use efficiency models: Model structure, parameters, input data, and spatial resolution. Agric. For. Meteorol. 263, 242–257. https://doi.org/10.1016/j.agrformet.2018.08.003

Zhou, Y., Xiao, X., Wagle, P., Bajgain, R., Mahan, H., Basara, J.B., Dong, J., Qin, Y., Zhang, G., Luo, Y., Gowda, P.H., Neel, J.P.S., Starks, P.J., Steiner, J.L., 2017. Examining the short-term impacts of diverse management practices on plant phenology and carbon fluxes of Old World bluestems pasture. Agric. For. Meteorol. 237–238, 60–70. https://doi.org/10.1016/j.agrformet.2017.01.018

5. COMPARISON OF SIMULATED ET USING THE DSSAT-CERES-MAIZE MODELING SYSTEM TO MEASURED ET USING THE EDDY COVARIANCE METHOD FOR A CORN CROP IN EAST TEXAS

5.1. Introduction

Quantifying the impacts of agriculture on regional and global hydrologic cycles is a pressing scientific issue given concerns over the effects of anthropogenic climate change on water availability. Agricultural production disturbs soils and plant communities, which alters surface characteristics, energy balance, and thus evapotranspiration (ET) patterns compared to natural ecosystems. Agricultural production contributes significantly to ET with global ET estimates suggesting that approximately 11.6% of terrestrial ET is from croplands (Oki and Shinjiro, 2006). However, it is important to note that large-scale, i.e. global, ET estimates are difficult to achieve due to the highly variable nature of ET processes and the lack of ground truth data in many regions (Rodell et al., 2015). Expanding ET measurement and modeling efforts can improve these large-scale ET monitoring efforts and assist in predicting how ecosystems will respond to a changing climate. In addition to contributing to regional and global hydrologic cycles, ET associated with crop production makes up the majority (85 – 90%) of human water use (Foley et al., 2005; Oki and Shinjiro, 2006; Ramankutty et al., 2008; Rost et al., 2008). Agricultural ET is a strong predictor of crop productivity and thus economic yield due to the role of ET in the process of CO_2 assimilation (Sinclair and Muchow, 2001). Increased use of irrigation, the introduction of higher-

yielding cultivars, and the expansion of agricultural lands have caused ET associated with crop production to increase over the past few decades (Rost et al., 2008; Spera et al., 2016). A better understanding of crop ET can lead to better crop water management, which can improve the sustainability of agricultural systems.

Crop modeling is the practice of simulating crop growth and relevant processes, such as ET and soil water balance. Crop modeling uses known agronomic principals, weather data, soil properties, and, information about the crop's physiology to simulate the agronomic system. Modeling efforts can expand on our ability to understand ET dynamics by expanding observed trends and applying them to areas where direct measurement is too costly or impractical. Direct measurement from the eddy covariance system requires specific equipment and large areas with uniform terrain and vegetation. Modeling is also useful in predicting how changes in management or climate will affect crop performance and water dynamics (Soler et al., 2007; Pathak et al., 2012; Jones et al., 2017). Incorporating modeling with ground measurements has the potential to improve our understanding of crop water use by validating models with ground truth data.

Modeling efforts often utilize software systems to perform the complex calculations needed to simulate crop growth and environmental impacts. There are a variety of crop modeling software platforms available, such as DSSAT, APSIM, and CropSyst. The Decision Support System for Agrotechnology Transfer, DSSAT, is a modular-style modeling software platform with ET modeling capabilities. The DSSAT system incorporates multiple modules and mathematical models into one system.

DSSAT models ET by first calculating potential ET and modifying it to using the crop model to calculate crop ET. Potential ET is calculated by one of two internal methods; Priestly-Taylor/Ritchie (default), and FAO-56. The default method in the DSSAT system is the Priestly-Taylor/Ritchie method, which was developed in 1972 as a simplified version of the Penman-Monteith ET equation. This method uses solar radiation and temperature to calculate potential ET (Agam et al., 2010; Priestly and Taylor, 1972; Ritchie, 1972; Xu and Chen, 2005). DSSAT has more recently incorporated an additional ET modeling method, FAO-56, the method described Paper No. 56 from the Food and Agriculture Organization. This method is a more complete variation on the Penman-Monteith ET equation, which uses wind speed and humidity in addition to temperature and radiation (Agam et al., 2010; Dejonge and Thorp, 2017; Doorenbos and Pruitt, 1977; Monteith, 1986). The DSSAT software manual recommends using the FAO-56 method for arid and windy climates and the Priestly-Taylor/Ritchie for humid environments (Hoogenboom et al., 2003; Jones et al., 2003).

Once potential ET is calculated it is then modified by the crop model to determine crop ET. In corn, this is achieved by one of two modeling systems, IXIM, and CERES, this paper focuses on the CERES method. The Crop Environment Resource Synthesis (CERES) is a crop model that was developed in the 1980s to simulate yield from grass crops (corn, wheat, rice). The CERES model was incorporated into DSSAT very early in the creation of DSSAT (Hoogenboom et al., 2003; Jones et al., 2003, 2017; Basso et al., 2016). The CERES model simulates growth as distinct growth phases that are determined by growing degree-day accumulation (Hoogenboom et al., 2003).

While DSSAT has been widely used to model corn ET, it has been less successful in dryland systems, indicating a need for further study. A meta-analysis (111 studies) ET modeling in corn using DSSAT's CERES-Maize model found that it often performs well in highly irrigated systems (error less than 10%), but that model performance in dryland systems was typically poorer with an error greater than 12% (Basso et al., 2016). The DSSAT system's ET modeling efforts often underestimate measured ET, particularly in dryland and deficit irrigation systems (Dokoohaki et al., 2016). Given the concerns over the success of modeling ET in dryland systems, it is important to expand efforts to model ET in such systems. This study aims to model ET in dryland, conventionally tilled corn in East-Central Texas. Our objective is to model ET using the CERES model and both of DSSAT's internal potential ET methods. Modeled ET will be compared to ET measured with an eddy covariance system.

5.2. Methods

5.2.1. Field Information

The study was conducted at the Agrilife Research Farm in Burleson County, TX (30.549749, -96.423949), which is shown in Figure 23. An eddy covariance (EC) system was installed in the center of a dryland, conventionally tilled cornfield field in February 2017. The field is 33.67 ha in area and is located adjacent to the Brazos River. Corn was planted on March 10 in 2017, on March 6 in 2018, and on March 7 in 2019. Corn was harvested on July 25 in 2017, on July 19 in 2018 and on August 12 in 2019. A longer senescence period delayed harvest in 2019. Disc tillage was performed prior to

planting in 2017 and 2018; however, wet soil conditions prevented it in 2019. Disc tillage was performed after harvest in all three years. The varieties planted were B-H 8845 VTB in 2017, Pioneer P1602 AM in 2018, and DeKalb 67-42 in 2019. Nitrogen fertilizer was applied at a rate of 125 kg ha^{-1} each year.

The local climate is humid subtropical (Köppen Classification: Cfa) with an average (30-year) annual temperature of 20.6°C and annual precipitation of 1000 mm. Precipitation is bi-modal with the majority of precipitation occurring in May, June, and October. Monthly 30-year averages for the typical corn growing season (March – July) are shown in Figure 24. All 30-year averages are from NOAA's 30-year climatic average (1980 - 2010) from a weather station approximately 11 km from the field site (National Oceanic and Atmospheric Administration, 2011). There are two dominant soil types in the field, the Weswood silt loam (Udifluventic Haplustepts, 38% clay in the surface horizon) and the Ships clay (Chromic Halpludert, 42% clay in the surface horizon), both of which contain predominantly shrink-swell clay minerals that cause the soil to heavily crack during dry weather.

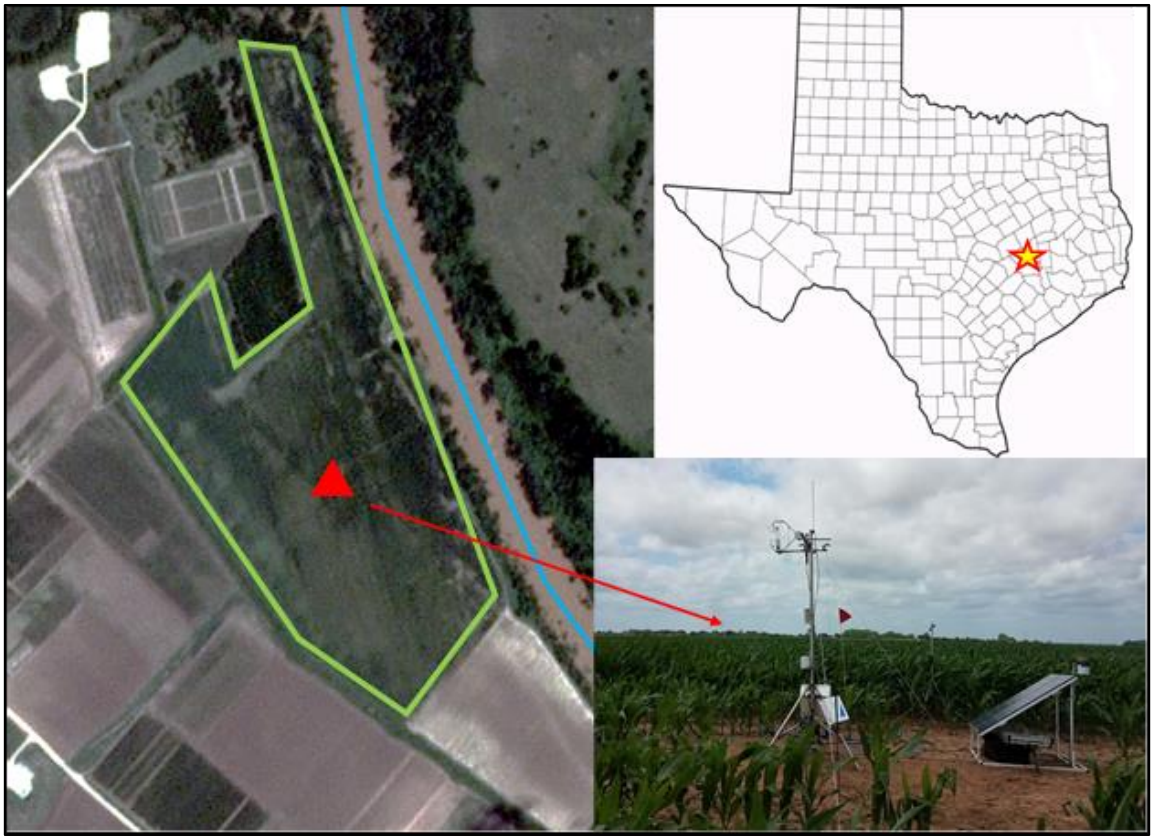

Figure 23: Image of corn site and eddy covariance tower
Images of the site and location are shown above. The image on the left is a satellite image of the field. The field is outlined in green with the location of the EC tower indicated by a red triangle. The Brazos River is highlighted with a blue line. The image on the upper right shows a map of Texas with the location of Burleson County marked with a star. The image on the lower right is a photograph of the EC tower.

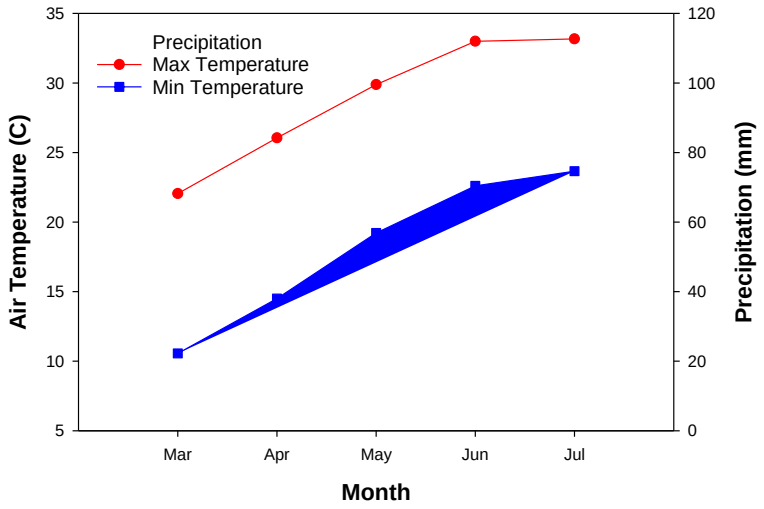

Figure 24: Monthly Average Weather for Location
Monthly temperature and precipitation averages for the typical growing season for corn in Burleson County, Texas are shown above. Averages are the 30-year average from the National Oceanic and Atmospheric Administration.

5.2.2. Instrumentation

The EC system is an open path system and consisted of an LI-7500 Infrared Gas Analyzer (IRGA; LI-COR, Lincoln, NE, USA) and a CSAT-3 Sonic Anemometer (Campbell Scientific, Logan, UT, USA). The EC instruments were connected to a SmartFlux system with embedded EddyPro (Version 6.2.2; L-COR, Lincoln, NE, USA) software. Data was collected at 10 Hz and then compiled into 30-minute summaries by the SmartFlux system. The EC instruments were installed on a tripod, facing due south (the direction of the prevailing winds), the height of the tower was maintained at 2 meters above the plant canopy. The instruments were calibrated and had their internal chemicals changed annually as recommended by the manufacturer.

Additional meteorological and soil instruments were installed at the site to augment the flux data and to allow for an energy balance calculation. Air temperature and relative humidity were collected using a temperature and relative humidity probe (HMP155A; Vaisala, Vantaa, Finland). Several aspects of solar radiation, incoming solar radiation, photosynthetically available radiation (PAR), and net radiation, were measured with the a pyranometer (LI-200R; LI-COR, Lincoln, NE, USA), a quantum sensor (LI-190R; LI-COR, Lincoln, NE, USA), and a net radiometer (NR-LITE2; Kipp & Zonen, Delft, Netherlands), respectively. Precipitation was measured with a tipping-bucket style rain-gauge (TE-525; Texas Electronics, Dallas, TX, USA). Soil instruments consisted of the following: seven soil moisture sensors (CS655; Campbell Scientific, Logan, UT, USA), four soil heat-flux plates (HPF01SC Hukseflux, Delft, Netherlands), and four soil thermocouples (TCAV; Campbell Scientific, Logan, UT, USA). Three of the soil moisture sensors were installed horizontally at 4 cm. Two soil moisture sensors were installed vertically between 10 and 20 cm. The remaining two soil moisture sensors were installed vertically between 10 and 20 cm. The soil heat-flux plates were buried at 8 cm and placed in pairs, 1 meter apart. The soil thermocouples were installed above the heat-flux plates with one probe at 2 cm and the other at 6 cm. All meteorological and soil instruments were connected to a datalogger (CR3000; Campbell Scientific, Logan, UT, USA) that was to collect measurements every 2 seconds and then compile the measurements into 30-minute summaries.

5.2.3. Eddy Covariance Data Processing and Analysis

The EddyPro software flagged data points that were likely to be erroneous based on internal turbulence tests; good quality data was marked with a "0", fair quality data was marked with a "1", and poor-quality data was marked with "2". Poor quality data was then manually removed. Gap filling was used to fill in missing (due to power loss and instrument malfunction) and removed data points. Gap filling was performed using the Max Plank Institute for Biogeochemistry's R-based program (R Gui 3.4.1) (Fritz et al., 2018). The EC data was also used to calculate an energy balance, a common method of correcting for any additional uncertainties in the EC data (Twine et al., 2000; Cook et al., 2004; Li et al., 2008; Hirschi et al., 2017). The energy balance formula is as follows:

$$R_n - G = LE + H.$$

Where:

$$G = (((1.02 + (VWC*4.19))*(\Delta T * 8) * (50/9))/G_{8\ cm}$$

Where Rn corresponds to the Net Radiation. LE and H correspond to the Latent and Sensible Heat, respectively, from the EC system. VWC corresponds to the Volumetric Water Content at four cm. ΔT was calculated as the difference in soil temperature from one thirty-minute time to the next. Soil heat at 8 cm ($G_{8\ cm}$) was the average of the 4-soil heat flux plates buried at 8 cm. Linear regression between Rn – G and LE + H was performed with the slope the regression line indicating the energy accounted for by the EC system. The unaccounted energy was redistributed to LE and H based on the Bowen ration.

5.2.4. DSSAT Model

The Decision Support System for Agrotechnology Transfer (DSSAT) software system (DSSAT Foundation, Gainsville, FL, USA) modeled crop growth and ET. Daily weather data from the meteorological instruments were added to the DSSAT system as a weather file. Separate soil files were created for each soil type found in the field (Ships clay and Weswood silt loam). Models were run using each soils file, models using the Ships clay as the input soils file will be referred to as Ships and models using the Weswood silt loam will be referred to as Weswood. The collected phenological data was added to DSSAT as a T-file to be used in calibrating the cultivar parameters. The Generalized Likelihood Uncertainty Estimation (GLUE) tool used the T-file to calibrate the cultivar file parameters used for the model, which are shown in Table 4. The GLUE tool creates many successive models and compares them to the actual recorded phenological information using a likelihood function and determines the best fit, this process has been shown to minimize uncertainty in parameter estimation (DSSAT, 2017, Pathak et al 2012). Since different cultivars were planted each year, calibration was done using each year's data alone. The species and ecotype files for corn were not modified. Following the creation of weather, soil, and cultivar files, the models themselves were set up using an experiment file.

Table 4: Optimized Corn Cultivars

Corn Cultivar Parameters				
Parameter	**Description**	**2017**	**2018**	**2019**
-	**Cultivar**	**B-H 8845 VTB**	**Pioneer P1602 AM**	**DeKalb 67-42**
P1	Growing Degree Days from emergence to end of vegetative growth	334.0	230.1	227.1
P2	Delay in development associated with day length longer than 12.5 hours	0.999	0.995	1.006
P5	Growing Degree Days from silk to maturity	842.0	793.2	791.2
G2	Kernels per plant	618.0	618.3	615.2
G3	Kernel growth rate	10.67	10.77	10.68
PHINT	Growing Degree Days between leaf appearances	38.90	45.00	38.90

The CERES-Maize model was used to simulate corn growth and development, CERES is one of two corn models available in DSSAT, the other being IXIM. CERES is primarily used for grass crops such as wheat, corn, and sorghum that uses a growing degree-day-based formula to model crop growth and development. The DSSAT system used a number of different sub-models to simulate environmental conditions (i.e. ET and soil moisture) that interact with the CERES model (Hoogenboom et al., 2003). Soil evaporation was modeled using the method developed by Suleiman and Ritchie in 1972. This method uses a two-step process, the first step occurs under high soil moisture and evaporation is limited only by available radiation energy. The second step occurs under

lower soil moisture and is limited by radiation, water availability, and soil properties (Hoogenboom et al., 2003; Suleiman and Ritchie, 2003; Ritchie et al., 2009). Soil organic matter was modeled the default DSSAT method, which is based on a modification of the PAPRAN model (Seligman and Van Keulen, 1981; Godwin and Jones, 1991; Godwin and Singh, 1998; Hoogenboom et al., 2003; Dejonge and Thorp, 2017). Soil water movement was modeled using the method developed for CERES; which is the default method. This model calculates water content in each soil layer on a daily time-scale using rainfall, ET, drainage, irrigation, and unsaturated water flow (Ritchie and Otter, 1985; Jones and Ritchie, 1991; Jones, 1993; Ritchie, 1998; Hoogenboom et al., 2003). The CERES-Maize model predicts daily canopy photosynthesis based on solar radiation, temperature, water availability, nitrogen availability, leaf biomass, row spacing, crop genetics, and atmospheric CO_2 concentration (Jones et al., 1989; Hoogenboom et al., 2003). Corn ET was modeled using both of DSSAT's built-in methods: FAO-56 and Priestly-Taylor/Ritchie, both of these methods model potential ET, which is then modified by CERES to estimate crop ET using soil water and crop growth information (Hoogenboom et al., 2003). Results from the ET methods will be compared to each other. Models using the Priestly-Taylor/Ritchie method will be referred to as PT, and models using the FAO-56 method will be referred to as FAO.

5.2.5. Statistical Analysis

Statistical analysis was performed using DSSAT's internal system and manual calculation. The following indices of model performance were manually calculated:

index of agreement (D-Index), normalized root mean square error (nRMSE), r-squared, and co-coefficient of residual mass (CRM). The D-index shows the degree of fit between the modeled data and the real data, with a perfect fit between the modeled and observed data giving a D-index of 1.0 and no fit giving a D-index of 0.0 (Soler et al., 2007; Adhikari et al., 2016; Basso et al., 2016; Amouzou et al., 2018). The calculation of the D-index is as follows, where x is the modeled value and y is the observed value:

$$d = 1 - [\frac{\sum(x - \bar{x})^2}{\sum(|x - \bar{x}| + |y - \bar{y}|)^2}]$$

The CRM shows the degree of over or underestimation between the model and the measured data. A perfect fit between a model and measurement would give a CRM of zero, positive numbers indicate underestimation and negative numbers indicate overestimation by the model (Xevi et al., 1996; Jalota et al., 2010; Dettori et al., 2011).

$$\text{CRM} = \frac{\sum y - \sum x}{\sum y}$$

5.3. Results and Discussion

5.3.1. Phenology Models

The phenology (height, biomass, and leaf area) models for 2017 are shown in Figure 25 and their statistical results are shown in Table 5. The Leaf Area Index (LAI) model (Figure 25A) slightly underestimated actual LAI during the earlier portion of the growing season. The Weswood LAI had a slight drop in LAI during the mid-growing season that was not seen in the Ships model or in the actual data. The Weswood model predicted a maximum LAI of 2.61, while the observed maximum LAI for the Weswood soil was 2.56. The RMSE for this model was 0.56. The Ships model predicted a

maximum LAI of 2.87, while the observed maximum LAI for the Ships soil was 2.59. The RMSE for this model was 0.42. A meta-analysis of 23 studies using DSSAT's CERES MAIZE to model LAI found a typical RMSE for dryland models to be 0.84 and that most studies had a d-Index above 0.8 (Basso et al., 2016). Other studies of LAI modeling using CERES-Maize produced similar results (Xevi et al., 1996). The result for these LAI models were well within the range of results observed in other studies.

The biomass models (Figure 25B) performed well. The Weswood model predicted a maximum aboveground biomass of 12951 kg ha^{-1}, while the observed maximum aboveground biomass for the Weswood soil was 13187 kg ha^{-1} with an RMSE of 1331.53 kg ha^{-1}. The Ships model predicted a maximum aboveground biomass of 14557 kg ha^{-1}, while the observed maximum aboveground biomass for the Ships soil was 12026 kg ha^{-1} with an RMSE of 772.16 kg ha^{-1}. The results of the 2017-biomass models were within those of other modeling efforts. Other modeling studies using CERES-Maize had a wide range of RMSE values (400 kg ha^{-1} – 5000 kg ha^{-1}) for the aboveground biomass, however most modeling efforts produced an RMSE approximately between 1500 kg ha^{-1} and 2000 kg ha^{-1} (Saseendran et al., 2005; Mubeen et al., 2013; Basso et al., 2016).

During 2017, the corn height model (Figure 25C) performed quite well for the first half of the growing season; however, it underestimated the actual plant height at maturity. This is due to a limitation in the CERES model, which sets a maximum plant height at 1.6 meters (Hoogenboom et al., 2003), thus the maximum predicted plant

height using both soil models was 1.6 meters while the actual maximum height was 2.02 m in the Ships soil and 2.17 m in the Weswood soil.

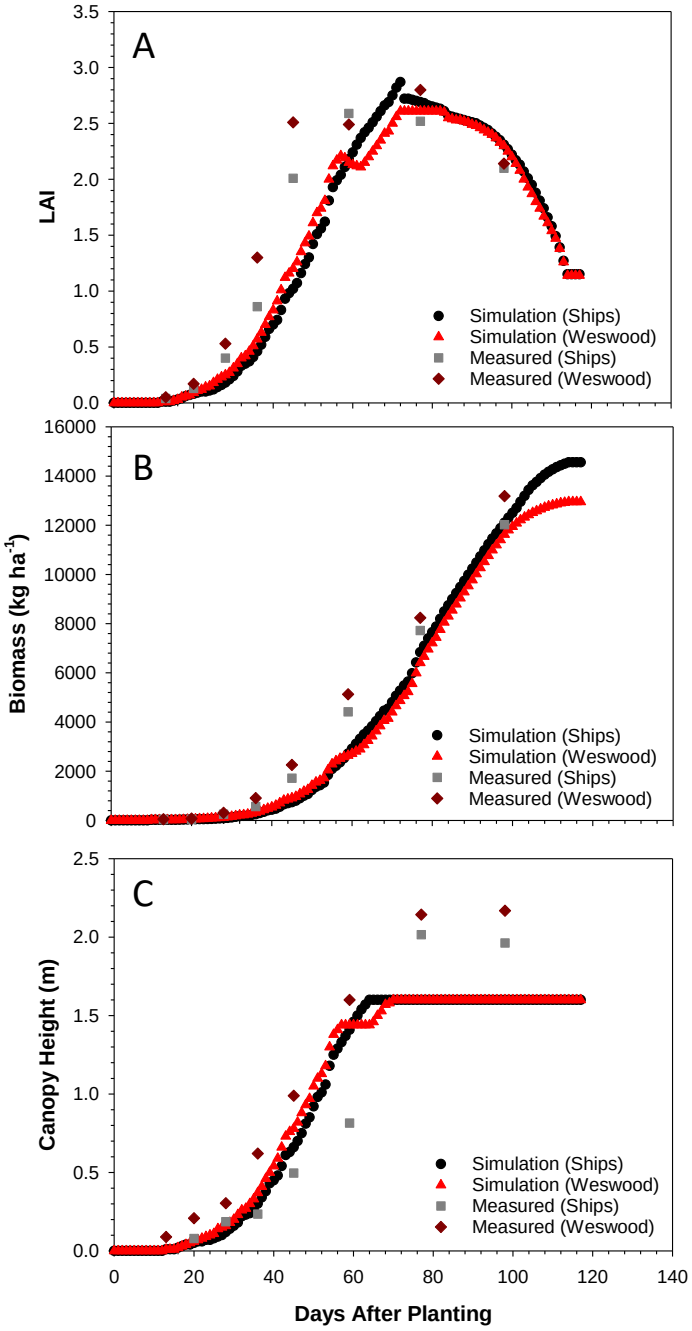

Figure 25: 2017 Corn Phenology Models

The 2017 Phenology models are shown above. Figure "A" is the LAI model, Figure "B" is the biomass model, and Figure "C" is the canopy height model. The black circles refer to the model using the Ships soil file. The grey squares refer to the measured points from

the area of the field with the Ships clay soil. The red triangles refer to the model using the Weswood soil file. The maroon diamonds refer to the measured points from the area of the field with the Weswood silt loam.

Table 5: Statistical Results for 2017 Phenology Model

2017 Phenology Models						
	Plant Height		Leaf Area Index		Biomass	
Statistic	**Ships Clay**	**Weswood Silt Loam**	**Ships Clay**	**Weswood Silt Loam**	**Ships Clay**	**Weswood Silt Loam**
RMSE	0.32	0.32	0.42	0.56	772.16	1331.53
R^2	0.84	0.98	0.88	0.83	0.98	0.98
D-Index	0.95	0.95	0.96	0.93	0.99	0.98

The phenology models for 2018 are shown in Figure 26 and Table 6. The LAI model (Figure 26A) using the Ships soils file simulated a lower LAI at maturity than the model using the Weswood file, which is the inverse of what was observed in 2017. The model using the Weswood soil file underestimated LAI during the dry-down period. The Weswood model predicted a maximum LAI of 3.11, while the observed maximum LAI for the Weswood soil was 3.06 with an RMSE for this model was 0.39. The Ships model predicted a maximum LAI of 2.80, while the observed maximum LAI for the Ships soil was 2.54. The RMSE for this model was 0.28. As with 2017, the error rate for the LAI model was similar to those seen in other modeling studies using CERES.

The biomass models (Figure 26B) both underestimated actual biomass, although the effect was more pronounced with the Ships model. The Weswood model predicted a maximum aboveground biomass of 12174 kg ha^{-1}, while the observed maximum aboveground biomass for the Weswood soil was 12649 kg ha^{-1} with an RMSE of 946.74

kg ha^{-1}. The Ships model predicted a maximum aboveground biomass of 13352 kg ha^{-1}, while the observed maximum aboveground biomass for the Ships soil was 8016 kg ha^{-1} with an RMSE of 2571.74 kg ha^{-1}. The error for the Ships model was greater than expected but still within the range observed by other studies (Basso et al., 2016). As with 2017, the CERES model set the maximum high to 1.6 meters, causing the mature height to be underestimated (Figure 26C). Additionally, the height model overestimated observed height during the early growing season. The observed maximum height was 2.5 m for the Ships soil and 2.8 m for the Weswood soil.

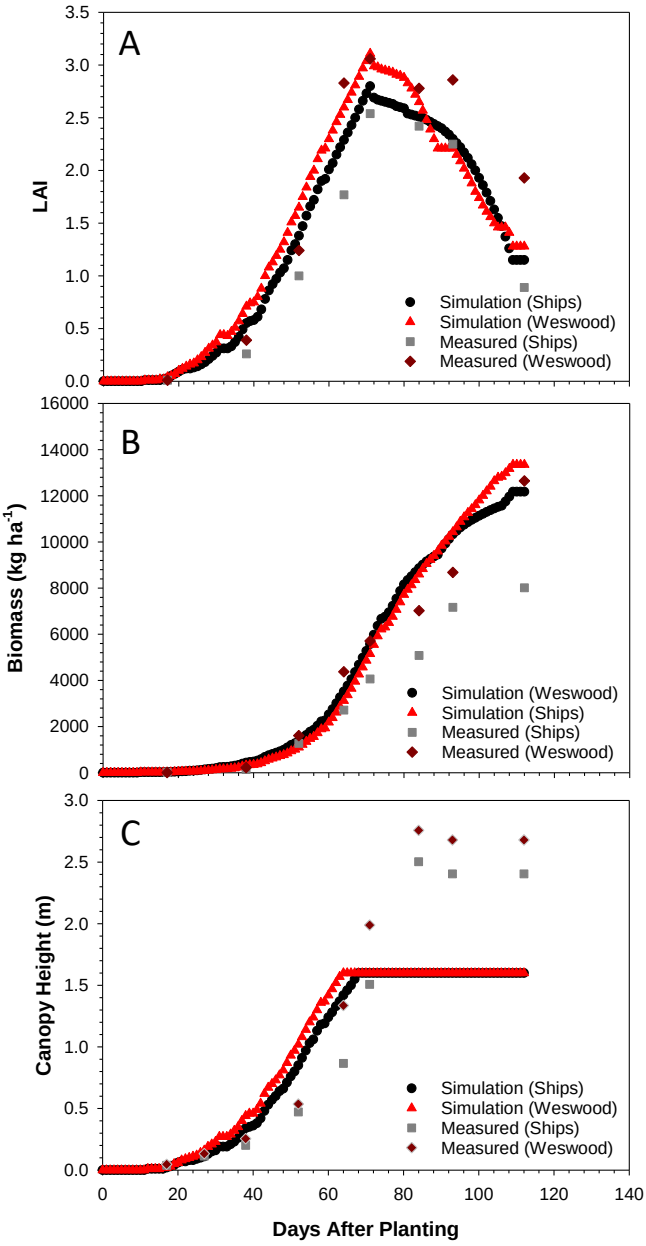

Figure 26: 2018 Corn Phenology Models

The 2018 Phenology models are shown above. Figure "A" is the LAI model, Figure "B" is the biomass model, and Figure "C" is the canopy height model. The black circles refer to the model using the Ships soil file. The grey squares refer to the measured points from the area of the field with the Ships clay soil. The red triangles refer to the model using

the Weswood soil file. The maroon diamonds refer to the measured points from the area of the field with the Weswood silt loam.

Table 6: Statistical Results for 2018 Corn Phenology Models

2018 Phenology Models						
	Plant Height		Leaf Area Index		Biomass	
Statistic	**Ships Clay**	**Weswood Silt Loam**	**Ships Clay**	**Weswood Silt Loam**	**Ships Clay**	**Weswood Silt Loam**
RMSE	0.54	0.68	0.28	0.39	2571.74	946.74
R^2	0.78	0.79	0.97	0.90	0.98	0.96
D-Index	0.89	0.85	0.98	0.97	0.89	0.99

The phenology models for 2019 are shown in Figure 27 and Table 7. The LAI model (Figure 27A) using the Weswood soil file overestimated LAI during the peak of the growing season. The model using the Ships clay file followed the measured data much more accurately, including data points from the areas of the field with Weswood soils. The Weswood model predicted a maximum LAI of 3.70, while the observed maximum LAI for the Weswood soil was 2.85 with an RMSE for this model was 0.49. The Ships model predicted a maximum LAI of 3.02, while the observed maximum LAI for the Ships soil was 2.46 with an RMSE for this model was 0.32.

The biomass model (Figure 27B) performed well with the Weswood model estimating a slightly higher biomass than the Ships model. The Weswood model predicted a maximum aboveground biomass of 13738 kg ha^{-1}, while the observed maximum aboveground biomass for the Weswood soil was 11349 kg ha^{-1} with an RMSE

of 1032.55 kg ha^{-1}. The Ships model predicted a maximum aboveground biomass of 12065 kg ha^{-1}, while the observed maximum aboveground biomass for the Ships soil was 8926 kg ha^{-1} with an RMSE of 1197.05 kg ha^{-1}. The height models (Figure 27C) performed similarly in 2019 to previous years.

Compared to each other, the 2018 models had the least agreement with the measured data, while the 2017 and 2019 models had a similar agreement with the measured data. The primary differences between the years were the weather data and the calibrated cultivar parameters. The model settings and methods were kept constant between the years. A comparison of 23 studies using CERES-Maize with DSSAT to model LAI found an average RMSE of 0.84 for dryland and limited irrigation systems. All RMSE values for this study were well within this range, and many were closer to the average RMSE value of 0.31 for irrigated systems (Basso et al., 2016; Jones et al., 2017). The same meta-analysis also looked at biomass models with 31 studies of biomass modeling with CERES-Maize. Reported errors in biomass studies varied widely with the average RMSE in dryland and deficit irrigation studies being 1998.8 kg ha^{-1}(Basso et al., 2016). The biomass model from 2018 using the Ships soils file was the only one to have an RMSE greater than this, however several studies reported an RMSE of over 5000 kg ha^{-1} (Carberry, 1991; Lopez-Cedron et al., 2008).

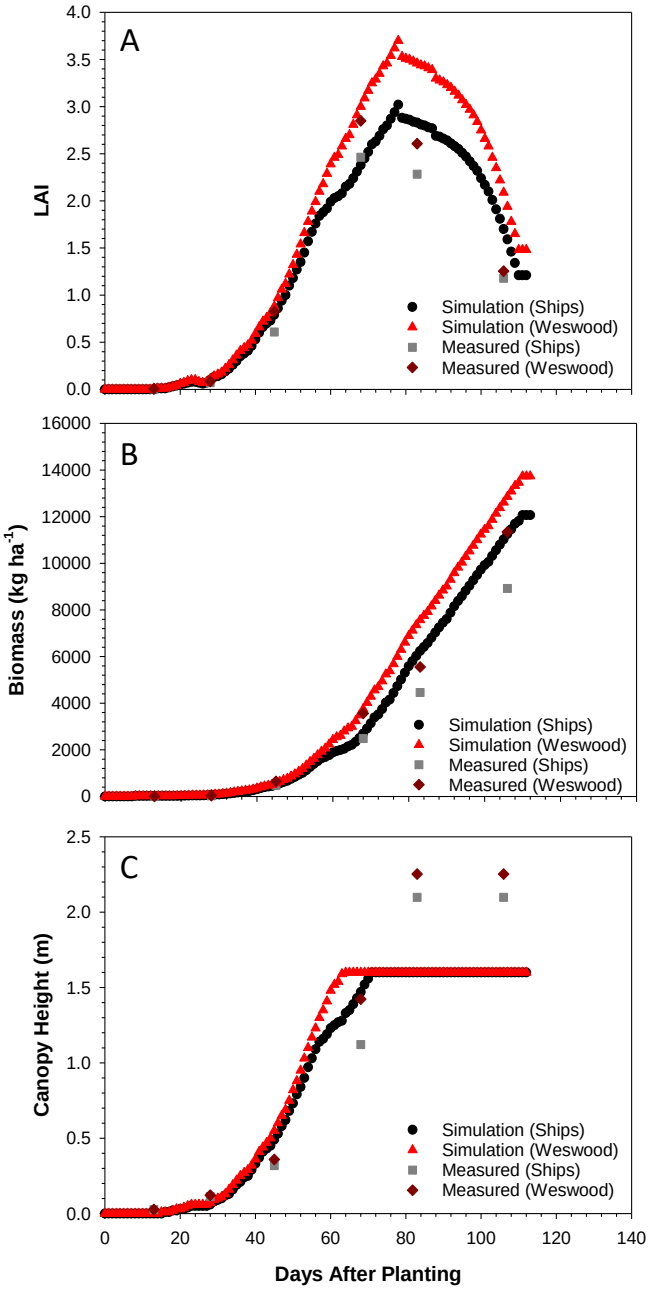

Figure 27: 2019 Corn Phenology Models

The 2019 Phenology models are shown above. Figure "A" is the LAI model, Figure "B" is the biomass model, and Figure "C" is the canopy height model. The black circles refer to the model using the Ships soil file. The grey squares refer to the measured points from the area of the field with the Ships clay soil. The red triangles refer to the model using the Weswood soil file. The maroon diamonds refer to the measured points from the area of the field with the Weswood silt loam.

Table 7: Statistical Results for 2019 Corn Phenology Models

2019 Phenology Models						
	Plant Height		**Leaf Area Index**		**Biomass**	
Statistic	**Ships Clay**	**Weswood Silt Loam**	**Ships Clay**	**Weswood Silt Loam**	**Ships Clay**	**Weswood Silt Loam**
RMSE	0.16	0.11	0.32	0.49	1197.05	1032.55
R^2	0.96	0.98	0.95	0.94	0.995	0.99
D-Index	0.99	0.99	0.98	0.96	0.97	0.9

5.3.2. Energy Balance

The energy balance closure is shown in Figure 28. The energy balance closure (the slope of the regression line for Rn-G v LE+H) was 0.70 in 2017, 0.86 in 2018, and 0.84 in 2019. These values are within the range of energy balance closures of other EC studies. One of the largest meta-analysis of EC sites and energy balance closure found an average closure of 0.79 with a range of 0.53 to 0.99 over 22 sites (Wilson et al., 2002). Studies in corn specifically have cited energy balance closure well within this range with most citing a closure between 0.75 and 0.90 (Twine et al., 2000; Saigusa et al., 2002; Baker and Griffis, 2005; Yu et al., 2006; Li et al., 2008, 2018; Carmelita et al., 2014).

The 2017 closure was on the lower end of the range of typical energy balance slopes. The 2018 and 2019 closures were typical for EC studies and were above the average closure for the meta-analysis by Wilson, et al.

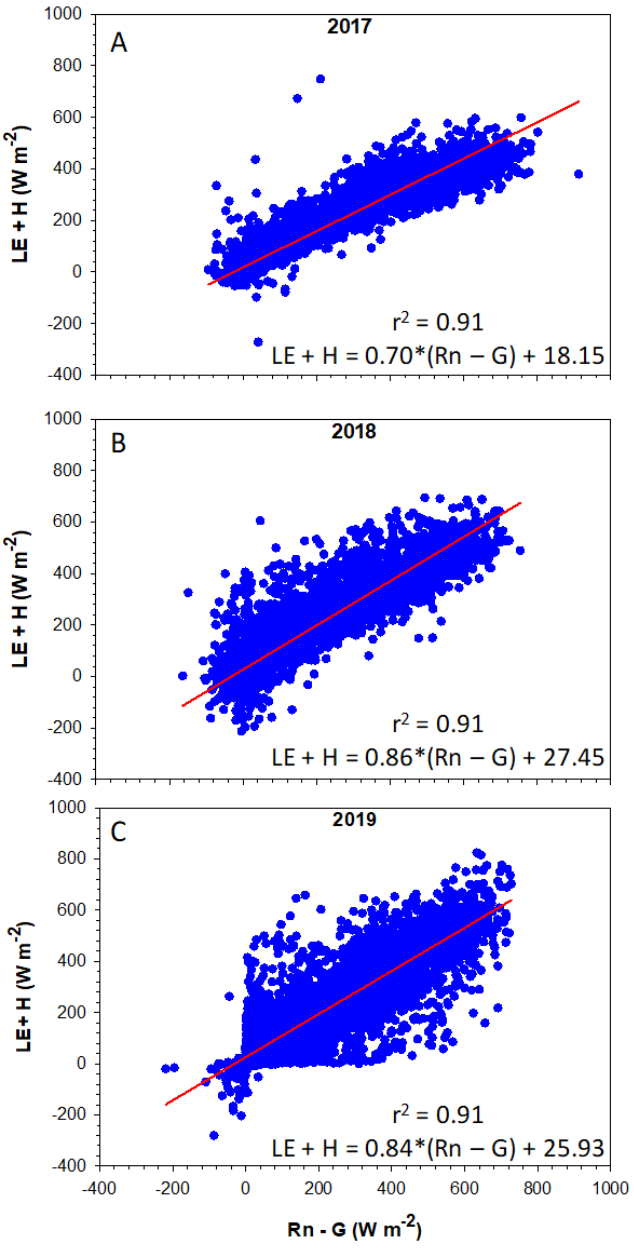

Figure 28: Corn Energy Balance Closure

The energy balance closure is shown above. Image “A” shows the closure for 2017. Image “B” shows 2018. Image “C” shows 2019. The red line shows the best fit for the data. Equation of the regression line and the r-square are also shown in the images above.

5.3.3. Evapotranspiration Models

The evapotranspiration models for 2017, 2018, and 2019 are shown in Figure 29, Figure 30, and Figure 3, respectively and the statistical analysis are shown in Table 8. The total measured ET in 2017 was 461.12 mm. The Priestly-Taylor model predicted a total ET of 459.20 mm using the Weswood soils file and a total ET of 500.70 mm using the Ships file. The FAO-56 model predicted a total ET of 456.39 mm using the Weswood soils file and 491.23 mm using the Ships soils file. In 2017, the best agreement between measured and modeled ET was during the late vegetative and reproductive growth periods in both models. Both models underestimated ET during the early vegetative and senescence periods. The Priestly-Taylor model had a tendency to overestimate ET during the main growing season, which was not seen in the FAO-56 model. The models using the Ships soils file had a greater tendency to overestimate ET. The lowest nRMSE (0.35 mm) was with the FAO-56 model using the Ships soils file. This is a higher nRMSE than ideal, however it is within the range of other dryland studies (Anothai et al., 2013; Basso et al., 2016).

The total measured ET in 2018 was 410.95 mm. The Priestly-Taylor model predicted a total ET of 323.72 mm using the Weswood soils file and a total ET of 376.78

mm using the Ships file. The FAO-56 model predicted a total ET of 334.05 mm using the Weswood soils file and 388.74 mm using the Ships soils file. All 2018 models greatly underestimated actual ET during the early vegetative phase, although this was less prominent for the FAO-56 models. The models (both FAO-56 and Priestly-Taylor) that used the Weswood soils file tended to underestimate ET during the late growing season compared to models using the Ships soils file. All 2018 models underestimated the actual ET (CRM greater than 0), however, it was only a slight overestimation for models using the Ships soils file. The Priestly-Taylor model using the Ships soil file had a good index of agreement (above 0.8) and had the lowest nRMSE of all of the 2018 models.

The total measured ET in 2019 was 410.86 mm. The Priestly-Taylor model predicted a total ET of 327.70 mm using the Weswood soils file and a total ET of 321.38 mm using the Ships file. The FAO-56 model predicted a total ET of 318.59 mm using the Weswood soils file and 310.49 mm using the Ships soils file. All 2019 models significantly underestimated ET; this was particularly true during the latter half of the growing season. Error between all 2019 models was similar (nRSME 0.31 mm & 0.33 mm). While the 2019 models underestimated ET, the pattern of the fluxes was modeled accurately, as all the models had a high index of agreement (D-Index above 0.8) and r-square values compared to the models in previous years. The model is likely underestimating ET in 2019 due to the change in tillage practices. As pre-plant tillage did not take place in 2019, pre-plant tillage was not included in 2019, which was different from the models in previous years.

Across all three years, the models in 2017 performed poorly compared to the models in 2018 and 2019. In all models except for the 2018 model with the Ships soils file, the FAO-56 method produced more accurate results than the Priestly-Taylor method. There was a tendency of most of the models to underestimate actual ET. Model error was within the typical range for DSSAT studies using dryland production. The use of DSSAT to model dryland production typically produces more error than with irrigated production (Sau et al., 2004; Anothai et al., 2013; Soldevilla-Martinez et al., 2014; Basso et al., 2016). This reduced accuaracy in dryland systems is a potential problem for modeling in regions where dryland farming the predominate management practice.

There is some evidence that the second stage of the soil water model used by DSSAT is contributing to this problem. In irrigated systems, regular water applications assure that the second-stage soil water flow is less prominent in determining soil water availability and evaporation (Suleiman and Ritchie, 2003; Ritchie et al., 2009). This is likely exacerbated by the presences of shrink-swell minerals at this site, which have been well-established to alter soil water processes by creating preferential flow and allowing for evaporation from deep within the soil via cracks (Patil and Rajput, 2009; Harmel et al., 2019). Finally, over the decades, in the time since the DSSAT system's crop coefficients were developed, corn breeder have been developing new traits that impact crop water use and evapotranspiration.

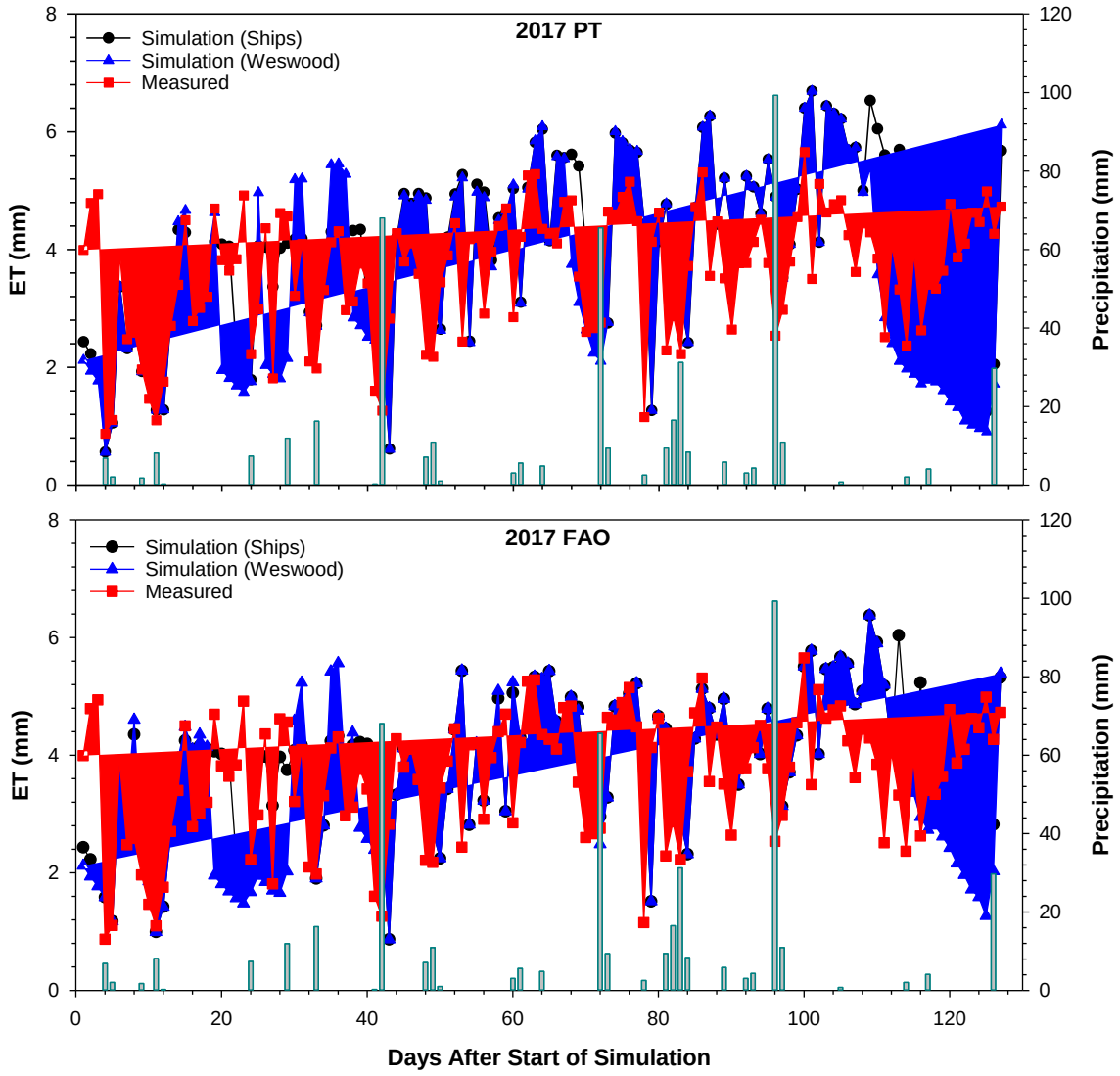

Figure 29: 2017 Corn Evapotranspiration Models
The ET models for 2017 are shown above against measured ET and rainfall. The top image shows the models using the Priestly-Taylor method. The bottom image shows the models using the FAO-56 method. The x-axis shows days after the start of the simulation. The left y-axis shows ET in millimeters. The right y-axis shows rainfall in millimeters. The vertical bars represent daily rainfall. The black circles show modeled

ET using the Ships soils file. The blue triangles show modeled ET using the Weswood soil file. The red squares show measured ET from the EC system.

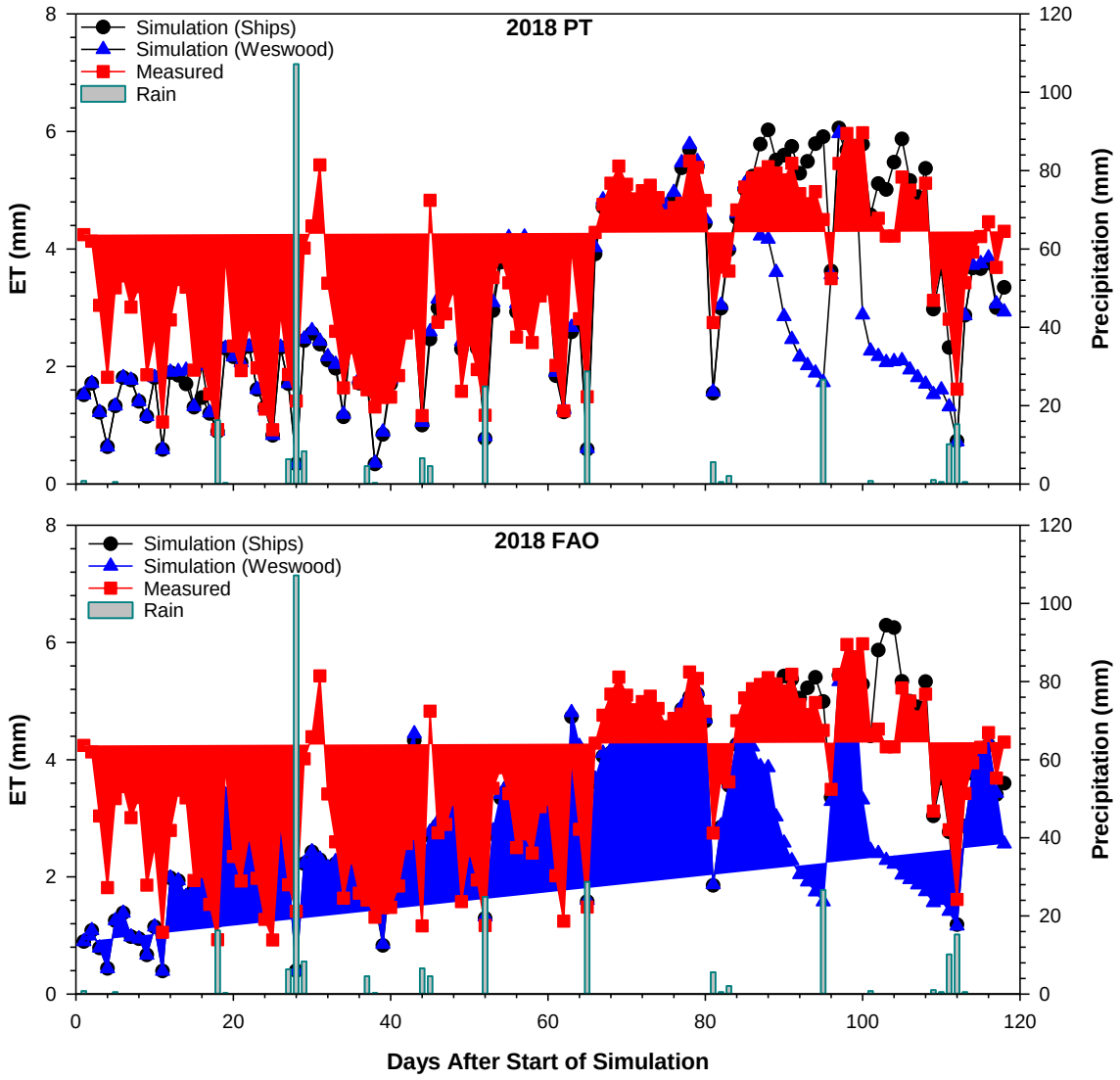

Figure 30: 2018 Corn Evapotranspiration Models
The ET models for 2018 are shown above against measured ET and rainfall. The top image shows the models using the Priestly-Taylor method. The bottom image shows the models using the FAO-56 method. The x-axis shows days after the start of the

simulation. The left y-axis shows ET in millimeters. The right y-axis shows rainfall in millimeters. The vertical bars represent daily rainfall. The black circles show modeled ET using the Ships soils file. The blue triangles show modeled ET using the Weswood soil file. The red squares show measured ET from the EC system.

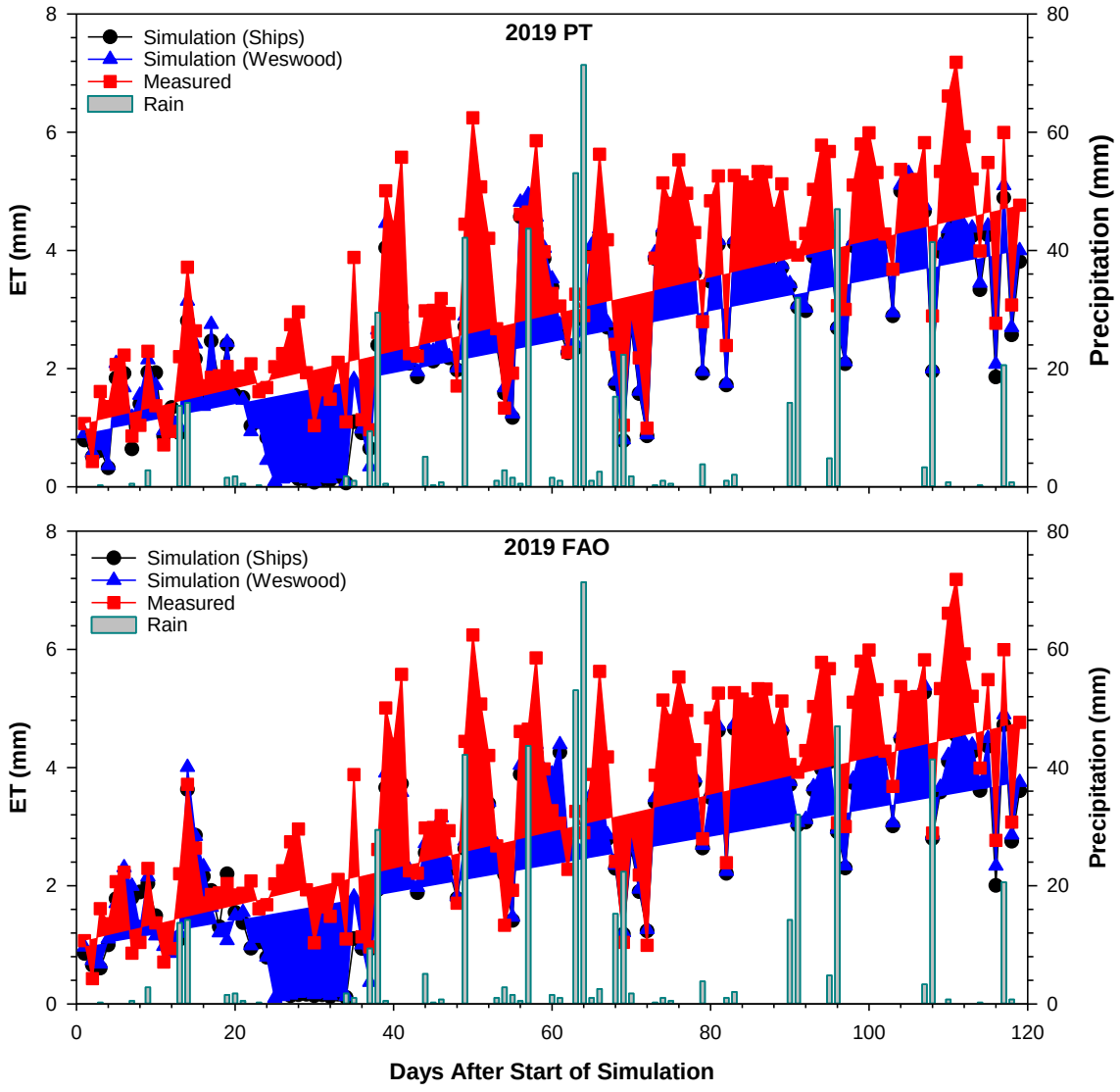

Figure 31: 2019 Corn Evapotranspiration Models

The ET models for 2017 are shown above against measured ET and rainfall. The top image shows the models using the Priestly-Taylor method. The bottom image shows the models using the FAO-56 method. The x-axis shows days after the start of the simulation. The left y-axis shows ET in millimeters. The right y-axis shows rainfall in millimeters. The vertical bars represent daily rainfall. The black circles show modeled ET using the Ships soils file. The blue triangles show modeled ET using the Weswood soil file. The red squares show measured ET from the EC system.

Table 8: Corn Evapotranspiration Model Statistical Results

ET Model Statistics						
	2017		2018		2019	
Statistic	**Weswood**	**Ships**	**Weswood**	**Ships**	**Weswood**	**Ships**
Priestly-Taylor/Ritchie Model						
nRMSE	0.46	0.43	0.39	0.26	0.31	0.33
CRM	-0.05	-0.15	0.21	0.08	0.22	0.24
D-index	0.75	0.76	0.79	0.86	0.87	0.86
R^2	0.13	0.16	0.45	0.74	0.79	0.80
FAO-56 Model						
nRMSE	0.39	0.35	0.42	0.30	0.31	0.32
CRM	0.01	-0.13	0.19	0.05	0.20	0.22
D-index	0.76	0.79	0.72	0.75	0.87	0.85
R^2	0.10	0.16	0.26	0.56	0.77	0.76

5.4. Conclusions

The phenology models were reasonably successful with the outcomes being similar to those reported in other studies of modeling corn growth in dryland production. The modeling efforts using the DSSAT system to model ET in dryland corn were met with mixed success. The nRMSE for the models ranged between 0.26 mm to 0.46 mm. The FAO-56 method produced results that are more consistent and usually had better agreement with the measured data. The inclusion of different soils files affected the modeling results, highlighting the potential problem of non-uniform soils in modeling efforts. The models often underestimated actual ET, which increased the error associated with the model. Unfortunately, mixed results like this are somewhat typical for ET modeling efforts in dryland systems. This effect is likely exacerbated by the presence of 2:1 shrink-swell clays at the site. The DSSAT system does not differentiate between clay minerals, which could be affecting model success. The gap in accuracy between irrigated and dryland modeling efforts is a particular problem in regions where dryland production is the predominate practice. Further work is needed to improve the accuracy of DSSAT's ET modeling in dryland systems.

5.5. Acknowledgment

This work is supported by NIFA-NLGCA [grant no. 2016-70001-24636/project accession no. 1008730] from the USDA National Institute of Food and Agriculture. The authors would like to thank Dr. Don T. Conlee (Department of Atmospheric Sciences, Texas A&M University) for providing missing meteorological data. The authors would like to thank Texas A&M Agrilife and the staff at the research farm, particularly Mr.

Alfred Nelson (Farm Manager) for planting and managing the cotton field. We would also like to thank Dr. Gerrit Hoogenboom (Department of Agricultural and Biological Engineering, University of Florida) and the DSSAT Foundation for their advice with operating and troubleshooting the DSSAT software system.

5.6. References

Adhikari, P., S. Ale, J.P. Bordovsky, K.R. Thorp, N.R. Modala, N. Rajan, and E.M. Barnes. 2016. Simulating future climate change impacts on seed cotton yield in the Texas High Plains using the CSM-CROPGRO-Cotton model. Agric. Water Manag. 164: 317–330. doi: 10.1016/j.agwat.2015.10.011.

Agam, N., W.P. Kustas, and M.C. Anderson. 2010. Application of the Priestley – Taylor Approach in a Two-Source Surface Energy Balance Model. Am. Meterorological Soc. 11: 185–198. doi: 10.1175/2009JHM1124.1.

Ahlrichs, J.S., and M.E. Bauer. 1983. Relation of Agronomic and Multispectral Reflectance Characteristics of Spring Wheat Canopies1. Agron. J. 75(6): 987–993. doi: 10.2134/agronj1983.00021962007500060029x.

Alganci, U., M. Ozdogan, E. Sertel, and C. Ormeci. 2014. Field Crops Research Estimating maize and cotton yield in southeastern Turkey with integrated use of satellite images , meteorological data and digital photographs. F. Crop. Res. 157: 8–19. doi: 10.1016/j.fcr.2013.12.006.

Altieri, M.A. 1999. The ecological role of biodiversity in agroecosystems. Agric. Ecosyst. Environ. 74(1–3): 19–31. doi: 10.1016/S0167-8809(99)00028-6.

Amouzou, K.A., J.B. Naab, J.P.A. Lamers, C. Borgemeister, M. Becker, and P.L.G.

Vlek. 2018. CROPGRO-Cotton model for determining climate change impacts on yield, water- and N- use efficiencies of cotton in the Dry Savanna of West Africa. Agric. Syst. 165(November 2017): 85–96. doi: 10.1016/j.agsy.2018.06.005.

Anothai, J., C.M.T. Soler, A. Green, T.J. Trout, and G. Hoogenboom. 2013. Evaluation of two evapotranspiration approaches simulated with the CSM–CERES–Maize model under different irrigation strategies and the impact on maize growth, development and soil moisture content for semi-arid conditions. Agric. For. Meteorol. 176(July): 64–76.

Anthoni, P.M., B.E. Law, and M.H. Unsworth. 1999. Carbon and water vapor exchange of an open-canopied ponderosa pine ecosystem. Agric. For. Meteorol. 95(3): 151–168. doi: 10.1016/S0168-1923(99)00029-5.

Asrar, G., M. Fuchs, E.T. Kanemasu, and J.L. Hatfield. 1984. (1984) Estimating Absorbed Photosynthetic Radiation and Leaf Area Index from Spectral Reflectance in Wheat (AJ).

Aubinet, M., T. Vesala, and D. Papale. 2012. Eddy Covariance: A Practical Guide to Measurement and Data Analysis. Springer Atmospheric Sciences, Berlin, Germany.

Bagavathiannan, M., and J.K. Norsworthy. 2012. Late-Season Seed Production in Arable Weed Communities: Management Implications. Weed Sci. 60(3): 325–334.

Bai, J., J. Wang, X. Chen, G.P. Lou, H. Shi, L.H. Li, and J. Li. 2015. Seasonal and inter-variations in carbon fluxes and evapotranspiration over cotton field under drip irrigation and plastic mulch in an arid region of Northwest China. J. Arid Land 7(2): 272–282.

Baker, J.M., and T.J. Griffis. 2005. Examining strategies to improve the carbon balance of corn / soybean agriculture using eddy covariance and mass balance techniques. Agric. For. Meteorol. 128: 163–177. doi: 10.1016/j.agrformet.2004.11.005.

Baldocchi, D.D. 2003. Assessing the eddy covariance technique for evaluating carbon dioxide exchange rates of ecosystems: past, present and future. Glob. Chang. Biol. 9(4): 479–492. doi: 10.1046/j.1365-2486.2003.00629.x.

Ballester, C., J. Brinkhoff, W.C. Quayle, and J. Hornbuckle. 2019. Monitoring the Effects of Water Stress in Cotton Using the Green Red Vegetation Index and Red Edge Ratio. Remote Sens. 11(7).

Baret, F., and G. Guyot. 1991. Potentials and limits of vegetation indices for LAI and APAR assessment. Remote Sens. Environ. 35(2–3): 161–173. doi: 10.1016/0034-4257(91)90009-U.

Basso, B., L. Liu, and J.T. Ritchie. 2016. A Comprehensive Review of the CERES-Wheat, -Maize and -Rice Models' Performances. Elsevier Inc.

Bednarz, C.W., and R.L. Nichols. 2005. Phenological and Morphological Components of Cotton Crop Maturity. Crop Sci. 45(4): 1497–1503.

Bell, J. 2017. Corn Growth Stages and Development.

Bennett, E.M., G.D. Peterson, and L.J. Gordon. 2009. Understanding relationships among multiple ecosystem services. Ecol. Lett. 12(12): 1394–1404. doi: 10.1111/j.1461-0248.2009.01387.x.

Boman, R., and R. Lemon. 2005. Soil Temperatures for Cotton Planting. College Station, Texas.

Boote, K.J., and N.B. Pickering. 1994. Modeling Photosynthesis of Row Crop Canopies. HortScience 29(12): 1423–1434.

Bozorov, T.A., R.M. Usmanov, H.L. Yang, S.A. Hamdullaev, S. Musayev, J. Shakiev, S. Nabiev, D.Y. Zhang, and A.A. Abdullaev. 2018. Effect of water deficiency on relationships between metabolism, physiology, biomass, and yield of upland cotton (Gossypium hirsutum L.). J. Arid Land 10(3): 441–456.

Bruinsma, J. 2003. World Agriculture: Towards 2015/2030.

Burba, G. 2013. Eddy Covariance Method (R Nelson, Ed.). LI-COR Biosciences, Lincoln, NE.

Carberry, P.S. 1991. Test of leaf-area development in CERES-Maize: a correction. F. Crop. Res. 27: 159–167.

Carmelita, M., R. Alberto, R. Wassmann, R.J. Buresh, J.R. Quilty, T.Q. Correa, J.M. Sandro, C. Arloo, and R. Centeno. 2014. Field Crops Research Measuring methane flux from irrigated rice fields by eddy covariance method using open-path gas analyzer. F. Crop. Res. 160: 12–21. doi: 10.1016/j.fcr.2014.02.008.

Chen, J.M., A. Govind, O. Sonnentag, Y. Zhang, A. Barr, and B. Amiro. 2006a. Leaf area index measurements at Fluxnet-Canada forest sites. Agric. For. Meteorol. 140(1): 257–268.

Chen, H., H. Tian, M. Liu, J. Melillo, S. Pan, and C. Zhang. 2006b. Effect of Land-Cover Change on Terrestrial Carbon Dynamics in the Southern United States. J. Environ. Qual. 35(4): 1533. doi: 10.2134/jeq2005.0198.

Collatz, G.J., J.T. Ball, C. Grivet, and J.A. Berry. 1991. Physiological and environmental

regulation of stomatal conductance, photosynthesis and transpiration: a model that includes a laminar boundary layer. Agric. For. Meteorol. 54(2–4): 107–136. doi: 10.1016/0168-1923(91)90002-8.

Collins, H.P., R.L. Blevins, L.G. Bundy, D.R. Christienson, W.A. Dick, D.R. Huggins, and E.A. Paul. 1999. Soil Carbon Dynamics in Corn-Based Agroecosystems: Results from Carbon-13 Natural Abundance. Soil Sci. Soc. Am. J. 63(3): 584–591.

Contay, W.C., J.J. Burke, J.R. Mahan, J.E. Neilsen, and B.G. Sutton. 2012. Determining the Optimum Plant Temperature of Cotton Physiology and Yield to Improve Plant-Based Irrigation and Scheduling. Crop Sci. 52(July): 1828–1836.

Cook, B.D., K.J. Davis, W. Wang, A. Desai, B.W. Berger, R.M. Teclaw, J.G. Martin, P. V. Bolstad, P.S. Bakwin, C. Yi, and W. Heilman. 2004. Carbon exchange and venting anomalies in an upland deciduous forest in northern Wisconsin, USA. Agric. For. Meteorol. 126(3–4): 271–295. doi: 10.1016/j.agrformet.2004.06.008.

Daughtry, C. 2000. Estimating Corn Leaf Chlorophyll Concentration from Leaf and Canopy Reflectance. Remote Sens. Environ. 74(2): 229–239. doi: 10.1016/S0034-4257(00)00113-9.

Dejonge, K.C., and K.R. Thorp. 2017. Implementing Standardized Reference Evapotranspiration and Dual Crop Coefficient Approach in the DSSAT Cropping System Model. Am. Soc. Agric. Biol. Eng. 60(6): 1965–1981.

Dettori, M., C. Cesaraccio, A. Montroni, D. Spano, and P. Duce. 2011. Using CERES-Wheat to simulate durum wheat production and phenology in Southern Sardinia, Italy. F. Crop. Res. 120(1): 179–188.

Dokoohaki, H., M. Gheysari, S.F. Mousavi, S. Zand-Parsa, F.E. Miguez, S.V. Archontoulis, and G. Hoogenboom. 2016. Coupling and testing a new soil water module in DSSAT CERES-Maize model for maize production under semi-arid condition. Agric. Water Manag. 163(1): 90–99.

Dolman, A.J., J. Noilhan, P. Durand, C. Sarrat, A. Brut, B. Piguet, A. Butet, N. Jarosz, Y. Brunet, D. Loustau, E. Lamund, L. Tolk, R. Ronda, F. Miglietta, B. Gioli, V. Magliulo, M. Esposito, C. Gerbig, S. Korner, P. Glademard, M. Ramonet, P. Ciais, B. Neininger, R.W.A. Hutjes, J.A. Elbers, R. Macatangay, O. Schrems, G. Perez-Landa, M.J. Sanz, Y. Scholz, G. Facon, E. Ceschia, and P. Beziat. 2006. The CarboEurope Regional Experiment Strategy. Am. Meteorol. Soc. (October): 1367–1379.

Doorenbos, J., and W.D. Pruitt. 1977. Guidelines for Predicting Crop Water Use. Rome, Italy.

Finnigan, J.J., R. Clement, Y. Malhi, R. Leuning, and H.A. Cleugh. 2003. A Re-Evaluation of Long-Term Flux Measurement Techniques Part 1: Averaging and Coordinate Rotation. Boundary-Layer Meteorol. (107): 1–48.

Foley, J.A., R. Defries, G.P. Asner, C. Barford, G. Bonan, S.R. Carpenter, F.S. Chapin, M.T. Coe, G.C. Daily, H.K. Gibbs, J.H. Helkowski, T. Holloway, E.A. Howard, C.J. Kucharik, C. Monfreda, J.A. Patz, I.C. Prentice, N. Ramankutty, and P.K. Snyder. 2005. Global Consequences of Land Use. Science (80-.). 309(July): 570–574. doi: 10.1126/science.1111772.

Food and Agriculture Organization. 2016. Land Use.

Frankenberg, C., J.B. Fisher, J. Worden, G. Badgley, S.S. Saatchi, J.E. Lee, G.C. Toon, A. Butz, M. Jung, A. Kuze, and T. Yokota. 2011. New global observations of the terrestrial carbon cycle from GOSAT: Patterns of plant fluorescence with gross primary productivity. Geophys. Res. Lett. 38(17): 1–7. doi: 10.1029/2011GL048738.

Fritz, E., S. Richter, S. Schott, S. Hejja, and S. Trumbore. 2018. Partitioning Algorithm. Max Planck Inst. Biogeochem.

Garbulsky, M.F., J. Penuelas, D. Papale, J. Ardo, M.L. Goulden, K. Gerard, A.D. Richardson, E. Rotenberg, E.M. Veenendall, and I. Filella. 2010. Patterns and controls of the variability of radiation use efficiency and primary productivity across terrestrial ecosystems. Glob. Ecol. Biogeogr. 19: 253–267.

Gitelson, A.A. 2019. Remote estimation of fraction of radiation absorbed by photosynthetically active vegetation : generic algorithm for maize and soybean. Remote Sens. Lett. 10(3): 283–291. doi: 10.1080/2150704X.2018.1547445.

Gitelson, A.A., Y. Peng, J.G. Masek, D.C. Rundquist, S. Verma, A. Suyker, J.M. Baker, J.L. Hat, and T. Meyers. 2012. Remote estimation of crop gross primary production with Landsat data. Remote Sens. Environ. 121: 404–414. doi: 10.1016/j.rse.2012.02.017.

Glenn, E.P., A.R. Huete, P.L. Nagler, and S.G. Nelson. 2008. Relationship Between Remotely-sensed Vegetation Indices, Canopy Attributes and Plant Physiological Processes: What Vegetation Indices Can and Cannot Tell Us About the Landscape. : 2136–2160.

Godwin, D.C., and C.A. Jones. 1991. Nitrogen dynamics in soil-plant systems. p. 287–321. *In* Modeling plant and soil systems. ASA, CSSA, and SSSA, Madison, Wisconsin.

Godwin, D.C., and U. Singh. 1998. Nitrogen balance and crop response to nitrogen in upland and lowland cropping systems. p. 55–77. *In* Tsuji, G.Y., Hoogenboom, G., Thornton, P.K. (eds.), Understanding options for agricultural production. System approaches for sustainable agricultural development. Kluwer Academic Publishers, Dordrecht, Netherlands.

Gonias, E.D., D.M. Oosterhuis, and A.C. Bibi. 2011. Light interception and radiation use efficiency of okra and normal leaf cotton isolines. Environ. Exp. Bot. 72(2): 217–222.

Gonzalez-Dugo, M.P., C.M.U. Neale, L. Mateos, W.P. Kustas, J.H. Prueger, M.C. Anderson, and F. Li. 2009. A comparison of operational remote sensing-based models for estimating crop evapotranspiration. Agric. For. Meteorol. 149(11): 1843–1853. doi: 10.1016/j.agrformet.2009.06.012.

Guo, L.B., and R.M. Gifford. 2002. Soil carbon stocks and land use change: A meta analysis. Glob. Chang. Biol. 8(4): 345–360. doi: 10.1046/j.1354-1013.2002.00486.x.

Gutierrez, M., R. Norton, K.R. Thorp, and G. Wang. 2012. Association of Spectral Reflectance Indices with Plant Growth and Lint Yield in Upland Cotton. Crop Sci. 52(2): 849–857.

Gwathmey, C.O., D.D. Tyler, and X. Yin. 2010. Prospects for Monitoring Cotton Crop

Maturity with Normalized Difference Vegetation Index. Agron. J. 102(5): 1352–1360.

Han, G., Q. Xing, J. Yu, Y. Luo, D. Li, L. Yang, G. Wang, P. Mao, B. Xie, and N. Mikle. 2014. Agricultural reclamation effects on ecosystem CO2exchange of a coastal wetland in the Yellow River Delta. Agric. Ecosyst. Environ. 196: 187–198. doi: 10.1016/j.agee.2013.09.012.

Harmel, R.D., D.R. Smith, R.L. Haney, and P.M. Allen. 2019. Comparison of nutrient loss pathways: Run-off and seepage flow in Vertisols. Hydrol. Process. 33(18): 2384–2393.

He, M., J.S. Kimball, M.P. Maneta, and B.D. Maxwell. 2018. Regional Crop Gross Primary Productivity and Yield Estimation Using Fused Landsat-MODIS Data. doi: 10.3390/rs10030372.

Hirschi, M., D. Michel, I. Lehner, and S.I. Seneviratne. 2017. A site-level comparison of lysimeter and eddy covariance flux measurements of evapotranspiration. Hydrol. Earth Syst. Sci. 21(3): 1809–1825. doi: 10.5194/hess-21-1809-2017.

Hoogenboom, G., J.W. Jones, C.H. Porter, P.W. Wilkens, K.J. Boote, W.D. Batchelor, L.A. Hunt, and G.Y. Tsuji. 2003. A Decision Support System for Agrotechnology Transfer Version 4.0. 4th ed. University of Hawaii, Honolulu, Hawaii.

Houghton, R.A. 2007. Balancing the Global Carbon Budget. Annu. Rev. Earth Planet. Sci. 35(1): 313–347. doi: 10.1146/annurev.earth.35.031306.140057.

Houghton, R.A., A. Baccini, and W.S. Walker. 2018. Where is the residual terrestrial carbon sink? Glob. Chang. Biol. 24(8): 3277–3279.

Howell, T.A., S.R. Evett, J.A. Tolk, and A.D. Schneider. 2004. Evapotranspiration of full-, deficit-irrigated, and dryland cotton on the Northern Texas High Plains. J. Irrig. Drain. Eng. 130(4).

Huemmrich, K.F., P. Campbell, D. Landis, and E. Middleton. 2019. Developing a common globally acceptable method for optical remote sensing of ecosystem light use efficiency. Remote Sens. Environ. 230.

Huete, A.R., H.Q. Liu, K. Batchily, and L. van W. J. 1997. A comparsion of vegetation indices over a Global set of TM images for EO -MODIS. Remote Sens. Environ. 59(Table 1): 440–451. doi: 10.1016/S0034-4257(96)00112-5.

Ibell, P.T., Z. Xu, and T.J. Blumfield. 2010. Effects of weed control and fertilization on soil carbon and nutrient pools in an exotic pine plantation of subtropical Australia. J. Soils Sediments (10): 1027–1038. doi: 10.1007/s11368-010-0222-6.

Ibrahim, M.E., and D.R. Buxton. 1981. Early Vegetative Growth of Cotton as Influenced by Leaf Type. Crop Sci. 21(5): 639–643.

Jaafar, H.H., and F.A.. Ahmad. 2015. Relationships Between Primary Production and Crop Yields in Semi-Arid and Arid Irrigated Agroecosystems. Int. Symp. Remote Sens. Environ. 47(W3): 27–30.

Jalota, S.K., S. Sukhvinder, G.B.S. Chahal, S.S. Ray, S. Panigraphy, F. Bhupinder-Singh, and K.B.. Singh. 2010. Soil texture, climate and management effects on plant growth, grain yield and water use by rainfed maize–wheat cropping system: Field and simulation study. Agric. Water Manag. 97(1): 83–90.

Jans, W.W.P., C.M.J. Jacobs, B. Kruijt, J.A. Elbers, S. Barendse, and E.J. Moors. 2010.

Carbon exchange of a maize (Zea mays L.) crop: Influence of phenology. Agric. Ecosyst. Environ. 139(3): 316–324. doi: 10.1016/j.agee.2010.06.008.

Johnson, D.M. 2016. A comprehensive assessment of the correlations between field crop yields and commonly used MODIS products. Int. J. Appl. EARTH Obs. Geoinf. 52: 65–81.

Jones, J.W. 1993. Decision Support System for agricultural development. p. 459–471. *In* de Vries, F.P., Teng, P., Metselaar, K. (eds.), Systems Approaches for Agricultural Development. Kluwer Academic Publishers, Boston.

Jones, J.W., J.M. Antle, B. Basso, K.J. Boote, R.T. Conant, I. Foster, H.C.J. Godfray, M. Herrero, R.E. Howitt, S. Janssen, B.A. Keating, R. Munoz-Carpena, C.H. Porter, C. Rosenzweig, and T.R. Wheeler. 2017. Brief history of agricultural systems modeling. Agric. Syst. 155(June): 240–254. doi: 10.1016/j.agsy.2016.05.014.

Jones, J.W., K.J. Boote, G. Hoogenboom, S.S. Jagtap, and G.G. Wilkerson. 1989. Soybean Crop Growth Simulation Model. Gainsville.

Jones, J.W., G. Hoogenboom, C.H. Porter, K.J. Boote, W.D. Batchelor, L.A. Hunt, P.W. Wilkens, U. Singh, and A.J. Gijsman. 2003. The DSSAT Cropping System Model.

Jones, J.W., and J.T. Ritchie. 1991. Crop Growth Models. p. 63–89. *In* Hoffman, G.J., Howell, T.A., Soloman, K.H. (eds.), Management of Farm Irrigation System. 9th ed. American Society of Agricultural Engineers.

Kaplan, J.O., K.M. Krumhardt, E.C. Ellis, F. Ruddiman, C. Lemmen, and K.K. Goldewijk. 2010. Holocene carbon emissions as a result of anthropogenic land cover change. The Holocene 21(June). doi: 10.1177/0959683610386983.

Kerr, J.T., and M. Ostrovsky. 2003. From space to species: Ecological applications for remote sensing. Trends Ecol. Evol. 18(6): 299–305. doi: 10.1016/S0169-5347(03)00071-5.

Kessavalou, A., A.R. Mosier, J.W. Doran, R.A. Drijber, D.J. Lyon, and O. Heinemeyer. 1998. Fluxes of Carbon Dioxide, Nitrous Oxide, and Methane in Grass Sod and Winter Wheat-Fallow Tillage Management. J. Environ. Qual. (27): 1094–1104.

King, A.W., L. Dilling, G.P. Zimmerman, D.M. Fairman, R.A. Houghton, G.H. Marland, A.Z. Rose, and T.J. Wilbanks. 2007. The North American Carbon Budget and Implications for the Global Carbon Cycle.

L'Ecuyer, T.S., H.K. Beaudoing, M. Rodell, W. Olson, B. Lin, S. Kato, C.A. Clayson, E. Wood, J. Sheffield, R. Adler, G. Huffman, M. Bosilovich, G. Gu, F. Robertson, P.R. Houser, D. Chambers, J.S. Famiglietti, E. Fetzer, W.T. Liu, X. Gao, C.A. Schlosser, E. Clark, D.P. Lettenmaier, and K. Hilburn. 2015. The observed state of the energy budget in the early twenty-first century. J. Clim. 28(21): 8319–8346. doi: 10.1175/JCLI-D-14-00556.1.

Laitala, K., and I.G. Klepp. 2015. Age and active life of clothing. Prod. Lifetimes Environ.: 182–186.

Lal, R. 2004. Soil Carbon Sequestration Impacts on Global Climate Change and Food Security. Am. Assoc. Adv. Sci. 304(5677): 1623–7. doi: 10.1126/science.1097396.

LI-COR. 2015. SmartFlux System Instruction Manual.

Li, S., S. Kang, F. Li, and L. Zhang. 2008. Evapotranspiration and crop coefficient of spring maize with plastic mulch using eddy covariance in northwest China. Agric.

Water Manag. 95(11): 1214–1222. doi: 10.1016/j.agwat.2008.04.014.

Li, X., L. Liu, H. Yang, and Y. Li. 2018. Relationships between carbon fluxes and environmental factors in a drip-irrigated, film-mulched cotton field in arid region. PLoS One 13(2): 1–18. doi: 10.1371/journal.pone.0192467.

Lindsey, R. 2009. Climate and Earth's Energy Budget. NASA Earth Obs.: 1–12. doi: 10.1007/s10712-011-9165-8.

Liu, P. 2017. The future of food and agriculture: Trends and challenges.

Lopez-Cedron, F.X., K.J. Boote, J. Pineiro, and F. Sau. 2008. Improving the CERES-Maize model ability to simulate water deficit impact on maize production and yield components. Agron. J. 100: 296–307.

Main, C.L. 2012. Cotton Growth and Development.

Matocha, M., C. Allen, R. Boman, G. Morgan, and P. Baumann. 2009. Crop Profile for Cotton in Texas. College Station, Texas.

Meyers, T.P. 2001. A comparison of summertime water and CO2fluxes over rangeland for well watered and drought conditions. Agric. For. Meteorol. 106(3): 205–214. doi: 10.1016/S0168-1923(00)00213-6.

Modala, N.R., S. Ale, N. Rajan, C.L. Munster, P.B. DeLaune, K.R. Thorp, S.S. Nair, and E.M. Barnes. 2015. Evaluation of the CSM-CROPGRO-COTTON MODEL for the Texas Rolling Plains Region and Simulation of Deficit Irrigation Strategies for Increasing Water Use Efficiency. Trans. ASABE 58(3): 658–696.

Möller, M., J. Tanny, Y. Li, and S. Cohen. 2004. Measuring and predicting evapotranspiration in an insect-proof screenhouse. Agric. For. Meteorol. 127(1–2):

35–51. doi: 10.1016/j.agrformet.2004.08.002.

Monteith, J.L. 1977. Climate and Efficiency of Crop Production in Britain. Phil. Trans. R. Soc. Lond. 281(980).

Monteith, J.L. 1986. How do crops manipulate water supply and demand ? Phil. Trans. R. Soc. Lond. 316: 245–259.

Mu, Q., M. Zhao, and S.W. Running. 2011. Improvements to a MODIS global terrestrial evapotranspiration algorithm. Remote Sens. Environ. 115(8): 1781–1800. doi: 10.1016/j.rse.2011.02.019.

Mubeen, M., A. Ahmad, T. Khaliqu, and A. Bakhsh. 2013. Evaluating CSM-CERESMaize model for irrigation scheduling in semi-arid conditions of Punjab, Pakistan. Int. J. Agric. Biol. 15(1): 1–10.

Murty, D., M.U.F. Kirschbaum, R.E. Mcmurtrie, and H. Mcgilvray. 2002. Does conversion of forest to agricultural land change soil carbon and nitrogen? A review of the literature. Glob. Chang. Biol. 8(2): 105–123. doi: 10.1046/j.1354-1013.2001.00459.x.

Myneni, R.B., R.R. Nemani, and S.W. Running. 1997. Estimation of global leaf area index and absorbed par using radiative transfer models. IEEE Trans. Geosci. Remote Sens. 35(6): 1380–1393.

National Oceanic and Atmospheric Administration. 2011. Climate Data Online. Natl. Centers Environ. Inf.

Oki, T., and K. Shinjiro. 2006. Global Hydrological Cycles and World Water Resources. Science (80-.). 313(August): 1068–1073.

Pace, P.F., H.T. Cralle, S.H.M. El-Halawany, J.T. Cothren, and S.A. Senseman. 1999. Drought-induced Changes in Shoot and Root Growth of Young Cotton Plants. J. Cotton Sci. 3(183–187).

Padilla, F.L.M., S.J. Maas, M.P. Gonzalez-Dugo, N. Rajan, F. Mansilla, P. Gavilan, and J. Dominguez. 2012. Wheat Yield Monitoring in Southern Spain Using the GRAMI Model and a Series of Satellite Images. F. Crop. Res. 139(29): 145–145.

Pathak, T.B., J.W. Jones, C.W. Fraisse, D. Wright, and G. Hoogenboom. 2012. Uncertainty analysis and parameter estimation for the CSM-CROPGRO-cotton model. Agron. J. 104(5): 1363–1373. doi: 10.2134/agronj2011.0349.

Patil, N.G., and G.S. Rajput. 2009. Evaluation of Water Retention Functions and Computer Program "Rosetta" in Predicting Soil Water Characteristics of Seasonally Impounded Shrink-Swell Soils. J. Irrig. Drain. Eng. 135(3): 286–294.

Paw, K.T., D.D. Baldocchi, T.P. Meyers, and K.B. Wilson. 2000. Correction of Eddy-Covariance Measurements Incorporating Both Advective Effects and Density Fluxes. Boundary-Layer Meteorol. (47): 487–511.

Pegelow, E.J., D.R. Buxton, R.E. Briggs, H. Muramoto, and W.G. Gensler. 1977. Canopy Photosynthesis and Transpiration of Cotton as Affected by Leaf Type. Crop Sci. 17(1): 1–4.

Peng, Y., and A.A. Gitelson. 2011. Application of chlorophyll-related vegetation indices for remote estimation of maize productivity. Agric. For. Meteorol. 151(9): 1267–1276.

Peng, Y., and A.A. Gitelson. 2012. Remote estimation of gross primary productivity in

soybean and maize based on total crop chlorophyll content. Remote Sens. Environ. 117: 440–448. doi: 10.1016/j.rse.2011.10.021.

Peng, Y., A.A. Gitelson, G. Keydan, D.C. Rundquist, and W. Moses. 2011. Remote estimation of gross primary production in maize and support for a new paradigm based on total crop chlorophyll content. Remote Sens. Environ. 115(4): 978–989.

Pettigrew, W.T. 2004. Physiological Consequences of Moisture Deficit Stress in Cotton. Crop Sci. 44(4): 1265–1272.

PhytoGen. 2019. PhytoGen Cotton Varieties. Corteva Agriscience. https://phytogencottonseed.com/varieties.

Planet Team. 2017. Planet Application Program Interface: In Space for Life on Earth. San Francisco, CA.

Planet Team. 2018. No Title. Planet Inc.

Priestly, C.H.B., and R.J. Taylor. 1972. On the Assessment of Surface Heat Flux and Evaporation Using Large-Scale Parameters. Mon. Weather Rev. 100(February): 81–92.

Qin, S., S. Li, S. Kang, T. Du, L. Tong, and R. Ding. 2016. Can the drip irrigation under film mulch reduce crop evapotranspiration and save water under the sufficient irrigation condition? Agric. Water Manag. 177: 128–137. doi: 10.1016/j.agwat.2016.06.022.

Rajan, N., S.J. Maas, and S. Cui. 2013a. Extreme Drought Effects on Carbon Dynamics of a Semi Arid Pasture. Crop Ecol. Physiol. 105(6): 1749–1760.

Rajan, N., S.J. Maas, and S. Cui. 2013b. Extreme Drought Effects on Carbon Dynamics

of a Semi-arid Pasture. 2013 105(6): 1749–1760.

Ramankutty, N., A.T. Evan, C. Monfreda, and J.A. Foley. 2008. Farming the planet : 1 . Geographic distribution of global agricultural lands in the year 2000. 22(February 2007): 1–19. doi: 10.1029/2007GB002952.

Raper, T.B., J.J. Varco, and K.J. Hubbard. 2013. Canopy-Based Normalized Difference Vegetation Index Sensors for Monitoring Cotton Nitrogen Status. Agron. J. 105(5): 1345–1354.

Reichstein, M., E. Falge, D. Baldocchi, D. Papale, M. Aubinet, P. Berbigier, C. Bernhofer, N. Buchmann, T. Gilmanov, A. Granier, T. Grunwald, K. Havrankova, H. Ilvesniemi, D. Janous, A. Knohl, T. Laurila, A. Lohila, D. Loustau, G. Matteucci, T. Meyers, F. Miglietta, J.-M. Ourcival, J. Pumpanen, S. Rambal, E. Rotenberg, M. Sanz, J. Tenhunen, G. Seufert, F. Vaccari, T. Vesala, D. Yakir, and R. Valentini. 2005. On the separation of net ecosystem exchange into assimilation and ecosystem respiration : review and improved algorithm. Glob. Chang. Biol. (11): 1424–1439. doi: 10.1111/j.1365-2486.2005.001002.x.

Ringrose-Voase, A.J., and A.J. Nadelko. 2013. Deep drainage in a Grey Vertosol under furrow-irrigated cotton. Crop Pasture Sci. 64(12): 1155–1170.

Ritchie, J.T. 1972. Model for Predicting Evaporation from a Row Crop with Incomplete Cover. Water Resour. Res. 8(5): 1204–1213.

Ritchie, J.T. 1998. Soil water balance and plant stress. p. 41–54. *In* Tsuji, G.Y., Hoogenboom, G., Thornton, P.K. (eds.), Understanding options for agricultural production. System approaches for sustainable agricultural development. Kluwer

Academic Publishers, Dordrecht, Netherlands.

Ritchie, G.L., C.W. Bednarz, P.H. Jost, and S.M. Brown. 2007. Cotton Growth and Development.

Ritchie, J.T., and S. Otter. 1985. Description and performance of CERES-Wheat: A User-oriented wheat yield model. ARS Wheat Yield Proj. 38: 159–175.

Ritchie, J.T., C.H. Porter, J. Judge, J.W. Jones, and A.A. Suleiman. 2009. Extension of an Existing Model for Soil Water Evaporation and Redistribution under High Water Content Conditions. Soil Sci. Soc. Am. J. 73(3): 792. doi: 10.2136/sssaj2007.0325.

Ritchie, G.L., D.G. Sullivan, W.K. Vencill, C.W. Bednarz, and J.E. Hook. 2010. Sensitivities of Normalized Difference Vegetation Index and a Green/Red Ratio Index to Cotton Ground Cover Fraction. Crop Sci. 50(3): 1000–1010.

Rodell, M., H.K. Beaudoing, T.S. L'Ecuyer, W.S. Olson, J.S. Famiglietti, P.R. Houser, R. Adler, M.G. Bosilovich, C.A. Clayson, D. Chambers, E. Clark, E.J. Fetzer, X. Gao, G. Gu, K. Hilburn, G.J. Huffman, D.P. Lettenmair, W.T. Liu, F.R. Robertson, C.A. Schlosser, J. Sheffield, and E.F. Wood. 2015. The Observed State of the Water Cycle in the Early Twenty-First Century. J. Clim. 28(November): 8289–8318. doi: 10.1175/JCLI-D-14-00555.1.

Rost, S., D. Gerten, A. Bondeau, W. Lucht, and J. Rohwer. 2008. Agricultural green and blue water consumption and its influence on the global water system. Water Resour. Res. 44: 1–17. doi: 10.1029/2007WR006331.

Saigusa, N., S. Yamamoto, S. Murayama, H. Kondo, and N. Nishimura. 2002. Gross primary production and net ecosystem exchange of a cool-temperate deciduous

forest estimated by the eddy covariance method. Agric. For. Meteorol. 112: 203–215.

Sakamoto, T., A.A. Gitelson, B.D. Wardlow, S.B. Verma, and A.E. Suyker. 2011. Estimating daily gross primary production of maize based only on MODIS WDRVI and shortwave radiation data. Remote Sens. Environ. 115(12): 3091–3101.

Saseendran, S.A., L. Ma, D.C. Nielsen, M.F. Vigil, and L.R. Ahuju. 2005. imulating planting date effects on corn production using RZWQM and CERES-Maize models. Agron. J. 97(1): 58–71.

Sau, F., K.J. Boote, M. Bostick, J.W. Jones, and M.I. Minguez. 2004. Testing and Improving Evapotranspiration and Soil Water Balance of the DSSAT Crop Models. Agron. J. 96(September): 1243–1257.

Schindler, D.W. 1999. The mysterious missing sink. Nature 398: 105–107.

Seligman, N.C., and H. Van Keulen. 1981. PAPRAN: a simulation model of annual pasture production limited by rainfall and nitrogen. p. 192–221. *In* Frissel, M.J., Van Veen, J.A. (eds.), Simulation of nitrogen behavior of soil-plant systems. Centrum voor Landbouwpublikaties en Landbouwdocumentatie, Wageningen, Netherlands.

Shafian, S., N. Rajan, R. Schnell, M. Bagavathiannan, J. Valasek, Y. Shi, and J. Olsenholler. 2018. Unmanned Aerial Systems-Based Remote Sensing for Monitoring Sorghum Growth and Development. PLoS One 13(5).

Sharma, S., N. Rajan, S. Cui, K. Casey, S. Ale, R. Jessup, and S. Maas. 2017. Seasonal variability of evapotranspiration and carbon exchanges over a biomass sorghum

field in the Southern U.S. Great Plains. Biomass and Bioenergy 105: 392–401.

Shelton, M.L. 1987. Irrigation induced change in vegetation and evapotranspiration in the Central Valley of California. Landsc. Ecol. 1(2): 95–105.

Sinclair, T.R., and R.C. Muchow. 2001. System Analysis of Plant Traits to Increase Grain Yield on Limited Water Supplies. 93(2): 263–270.

Skinner, H.R. 2007. High Biomass Removal Limits Carbon Sequestration Potential of Mature Temperate Pastures. J. Environ. Qual. 37(4): 1319–1326.

Smith, P., M. Bustamante, H. Ahammad, H. Clark, H. Dong, E.A. Elsiddi, H. Haberl, R. Harper, J. House, M. Jafari, O. Masera, C. Mbow, N.H. Ravindranath, C.W. Rice, C.R. Abad, A. Romanovskaya, F. Sperling, and F. Tubiello. 2014. Agriculture, forestry and other land use.

Snowden, M.C., G.L. Ritchie, F.R. Simao, and J.P. Bordovsky. 2014. Timing of Episodic Drought Can Be Critical in Cotton. Agron. J. 106(2): 452–458.

Soldevilla-Martinez, M., M. Quemada, R. Lopez-Urrea, R. Munoz-Carpena, and J.I. Lizaso. 2014. Soil water balance: Comparing two simulation models of different levels of complexity with lysimeter observations. Agric. Water Manag. 139(June): 53–63.

Soler, C.M.T., P.C. Sentelhas, and G. Hoogenboom. 2007. Application of the CSM-CERES-Maize model for planting date evaluation and yield forecasting for maize grown off-season in a subtropical environment. Eur. J. Agron. 27(2–4): 165–177. doi: 10.1016/j.eja.2007.03.002.

Sonnentag, O., M. Detto, R. Vargas, Y. Ryu, B.R.K. Runkle, M. Kelly, and D.D.

Baldocchi. 2011. Agricultural and Forest Meteorology Tracking the structural and functional development of a perennial pepperweed (Lepidium latifolium L .) infestation using a multi-year archive of webcam imagery and eddy covariance measurements. Agric. For. Meteorol. 151(7): 916–926. doi: 10.1016/j.agrformet.2011.02.011.

Spera, S.A., G.L. Galford, and M.T. Coe. 2016. Land-use change affects water recycling in Brazil ' s last agricultural frontier. Glob. Chang. Biol. 22: 3405–3413. doi: 10.1111/gcb.13298.

Suleiman, A.A., and G. Hoogenboom. 2007. Comparison of Priestley–Taylor and FAO-56 Penman–Monteith for daily reference evapotranspiration estimation in Georgia, USA. J. Irrig. Drain. Eng. 133(2).

Suleiman, A.A., and J.T. Ritchie. 2003. Modeling Soil Water Redistribution during Second-Stage Evaporation. Soil Sci. Soc. Am. J. 67(2): 377–386. doi: 10.2136/sssaj2003.0377.

Suleiman, A.A., C.M.T. Soler, and G. Hoogenboom. 2007. Evaluation of FAO-56 crop coefficient procedures for deficit irrigation management of cotton in a humid climate. Agric. Water Manag. 91(1): 33–42.

Suyker, A.E., S.B. Verma, G.G. Burba, T.J. Arkebauer, D.T. Walters, and K.G. Hubbard. 2004a. Growing season carbon dioxide exchange in irrigated and rainfed maize. Agric. For. Meteorol. 124(1–2): 1–13. doi: 10.1016/j.agrformet.2004.01.011.

Suyker, A.E., S.B. Verma, G.G. Burba, T.J. Arkebauer, D.T. Walters, and K.G.

Hubbard. 2004b. Growing season carbon dioxide exchange in irrigated and rainfed maize. Agric. For. Meteorol. 124(1): 1–13.

Texas A&M Agrilife. 2019. Cotton Production Regions of Texas. Cott. Insect Manag. Guid.

Texas Parks and Wildlife. 2019. Post Oak Savannah and Blackland Prairie Wildlife Management. Habitats.

Thorp, K.R., E.M. Barnes, D.J. Hunsaker, and B.A. Kimball. 2014. Evaluation of CSM-CROPGRO-Cotton for Simulating Effects of Management and Climate Change on Cotton Growth and Evapotranspiration In An Arid Environment. Trans. ASABE 57(6): 1627–1642.

Thorp, K.R., D.J. Hunsaker, A.N. French, E. Bautista, and K.F. Bronson. 2015. Integrating geospatial data and cropping system simulation within a geographic information system to analyze spatial seed cotton yield, water use, and irrigation requirements. Precis. Agric. 16(5): 532–557.

Tian, H., G. Chen, M. Liu, C. Zhang, G. Sun, C. Lu, X. Xu, W. Ren, S. Pan, and A. Chappelka. 2010. Model estimates of net primary productivity, evapotranspiration, and water use efficiency in the terrestrial ecosystems of the southern United States during 1895-2007. For. Ecol. Manage. 259(7): 1311–1327. doi: 10.1016/j.foreco.2009.10.009.

Tscharntke, T., A.M. Klein, A. Kruess, I. Steffan-Dewenter, and C. Thies. 2005. Landscape perspectives on agricultural intensification and biodiversity - Ecosystem service management. Ecol. Lett. 8(8): 857–874. doi: 10.1111/j.1461-

0248.2005.00782.x.

Tubiello, F.N., M. Salvatore, R.D. Cóndor Golec, A. Ferrara, S. Rossi, R. Biancalani, S. Federici, H. Jacobs, and A. Flammini. 2014. Agriculture, Forestry and Other Land Use Emissions by Sources and Removals by Sinks. ESS Work. Pap. No.2 2: 4–89. doi: 10.13140/2.1.4143.4245.

Twine, T.E., W.P. Kustas, J.M. Norman, D.R. Cook, P.R. Houser, and T.P. Meyers. 2000. Correcting eddy-covariance flux underestimates over a grassland. Agric. For. Meteorol. 103: 279–300.

Uddin, J., R.J. Smith, N.H. Hancock, and J.P. Foley. 2013. Evaporation and sapflow dynamics during sprinkler irrigation of cotton. Agric. Water Manag. 125: 35–45. doi: 10.1016/j.agwat.2013.04.001.

USDA-NASS. 2017. 2017 Census of Agriculture County Profile: Burleson County Texas.

Verlag, F., A.A. Gitelson, Y. Gritz, and M.N. Merzlyak. 2003. Relationships between leaf chlorophyll content and spectral reflectance and algorithms for non-destructive chlorophyll assessment in higher plant leaves. J. Plant Physiol. 160(3): 271–282.

Verma, S.B., A. Dobermann, K.G. Cassman, D.T. Walters, J.M. Knops, T.J. Arkebauer, A.E. Suyker, G.G. Burba, B. Amos, H. Yang, D. Ginting, K.G. Hubbard, A.A. Gitelson, and E.A. Walter-Shea. 2005. Annual carbon dioxide exchange in irrigated and rainfed maize-based agroecosystems. Agric. For. Meteorol. 131(1–2): 77–96. doi: 10.1016/j.agrformet.2005.05.003.

Vitale, L., P. Di Tommasi, G. D'Urso, and V. Magliulo. 2016. The response of

ecosystem carbon fluxes to LAI and environmental drivers in a maize crop grown in two contrasting seasons. Int. J. Biometeorol. 60(3): 411–420. doi: 10.1007/s00484-015-1038-2.

Wang, Y., C.E. Woodcock, W. Buermann, P. Stenberg, P. Voipio, H. Smolander, T. Hame, Y. Tian, H. Jiannan, Y. Knyazikhin, and R.B. Myneni. 2004. Evaluation of the MODIS LAI algorithm at a coniferous forest site in Finland. Remote Sens. Environ. 91(1): 114–127.

Wang, C., Z. Zhang, S. Fan, R. Mwiya, and M. Xie. 2018. Effects of straw incorporation on desiccation cracking patterns and horizontal flow in cracked clay loam. Soil Tillage Res. 182: 130–143.

Webb, E.K., G.I. Pearman, and R. Leuning. 1980. Correction of flux measurements for density effects due to heat and water vapour transfer. Q. J. R. Meteorol. Soc. 106(447): 85–100.

West, T.O., and W.M. Post. 2002. Soil Organic Carbon Sequestration Rates by Tillage and Crop Rotation : A Global Data Analysis. Soil Sci. Soc. Am. J. 66(6): 1930–1946. doi: 10.2136/sssaj2002.1930.

Wharton, S., M. Falk, K. Bible, M. Schroeder, and K.T.U. Paw. 2012. Old-growth CO2 flux measurements reveal high sensitivity to climate anomalies across seasonal, annual and decadal time scales. Agric. For. Meteorol. 161: 1–14. doi: 10.1016/j.agrformet.2012.03.007.

Wilson, K., A. Goldstein, E. Falge, M. Aubinet, D. Baldocchi, P. Berbigier, C. Bernhofer, R. Ceulemans, H. Dolman, C. Field, A. Grelle, A. Ibrom, B.E. Law, A.

Kowalski, T. Meyers, J. Moncrieff, R. Monson, W. Oechel, J. Tenhunen, R. Valentini, and S. Verma. 2002. Energy balance closure at FLUXNET sites. Agric. For. Meteorol. 113: 223–243.

Woodbury, P.B., L.S. Heath, and J.E. Smith. 2006. Land Use Change Effects on Forest Carbon Cycling Throughout the Southern United States. J. Environ. Qual. 35(4): 1348. doi: 10.2134/jeq2005.0148.

Wu, H., X. Wang, M. Xu, and J. Zhang. 2018. The Effect of Water Deficit and Waterlogging on the Yield Components of Cotton. Crop Sci. 58(4): 1751–1761.

Xevi, E., J. Gilley, and J. Feyen. 1996. Comparative study of two crop yield simulation models. Agric. Water Manag. 30(2): 155–173.

Xiao, J., G. Sun, J. Chen, H. Chen, S. Chen, G. Dong, S. Gao, H. Guo, J. Guo, S. Han, T. Kato, Y. Li, G. Lin, L. Weizhi, M. Ma, S. McNulty, C. Shao, X. Wang, and J. Zhou. 2013. Carbon fluxes, evapotranspiration, and water use efficiency of terrestrial ecosystems in China. Agric. For. Meteorol. 182(12): 76–90.

Xu, C.Y., and D. Chen. 2005. Comparison of seven models for estimation of evapotranspiration and groundwater recharge using lysimeter measurement data in Germany. Hydrol. Process. 19(18): 3717–3734. doi: 10.1002/hyp.5853.

Yan, H., Y. Fu, X. Xiao, H.Q. Huang, H. He, and L. Ediger. 2009. Modeling gross primary productivity for winter wheat-maize double cropping system using MODIS time series and CO2eddy flux tower data. Agric. Ecosyst. Environ. 129(4): 391–400. doi: 10.1016/j.agee.2008.10.017.

Yoder, B.J., and R.E. Pettigrew-Crosby. 1995. Predicting nitrogen and chlorophyll

content and concentration for reflectance spectra (400 - 2500 nm) at leaf and canopy scales. Remote Sens. Environ. 53(September 1994): 199–211.

Yuan, W., S. Liu, G. Yu, J.M. Bonnefond, J. Chen, K. Davis, A.R. Desai, A.H. Goldstein, D. Gianelle, F. Rossi, A.E. Suyker, and S.B. Verma. 2010. Global estimates of evapotranspiration and gross primary production based on MODIS and global meteorology data. Remote Sens. Environ. 114(7): 1416–1431. doi: 10.1016/j.rse.2010.01.022.

Yu, G., X. Wen, X. Sun, B.D. Tanner, X. Lee, and J. Chen. 2006. Overview of ChinaFLUX and evaluation of its eddy covariance measurement. Agric. For. Meteorol. 137: 125–137. doi: 10.1016/j.agrformet.2006.02.011.

Zapata, D., N. Rajan, and F. Hons. 2017. Does high soil moisture in no-till systems increase CO2 emissions and reduce carbon sequestration? Tampa, FL.

Zapata, D., N. Rajan, J. Mowrer, K. Casey, R. Schnell, and F. Hons. 2019. Impact of Long-Term Tillage on Soil CO2 Emissions and Soil Carbon Sequestration in Monoculture and Rotational Cropping Systems. Soil Tillage Res.

Zhao, M., F.A. Heinsch, R.R. Nemani, and S.W. Running. 2005. Improvements of the MODIS terrestrial gross and net primary production global data set. Remote Sens. Environ. 95(2): 164–176. doi: 10.1016/j.rse.2004.12.011.

Zheng, Y., L. Zhang, J. Xiao, W. Yuan, M. Yan, and T. Li. 2018. Sources of uncertainty in gross primary productivity simulated by light use efficiency models: Model structure, parameters, input data, and spatial resolution. Agric. For. Meteorol. 263(December 2017): 242–257. doi: 10.1016/j.agrformet.2018.08.003.

Zhou, Y., X. Xiao, P. Wagle, R. Bajgain, H. Mahan, J.B. Basara, J. Dong, Y. Qin, G. Zhang, Y. Luo, P.H. Gowda, J.P.S. Neel, P.J. Starks, and J.L. Steiner. 2017. Examining the short-term impacts of diverse management practices on plant phenology and carbon fluxes of Old World bluestems pasture. Agric. For. Meteorol. 237–238: 60–70. doi: 10.1016/j.agrformet.2017.01.018.

6. COMPARISON OF SIMULATED ET USING DSSAT-CROPGRO-COTTON AND MEASURED ET USING THE EDDY COVARIANCE METHOD

6.1. Introduction

Improving our understanding of crop water use and its impact of regional and global hydrologic cycles is an important topic of research given current concerns over the effects of a rising human population and climate change on the availability of water for using in agriculture. Evapotranspiration (ET), is the combination of evaporation and plant transpiration, and over terrestrial areas, ET is largely plant transpiration plus some soil water evaporation. Agriculture can change ET patterns compared to natural ecosystems due to changes in soil management and plant cover. For example, the clearing of forest for cropland typically results in a decrease in ET as deep-rooted trees with access to groundwater are replaced with short rooted crops with access only to the surface soil (Shelton, 1987; Rost et al., 2008; Tian et al., 2010; Spera et al., 2016). Current global ET estimates suggest that approximately 12% of terrestrial ET comes from crop production, irrigated and dryland (Oki and Shinjiro, 2006; Rost et al., 2008). However, large-scale ET estimates can be difficult due to the highly variable nature of ET processes and the lack of actual measurements in many areas (Rodell et al., 2015). While cropping systems account for a low percentage of terrestrial ET, it accounts the majority (85 – 90%) of human water use (Foley et al., 2005; Oki and Shinjiro, 2006). Agricultural ET also important because it is correlated with yield and productivity due to the role of transpiration in the CO_2 assimilation process (Sinclair and Muchow, 2001).

Increasing our efforts to understand crop water use via measurement and modeling can improve our ability to predict how ecosystems will respond to a changing climate.

Eddy covariance (EC) is a well-established technique for measuring gas fluxes, including water vapor, from larger-scale ecosystems and agricultural settings (Suyker et al., 2004a; Yu et al., 2006; Burba, 2013; Hirschi et al., 2017). Gas fluxes are calculated as the covariance between the vertical wind speed and the concentration of the interest. The eddy covariance method is comparable to older lysimeter based methods, although it does have a tendency towards error immediately after rain events (Möller et al., 2004; Hirschi et al., 2017). The EC method has successfully been used with cotton, although studies of EC in cotton are limited compared to more common crops, such as corn or wheat (Uddin et al., 2013; Han et al., 2014; Qin et al., 2016; Li et al., 2018). While the EC method is useful for measuring ET, the cost of establishing and maintaining a system is high. Additionally, the EC method requires a large uniform and level area with the same crop to perform adequately, as such it is not applicable to non-uniform fields, smaller fields, and fields on sloped land (Burba, 2013; Hirschi et al., 2017). Simulation of ET, via various modeling systems, is thus important for fully understanding ET, particularly where direct measurement is not possible or practical.

Crop modeling uses known agronomic principals, weather information, soil information, and management information to predict the growth and development of a crop. Crop models often incorporate ET as part of the modeling effort to determine crop water use. Most ET modeling platforms use the Penman-Monteith equation or a modified version thereof to model potential ET and then modify that to simulate crop ET

(Soler et al., 2007; Pathak et al., 2012; Jones et al., 2017). Some of the more commonly used crop-modeling software platforms include DSSAT, CropSyst, and APSIM.

The Decision Support System for Agrotechnology Transfer (DSSAT) is a crop-modeling software platform with ET modeling capabilities. DSSAT has a modular approach that incorporates multiple models, i.e. CERES, CROPGRO, IXIM, into one software platform with internal soil and water modeling methods. Cotton is modeled using the CROPGRO method, which was initially developed for soybean and peanut and has since been modified for use in a variety of dicot (broadleaf) crops, including cotton (Hoogenboom et al., 2003; Jones et al., 2017). In the DSSAT system, ET is modeled in a two-step process. The first step is to calculate potential ET and the second is to modify potential ET with the soils file and crop model to produce ET. There are two internal methods for calculating potential ET within DSSAT, Priestly-Taylor/Ritchie (default) method, and the FAO-56 method. The Priestly-Taylor method is a modification of the Penman-Monteith equation published by C.H.B. Priestly and R.J. Taylor in 1972. This method calculates potential ET using air temperature and solar radiation (Priestly and Taylor, 1972; Hoogenboom et al., 2003; Jones et al., 2003). This method has been found to work adequately in low wind and humid conditions (Jones, 1993; Xu and Chen, 2005). The FAO-56 method a more complete version of the Penman-Monteith equation that was published in the Food and Agriculture Organization's paper number 56. This method calculated potential ET using air temperature, solar radiation, wind speed, and relative humidity. This method is recommended by DSSAT for use in arid and windy climates (Jones, 1993; Jones et al., 2003; Monteith, 1986). However several studies have

found that the FAO-56 method is preferred even in humid climates as it produces less error than the Priestly-Taylor/Ritchie model (Suleiman and Hoogenboom, 2007; Suleiman et al., 2007; Thorp et al., 2014).

While DSSAT's ET modeling capabilities have been used widely in some crops, like corn, there have been limited applications in cotton. The studies that have been done in cotton have generally had more success in irrigated cropping compared to dryland (Howell et al., 2004; Thorp et al., 2014; Dejonge and Thorp, 2017). As such, the overall goal of this study is to improve our knowledge of modeling ET in cotton using the DSSAT system. This study will model ET from a cotton crop in Texas using both of DSSAT's internal methods. The modeled ET will be compared to observed ET from an EC tower in the cotton field.

6.2. Methods

6.2.1. Instrumentation

Continuous 10 Hz measurements of CO_2 and water vapor flux were made using an eddy covariance system (EC). The EC system consisted of a sonic anemometer (C-SAT3; Campbell Scientific, Logan, UT, USA) and an infrared gas analyzer, IRGA (LI-7500; LI-COR, Lincoln, NE, USA). The sonic anemometer and IRGA were connected to LI-COR's SmartFlux system, which used EddyPro (version 6.2.2) software to process 10 Hz fluxes and compile them into 30-minute summaries. Eddy covariance instruments were maintained at 2 m above the plant canopy and were installed facing due south, which was the direction of the prevailing winds. Instruments were calibrated and had their internal chemicals changed annually as recommended by the manufacturer.

Additional meteorological instruments were installed at the site to accompany the EC measurements and to allow for an energy balance closure. Air temperature and relative humidity were measured using a temperature and relative humidity probe (HMP155A; Vaisala, Vantaa, Finland). Solar instruments consisted of a pyranometer (LI-200R; LI-COR, Lincoln, NE, USA), a quantum (PAR) sensor (LI-190R; LI-COR, Lincoln, NE, USA), and a net radiometer (NR-LITE2; Kipp and Zonen, Delft, Netherlands). Precipitation was measured using a tipping bucket style rain gauge (TE525; Texas Electronics, Dallas, TX, USA). Soil instruments consisted of seven soil moisture sensors (CS655; Campbell Scientific, Logan, UT, USA), four soil thermocouples (TCAV; Campbell Scientific, Logan, UT, USA), and four soil heat-flux plates (HPF01SC; Hukseflux, Delft, Netherlands). Three soil moisture sensors were placed horizontally at a depth of 4 cm; two were placed vertically between 10 and 20 cm; the last two were placed vertically between 20 and 30 cm. Soil heat-flux plates were placed in pairs, 1 meter apart, and buried at 8 cm. Soil thermocouples were buried at 2 and 6 cm above the soil heat-flux plates. Additional meteorological instruments and soil instruments were connected to a datalogger (CR-3000; Campbell Scientific, Logan, UT, USA). Readings were collected every 2 seconds and compiled into 30-minute summaries.

6.2.2. Field Information

The study was conducted in a 12.14 ha conventionally managed dryland cotton (*Gossypium hirsutum*) field, which is shown in Figure 32. The field was located at the Texas A&M Agrilife Research Farm in Burleson County, Texas (30°32’46.2” N,

96°25’19.7”W), approximately 15 km from the College Station campus. The cotton crop was planted on April 6 (DOY 96) in 2017, April 18 (DOY 108) in 2018, and April 30 (DOY 120) in 2019. Wet and cool soil conditions delayed planting in 2019 The cotton crop was defoliated using GinSTAR (BayerCrop Science, Leverkusen, Germany) on August 21 (DOY 233) 2017, August 21 (DOY 233) in 2018, and September 3 (DOY 246) in 2019. The cotton crop was harvested on September 11 (DOY 254) in 2017, September 17 (DOY 260) in 2018, and September 16 (259) in 2019. The variety was Phytogen 333WRF in 2017 and 2018 and Phytogen 350 in 2019. The plant population was 6.24 plants m^{-2} in 2017, 6.22 plants m^{-2} in 2018, and 6.11 plants m^{-2} in 2019. Nitrogen 95 kg N ha^{-1} was applied to the cotton crop in all years. The field was tilled and hilled prior to planting. After harvest, the residues were shredded and then tilled into the soil.

The climate of the location is humid subtropical (Köppen Cfa) with an average annual temperature of 20.58°C and an average annual precipitation of 1018 mm (National Oceanic and Atmospheric Administration, 2011). Rainfall typically follows a bimodal pattern with the most precipitation occurring in May, June, and October. The dominant soil type in the field is Weswood silt loam (Udifluventic Haplustepts, 38% clay in surface horizon, floodplain), which contains high amounts of 2:1 shrink-swell clays. The site is located in the Texas Blacklands and Post-Oak Savanah region, where the majority of cotton grown in the region (80 – 95%) is dryland (Matocha et al., 2009; Texas A&M Agrilife, 2019). Cotton is the most common crop in Burleson Country, where this study is located (USDA-NASS, 2017).

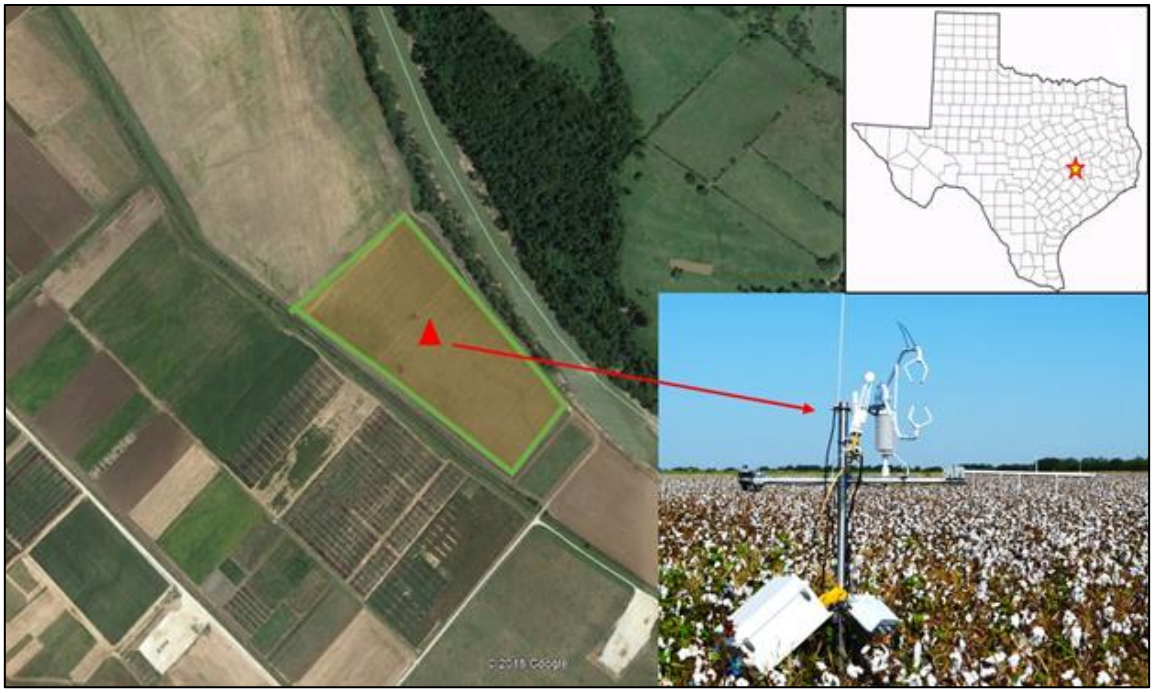

Figure 32: The Cotton EC Tower and Location.
The study site is shown above. The left image is a satellite image of the site with the cotton field outlined in green. The red triangle represents the location of the EC system, which is shown in the lower right. The upper right image shows the location of the site within Texas (Google Earth, 2018).

6.2.3. Data Analysis

The EddyPro (6.2.2) embedded within SmartFlux computed 30-minute fluxes from the 10 Hz input data. The sign convention used was that positive numbers indicate fluxes away from the canopy and negative numbers indicate fluxes toward the canopy. The EddyPro software flagged data for quality based on internal turbulence tests. High-quality data was marked with a "0", moderate quality with a "1" and low quality with a "2". Low-quality points were manually removed during data inspection for gap filling.

Gap filling was used to fill in missing and removed data points. Gap filling and flux partitioning (partitioning CO_2 uptake {GPP} and respiration {R_{eco}}) were done using the Max Plank Institute for Biogeochemistry's online R-based program (R Gui 3.4.1) using the default settings.

Evapotranspiration (ET) was calculated from Latent heat (LE), after gap filling.

$$ET = \frac{LE * 0.0018}{2.5}$$

6.2.4. Energy Balance Calculation

After gap filling, an energy balance was calculated with the data in order to verify the data quality and correct for unaccounted energy. Net radiation (from net radiometer) minus soil heat storage (calculated from soil heat -plates) was regressed against LE + Sensible Heat (H) (both from EC instruments).

$$Rn - G = LE + H$$

$$G = G_{8cm} + \left(\left(1.02 + (VWC * 4.19)\right) * (\Delta T * 8) * \frac{100}{18}\right.$$

Where G_{8cm} is the soil heat from the flux plate at 8 cm, VWC is the volumetric water content at 4 cm, and ΔT is the temperature difference between the soil heat-flux plates and the soil surface. The slope of Rn – G vs LE + H represented the amount of energy correctly accounted for by the EC system. The inverse of the slope was equivalent to the energy unaccounted for by the EC system. The unaccounted energy was redistributed to LE and H based on the Bowen ratio. Due to an instrument malfunction, an energy balance calculation was not possible for 2017.

6.2.5. DSSAT Modelling

The Decision Support System for Agrotechnology Transfer (DSSAT) software system (Version 4.7; The DSSAT Foundation, Gainesville, FL, USA) modeled crop growth and ET. The simulation was started on March 1 (DOY 60) in 2017, on April 1 (DOY 91) in 2018, and on April 1 (DOY 91) in 2019. The following weather variables were input into the DSSAT model as a daily summary: precipitation, maximum temperature, minimum temperature, dew point, relative humidity, solar radiation, plant-available radiation, and wind speed. Soils files were created in DSSAT using soil information from direct sampling as well as information from the NRCS soil survey. A soil file was created for each soil type found in the field. The soil files contained the following information: texture, pH, and CEC (estimated from soil texture and mineralogy).

The collected phenological data was used alongside DSSAT's Generalized Likelihood Uncertainty Estimation (GLUE) tool to calibrate the cultivar file parameters used for the model (Table 9). GLUE creates many successive models and compares them to the actual recorded phenological information using a likelihood function. The cultivar parameters are adjusted until the closest match is obtained. This process minimizes uncertainty in parameter estimation (DSSAT, 2017, Pathak et al 2012). The species and ecotype files were not modified. Following the creation of weather, soil, and cultivar files, the models themselves were set up using the X-build feature.

Table 9: Cotton Cultivar Parameters

Cotton Cultivar Parameters				
Parameter	**Description**	**Calibrated 2017**	**Calibrated 2018**	**Calibrated 2019**
EM-FL	Time between emergence and first flower	37.1	37.0	36.1
FL-SD	Time between first flower and first seed	15.0	17.5	12.7
SD-PM	Time between first seed and maturity	47.11	40.47	47.96
FL-LF	Time between first flower and end of leaf expansion	50.0	50.0	75.0
LFMAX	Maximum leaf photosynthesis rate	1.05	1.03	1.11
SLAVR	Leaf area under standard conditions	210	191	241.7
SIZLF	Maximum leaf size	275	250.2	280.0
XFRT	Max portion of growth used in seed development	0.75	0.75	0.75
SFDUR	Seed filling duration under standard conditions	29.9	27.3	23.25
SDPDV	Average # seeds per pod.	23.53	20.84	25.84

The CROPGRO-Cotton model was used to model cotton growth and development. CROPGRO is the only cotton growth model in the DSSAT system. CROPGRO is a broad range model that has applications with many crops, including cotton. CROPGRO uses a growing degree-day based formula that changes with the phenological stage of the cotton crop to model cotton growth and development (DSSAT, 2017). DSSAT used a number of different sub-models to simulate environmental conditions (i.e. ET, soil moisture) for the CROPGRO model.

Soil evaporation was modeled using the method developed by Suleiman and Ritchie in 1972. This method uses a two-step process, the first step occurs under high soil moisture and evaporation is limited only by available radiation energy. The second step occurs under lower soil moisture and is limited by radiation, water availability, and soil properties (Hoogenboom et al., 2003; Suleiman and Ritchie, 2003; Ritchie et al., 2009). Soil organic matter was modeled the default DSSAT method, which is based on a modification of the PAPRAN model (Seligman and Van Keulen, 1981; Godwin and Jones, 1991; Godwin and Singh, 1998; Hoogenboom et al., 2003; Dejonge and Thorp, 2017). Soil water movement was modeled using the method developed for CERES-Wheat; all DSSAT models use this soil water model. This model calculates water content in each soil layer on a daily time-scale using rainfall, ET, drainage, irrigation, and unsaturated water flow (Ritchie and Otter, 1985; Jones and Ritchie, 1991; Jones, 1993; Ritchie, 1998; Hoogenboom et al., 2003). CROPGRO uses an hourly photosynthesis model that uses climate and weather information, canopy height, width, LAI, leaf angle, row spacing, day of year, and time of day to compete total C fixation. For sunlit leaves, photosynthesis is largely controlled by CO_2 concentration and temperature. For shaded leaves, the complication is more complex (Boote and Pickering, 1994; Hoogenboom et al., 2003).

Cotton ET was modeled using both of DSSAT's built-in methods: FAO-56 and Priestly-Taylor/Ritchie. Both of these methods are used to model potential ET, which is then modified by CROPGRO in DSSAT to simulate actual ET. The default method is the Priestly-Taylor/Ritchie method, which was developed in 1972 as a simplified

modification of the Penman-Monteith equation. This method uses solar radiation and temperature to calculate potential ET (Priestly and Taylor, 1972; Ritchie, 1972; Xu and Chen, 2005; Agam et al., 2010). DSSAT has recently incorporated the potential ET model described in FAO paper number 56, which is a more complete version of the Penman equation. This method uses wind speed and humidity in addition to temperature and radiation (Doorenbos and Pruitt, 1977; Monteith, 1986; Agam et al., 2010; Dejonge and Thorp, 2017). DSSAT recommends using the FAO-56 method for arid and windy climates and the Priestly-Taylor/Ritchie for humid environments. Following the calculation of potential ET by one of two methods DSSAT then converts potential ET to actual ET using the soil water models and the crop growth model (Hoogenboom et al., 2003).

6.2.6. Statistical Analysis

Statistical analysis was performed using manual calculation, DSSAT's internal system, and SigmaPlot (Version 14.0). Regression analysis of the energy balance was calculated using SigmaPlot. The following indices of model performance were manually calculated: index of agreement (d-Index), normalized root mean square error (nRMSE), r-squared, and co-coefficient of residual mass (CRM). The d-index shows the degree of agreement between the modeled data and the observed data, with a perfect fit between the modeled and observed data resulting in a d-index of 1.0 and no fit with a d-index of 0.0 (Soler et al., 2007; Adhikari et al., 2016; Basso et al., 2016; Amouzou et al., 2018). The calculation of the d-index is as follows, where x is the modeled value and y is the observed value:

$$d = 1 - [\frac{\sum(x - \bar{x})^2}{\sum(|x - \bar{x}| + |y - \bar{y}|)^2}]$$

The CRM shows the degree of over- or underestimation between the modeled and the observed data. A perfect fit between a model and measurement would result in a CRM of zero, positive numbers indicate underestimation and negative numbers indicate overestimation by the model (Xevi et al., 1996; Jalota et al., 2010; Dettori et al., 2011).

$$\text{CRM} = \frac{\sum y - \sum x}{\sum y}$$

6.3. Results and Discussion

6.3.1. Energy Balance

The energy balance closure is shown in Figure 33. The energy balance closure (the slope of the regression line between Rn-G and LE+H) was, 0.71 in 2018, and 0.78 in 2019. As previously mentioned, an energy balance calculation was not possible in 2017 due to a malfunction with the net radiometer. However, the energy balance closure for 2018 and 2019 was similar to that seen of energy balance closures in other EC studies. One of the largest meta-analysis of EC studies found an average energy balance closure of 0.79 with a range of 0.53 to 0.99 over 22 sites (Wilson et al., 2002). Studies in specifically cotton have found similar energy balance closure values (Gonzalez-Dugo et al., 2009; Hirschi et al., 2017; Li et al., 2018). Hirschi et al (2017) found an average closure of 0.77. Li et al (2018) found a range of closure values between 0.57 and 0.95 across several EC sites in cotton across China and Kazakhstan. The energy balance for this site was better in 2019, but both were acceptable. The closure allowed LE to be

corrected, which improved model accuracy. Despite the lack of energy balance closure in 2017, the model efficacy was still adequate.

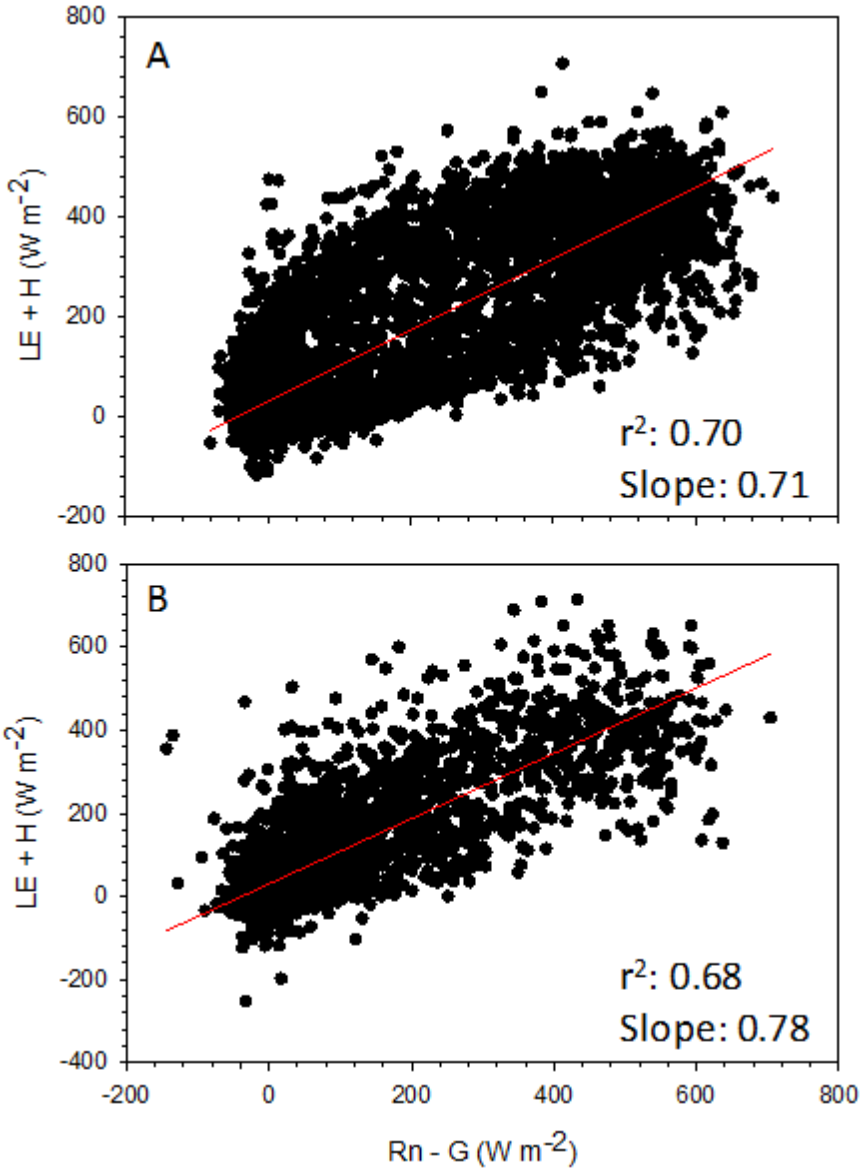

Figure 33: Cotton Energy Balance Closure
Energy Balance closure is shown above. Image "A" refers to the closure for 2018. Image "B" refers to the closure for 2019. The slope and r-square of the linear regression is shown on the graph.

6.3.2. Phenology Models

The phenology models for 2017 are shown in Figure 34 and their statistical results are shown in Table 10. These phenology models were used to verify the model performance. The 2017 cotton height (Figure 34A) model overestimated mature plant height. The maximum plant height in 2017 was 0.90 ± 0.01 meters, whereas the simulated maximum plant height was 1.12 meters. The RMSE of this estimation was 0.16 meters with a d-index of 0.93. Other modeling efforts using CROPGRO-Cotton have achieved lower RMSE, however many of these were in irrigated cotton. Studies in dryland and deficit irrigation have produced results similar to these (Thorp et al., 2014, 2015; Modala et al., 2015). The reduced model efficiency found in studies of dryland cropping systems indicates a need for further study and model improvement.

The 2017 LAI model (Figure 34B) simulated the early growing season well, although it underestimated the actual maximum LAI. The actual maximum LAI was 2.55 ± 0.09, while CROPGRO predicted a maximum LAI of 2.24. The LAI model had an RMSE of 0.26 and a d-index of 0.98. Compared to other studies using CROPGRO-Cotton, this is an ideal result, even when compared to studies in irrigated cotton. Other studies of LAI in cotton have reported a range of RMSE values from 0.16 to 1.11 (Pathak et al., 2012; Modala et al., 2015; Thorp et al., 2015).

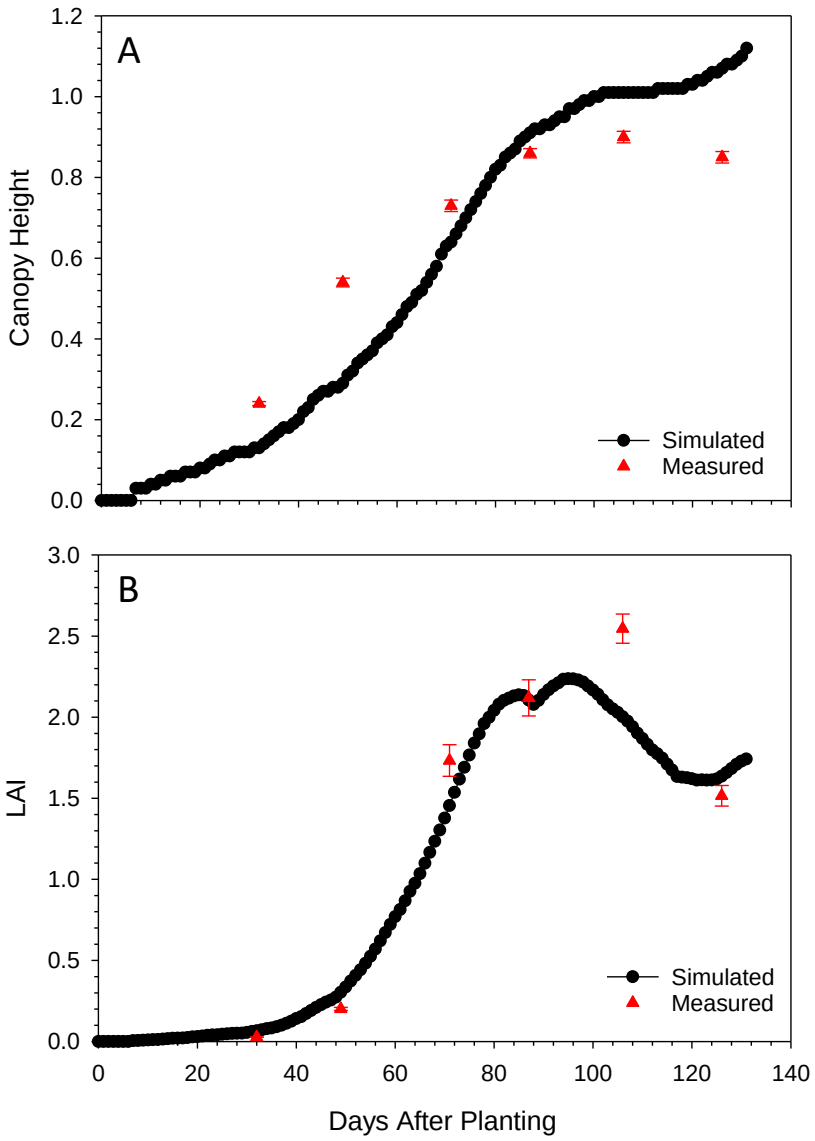

Figure 34: Cotton Phenology Model 2017
Cotton Phenology Models for 2017 are shown above. Image "A" refers to the canopy height model. Image "B" refers to the LAI model. Black circles show the simulated values and red triangles show the measured values. Error bars show standard error of the mean.

Table 10: Cotton Phenology Models - 2017

2017		
Statistic	**Height Model**	**LAI Model**
RMSE	0.16	0.26
R^2	0.90	0.95
D-index	0.93	0.98

The phenology for 2018 models are shown in Figure 35 and their statistical results are shown in Table 11. The 2018 height model (Figure 35A) was more accurate than the 2017 model with only a slight overestimation and better agreement in the early growing season. The maximum observed height was 0.95 ± 0.01 meters while the maximum simulated height was 0.99 meters. The RMSE of this estimation was 0.07 meters with a d-index of 0.99. The results of this modeling effort are more in line with those observed in other studies utilizing DSSAT's CROPGRO-Cotton model (Modala et al., 2015; Thorp et al., 2015).

The 2018 LAI model (Figure 35B) performed slightly worse than the 2017 model, primarily due to measurements later in the season. Cotton LAI decreased more quickly with drought stress than predicted in the model. This indicates a deficit in the model with simulating the effects of drought-stress and soil water storage. The prior to defoliation, the observed LAI was 0.66 ± 0.07 while the simulated LAI was 1.39. The maximum observed LAI was 2.80 ± 0.24 while the maximum simulated LAI was 2.41. The RMSE of this model was 0.34 meters and the d-index was 0.97. While not as precise

as the 2017 model, the results for the 2018 LAI model were still within the typical range observed by other studies (Pathak et al., 2012; Modala et al., 2015; Thorp et al., 2015).

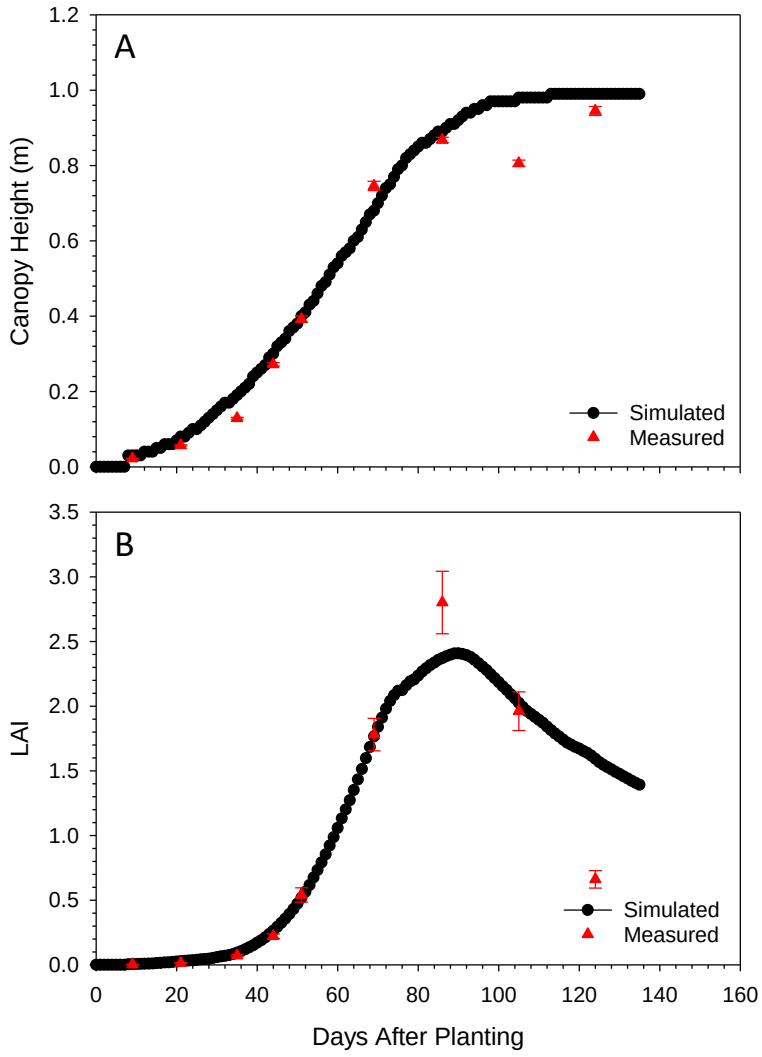

Figure 35: 2018 Cotton Phenology Models
Cotton phenology models for 2018 are shown above. Image "A" refers to the canopy height model. Image "B" refers to the LAI model. Black circles show the simulated values and red triangles show the measured values. Error bars show standard error of the mean.

Table 11: Cotton Phenology Models - 2018

2018		
Statistic	**Height Model**	**LAI Model**
RMSE	0.07	0.34
R^2	0.97	0.88
D-index	0.99	0.97

The phenology models for 2019 are shown in Figure 36 and their statistical results are shown in Table 12. The 2019 height model (Figure 36A) significantly overestimated actual height resulting in a high RMSE of 0.22 meters. The d-index in 2019 was 0.93, similar to that of 2017. The actual maximum height was 1.03 ± 0.09, while the model predicted a maximum height of 1.25 meters. While the model overestimates mature plant height all three years, this effect was most pronounced in 2019. DSSAT's CROPGRO-Cotton performs most adequately when run and calibrated under irrigated conditions. This model could be improved by calibrating the cultivar co-efficient with data from an irrigated plot (Hoogenboom et al., 2003; Modala et al., 2015; Thorp et al., 2015). The lack of model efficiency in dryland settings is a potential problem with this modeling system.

The 2019 LAI model (Figure 36B) performed similarly to previous years. The model did underestimate cotton LAI late in the season; however, this effect was similar to that of previous years. The maximum observed LAI was 2.41 ± 0.13 while the model

predicted a maximum LAI of 2.29. The RMSE of the 2019 LAI model was 0.28 and the d-index was 0.97. Model efficacy for the 2019 phenology model is limited by the lower number of observations (4) due to poor weather conditions early in the season. In spite of this, the LAI model performed well, similar to the results seen in other studies using DSSAT's CROPGRO-Cotton.

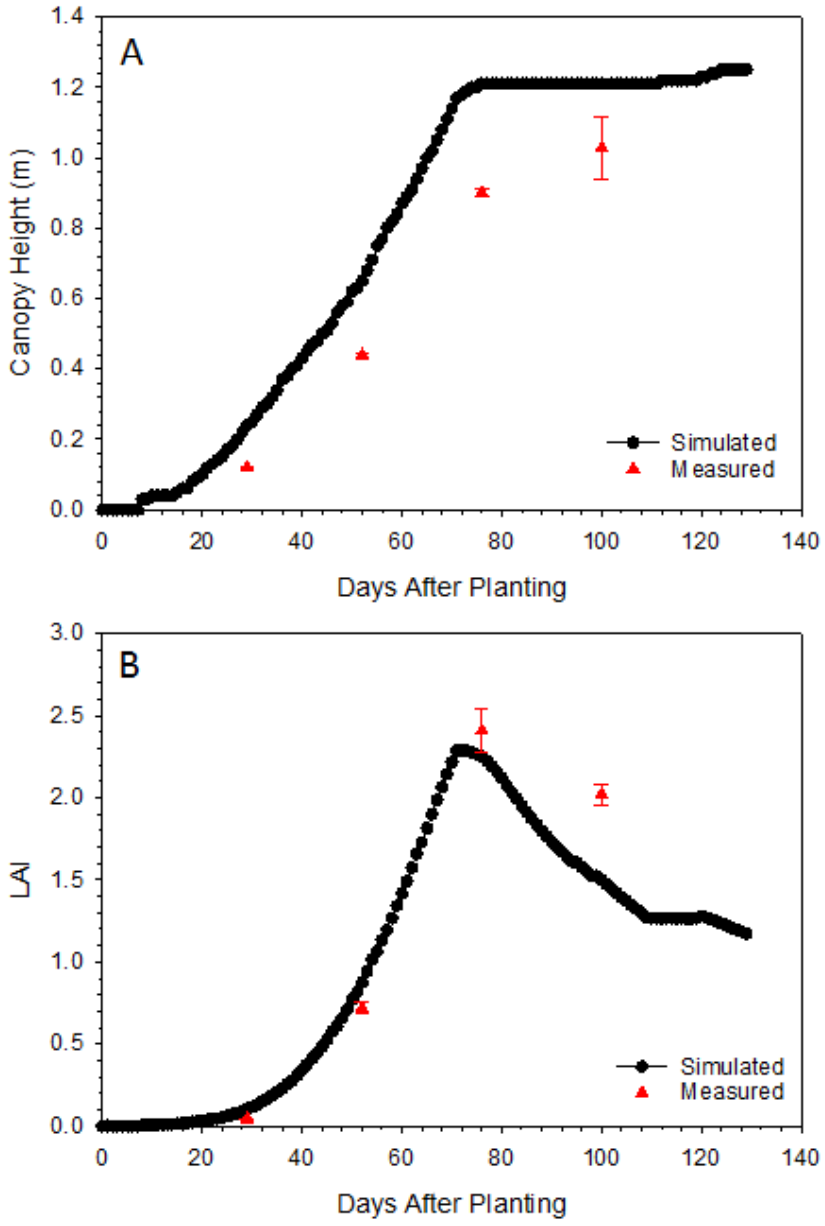

Figure 36: 2019 Cotton Phenology Models
Cotton phenology models for 2019 are shown above. Image "A" refers to the canopy height model. Image "B" refers to the LAI model. Black circles show the simulated values and red triangles show the measured values. Error bars show standard error of the mean.

Table 12: Cotton Phenology Models - 2019

2019		
Statistic	**Height Model**	**LAI Model**
RMSE	0.22	0.28
R^2	0.98	0.95
D-index	0.93	0.97

6.3.3. Evapotranspiration Modeling

The ET modeling efforts for 2017 is shown in Figure 37 and the associated statistical analysis is shown in Table 13. The FAO-56 model simulated ET well throughout most of the growing season. The model did have a slight tendency to overestimate ET pulses after rain events, particularly in the early growing season. The Priestly-Taylor ET had a greater tendency to over and under-estimate ET following rain events. The negative CRM values (-0.05 for the Priestly-Taylor model and -0.01 for the FAO-56 model) indicate that the model had a tendency to overestimate actual ET, although that trend was very slight with the FAO-56 models.

Total observed cumulative ET during the 2017 modeled period (March 1 to August 15; DOY 60 – DOY 227) was 547.61 mm m^{-2}, while precipitation during this period was 561.83 mm m^{-2}. The FAO-56 model predicted a cumulative ET of 545.38 mm m^{-2}, which is a cumulative underestimation of 2.23 mm m^{-2}. The normalized RMSE of this estimation was 0.12 mm m^{-2} day^{-1}. The error of this modeling effort is within the range observed in other modeling efforts using DSSAT's CROPGRO-Cotton (Thorp et

al., 2015). The Priestly-Taylor model predicted a cumulative ET of 558.98 mm m^{-2}, resulting in a cumulative overestimation of 11.37 mm m^{-2}. The normalized RMSE of this estimation was 0.58 mm m^{-2} day^{-1}, which although greater than that observed by the FAO-56 model was still within the range of results seen by Thorp et al (2015).

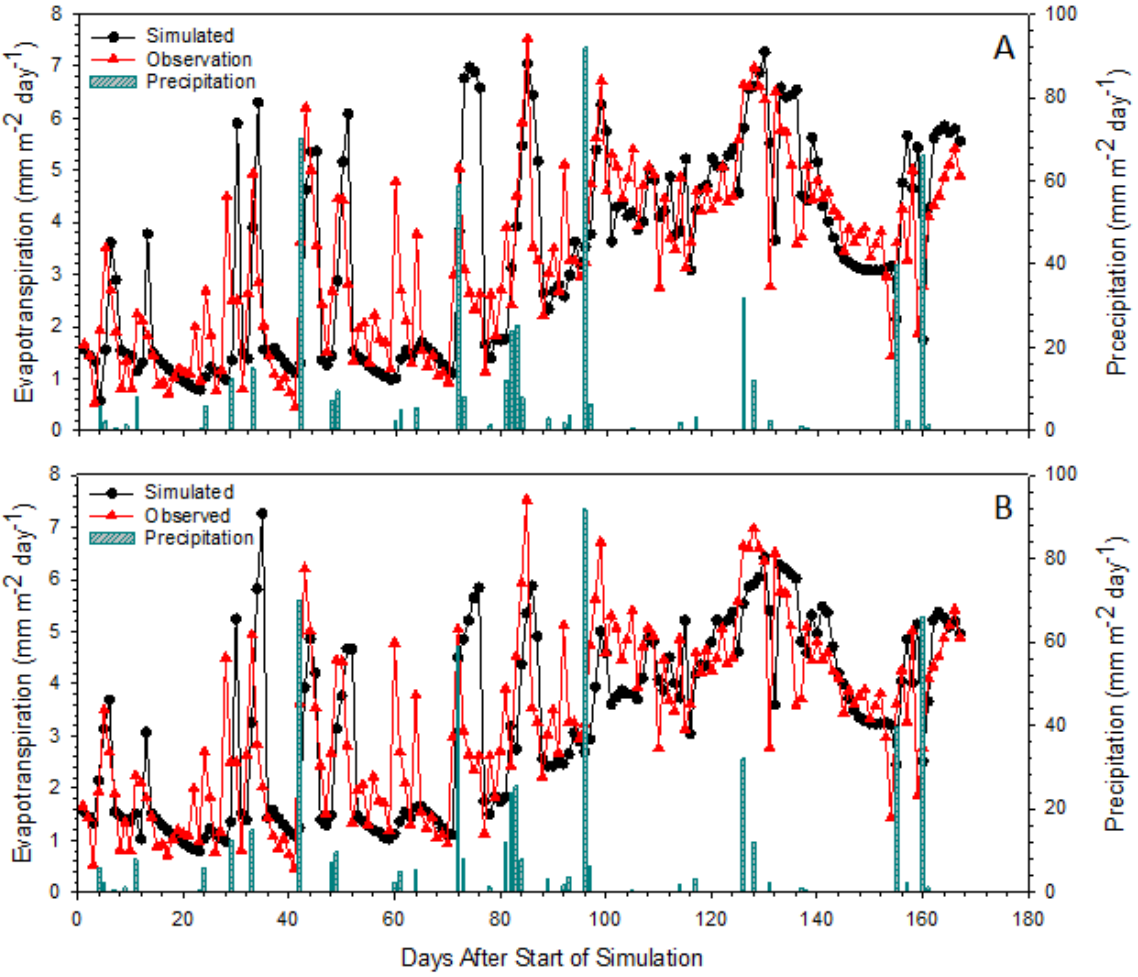

Figure 37: 2017 Cotton Evapotranspiration Models
The cotton evapotranspiration models for 2017 are shown above. Image "A" shows the Priestly-Taylor/Ritchie model. Image "B" shows the FAO-56 model. Black circles in

both images refer to simulated ET values. Red triangles show observed ET values in both images. Teal-stripped bars show precipitation. The simulation was started on April 1 (DOY 91).

The evapotranspiration models for 2018 are shown in Figure 38 and their statistical analysis is shown in Table 13. In 2018, the Priestly-Taylor model performed similarly to that of 2017. However, the 2018 FAO-56 model had much more error than the Priestly-Taylor model. The FAO-56 model overestimated ET following rain events and underestimated ET during dry spells. This is a significant change in model efficiency between the years, 2018 was an unusually dry year. While the FAO-56 model is traditionally thought to perform better in arid conditions, this was not the case for 2018 at this location (Hoogenboom et al., 2003; Jones et al., 2003). It is possible that the unique shrink-swell nature of the soils at this site are affecting soil water evaporation in ways not anticipated by the model (Patil and Rajput, 2009).

Total observed cumulative ET during the 2018 modeled period (April 1 to August 31; DOY 60 – DOY 227) was 485.84 mm m^{-2}, while precipitation during this period was 201.42 mm m^{-2}. The FAO-56 model predicted a cumulative ET of 410.53 mm m^{-2}, which is a cumulative underestimation of 75.31 mm m^{-2}. The normalized RMSE of this estimation was 2.04 mm m^{-2} day^{-1}. The error of this modeling effort is within the range observed in other modeling efforts using DSSAT's CROPGRO-Cotton (Thorp et al., 2015). The Priestly-Taylor model predicted a cumulative ET of 447.64 mm

m^{-2}, resulting in a cumulative underestimation of 38.2 mm m^{-2}. The normalized RMSE of this estimation was 0.61 mm m^{-2} day^{-1}

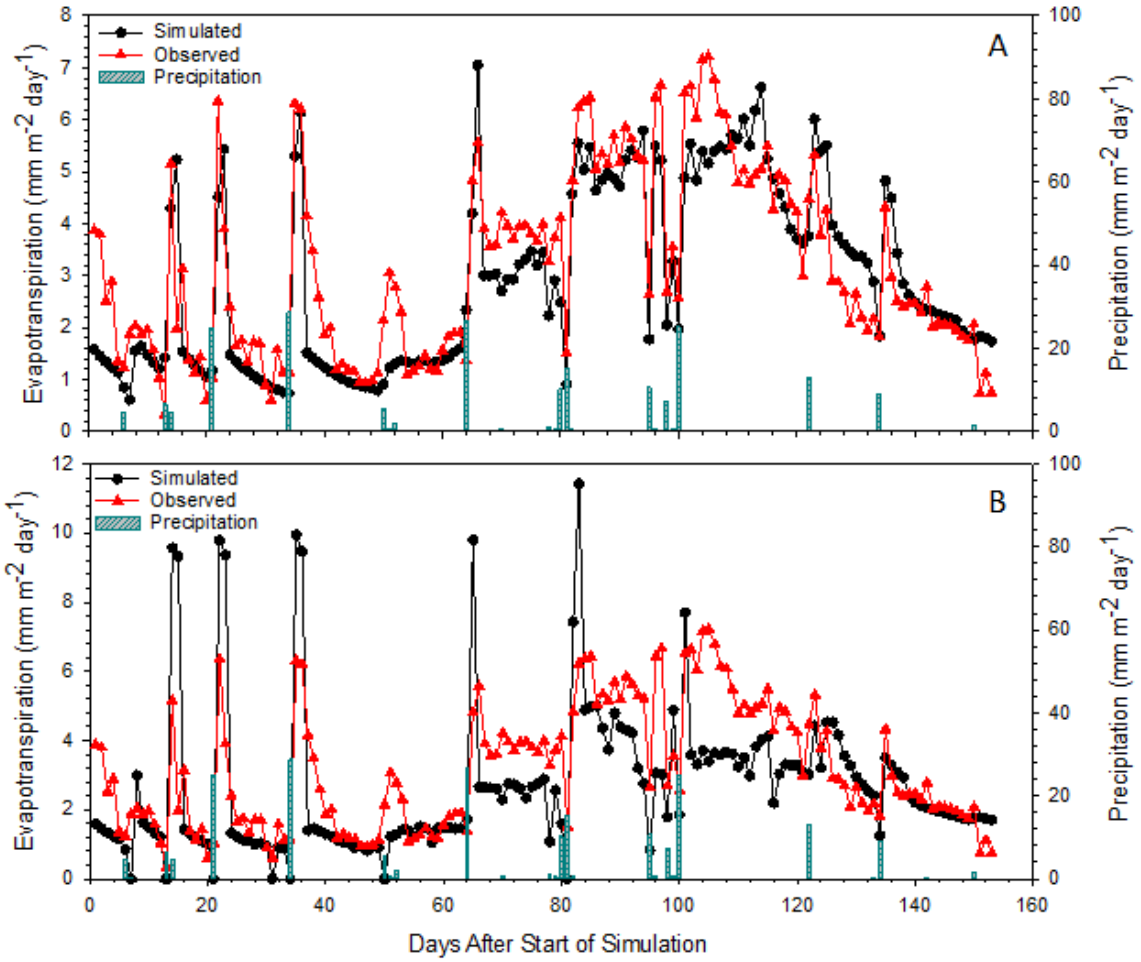

Figure 38: 2018 Cotton Evapotranspiration Models
The 2018 cotton evapotranspiration models are shown above. Image "A" shows the Priestly-Taylor/Ritchie model. Image "B" shows the FAO-56 model, note that the left Y-axis is different for the FAO-model. Black circles in both images refer to simulated ET values. Red triangles show observed ET values in both images. Teal-stripped bars show precipitation. The simulation was started on April 1 (DOY 91).

The evapotranspiration models for 2019 are shown in Figure 39 and their statistical analysis is shown in Table 13. In 2019, the Priestly-Taylor model underestimated ET throughout the early 2019 growing season. During a dry period later in the growing season, the Priestly-Taylor model significantly underestimated actual ET. The FAO-56 model performed similarly to the Priestly-Taylor model, however the under- and overestimation was less pronounced. The tendency of the model to estimate the effect of a rain-pulse on ET incorrectly was more pronounced in 2019 and was exacerbated by frequent rain events in the early growing season. Additionally the models both underestimated ET during dry-spells, possibly indicating an issue with modeling soil water storage.

Total observed cumulative ET during the 2019 modeled period (April 1 to September 6; DOY 60 – DOY 249) was 637.08 mm m^{-2}, while precipitation during this period was 603.74 mm m^{-2}. The FAO-56 model predicted a cumulative ET of 588.05 mm m^{-2}, which is a cumulative underestimation of 49.03 mm m^{-2}. The normalized RMSE of this estimation was 0.43 mm m^{-2} day^{-1}; however, the overall correlation was poor with an r^2 of only 0.13. The Priestly-Taylor model predicted a cumulative ET of 585.06 mm m^{-2}, resulting in a cumulative underestimation of 52.01 mm m^{-2}. The normalized RMSE of this estimation was 0.46 mm m^{-2} day^{-1}. This model had a poor correlation with an r^2 of only 0.15. Both models overall performed poorly for 2019, which was more pronounced with the Priestly-Taylor.

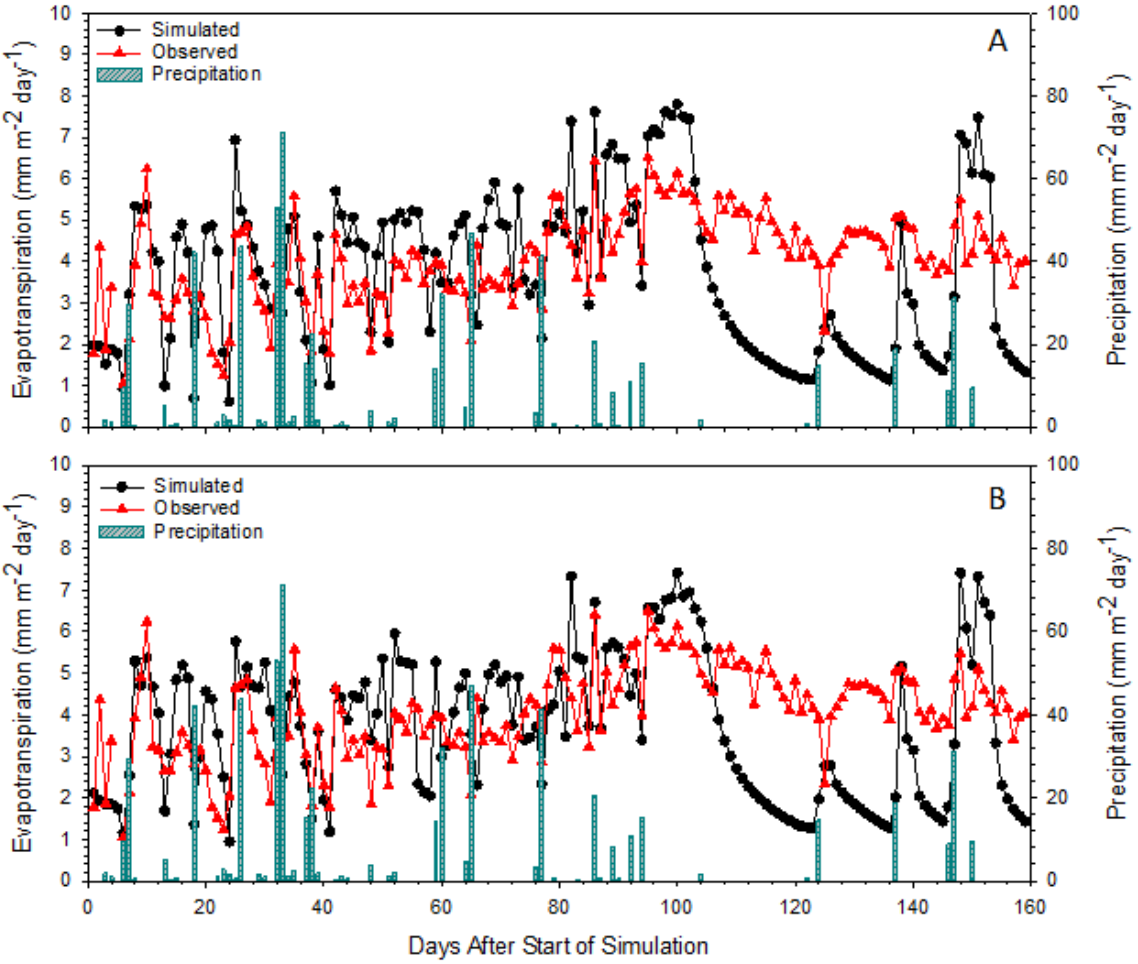

Figure 39: 2019 Cotton Evapotranspiration Models
The 2019 cotton evapotranspiration models are shown above. Image "A" shows the Priestly-Taylor/Ritchie model. Image "B" shows the FAO-56 model. Black circles in both images refer to simulated ET values. Red triangles show observed ET values in both images. Teal-stripped bars show precipitation. The simulation was started on April 1 (DOY 91).

Table 13: Cotton Evapotranspiration Model Statistical Analysis

Statistical Analysis						
	Priestly-Taylor			**FAO-56**		
Statistic	**2017**	**2018**	**2019**	**2017**	**2018**	**2019**
nRMSE	0.58	0.61	0.46	0.12	2.04	0.43
CRM	-0.05	0.08	0.08	-0.01	0.16	0.08
D-Index	0.87	0.93	0.77	0.87	0.70	0.78
r^2	0.68	0.76	0.15	0.66	0.43	0.13

While there was some success in modeling cotton evapotranspiration using DSSAT's CROPGRO-Cotton, there was also a considerable error in some for the models. Throughout all three years, the model frequently misrepresented the effect of both rain-pulses and dry spells. Other attempts at modeling ET in dryland cotton have also been met with mixed-to-low success (Thorp et al., 2015; Dejonge and Thorp, 2017). The reduced model in dryland systems has been observed in other crops, indicating a need to make improvements in the model (Sau et al., 2004; Anothai et al., 2013; Soldevilla-Martinez et al., 2014; Thorp et al., 2014; Modala et al., 2015; Basso et al., 2016). Dejonge and Thorp et al. (2017) were able to improve the model efficacy in CROPGRO-Cotton by altering the wind component of the FAO-56 method within DSSAT, indicating a possible cause of these issues. An additional study found that the soil water distribution during the second stage may be causing some of the issues with dryland modeling (Ritchie et al., 2009). These issues with modeling ET in dryland

systems are potential problems for regional ET estimates in Eastern Texas as the majority of cotton grown in this region is dryland (Matocha et al., 2009; USDA-NASS, 2017; Texas A&M Agrilife, 2019).

A possible complication at this site is the presence of 2:1 shrink-swell clays. The soils file in DSSAT only includes total clay, with no consideration given to the type of clay minerals. 2:1 shrink-swell clays interact with water in a different manner than non-shrink-swell clays. During dry periods, cracks form that create preferential flow pathways for water, altering its movement into and through the soil profile. Early-stage water infiltration after a dry period in shrink-swell soils is more rapid due to the presence of the preferential flow pathways. However, as the soil absorbs water and the cracks close, infiltration is greatly reduced (Wang et al., 2018; Harmel et al., 2019). The effect of shrink-swell properties on soil water movement has been found to make predicting crop water use more unpredictable and more difficult to manage (Ringrose-Voase and Nadelko, 2013). Traditional soil water movement and storage models, which are incorporated into DSSAT's ET model during the calculation of crop ET from potential ET, have been found to be less effective in soils high in shrink-swell clays (Patil and Rajput, 2009). All of this together suggests a need for greater study and modeling efforts in dryland agriculture and in soils with shrink-swell properties.

6.4. Conclusions

The phenology models were somewhat successful. The cotton height model had a tendency to overestimate mature plant height and the leaf area model often overestimated leaf area index late in the growing season. The energy balance closure

computed for 2018 and 2019 was well within the range of results observed in other studies, indicating that the observed ET data was good. The ET modeling effort using the DSSAT CROPGRO-cotton was less successful. Of the two internal potential ET methods, the Priestly/Taylor method was more consistent (average nRMSE: 0.55). The accuracy of the FAO-56 method was highly variable between the years, with a good fit in 2017 (nRMSE: 0.12) and a poor fit in 2019 (nRMSE: 2.04). The 2019 modeling effort had a problem with significantly underestimating ET late in the season; this problem was observed for both internal methods. Unfortunately, there is less literature on modeling ET in cotton than other crops. Most work modeling ET using the DSSAT system has found that modeling ET in dryland systems is less accurate than modeling in irrigated systems. There is some evidence that the second-stage soil water model might be a contributing factor. The presences of shrink-swell minerals at this study site likely complicated the modeling effort. The shrink-swell minerals interact with water in a different manner than non-shrink-swell clay minerals, potentially influencing crop ET. Given the predominance of dryland farming in this region, the lack of model accuracy in dryland systems is a problem with estimating crop water use and energy balance in this region and in others where dryland farming is common.

6.5. Acknowledgments

This work is supported by NIFA-NLGCA [grant no. 2016-70001-24636/project accession no. 1008730] from the USDA National Institute of Food and Agriculture. This work was also supported partially through cotton incorporated grant # 17-614. The authors would like to thank Dr. Don T. Conlee (Department of Atmospheric Sciences,

Texas A&M University) for providing missing meteorological data. The authors would like to thank Texas A&M Agrilife and the staff at the research farm, particularly Mr. Alfred Nelson (Farm Manager) for planting and managing the cotton field. We would also like to thank Dr. Gerrit Hoogenboom (Department of Agricultural and Biological Engineering, University of Florida) and the DSSAT Foundation for their advice with operating and troubleshooting the DSSAT software system.

6.6. References

Adhikari, P., Ale, S., Bordovsky, J.P., Thorp, K.R., Modala, N.R., Rajan, N., Barnes, E.M., 2016. Simulating future climate change impacts on seed cotton yield in the Texas High Plains using the CSM-CROPGRO-Cotton model. Agric. Water Manag. 164, 317–330. https://doi.org/10.1016/j.agwat.2015.10.011

Agam, N., Kustas, W.P., Anderson, M.C., 2010. Application of the Priestley – Taylor Approach in a Two-Source Surface Energy Balance Model. Am. Meteorological Soc. 11, 185–198. https://doi.org/10.1175/2009JHM1124.1

Amouzou, K.A., Naab, J.B., Lamers, J.P.A., Borgemeister, C., Becker, M., Vlek, P.L.G., 2018. CROPGRO-Cotton model for determining climate change impacts on yield, water- and N- use efficiencies of cotton in the Dry Savanna of West Africa. Agric. Syst. 165, 85–96. https://doi.org/10.1016/j.agsy.2018.06.005

Anothai, J., Soler, C.M.T., Green, A., Trout, T.J., Hoogenboom, G., 2013. Evaluation of two evapotranspiration approaches simulated with the CSM–CERES–Maize model under different irrigation strategies and the impact on maize growth, development and soil moisture content for semi-arid conditions. Agric. For. Meteorol. 176, 64–

76.

Basso, B., Liu, L., Ritchie, J.T., 2016. A Comprehensive Review of the CERES-Wheat, -Maize and -Rice Models' Performances, Advances in Agronomy. Elsevier Inc. https://doi.org/10.1016/bs.agron.2015.11.004

Boote, K.J., Pickering, N.B., 1994. Modeling Photosynthesis of Row Crop Canopies. HortScience 29, 1423–1434.

Burba, G., 2013. Eddy Covariance Method. LI-COR Biosciences, Lincoln, NE.

Dejonge, K.C., Thorp, K.R., 2017. Implementing Standardized Reference Evapotranspiration and Dual Crop Coefficient Approach in the DSSAT Cropping System Model. Am. Soc. Agric. Biol. Eng. 60, 1965–1981.

Dettori, M., Cesaraccio, C., Montroni, A., Spano, D., Duce, P., 2011. Using CERES-Wheat to simulate durum wheat production and phenology in Southern Sardinia, Italy. F. Crop. Res. 120, 179–188.

Doorenbos, J., Pruitt, W.D., 1977. Guidelines for Predicting Crop Water Use. Rome, Italy.

Foley, J.A., Defries, R., Asner, G.P., Barford, C., Bonan, G., Carpenter, S.R., Chapin, F.S., Coe, M.T., Daily, G.C., Gibbs, H.K., Helkowski, J.H., Holloway, T., Howard, E.A., Kucharik, C.J., Monfreda, C., Patz, J.A., Prentice, I.C., Ramankutty, N., Snyder, P.K., 2005. Global Consequences of Land Use. Science (80-.). 309, 570–574. https://doi.org/10.1126/science.1111772

Godwin, D.C., Jones, C.A., 1991. Nitrogen dynamics in soil-plant systems, in: Modeling Plant and Soil Systems. ASA, CSSA, and SSSA, Madison, Wisconsin, pp. 287–

321.

Godwin, D.C., Singh, U., 1998. Nitrogen balance and crop response to nitrogen in upland and lowland cropping systems, in: Tsuji, G.Y., Hoogenboom, G., Thornton, P.K. (Eds.), Understanding Options for Agricultural Production. System Approaches for Sustainable Agricultural Development. Kluwer Academic Publishers, Dordrecht, Netherlands, pp. 55–77.

Gonzalez-Dugo, M.P., Neale, C.M.U., Mateos, L., Kustas, W.P., Prueger, J.H., Anderson, M.C., Li, F., 2009. A comparison of operational remote sensing-based models for estimating crop evapotranspiration. Agric. For. Meteorol. 149, 1843–1853. https://doi.org/10.1016/j.agrformet.2009.06.012

Google Earth, 2018. Map showing location of cotton field. earth.google.com/web/.

Han, G., Xing, Q., Yu, J., Luo, Y., Li, D., Yang, L., Wang, G., Mao, P., Xie, B., Mikle, N., 2014. Agricultural reclamation effects on ecosystem CO2exchange of a coastal wetland in the Yellow River Delta. Agric. Ecosyst. Environ. 196, 187–198. https://doi.org/10.1016/j.agee.2013.09.012

Harmel, R.D., Smith, D.R., Haney, R.L., Allen, P.M., 2019. Comparison of nutrient loss pathways: Run-off and seepage flow in Vertisols. Hydrol. Process. 33, 2384–2393.

Hirschi, M., Michel, D., Lehner, I., Seneviratne, S.I., 2017. A site-level comparison of lysimeter and eddy covariance flux measurements of evapotranspiration. Hydrol. Earth Syst. Sci. 21, 1809–1825. https://doi.org/10.5194/hess-21-1809-2017

Hoogenboom, G., Jones, J.W., Porter, C.H., Wilkens, P.W., Boote, K.J., Batchelor, W.D., Hunt, L.A., Tsuji, G.Y., 2003. A Decision Support System for

Agrotechnology Transfer Version 4.0, 4th ed, University of Hawaii. University of Hawaii, Honolulu, Hawaii.

Howell, T.A., Evett, S.R., Tolk, J.A., Schneider, A.D., 2004. Evapotranspiration of full-, deficit-irrigated, and dryland cotton on the Northern Texas High Plains. J. Irrig. Drain. Eng. 130.

Jalota, S.K., Sukhvinder, S., Chahal, G.B.S., Ray, S.S., Panigraphy, S., Bhupinder-Singh, F., Singh, K.B.., 2010. Soil texture, climate and management effects on plant growth, grain yield and water use by rainfed maize–wheat cropping system: Field and simulation study. Agric. Water Manag. 97, 83–90.

Jones, J.W., 1993. Decision Support System for agricultural development, in: de Vries, F.P., Teng, P., Metselaar, K. (Eds.), Systems Approaches for Agricultural Development. Kluwer Academic Publishers, Boston, pp. 459–471.

Jones, J.W., Antle, J.M., Basso, B., Boote, K.J., Conant, R.T., Foster, I., Godfray, H.C.J., Herrero, M., Howitt, R.E., Janssen, S., Keating, B.A., Munoz-Carpena, R., Porter, C.H., Rosenzweig, C., Wheeler, T.R., 2017. Brief history of agricultural systems modeling. Agric. Syst. 155, 240–254. https://doi.org/10.1016/j.agsy.2016.05.014

Jones, J.W., Hoogenboom, G., Porter, C.H., Boote, K.J., Batchelor, W.D., Hunt, L.A., Wilkens, P.W., Singh, U., Gijsman, A.J., 2003. The DSSAT Cropping System Model, European Journal of Agronomy.

Jones, J.W., Ritchie, J.T., 1991. Crop Growth Models, in: Hoffman, G.J., Howell, T.A., Soloman, K.H. (Eds.), Management of Farm Irrigation System. American Society

of Agricultural Engineers, pp. 63–89.

Li, X., Liu, L., Yang, H., Li, Y., 2018. Relationships between carbon fluxes and environmental factors in a drip-irrigated, film-mulched cotton field in arid region. PLoS One 13, 1–18. https://doi.org/10.1371/journal.pone.0192467

Matocha, M., Allen, C., Boman, R., Morgan, G., Baumann, P., 2009. Crop Profile for Cotton in Texas. College Station, Texas.

Modala, N.R., Ale, S., Rajan, N., Munster, C.L., DeLaune, P.B., Thorp, K.R., Nair, S.S., Barnes, E.M., 2015. Evaluation of the CSM-CROPGRO-COTTON MODEL for the Texas Rolling Plains Region and Simulation of Deficit Irrigation Strategies for Increasing Water Use Efficiency. Trans. ASABE 58, 658–696.

Möller, M., Tanny, J., Li, Y., Cohen, S., 2004. Measuring and predicting evapotranspiration in an insect-proof screenhouse. Agric. For. Meteorol. 127, 35–51. https://doi.org/10.1016/j.agrformet.2004.08.002

Monteith, J.L., 1986. How do crops manipulate water supply and demand ? Phil. Trans. R. Soc. Lond. 316, 245–259.

National Oceanic and Atmospheric Administration, 2011. Climate Data Online [WWW Document]. Natl. Centers Environ. Inf.

Oki, T., Shinjiro, K., 2006. Global Hydrological Cycles and World Water Resources. Science (80-.). 313, 1068–1073.

Pathak, T.B., Jones, J.W., Fraisse, C.W., Wright, D., Hoogenboom, G., 2012. Uncertainty analysis and parameter estimation for the CSM-CROPGRO-cotton model. Agron. J. 104, 1363–1373. https://doi.org/10.2134/agronj2011.0349

Patil, N.G., Rajput, G.S., 2009. Evaluation of Water Retention Functions and Computer Program “Rosetta” in Predicting Soil Water Characteristics of Seasonally Impounded Shrink-Swell Soils. J. Irrig. Drain. Eng. 135, 286–294.

Priestly, C.H.B., Taylor, R.J., 1972. On the Assessment of Surface Heat Flux and Evaporation Using Large-Scale Parameters. Mon. Weather Rev. 100, 81–92.

Qin, S., Li, S., Kang, S., Du, T., Tong, L., Ding, R., 2016. Can the drip irrigation under film mulch reduce crop evapotranspiration and save water under the sufficient irrigation condition? Agric. Water Manag. 177, 128–137. https://doi.org/10.1016/j.agwat.2016.06.022

Ringrose-Voase, A.J., Nadelko, A.J., 2013. Deep drainage in a Grey Vertosol under furrow-irrigated cotton. Crop Pasture Sci. 64, 1155–1170.

Ritchie, J.T., 1998. Soil water balance and plant stress, in: Tsuji, G.Y., Hoogenboom, G., Thornton, P.K. (Eds.), Understanding Options for Agricultural Production. System Approaches for Sustainable Agricultural Development. Kluwer Academic Publishers, Dordrecht, Netherlands, pp. 41–54.

Ritchie, J.T., 1972. Model for Predicting Evaporation from a Row Crop with Incomplete Cover. Water Resour. Res. 8, 1204–1213.

Ritchie, J.T., Otter, S., 1985. Description and performance of CERES-Wheat: A User-oriented wheat yield model. ARS Wheat Yield Proj. 38, 159–175.

Ritchie, J.T., Porter, C.H., Judge, J., Jones, J.W., Suleiman, A.A., 2009. Extension of an Existing Model for Soil Water Evaporation and Redistribution under High Water Content Conditions. Soil Sci. Soc. Am. J. 73, 792.

https://doi.org/10.2136/sssaj2007.0325

Rodell, M., Beaudoing, H.K., L'Ecuyer, T.S., Olson, W.S., Famiglietti, J.S., Houser, P.R., Adler, R., Bosilovich, M.G., Clayson, C.A., Chambers, D., Clark, E., Fetzer, E.J., Gao, X., Gu, G., Hilburn, K., Huffman, G.J., Lettenmair, D.P., Liu, W.T., Robertson, F.R., Schlosser, C.A., Sheffield, J., Wood, E.F., 2015. The Observed State of the Water Cycle in the Early Twenty-First Century. J. Clim. 28, 8289–8318. https://doi.org/10.1175/JCLI-D-14-00555.1

Rost, S., Gerten, D., Bondeau, A., Lucht, W., Rohwer, J., 2008. Agricultural green and blue water consumption and its influence on the global water system. Water Resour. Res. 44, 1–17. https://doi.org/10.1029/2007WR006331

Sau, F., Boote, K.J., Bostick, M., Jones, J.W., Minguez, M.I., 2004. Testing and Improving Evapotranspiration and Soil Water Balance of the DSSAT Crop Models. Agron. J. 96, 1243–1257.

Seligman, N.C., Van Keulen, H., 1981. PAPRAN: a simulation model of annual pasture production limited by rainfall and nitrogen, in: Frissel, M.J., Van Veen, J.A. (Eds.), Simulation of Nitrogen Behavior of Soil-Plant Systems. Centrum voor Landbouwpublikaties en Landbouwdocumentatie, Wageningen, Netherlands, pp. 192–221.

Shelton, M.L., 1987. Irrigation induced change in vegetation and evapotranspiration in the Central Valley of California. Landsc. Ecol. 1, 95–105.

Sinclair, T.R., Muchow, R.C., 2001. System Analysis of Plant Traits to Increase Grain Yield on Limited Water Supplies 93, 263–270.

Soldevilla-Martinez, M., Quemada, M., Lopez-Urrea, R., Munoz-Carpena, R., Lizaso, J.I., 2014. Soil water balance: Comparing two simulation models of different levels of complexity with lysimeter observations. Agric. Water Manag. 139, 53–63.

Soler, C.M.T., Sentelhas, P.C., Hoogenboom, G., 2007. Application of the CSM-CERES-Maize model for planting date evaluation and yield forecasting for maize grown off-season in a subtropical environment. Eur. J. Agron. 27, 165–177. https://doi.org/10.1016/j.eja.2007.03.002

Spera, S.A., Galford, G.L., Coe, M.T., 2016. Land-use change affects water recycling in Brazil ' s last agricultural frontier. Glob. Chang. Biol. 22, 3405–3413. https://doi.org/10.1111/gcb.13298

Suleiman, A.A., Hoogenboom, G., 2007. Comparison of Priestley–Taylor and FAO-56 Penman–Monteith for daily reference evapotranspiration estimation in Georgia, USA. J. Irrig. Drain. Eng. 133.

Suleiman, A.A., Ritchie, J.T., 2003. Modeling Soil Water Redistribution during Second-Stage Evaporation. Soil Sci. Soc. Am. J. 67, 377–386. https://doi.org/10.2136/sssaj2003.0377

Suleiman, A.A., Soler, C.M.T., Hoogenboom, G., 2007. Evaluation of FAO-56 crop coefficient procedures for deficit irrigation management of cotton in a humid climate. Agric. Water Manag. 91, 33–42.

Suyker, A.E., Verma, S.B., Burba, G.G., Arkebauer, T.J., Walters, D.T., Hubbard, K.G., 2004. Growing season carbon dioxide exchange in irrigated and rainfed maize. Agric. For. Meteorol. 124, 1–13. https://doi.org/10.1016/j.agrformet.2004.01.011

Texas A&M Agrilife, 2019. Cotton Production Regions of Texas [WWW Document]. Cott. Insect Manag. Guid.

Thorp, K.R., Barnes, E.M., Hunsaker, D.J., Kimball, B.A., 2014. Evaluation of CSM-CROPGRO-Cotton for Simulating Effects of Management and Climate Change on Cotton Growth and Evapotranspiration In An Arid Environment. Trans. ASABE 57, 1627–1642.

Thorp, K.R., Hunsaker, D.J., French, A.N., Bautista, E., Bronson, K.F., 2015. Integrating geospatial data and cropping system simulation within a geographic information system to analyze spatial seed cotton yield, water use, and irrigation requirements. Precis. Agric. 16, 532–557.

Tian, H., Chen, G., Liu, M., Zhang, C., Sun, G., Lu, C., Xu, X., Ren, W., Pan, S., Chappelka, A., 2010. Model estimates of net primary productivity, evapotranspiration, and water use efficiency in the terrestrial ecosystems of the southern United States during 1895-2007. For. Ecol. Manage. 259, 1311–1327. https://doi.org/10.1016/j.foreco.2009.10.009

Uddin, J., Smith, R.J., Hancock, N.H., Foley, J.P., 2013. Evaporation and sapflow dynamics during sprinkler irrigation of cotton. Agric. Water Manag. 125, 35–45. https://doi.org/10.1016/j.agwat.2013.04.001

USDA-NASS, 2017. 2017 Census of Agriculture County Profile: Burleson County Texas.

Wang, C., Zhang, Z., Fan, S., Mwiya, R., Xie, M., 2018. Effects of straw incorporation on desiccation cracking patterns and horizontal flow in cracked clay loam. Soil

Tillage Res. 182, 130–143.

Wilson, K., Goldstein, A., Falge, E., Aubinet, M., Baldocchi, D., Berbigier, P., Bernhofer, C., Ceulemans, R., Dolman, H., Field, C., Grelle, A., Ibrom, A., Law, B.E., Kowalski, A., Meyers, T., Moncrieff, J., Monson, R., Oechel, W., Tenhunen, J., Valentini, R., Verma, S., 2002. Energy balance closure at FLUXNET sites. Agric. For. Meteorol. 113, 223–243.

Xevi, E., Gilley, J., Feyen, J., 1996. Comparative study of two crop yield simulation models. Agric. Water Manag. 30, 155–173.

Xu, C.Y., Chen, D., 2005. Comparison of seven models for estimation of evapotranspiration and groundwater recharge using lysimeter measurement data in Germany. Hydrol. Process. 19, 3717–3734. https://doi.org/10.1002/hyp.5853

Yu, G., Wen, X., Sun, X., Tanner, B.D., Lee, X., Chen, J., 2006. Overview of ChinaFLUX and evaluation of its eddy covariance measurement. Agric. For. Meteorol. 137, 125–137. https://doi.org/10.1016/j.agrformet.2006.02.011

7. CONCLUSIONS

7.1. Conclusions

The overarching goal of this dissertation was to improve our understanding of carbon and water fluxes in East-Central Texas agroecosystems. Agroecosystems are unique compared to natural ecosystems due to their inputs and management practices (Foley et al., 2005; Tscharntke et al., 2005; Tian et al., 2010; Han et al., 2014). Carbon and water vapor fluxes are extremely important ecosystem processes that are part of nutrient cycling and energy transfer. Understanding these fluxes from agroecosystems can allow for improved management that preserves the function of these vital ecosystem services (Tscharntke et al., 2005; Bennett et al., 2009; Tian et al., 2010; Han et al., 2014). By incorporating modeling and measurements, this dissertation explored carbon and water vapor fluxes from conventional corn production and conventional cotton production.

The first chapter (after the introduction) described the observations of carbon fluxes in dryland production cotton over two full years, including off-season (fallow). Carbon fluxes were compared to weather conditions and NDVI from PlanetScope satellite images. There were substantial differences between the two years, likely caused by meteorological conditions. Precipitation was the greatest predictor of gross primary productivity (GPP) compared to photosynthetically active radiation, and air temperature. High off-season precipitation in 2018 caused a growth of weeds, which increased off-

season carbon uptake. The overall carbon balance for 2017 was a net emission of 175.4 g C m^{-2} and the overall carbon balance for 2018 was a net sequestration of 5.1 g C m^{-2}.

In the second chapter, high-resolution satellite imagery from Planet Labs, Inc. was used to model GPP in conventionally tilled, dryland corn. A variation on the light use efficiency model where light use efficiency is replaced by a remotely sensed vegetation index was used (Monteith, 1977; Yan et al., 2009; Zhou et al., 2017; Shafian et al., 2018). GPP was correlated with vegetation index multiplied by photosynthetically active radiation and leaf area index to develop the models using data from 2017. The models were validated using data from 2018 and 2019. The vegetation indices used were the normalized difference vegetation index (NDVI), soil adjusted vegetation index (SAVI), weighted difference vegetation index (WDVI), and the enhanced vegetation index (EVI). The SAVI-based models were the most successful with a standard error of the estimate of 1.74 g C m^{-2} for the 2018 validation and 1.50 g C m^{-2} for 2019. The slope of the modeled GPP using SAVI compared to observed GPP from the eddy covariance system was not different from one.

The third chapter highlighted the efforts to model GPP in dryland, conventionally tilled cotton using Planet Labs, Inc.'s high-resolution satellite data. The same method based on Monteith's light-use efficiency that was used to model corn GPP was also used to model cotton GPP. The following vegetation indices were used to model GPP in cotton: the normalized difference vegetation index (NDVI), soil adjusted vegetation index (SAVI), Green Chlorophyll Index (CI_{Green}), and the enhanced vegetation index (EVI). The 2018 model validation was somewhat successful with an average standard

error across all VI-based models of 1.78 g C m^{-2}, while the 2019 validation was less successful with an average standard error of 2.36 across all VI-based models. The most successful model in 2018 was the NDVI-based model and the most successful model in 2019 was the SAVI-based model.

In the fourth chapter, the Decision Support System for Agrotechnology Transfer (DSSAT) was used to model corn growth and evapotranspiration in a dryland, conventionally tilled system. Modeled evapotranspiration was then compared statistically to evapotranspiration observed using the eddy covariance system. Of DSSAT's internal potential evapotranspiration methods, the FAO-56 method generally was less error-prone than the Priestly-Taylor model. The models had the most error shortly after precipitation events. Evapotranspiration modeling in corn was successful with standard error and index of agreement within the range seen by other studies in dryland corn (Gonzalez-Dugo et al., 2009; Basso et al., 2016).

. In the fifth chapter, DSSAT was used to model cotton growth and evapotranspiration in dryland, conventionally tilled cotton. The eddy covariance water vapor flux data was then used to validate the evapotranspiration models. Once again, the FAO-56 method produced fewer errors, especially following rain events. The cotton models were less successful than the corn models, with the 2019 models having low agreement with observed ET ($r^2 = 0.14$). In both modeling efforts (DSSAT and remote sensing), the modeling with cotton was less successful than that with corn. Cotton has a more complex growth habit that is likely more difficult for models to accurately simulate. In the early growing season, cotton plants grow slowly, putting most of their

energy belowground. Despite potentially high PAR and air temperatures, plant growth can remain slow. In the later season, the application of growth regulators and defoliants further alters the response of cotton ET and GPP to meteorological conditions. Additionally, the unique shrink-swell characteristics of the soil at the site are likely further complicating modeling efforts (Ringrose-Voase and Nadelko, 2013; Zapata et al., 2017, 2019; Harmel et al., 2019).